



UNIL | Université de Lausanne

Unicentre

CH-1015 Lausanne

<http://serval.unil.ch>

Year : 2019

Molecular and functional immune déterminants associated with the optimal immunogenicity of Yellow Fever vaccination in humans.

Bovay Amandine

Bovay Amandine, 2019, Molecular and functional immune déterminants associated with the optimal immunogenicity of Yellow Fever vaccination in humans.

Originally published at : Thesis, University of Lausanne

Posted at the University of Lausanne Open Archive <http://serval.unil.ch>

Document URN : urn:nbn:ch:serval-BIB_5EBE536D2CB33

Droits d'auteur

L'Université de Lausanne attire expressément l'attention des utilisateurs sur le fait que tous les documents publiés dans l'Archive SERVAL sont protégés par le droit d'auteur, conformément à la loi fédérale sur le droit d'auteur et les droits voisins (LDA). A ce titre, il est indispensable d'obtenir le consentement préalable de l'auteur et/ou de l'éditeur avant toute utilisation d'une oeuvre ou d'une partie d'une oeuvre ne relevant pas d'une utilisation à des fins personnelles au sens de la LDA (art. 19, al. 1 lettre a). A défaut, tout contrevenant s'expose aux sanctions prévues par cette loi. Nous déclinons toute responsabilité en la matière.

Copyright

The University of Lausanne expressly draws the attention of users to the fact that all documents published in the SERVAL Archive are protected by copyright in accordance with federal law on copyright and similar rights (LDA). Accordingly it is indispensable to obtain prior consent from the author and/or publisher before any use of a work or part of a work for purposes other than personal use within the meaning of LDA (art. 19, para. 1 letter a). Failure to do so will expose offenders to the sanctions laid down by this law. We accept no liability in this respect.



UNIL | Université de Lausanne

Faculté de biologie
et de médecine

Département d'Oncologie Fondamentale (DOF), CHUV

Molecular and functional immune determinants associated with the optimal immunogenicity of Yellow Fever vaccination in humans.

Thèse de doctorat ès sciences de la vie (PhD)

présentée à la

Faculté de biologie et de médecine
de l'Université de Lausanne

par

Amandine BOVAY

Master de l'Université de l'Ecole Polytechnique Fédérale de Zurich (ETHZ)

Jury

Prof. David Vernez, Président
Prof. Daniel Speiser, Directeur de thèse
Prof. Silvia Fuertes-Marraco, Co-directeur
Prof. Sanjiv Luther, représentant du programme PhD
Prof. Immanuel Luescher, expert interne
Prof. Enrico Lugli, expert externe

Lausanne 2019



UNIL | Université de Lausanne

Faculté de biologie
et de médecine

Ecole Doctorale

Doctorat ès sciences de la vie

Imprimatur

Vu le rapport présenté par le jury d'examen, composé de

Président·e	Monsieur	Prof.	David	Vernez
Directeur·trice de thèse	Monsieur	Prof.	Daniel	Speiser
Co-directeur·trice	Madame	Prof.	Silvia	Fuertes-Marraco
Expert·e·s	Monsieur	Dr	Immanuel	Luescher
	Monsieur	Prof.	Sanjiv	Luther
	Monsieur	Dr	Enrico	Lugli

le Conseil de Faculté autorise l'impression de la thèse de

Madame Amandine Bovay

Master en Biologie, ETHZ, Zürich

intitulée

**Molecular and functional immune determinants associated
with the optimal immunogenicity of Yellow Fever
vaccinations in humans**

Lausanne, le 7 juin 2019

pour le Doyen
de la Faculté de biologie et de médecine

Prof. David Vernez

TABLE OF CONTENT

TABLE OF CONTENT	5
ACKNOWLEDGEMENT	7
SUMMARY.....	8
RÉSUMÉ.....	9
RÉSUMÉ (large public).....	10
LIST OF ABBREVIATIONS	11
PREFACE	13
1. INTRODUCTION.....	15
1.1 BASIC PRINCIPLES OF INNATE AND ADAPTIVE IMMUNITY	15
1.2 T CELL DEVELOPMENT.....	16
1.2.1 T CELL DIFFERENTIATION.....	16
1.2.2 TCR GENE ASSEMBLY AND SOMATIC RECOMBINATION.....	22
1.2.3 TCR:pMHC RECOGNITION	23
1.2.4 DIVERSITY OF THE TCR REPERTOIRE	27
1.3 CANCER IMMUNOTHERAPIES	28
1.4 YELLOW FEVER VACCINATION AS A MODEL OF OPTIMAL IMMUNOGENICITY IN HUMANS	31
1.4.1 YELLOW FEVER VIRUS VACCINE (YF-17D).....	31
1.4.2 HUMAN IMMUNE RESPONSE TO YF-17D VACCINATION.....	32
1.4.3 YELLOW FEVER AS A MODEL	35
2. PROJECT NETWORK OVERVIEW AND AIMS OF THESIS	38
3. RESULTS.....	41
3.1 AXIS 1: TRAV12-2 bias and TCR:pMHC studies.....	41
3.1.1 TRAV12-2 bias in the immunodominant response to YFV	42
3.1.2 Fishing out new A2/LLW-specific clonotypes using an optimized multimer staining procedure	57
3.1.3 Detailed description of the soluble TCR:pMHC production process.....	66
3.1.4 in vivo analysis of the TRAV12-2 bias using the transgenic ABAbDII mouse model	80
3.1.5 Characterization of potential superagonist variants of the A2/LLW epitope	92
3.1.6 CONCLUDING REMARKS.....	114
3.2 AXIS 2: Longitudinal analysis of the human immune responses to YF-17D vaccination.....	115
3.2.1 Characterization of all major immune cell populations following primary and booster YF-17D vaccination (aims a and b).....	118
3.2.2 Analysis of A2/LLW-specific effector and long-lasting memory CD8 T cells in the early response to YF-17D (aim c).....	172
4. ONGOING WORK AND PERSPECTIVES.....	176
5. CONCLUDING REMARKS.....	180
6. MATERIAL AND METHODS	181
6.1 Clinical studies: design, population and ethics statement	181
6.2 Biobank: Peripheral blood collection and processing	181
6.3 Viral load quantification.....	182
6.4 Plaque reduction neutralizing test (PRNT)	182
6.5 Generation and maintenance of T cell clones.....	182
6.6 Generation of T cell lines	183
6.7 TCR repertoire and clonotype analysis in A2/LLW-specific CD8 ⁺ T cell clones...	183
6.8 TCR sequencing and analysis of the A2/LLW-specific T cell line	183

6.9 ⁵¹ Chromium release assays	184
6.10 Flow cytometry	184
6.10.1 Flow cytometry: list of reagents	186
6.10.2 Intracellular cytokine staining assay	188
6.10.4 Data processing and statistical analysis	188
6.10.5 Bioinformatics analysis of broad datasets	188
6.11 NTAmer staining and dissociation kinetic measurements	189
6.12 Sizing scan	189
6.13 Combinatorial peptide library (CPL) scans	190
6.14 Protein expression, refolding and purification	190
6.15 Crystallization, diffraction data collection, and model refinement	191
6.16 Measuring the thermal stability of HLA-A*0201–peptide complexes	192
6.17 In silico TCR:pMHC analyses: Modeling the TCR:pMHC complex and Molecular Dynamics (MD) simulations	192
7. REFERENCES	194
APPENDIX 1: European Journal of Immunology – Cover 2/18	224
APPENDIX 2: T cell receptor alpha variable 12-2 bias in the immunodominant response to Yellow fever virus	225
APPENDIX 3: Human stem cell-like memory CD8 T cells establish early in the acute response to Yellow Fever virus vaccination	240
CURRICULUM VITAE	278

ACKNOWLEDGEMENT

I would like to thank the Swiss National Science Foundation and the Quealth Foundation for funding the research documented in this thesis.

I would like to express my sincerest gratitude to my thesis director, Prof. Daniel Speiser, for giving me the opportunity to carry out my PhD thesis in his laboratory and his involvement in my work.

To my co-director and main supervisor, Dr. Silvia Fuertes Marraco, thank you so much for your dedication to the project. Many thanks also for your constant support. Without your encouragement, it would have been a lonely road. Your guidance helped me in all time of research and writing of this thesis. Not only you are a great scientist but also you are a beautiful person. I have learnt so many things from you, I owe you a lot!

I am grateful to the whole group of Prof. Andrew Sewell who gave me the chance to discover new scientific and personal horizons. Andy, it was quite a battle wasn't it? But you taught me to keep a positive attitude and accept new challenges with philosophy (and a bit of whisky :p).

In addition, I would like to thank Dr. David Cole, Dr. Pierre Rizkallah, Dr. Anna Bulek and Anna Fuller for their help with the protein work. I would like to acknowledge the good time spent in the 2F04 office. An enormous thanks goes to Dr. Valentina Bianchi who helped me settling in Cardiff.

I also would like to thank my committee members, Prof. Sanjiv Luther, Prof. Immanuel Luescher and Dr. Enrico Lugli, for their numerous advice and constructive critique during exams.

Special thanks to my colleagues for the enjoyable atmosphere in the lab, passionate discussions (scientific or not) and emotional support throughout the years. In particular, I would like to mention Kaat De Jonge, Amélie Cachot, Bérengère Salomé, Claire Imbratta, Alexander Rockinger and Christophe Martignier.

Je tiens à remercier très chaleureusement ma famille: Papa, Maman, Viviane. Vous avez toujours été là pour moi et m'avez encouragée dans cette voie surtout dans les moments les plus difficiles. Merci pour votre soutien et amour inconditionnel, en particulier en cette fin de thèse qui s'est avérée plus mouvementée que prévu.

À toi Estelle, mon rayon de soleil, pour l'avenir!

SUMMARY

It is well established that strong immune responses by cytotoxic CD8 T cells are often key for the clinical outcome of patients with viral infection and cancer. In recent years, novel immunotherapies to activate the patient's immune system have shown unprecedented benefits for the treatment of cancer patients. However, immune responses are still often insufficient, even despite immunotherapy, which therefore must be optimized.

Our group has elaborated clinical studies on vaccination against Yellow Fever virus (YFV) with the YF-17D vaccine, because this live-attenuated virus vaccine is the most potent vaccine in humans, and it is increasingly renowned as a unique opportunity to study human CD8 T cells to model optimal immunotherapies.

First, I characterized the molecular basis of the high frequency and prevalence of an immunodominant HLA-A*02- restricted YFV-specific epitope, in analogy to the HLA-A*02-restricted Melan-A epitope in melanoma. Secondly, I focused on the characterization of a longitudinal study in healthy individuals before and up to six months after YF-17D vaccination, analyzing various innate and adaptive parameters using multiparameter flow cytometry. We gained insights into key parameters involved in strong, protective and long-term immune responses in humans. Furthermore, we compared primary and booster response to YF-17D with respect to CD8 T cell heterogeneity and the proportion and profiles of all major immune cell populations.

Overall, I obtained detailed and broad insight of the optimal acute immune response in humans based on vaccination against Yellow Fever virus (YFV) with YF-17D. This knowledge supports the identification of optimal immune parameters that may transcend and sustain optimization of anti-cancer T cell-based therapies.

RÉSUMÉ

Il est maintenant établi que les cellules CD8 T cytotoxiques sont un élément clé de l'issue clinique des patients souffrant d'infection virale ou de cancer. Ces dernières années, de nouvelles immunothérapies ont vu le jour et ont apportés des bénéfices sans précédent et l'espoir de traiter des cas très avancés. Cependant, les réponses immunitaires contre les tumeurs restent le plus souvent insuffisantes malgré l'immunothérapie. Il est donc primordial de trouver des moyens de les améliorer.

Notre groupe de recherche a élaboré des études cliniques portant sur la vaccination contre le virus de la fièvre jaune avec le vaccin vivant atténué YF-17D. Il s'agit du vaccin le plus efficace qui existe à ce jour chez l'humain. Il offre l'opportunité unique d'étudier les réponses immunitaires dans un contexte contrôlé chez l'être humain, en particulier les cellules T cytotoxiques. Ce vaccin est donc considéré comme un modèle optimal pour améliorer les immunothérapies.

Durant ma thèse, j'ai d'abord caractérisé les bases moléculaires de la haute fréquence and prévalence de l'épitope immunodominant spécifique à la fièvre jaune et restreint à la molécule HLA-A*02. Deuxièmement, j'ai analysé les échantillons sanguins d'individus sains avant et après avoir reçu le vaccin YF-17D pour la première fois ou le rappel après 10 ans. J'ai analysé les différents paramètres de la réponse immunitaire innée et adaptative grâce à la cytométrie de flux. Le but de ma thèse est de déterminer quels sont les paramètres associés à une réponse immunitaire robuste, protectrice et durable. Ces connaissances permettront d'identifier les paramètres immunitaires qui serviront à optimiser les immunothérapies contre le cancer.

RÉSUMÉ (large public)

Il est maintenant établi que certains types cellulaires du système immunitaire sont capables de reconnaître et de tuer non seulement les agents pathogènes externes tels que les virus et les bactéries mais également les cellules tumorales. Ces dernières années, de nouvelles stratégies visant à mobiliser efficacement les propres cellules immunitaires de patients atteints de cancer ont vu le jour. Appelées “immunothérapies”, ces thérapies ont apportés des bénéfices sans précédent et l’espoir de traiter des cas très avancés. Cependant, les réponses immunitaires contre les tumeurs restent le plus souvent insuffisantes malgré l’immunothérapie. Il est donc primordial de trouver des moyens de les améliorer.

Ma thèse de doctorat porte sur le vaccin contre la fièvre jaune car il s’agit du vaccin le plus efficace qui existe à ce jour chez l’humain. Il offre l’opportunité unique d’étudier les réponses immunitaires dans un contexte contrôlé chez l’être humain, en particulier les cellules T cytotoxiques, une classe de globules blancs capables d’éradiquer les tumeurs. Ce vaccin est donc considéré comme un modèle optimal pour améliorer les immunothérapies.

Le but de ma thèse est de déterminer quels sont les paramètres associés à une réponse immunitaire robuste, protectrice et durable. Pour ce faire, j’ai utilisé une combinaison de techniques à la fois moléculaires et fonctionnelles. J’ai analysé les échantillons sanguins d’individus avant et après avoir reçu le vaccin pour la première fois ou le rappel après 10 ans. J’ai ainsi pu examiner de manière détaillée la dynamique et l’activation des principaux types cellulaires du système immunitaire tenant compte d’une large combinaison de paramètres immunitaires pour obtenir un portrait détaillé de la réponse immunitaire optimale chez l’humain.

LIST OF ABBREVIATIONS

A2	HLA-A2*0201
Ag	Antigen
APC	Antigen-Presenting Cell
Bcl-2	B cell lymphoma protein-2
C	Core
CAR	chimeric antigen receptor
CD	Circular Dichroism
CDR	Complementarity- Determining Region
CM	Central Memory
CMV	Cytomegalovirus
CPL	Combinatorial Peptide Library
CSnT	Cytometer Set-up and Tracking
CTLA-4	Cytotoxic T-Lymphocyte Associated Protein 4
DAG	Diacylglycerol
DC	Dendritic cell
E	Envelope
EBV	Epstein-Barr Virus
EM	Effector Memory
ER	Endoplasmic Reticulum
FDA	Food and Drug Administration
FDA	Functional Data Analysis
FTOC	Fetal Thymus Organ Culture
HTLV-1	Human T-cell leukemia virus type 1
IB	Inclusion Body
IFA	Incomplete Freud's Adjuvant
ILC	Innate Lymphoid Cell
IP3	Inositol triphosphate
LLW	LLWNGPMAV
M	Membrane
mDC	Myeloid dendritic cell
MHC-I	Major Histocompatibility Complex class I

nAbs	neutralizing antibodies
NK	Natural Killer
NS	Non-Structural
NTA	Ni ²⁺ -nitrilotriacetic acid
PBMCs	Peripheral Blood Mononuclear Cells
PBS	Phosphate Buffered Saline
PD1	Programmed cell Death 1
pDC	plasmacytoid DC
PIP2	Phosphatidylinositol triphosphate
PLC-γ1	phospholipase C gamma 1
pMHC	peptide: Major Histocompatibility Complex
PRNT	Plaque Reduction Neutralizing Test
RAG	Recombinase Activating Gene
RNA	RiboNucleic Acid
S1PR	Sphingosine 1-Phosphate Receptor 1
SAGE	Strategic Advisory Group of Experts
Sca-1	Stem Cell Antigen-1
SCM	Stem Cell Memory
scRNA	single-cell RNA sequencing
SPR	Surface Plasmon Resonance
SWATH-MS	Sequential Window Acquisition of all Theoretical Mass Spectra
T	Thymus
t-SNE	t-stochastic neighbor embedding
TAP	Transporter associated with Antigen Processing
TCR	T-Cell Receptor
TIL	Tumor-Infiltrating lymphocyte
TraCeR	T cell receptor sequence Reconstruction
WHO	World Health Organization
YEL-AND	YF-17D vaccine-associated neurotropic disease
YEL-AVD	YF-17D vaccine-associated viscerotropic disease
YF	Yellow Fever
YFV	Yellow Fever Virus

PREFACE

My PhD thesis work can be divided into two main axes. The first axis consisted in characterizing the molecular and functional aspects of the TCR:pMHC interaction in HLA-A2/LLW-specific CD8 T cells. The second axis focused on the longitudinal clinical protocol, in which we collected blood samples before and several time-points after YF-17D vaccination, in order to uncover the major immune parameters and their relationships during this strong human acute T cell response.

The work conducted during my PhD thesis has led to an accepted first-author paper and several manuscripts are currently in preparation:

- **Bovay A**, Zoete V, Dolton G, Bulek Am, Cole DK, Rizkallah PJ, Fuller A, Beck K, Michielin O, Speiser DE, Sewell AK, Fuertes Marraco SA. T cell Receptor Alpha Variable 12-2 bias in the immunodominant response to Yellow fever virus. *Eur J Immunol.* 2018 Feb; 48(2):258-272. doi: 10.1002/eji.201747082.
This article was selected for the journal front cover.
- Rius C*, Attaf M*, Tungatt K, Bianchi V, Legut M, **Bovay A**, Donia M, Straten PT, Peakman M, Svane IM, Ott A, Connor T, Szomolay B, Dolton G, Sewell AK. Peptide-MHC class I multimer staining can fail to detect relevant functional T-cell clonotypes and underestimate antigen-specific T cell populations. *J Immunol.* 2018 Feb 26;. doi: 10.4049/jimmunol.1700242.
- Fuertes Marraco SA, **Bovay A**, Nassiri S, Maby-El Hajjami H, Ouertatani-Sakouhi H, Held W, Speiser DE. Human stem cell-like memory CD8 T cells establish early in the acute response to Yellow Fever virus. *In preparation.*
- **Bovay A**, Zoete V, Rizkallah PJ, Beck K, Delbreil P, Speiser DE, Cole DK, Fuertes Marraco SA. Functionally optimized peptide rigidity in a novel superagonist mutant of the immunodominant Yellow Fever Virus epitope NS4b₂₁₄₋₂₂₂. *In preparation.*
- **Bovay A**, Nassiri S, Maby-El Hajjami H, Marcos Mondéjar P, Akondy AS, Ahmed R, Lawson B, Speiser DE, Fuertes Marraco SA. Pre-existing neutralizing antibodies restricts adaptive and innate immune responses to Yellow Fever virus YF-17D vaccination. *In preparation.*

I structured the present PhD report in the format “thesis without published articles”, keeping all data output and report as maintext, and the corresponding manuscripts are found as Appendixes at the end of the report.

My thesis was conducted in a collaborative framework coordinated by my direct supervisor Dr. Silvia Fuertes and closely supported by Prof. Daniel Speiser, with specific projects led by myself. The specific contributions are stated in each chapter of the results. Briefly, the work of the first axis was predominantly achieved and led by myself, including a 9-month scientific visit in Prof. Andrew Sewell’s laboratory in Cardiff. I also mainly conducted the collaborations that subsequently arose from this project. The work that I carried out for the second axis was wired within a collaborative network of world-leading experts involving multiple analyses using comprehensive and cutting-edge technology.

1. INTRODUCTION

1.1 BASIC PRINCIPLES OF INNATE AND ADAPTIVE IMMUNITY

To protect the human body against disease, the immune system must fulfill several tasks. The initial defenses against pathogens are the physical and chemical barriers, such as the skin and mucous membranes. When an individual encounters an infectious agent, its presence inside the body must be detected as a foreign component by cells from both the innate and adaptive systems. Then, an effector response is mounted to contain the infection and eliminate it. The innate immune response occurs rapidly and in a non-specific manner. In contrast, the adaptive immune response takes longer to develop but is more efficient at eliminating infections, as it is highly specific (antigen-specific). The main functions of the various cell types of both the innate and adaptive response are illustrated in Figure 1.

Concurrently, the immune response must be tightly and finely regulated to overcome pathogenic invasion while avoiding tissue damage, allergy and autoimmune diseases. A remarkable property of the adaptive immune system is the generation of an immunological memory, providing long-lasting specific protection. As a result, the immune system can react more efficiently to a secondary exposure to a particular antigen. As my work largely focused on the immune responses mediated by cytotoxic CD8 T cells, I will give particular attention to major concepts concerning the function and quality of these cells.

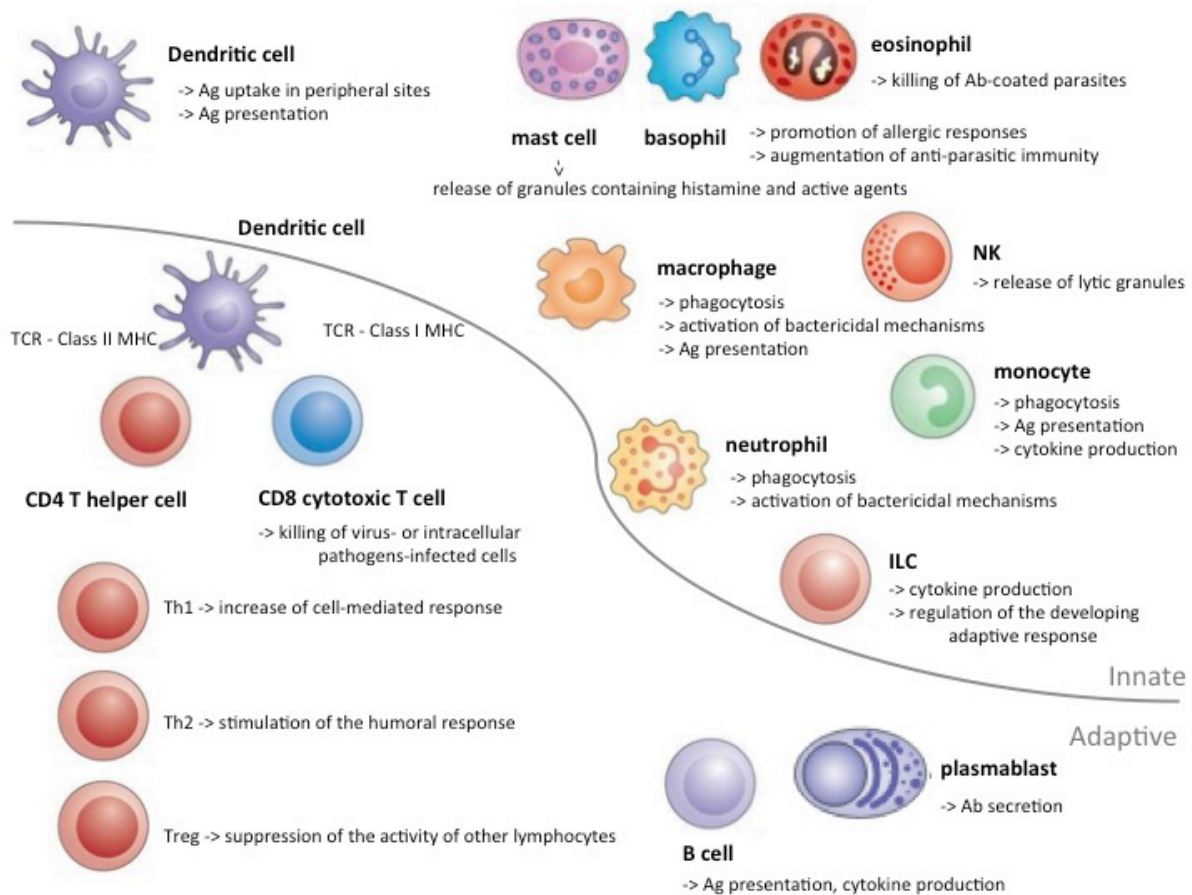


Figure 1 Overview of the primary functions of the main innate and adaptive immune. Adapted from [1]

1.2 T CELL DEVELOPMENT

1.2.1 T CELL DIFFERENTIATION

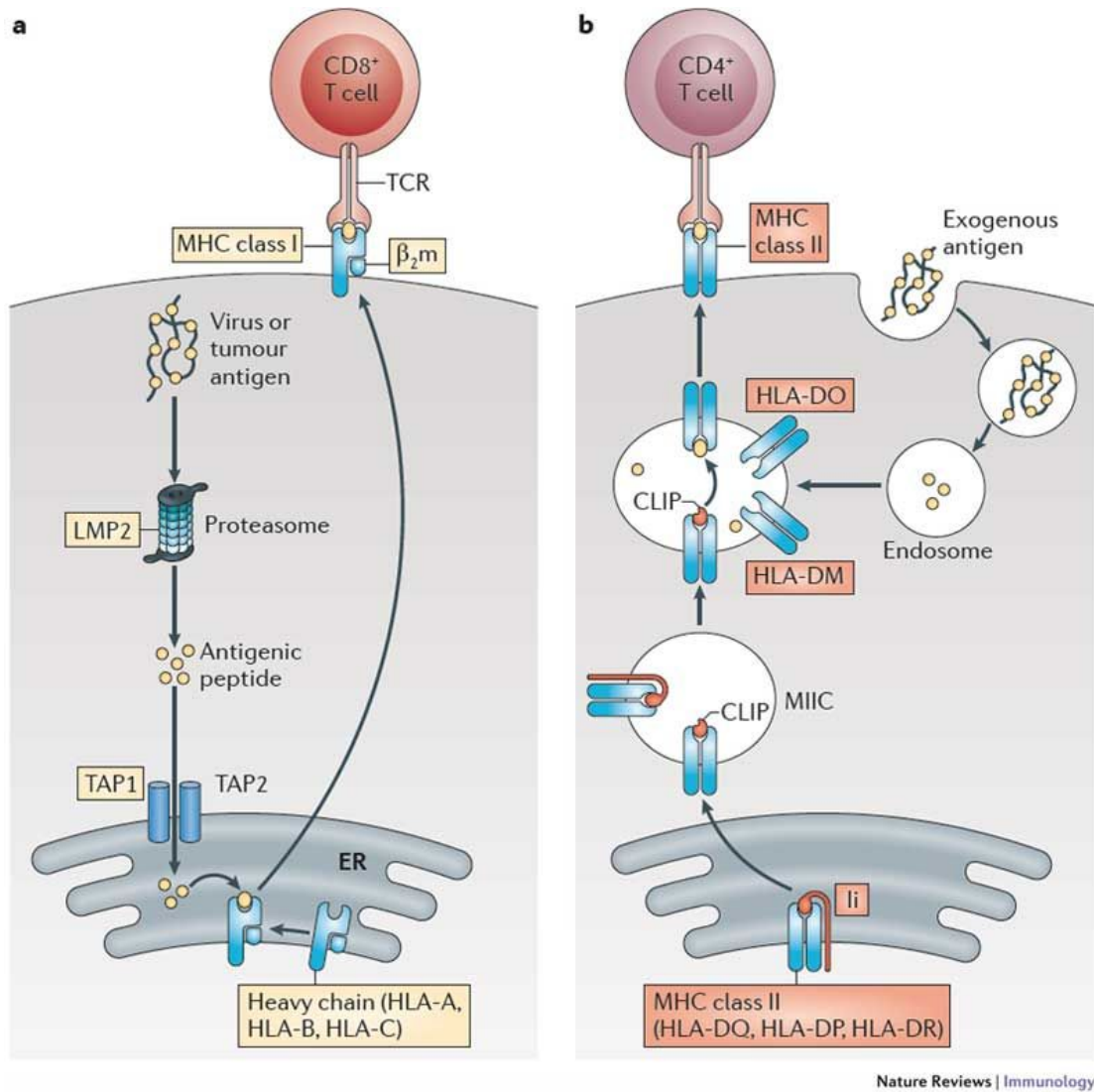
T cells derive from the hematopoietic stem cells found in the bone marrow. Unlike B lymphocytes that continue their development in the bone marrow (hence named “B” cells), T cell progenitors migrate to and colonize the thymus, hence their name thymus-dependent (T) lymphocytes. Developing T cells, known as thymocytes, undergo a series of maturation steps across thymic compartments, which are marked by changes in cell surface proteins such as the CD3 complex and the co-receptor molecules CD4 and CD8. Importantly, it is here that thymocytes rearrange their T-cell receptor (TCR) genes (this process is described in more detail below). Then, immature T cells face positive and negative selection depending on the interaction of the TCR with antigenic peptide in the context of major histocompatibility complex (peptide:MHC complex, pMHC). In the thymus cortex, epithelial cells present self MHC molecules. For positive

selection, only thymocytes that recognize self MHC with sufficient strength receive signals to survive. Autoimmune regulator (AIRE) is an important transcriptional regulator mainly expressed by thymic epithelial cells in the medulla of the thymus (mTECs). AIRE functions in immune central tolerance by clearance of auto-reactive T cells. Through negative selection, AIRE enhances the clonal deletion of thymocytes that recognize self antigens (self pMHC) and are thus potentially auto-immune. AIRE also induces the production of regulatory T cells (Tregs) which are tolerogenic. Mature T cells exit the thymus and enter the blood circulation: recirculate in blood and migrate in the blood to the peripheral lymphoid tissues, where they encounter foreign antigens and are activated. In addition to central tolerance, not all self-reactive lymphocytes are eliminated, in part because not all self-antigens are expressed in the thymus. Therefore, both anergy (tolerance mechanism by which a lymphocyte is intrinsically functionally inactivated following antigen encounter) and deletion of self-reactive T cells can occur in the periphery.

MHC class I molecules are expressed on all nucleated cell types (i.e. with the exception of red blood cells) and can load relatively small peptides derived from proteins degraded in the cytosol. The resulting pMHC class I complexes are presented at the surface of the cell for interaction with the CD8 co-receptor and the T cell receptor, namely to cytotoxic CD8⁺ T cells (Figure 2a). In this process, intracellular antigens are processed into peptides by the immunoproteasome. Peptides are transported by the Transporter associated with antigen processing (TAP) complex into the endoplasmic reticulum (ER). They are then loaded into the groove the MHC class I complex composed of a heavy chain and a smaller subunit β 2-microglobulin. Cytotoxic CD8 T cells are able to eliminate virally-infected or malignant cells.

Conversely, CD4 T cells recognize antigens associated with MHC class II molecules that are expressed on professional antigen-presenting cells (APCs) such as B cells, dendritic cells (DCs), monocytes and macrophages (Figure 2b). These antigens originate from extracellular proteins endocytosed into vesicles (e.g bacteria) and are processed by endolysosomal enzymes into peptides. These peptides bind to the MHC class II complex by displacing the class II-associated invariant chain peptide (CLIP), which is derived from the MHC class II-associated invariant chain (Ii).

Although direct cytotoxicity has also been found in a subset of CD4 T cells, the effector qualities attributed to CD4 T cells rather serve “helper” functions and are thus called “CD4 helper T (Th) cells”. CD4 Th cells may produce a large variety of cytokines and chemokines to support the immune response in various tasks: stimulate the production of antibodies by B cells, enhance the antimicrobial mechanisms of macrophages, recruit neutrophils, eosinophils, and basophils. Upon activation, and depending on the immune cues, naïve CD4 T cells can differentiate into several Th subtypes, associated with particular transcription factors, and cytokine sensitivity, cytokine production potential, and helper function. The two major traditional Th1/Th2 polarizations can be distinguished: Th1 CD4 T cells secrete IFN- γ and are involved in the immunity against intracellular pathogens and autoimmunity, whereas Th2 CD4 T cells secrete IL-4, IL-5, IL-10 and IL-13 and function in the response to large extracellular organisms, asthma and allergy. Relatively more recent Th types have been described: Th9 secrete the cytokines IL-9, IL-10 and IL-21 and participate in the response to parasite infections and large extracellular pathogens. Th17 secrete IL-17, IL-21 and IL-22 and are involved in the response to fungi and extracellular bacteria. Th22 secrete IL-13 and IL-22 and potentially contribute to host defense against microbial infection in the skin. T Follicular helper cells are specialized to help B cells produce antibody. Tregs maintain homeostasis and tolerance during an immune response.



Nature Reviews | Immunology

Figure 2 The MHC class I (a) and class II (b) antigen-presentation pathways. From [2]

Certain APCs such as a highly specialized subset of dendritic cells (Clec9A+ in humans, CD8+ or the cDC1 subset in mice) can phagocytize and process extracellular antigens then load these onto MHC class I molecules for presentation to CD8 T cells. This process is known as antigen cross-presentation, it allows CD8 T cells to be “cross-primed” to respond to extracellular antigens as opposed to the traditionally attributed response to intracellular antigens.

I will now focus on the CD8 T cells as they are at the center of the first axis of my PhD thesis and a major component of my studies in Axis 2; the TCR:pMHC interaction is also central to Axis 1 and thus given particular introductory attention further below.

Naïve antigen-specific CD8 T cells are activated after receiving at least three signals: TCR engagement (by binding to cognate pMHC on the APC), co-stimulation (binding co-stimulatory molecules on the T cell such as CD28 by co-stimulatory ligands such as CD80/CD86 on APC), and stimulation with inflammatory cytokines such as type 1 IFN and IL-12. When all three signals are delivered to a naïve cell, the latter is induced to massively proliferate by clonal expansion, and further differentiate into a heterogeneity of cells, with varying degrees of memory and effector functions. CD8 T cell effector function comprises cytotoxic cytokine production: the expression of perforin and granzyme molecules. Upon encounter with a target cell presenting cognate antigen, the release of these cytokines by degranulation leads to cytolytic activity. T cells migrate throughout the body based on patterns of chemokine receptor and selectin expression, and thus differential response to chemotactic and retention cues. Typically for example, naïve and memory cells express the chemokine receptor CCR7, responding to the secondary lymphoid ligands CCL19 and CCL21, and the L-selectin (CD62L) allowing the homing of these cells into lymph nodes. Differentiated cells express high levels of CXCR3 which responds to the inflammatory chemokines CXCL9, CXCL10 and CXCL11, supporting the recruitment of effector cells into sites of inflammation.

Initially, the view on CD8 T cell differentiation was very simplistic and cells were classified into effector or memory subsets. Conventionally, the expression of the surface markers CCR7 and CD45RA has been used to define the differentiation subsets in human CD8 T cells (Figure 3). Thanks to new broad-spectrum technologies such as transcriptomic and epigenetic analyses, recent studies have highlighted the heterogeneity of CD8 T cells expressing varying phenotypes of both effector and memory-associated molecules [3]–[5] (Figure 3). While effector cells have potent cytotoxicity, memory cells retain high proliferative capacity and potential to generate an effector progeny, together with long-term persistence and self-renewal.

Elucidating the differentiation path of a naïve T cell into this heterogeneity of CD8 T cell phenotypes and functions has been debated for a long time. Although difficult to assign, the generation of memory T cells and the plasticity among subsets have cumulated increasing knowledge especially in the last decade and a number of CD8 T cell differentiation models have been proposed. Initially, the linear model suggested sequential differentiation: first from naïve cells into effector cells in the acute phase, then upon antigen clearance the effector cells contract (the majority die) while a

fraction of effectors serve as precursors for memory cells [6] [7]. The observation in mouse models that both memory precursors (MPECs) and effector cells could be observed in the early response, before viral clearance and the contraction phase, challenged this view [8]. Today, markers such as the IL7Ra and the transcription factor T cell factor 1 (TCF1) allow distinguishing acute precursors of long-lived memory and activated cells [9]–[13]. Recent studies have therefore proposed non-linear models, where memory cells arise directly from naïve cells, e.g. by asymmetric cell division leaving one daughter cell committed to the memory fate, the other to become an effector cell [14]–[16]. These studies have mainly been driven in mouse models of acute immune responses. While some aspects of CD8 T cell differentiation might be shared between mice and humans, there are fundamental differences in the markers used to classify CD8 T cell subsets.

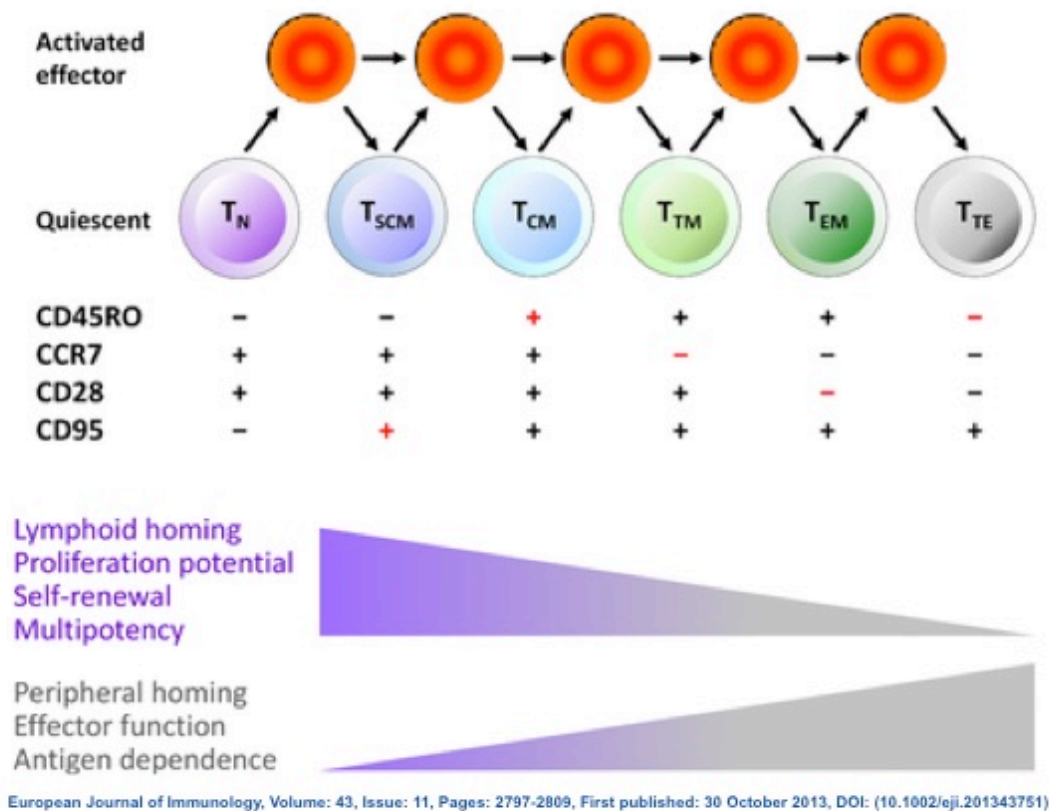


Figure 3 Properties and qualities of T cells across differentiation. The latest gradual model proposes that naïve T cells are driven towards progressive stages of differentiation: memory stem cells (SCM), central memory (CM), transitional memory (TM), effector memory (EM), terminally effector (TE). Adapted from Mahnke et al, 2013 [17]

1.2.2 TCR GENE ASSEMBLY AND SOMATIC RECOMBINATION

A TCR is a heterodimer composed of one α - and one β - chains. Each consists of a variable (V) amino-terminal region and a constant (C) region. The TCR α locus contains V and J gene segments ($V\alpha$ and $J\alpha$). The TCR β locus contains D gene segments (2 TRBD genes) in addition to $V\beta$ and $J\beta$ gene segments (52 TRBV and 13 TRBJ genes respectively) [1]. The process of functional TCR gene assembly is called somatic recombination (or somatic rearrangement) and takes place as part of the T cell development process in the thymus (Figure 4). It involves the sequential random germline DNA rearrangement of a $V\alpha$ gene segment (among 70-80 TRAV genes) with a $J\alpha$ gene segment (among 61 TRAJ genes) to create a functional V- region exon [1]. This is controlled by the Recombinase-activating gene 1 and 2 (RAG-1 and RAG-2) [18]. Transcription and splicing of the $VJ\alpha$ exon to $C\alpha$ generates the complete mRNA translated into the TCR α -chain protein. The same somatic recombination principle applies to the β - chain. The α - and β - chains are linked by a disulfide bond and pair to form the $\alpha\beta$ TCR heterodimer. The overall variety of $\alpha\beta$ TCRs produced during somatic recombination is the result of both combinatorial and junctional diversity [19]. The combinatorial diversity relies on both the number of combinations of both the germline gene segments that can rearrange at the TCR loci and the pairing of the α - and β - chains. Junctional diversity further increases TCR variety by the presence of P-nucleotides (making up palindromic sequences) and N-nucleotides (non-template encoded) in the junctions between the V, (D), and J gene segments [1] [19]. Nucleotides can also be deleted at gene segments junctions. The junctional diversity is believed to produce most of the TCR genetic variability. It has been estimated that somatic recombination is able to generate 10^{15} - 10^{20} unique TCRs [20]–[23].

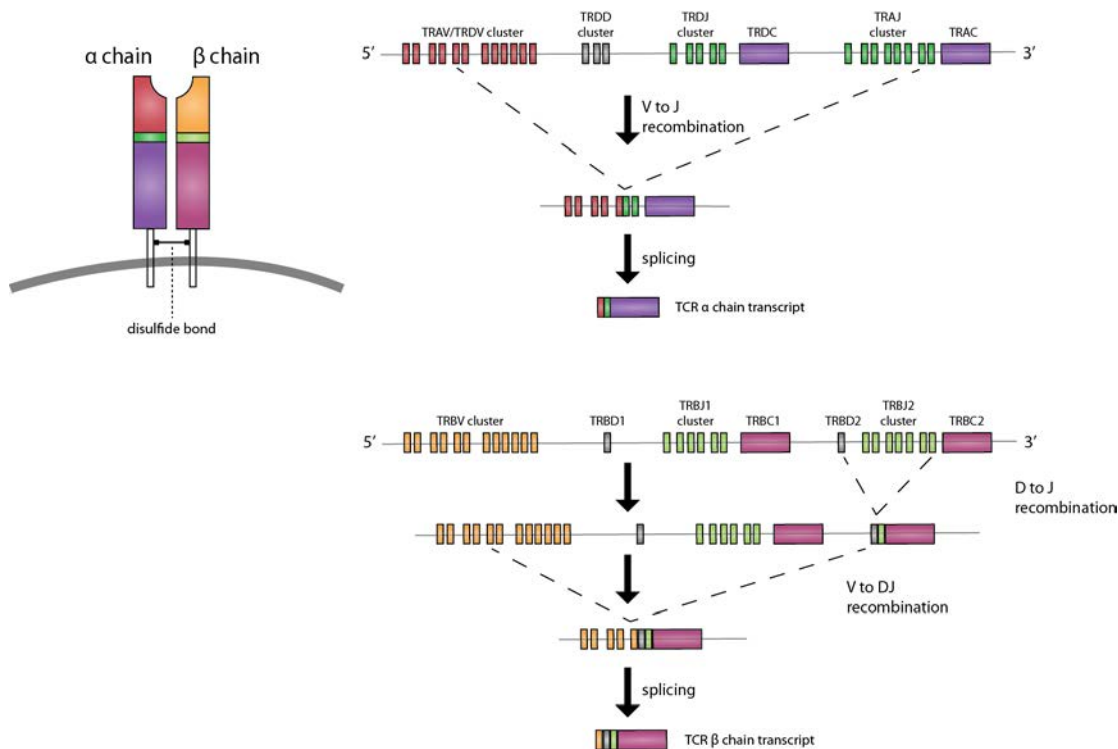


Figure 4 Description of TCR gene assembly steps. Functional TCRs are heterodimers consisting of an α - and a β -chain that are generated by somatic rearrangement of variable (V), diversity (D) and junctional (J) gene segments for the β - chain, and V and J gene segments for the α - chain. During T-cell development, gene segments recombine and are splice together with the constant (C) region to form the functional $\alpha\beta$ TCR.

1.2.3 TCR:pMHC RECOGNITION

As previously mentioned, TCRs expressed on the surface of CD8 T cells recognize foreign antigens derived from intracellular degradation of proteins in the cytosol and presented by MHC class I (MHC-I) molecules. MHC-I molecules are formed by one α chain encoded in the MHC gene and a non-covalently associated smaller protein, the invariant β 2-microglobulin. MHC genes are highly polymorphic. MHC-I molecules usually bind short peptides (8-13 amino acids) lying in an elongated conformation along the MHC cleft, with the termini and anchor residues (typically residues 2 and the C-terminus of MHC-I peptides) buried in pockets within the peptide-binding groove of MHC. The peptide side chains are therefore pointing outwards of the pMHC complex for interaction with the TCR. Furthermore, the peptides are bulging out of the groove providing additional surface area for TCR recognition. Within the TCR, there are six hypervariable complementarity-determining regions (CDRs) that mediate recognition, with 3 CDRs per TCR chain (Figure 5) [24]. The CDR1 and CDR2 loops are encoded

within the germline TRAV and TRBV genes. The CDR3 loops are formed at the junction of the V(D)J gene rearrangements and are therefore the most variable regions of the TCR [25]. The diversity of the naïve TCR repertoire is further increased by a lack of precision during V(D)J gene rearrangement, therefore adding or deleting N-nucleotides at the V(D)J junction [26] [27].

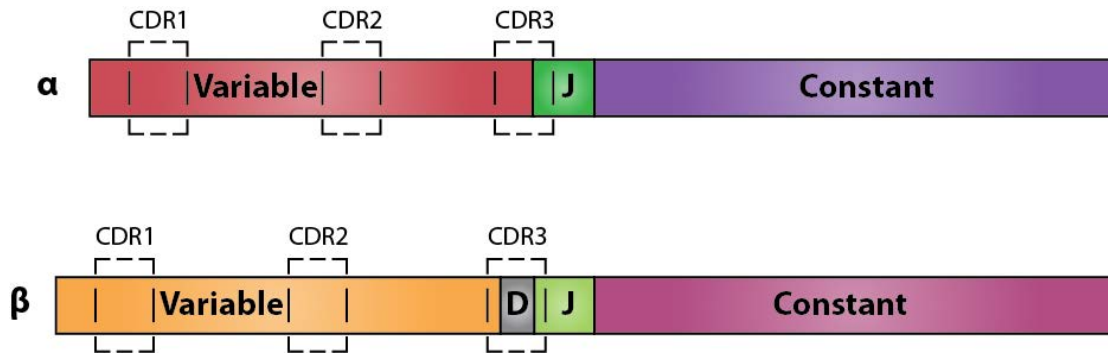


Figure 5 Protein structure of TCR chains. Regions of hypervariability, known as complementarity-determining regions (CDRs), are encoded in the V gene segments. The CDR1 and CDR2 regions are germline-encoded, whereas the CDR3 region is created by the juxtaposition of different V(D)J germline segments after somatic rearrangement. The diversity of the CDR3 region is further increased by the addition or deletion of N-nucleotides at the V(D)J junction.

The first X-ray crystallographic structures of TCR:pMHC-I complexes have provided a lot of information on T cell recognition [28]–[30]. They show that most TCRs align diagonally over the peptide with the CD3 loops of both α and β TCR chains meeting over the central amino residues of the peptide (Figure 6). The CDR1 α and CDR2 α loops primarily mediate MHC contacts at the amino terminus of the bound peptide, whereas the CDR1 β and CDR2 β loops interact with the complex around at the carboxy terminus of the bound peptide. As discussed in the 3.1.1, this general view regarding the TCR binding mode has been challenged by the growing database of TCR:pMHC structures as the TCR:pMHC interface presented a poor fit, which is consistent with the generally weak affinity of the interaction [31], and interaction with the pMHC complex induced a conformational change in the CDR3 loops [32].

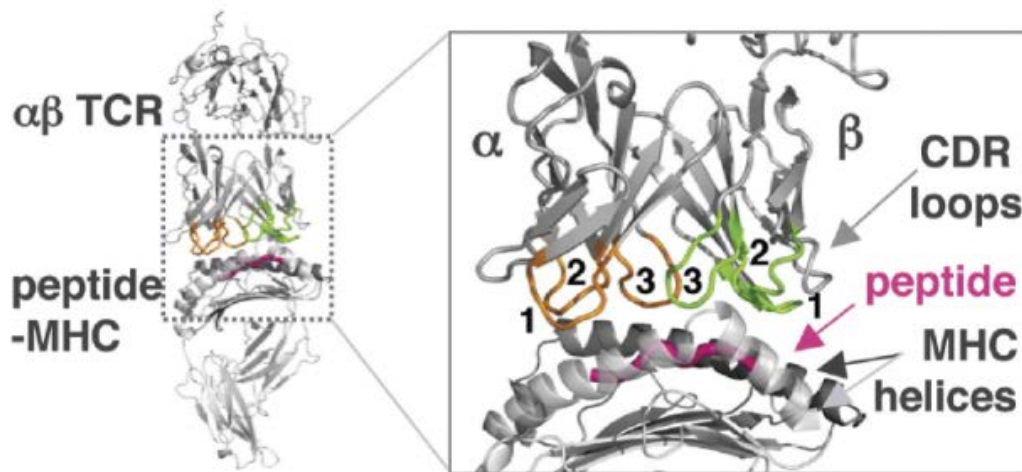


Figure 6 Structural view of the pMHC-TCR interface. The germline- encoded CDR1 and CDR2 loops mainly interact with the MHC, whereas the rearranged CDR3 loops is placed centrally above the peptide. Figure from [33].

The TCR is located in close proximity to a complex of signaling molecules, including the CD3 family of proteins (CD3 δ , CD3 ϵ , and CD3 γ) as well as a TCR zeta (ζ) chain [34]. Upon TCR engagement by an agonist peptide, the TCR transmits a signal to the CD3 complex, which subsequently triggers intracellular signaling cascades that regulate cytokine production, cell survival, proliferation, and differentiation. An early event in TCR activation is the phosphorylation of the immunoreceptor tyrosine-based activation motifs (ITAMs) on the cytosolic side of the TCR/CD3 complex by lymphocyte protein tyrosine kinase (Lck) [35] [36]. The TCR ζ chain is also phosphorylated upon TCR engagement. Zeta-chain associated protein kinase (Zap-70) is recruited to the TCR/CD3 complex where it becomes activated, promoting recruitment and phosphorylation of downstream adaptor or scaffold proteins [37]. This promotes phosphorylation of the effector molecule phospholipase C gamma 1 (PLC- γ 1). PLC- γ 1 transduces TCR signals by hydrolyzing phosphatidylinositol triphosphate (PIP2) in the plasma membrane to generate the second messengers diacylglycerol (DAG) and inositol trisphosphate (IP3). DAG activates several isoforms of protein kinase C and the MAPK/Erk pathways, promoting transcription factor NF- κ B activation [37]. IP3 triggers the efflux of Ca²⁺ from the ER into the cytoplasm [38]. Elevated Ca²⁺ activates the phosphatase calcineurin, which promotes IL-2 gene transcription through the transcription factor NFAT.

Signaling exclusively through the TCR is not sufficient for T cell activation, and can result in induction of an anergic state in which T cells fail to respond to antigen stimulation. Therefore, the cellular interface is reinforced by T cell surface

glycoproteins. The CD8 co-receptor binds to invariant regions of the MHC-I molecules. The binding is further stabilized by co-stimulatory and adhesion molecules, such as CD2-CD58, and the CTLA-4/CD28 and CD80/CD86 interaction. This combination of interactions and events lead to an effective T cell response.

Several parameters have been used to describe the strength of TCR:pMHC interactions, including TCR affinity, TCR avidity and functional avidity (Figure 7). The potency of a T cell response described in terms of biological outcomes is called functional avidity. The functional avidity of a given T cell clone is measured by assessing its functions *in vitro* (cytotoxicity, cytokine production) after exposure to titrating amounts of antigen concentration. TCR avidity is impacted by the TCR affinity (binding strength between one TCR and one pMHC molecule), expression levels of the TCR and coreceptors, the expression of signaling molecules, and the overall dynamic functions of the immune synapse.

The TCR affinity is measured by surface plasmon resonance (SPR) to calculate the dissociation constant (K_D) in the interaction between pMHC complex immobilized on a sensor surface and the TCR molecule added in soluble form (Figure 7). The TCR avidity concerns the measure of the strength of TCR:pMHC interaction involving multiple TCRs and pMHC molecules; it can be assessed for instance by dually labeled pMHC multimers built on NTA-Ni²⁺-His-tag interactions called NTAmers, assessing interaction with multiple TCR molecules on the surface of cells. Monomeric dissociation constant rates k_{off} can therefore be determined. K_D and k_{off} are related as following:

$$K_D = \frac{k_{off}}{k_{on}}$$

Several studies suggested that a potent T cell response is related to a lower K_D and/or a longer k_{off} [39]–[44]. A recent report on self/tumor and virus-specific CD8 T cell clones showed that k_{off} values offer a better prediction of the CD8 T cell potency [45]. TCRs often weakly interact with pMHC complexes (1-100 μ M) and with fast dissociation kinetics ($t_{1/2} < 60$ s) [46]–[48].



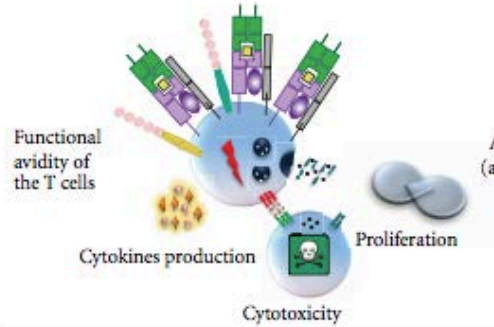


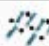


	Schematic representation	Definition	Technique of measurement	Measurement readout
TCR affinity		Strength of the binding between one peptide-MHC (pMHC) molecule and one TCR	Surface plasmon resonance (SPR)	- Direct assessment of ligand binding to surface immobilized receptors - K_D values, on- and off-rates, and $T_{1/2}$ can precisely be determined
TCR avidity		Strength of interaction between multiple TCR and pMHC molecules	Surface staining with fluorescent peptide-MHC multimers	- Fluorescence intensity of surface bound pMHC multimers - Cell surface bound tetramer off-rates
Functional avidity of the T cells		Antigen sensitivity (activation threshold)	Assessment of T-cell functions in presence of decreasing antigen concentration	Biological read-out: - Cytokines production - Cytotoxic activity (ability to lyse target cells) - Proliferation capacity
	 Peptide-MHC (pMHC) molecule and TCR	 Coreceptor	 Granzymes and perforin	
	 Costimulatory/coinhibitory molecules and their ligands	 Fas/FasL		

Figure 7 Description of TCR affinity, TCR avidity and functional avidity. Figure from [49]

1.2.4 DIVERSITY OF THE TCR REPERTOIRE

The generation and maintenance of an effective repertoire of TCRs are crucial for the effectiveness of the adaptive immune system, as the organism might encounter a wide variety of foreign antigens. It means that the size and diversity of the pre-immune T cell repertoire are critical in shaping the immune response to a given antigen. Theoretically, as mentioned above (1.2.2.), the V(D)J somatic recombination is able to produce 10^{15} - 10^{20} unique TCR sequences and therefore to recognize as many potential antigens [23]. However, there are only 10^{13} T cells in humans and the pre-immune T cell repertoire has been estimated to 10^8 distinct $\alpha\beta$ TCRs [20] [50]. Therefore, in order to provide a full antigenic protection, TCR are able to recognize more than one pMHC molecule, a phenomenon defined as cross-reactivity [23].

Despite this enormous TCR diversity, several studies showed that TCR repertoires generated during an immune response are biased for the preferential use of particular TCRs. Examples of TCR bias were observed in infectious diseases, autoimmunity and cancer (reviewed in [51]–[55]). Turner et al proposed a classification for TCR bias into three main categories. Type I bias is characterized by selecting a single TCR gene family (TRBV or TRAV gene), still with diversity in the CDR3 loops. Type II bias refers to the selection of conserved residue motifs in antigen-specific TCR V α or V β chains. Type III bias, the least common category, indicates a complete TCR α and/or TCR β sequence similarity.

The parameters resulting to the generation of TCR bias are emerging. First of all, studies demonstrated that TCR gene usage is already highly biased [56] [57]. Therefore, only a fraction of the theoretical diversity is generated during somatic rearrangement. The TCR bias can also result from convergent recombination producing the same amino acid sequence from multiple nucleotide sequences [58]. The naïve T-cell repertoire is also shaped during thymic selection. The TCR bias can be generated during the initiation of an immune response by mechanisms including affinity, antigen load and duration of the TCR:pMHC interaction [51] [59] [60]. Structural studies revealed the importance of the pMHC structural landscape in skewing the TCR repertoire (e.g. bulged or featureless peptides). Persistent infection may also favor TCR bias. For instance, dominant T-cell clones present in the early response to HIV tend to be lost during the course of the infection [61]. Studies on immune responses to Epstein-Barr virus (EBV) and cytomegalovirus (CMV) indicates that TCRs with high affinity for their cognate antigen are preferentially used [60] [62].

1.3 CANCER IMMUNOTHERAPIES

For a long time, the conventional anticancer treatment strategies have been surgery, chemotherapy, and radiotherapy [63] [64]. However, patients often experience relapses from residual malignant cells or metastasis, or become resistant to therapy [65] [66]. Therefore, optimized and new approaches to achieve durable and complete remission are needed.

Multiple studies showed that anti-cancer CD8 T cells have the potential to limit cancer progression and to eradicate a wide variety of tumors, with vast evidence that CD8 T cell infiltration inside the tumor mass is a solid good prognostic indicator [67]. However,

immunosuppressive mechanisms are inherent to anti-cancer T cell responses [68]. First, cancer antigens being close to the “self”, anti-cancer T cells are deleted by the negative selection. Therefore, the low frequency of precursor anticancer T cells hampers the outcome of the response. Besides, these anti-cancer T cells harbor TCRs of low affinity. Secondly, unlike APCs, cancer cells poorly trigger activation of CD8 T cells due to limited antigen priming and inefficient co-stimulation. Finally, T cells become functionally deficient due to the hostile tumor microenvironment and the chronic inflammation and stimulation. They are driven to “exhaustion”, characterized by poor effector function and sustained expression of inhibitory receptors.

Several T cell extrinsic mechanisms lead to the hyporesponsiveness of anticancer T cells. Tumors can escape the immune surveillance by downregulation of MHC molecules, hiding surface antigens, releasing immunosuppressive factors or inducing T cell apoptosis [69]. Other cell types such as regulatory T cells, tolerogenic DCs, so-called M2 macrophages and Myeloid-Derived Suppressor Cells can inhibit the anticancer response [70]–[73]. Also, cancer-associated fibroblasts can secrete tumor-promoting factors or retain T cells at the tumor edge [74].

Immunotherapy has emerged as an exciting strategy in cancer treatment in recent years, appointed breakthrough of the year by the Science journal in 2013 and meriting the Nobel Prize for Medicine or Physiology to James P. Allison and Tasuku Honjo in 2018. This approach is based on the ability of the immune system to recognize tumor antigens and supports thus the own body’s capacity to detect and destroy tumor cells. First, active immunization aims at generating or boosting anti-cancer T cell responses to kill tumor cells. This includes vaccination with tumor antigens or enhancement of antigen presentation. Secondly, passive immunization, also known as adoptive cell transfer, relies on the administration of immune cells directly to the patient. It uses autologous peripheral blood mononuclear cells (PBMCs) or tumor-infiltrating lymphocytes (TILs) that are expanded *in vitro* and selected for tumor reactivity before being infused back into the patient [75]. T cells can be modified before adoptive cell transfer. This comprises modifications in cytokine and/or signaling pathways, inserting T cell receptors (TCRs), or chimeric antigen receptors (CARs) [76] [77]. Finally, one approach to trigger antitumor immune responses includes T-cell immune receptor modulating monoclonal antibodies. It consists either in blocking immune-inhibitory

pathways activated by cancer cells with antibodies, which is called “checkpoint blockade”, or using agonistic antibodies to target and activate the co-stimulatory molecules such as 4-1BB, OX40 or CD28 [78]. The first targets to be discovered were the inhibitory molecules Cytotoxic T lymphocyte-associated protein 4 (CTLA-4) and Programmed cell death 1 (PD1) and its ligand PD-L1 (Figure 8). Ipilimumab (Yervoy®) is a monoclonal antibody that blocks the inhibitory receptor CTLA-4 expressed on T cells. It was approved by the Food and Drug Administration (FDA) in 2011 as a first-line therapy for melanoma patients with metastatic disease [79] [80]. Unfortunately, only a relatively small fraction of patients obtains clinical benefit and severe immune-related adverse events have been observed. More recently, antibodies targeting PD1 (Nivolumab, Pembrolizumab) or its ligand PD-L1 demonstrated remarkable benefit in a variety of cancer types including melanoma, kidney and lung [81]–[83].

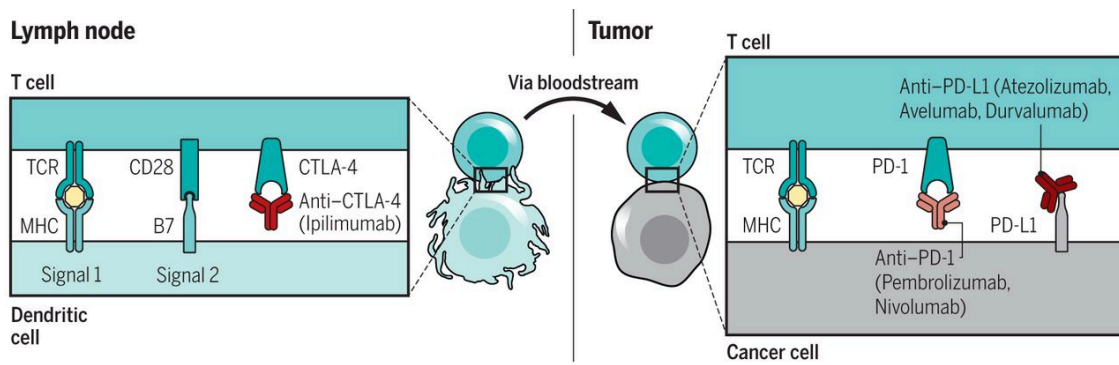


Figure 8 Blockade of CTLA-4 and PD1 and PD-L1 induces antitumor responses. From [84]

1.4 YELLOW FEVER VACCINATION AS A MODEL OF OPTIMAL IMMUNOGENICITY IN HUMANS

1.4.1 YELLOW FEVER VIRUS VACCINE (YF-17D)

Yellow Fever disease is caused by the Yellow Fever Virus (YFV) and occurs predominantly in sub-Saharan African regions as well as tropical and subtropical regions of South America [85] [86]. The YFV is transmitted by a mosquito belonging to the genus *Aedes* [87]. Yellow fever illness can present subclinical infection to acute hemorrhagic disease, including fever, hemorrhagic shock and multi-organ failure of the liver, kidneys and myocardial tissues [87]. The liver is a major target organ and liver dysfunction results in jaundice-like symptoms, hence the name “yellow fever”. While a majority of infected people develop no or minor symptoms, an estimated 1 in 7 infected people enter a toxic phase which half of them do not survive ¹.

The YFV is the prototype of the family of *Flaviviridae*. It is a single-stranded, positive sense RNA virus that varies in size between 40-60nm. The virus consists of three structural proteins (core C, membrane M and envelope E), and seven non-structural proteins (NS1, NS2A, NS2B, NS3, NS4A, NS4B and NS5) that are necessary for viral replication [85] [86]. The virus particle consists of the C protein that surrounds the genome (approximately 10'800 nucleotides) and the viral proteins (M- and E-proteins) are imbedded in the virus envelope.

There is no antiviral therapy to treat the disease but prophylaxis is maximized by a live-attenuated virus vaccine that is considered as one of the most efficient vaccines ever made for humans: the YF-17D vaccine strain. The YF-17D vaccine has been applied to more than 600 million people worldwide [85] [86]. The original 17D strain was developed in 1937 by Max Theiler and his colleagues [88]. It included isolation of the virus from a cured African patient (Mr. Asibi) and 176 passages of this wild-type strain Asibi in mouse and chicken tissue. This process led to viral attenuation while maintaining the immunogenicity. This discovery was awarded with the Nobel Prize in Physiology or Medicine in 1951. Two substrains are currently used for vaccine production, 17D-204 and 17DD, originating from the 17D strain. Although the genomes of Asibi, 17D-204 and 17DD viruses have been determined, the molecular mechanism

¹ <https://www.who.int/news-room/fact-sheets/detail/yellow-fever>;
<https://www.cdc.gov/yellowfever/symptoms/index.html>

leading to attenuation remains unclear. The mutations observed in the gene encoding the E protein are thought to have a role in attenuation [89]–[91]. The vaccine substrains show only subtle nucleotide variations (ca. 99.9% nucleotide sequence identity) [92].

Immunogenicity and protection by YF-17D vaccination have mainly been assessed by measuring neutralizing antibodies (nAbs). Since May 2013, the Strategic Advisory Group of Experts on immunization (SAGE) of the WHO organization concluded that a single dose of the YF-17D vaccine is sufficient for life-long protection [93]. This was supported by several studies on the duration of nAbs and T cell responses following vaccination with YF-17D showing that neutralizing antibodies can last up to 38 years and that T cell responses can still be detected after decades [94]–[99]. However, contrasting studies conducted in Brazil have raised concerns over T cell responses and nAbs titers as they observed reduction over time [100] [101]. To date, the Brazilian national immunization policy still includes a booster dose every 10 years [102]. Interestingly, Hepburn et al showed that the humoral efficacy of booster vaccination depends on the pre-booster level of antibodies. If the serological levels are low, the booster induces a 4-fold increase in the vast majority of the 35 vaccinees. On the contrary, if the antibody titers are high, only 10% have an appropriate secondary response [96].

In addition to its exceptional efficacy, the YF-17D vaccine has an acceptable safety record. Neurotropic and viscerotropic serious adverse events occur rarely (1 in 250'000 cases). However, YF-17D vaccine-associated neurotropic and viscerotropic disease (YEL-AND and YEL-AVD, respectively) are often lethal [103]–[108] and thus although rare, these adverse events do tilt the balance of benefit/risk and limits vaccination to the strictest minimum with a strong weight of epidemiological and operational considerations in endemic versus non-endemic countries. E.g.: in endemic countries, vaccination is given to children at 9-12 months, while only travelers aged ≥ 9 months, traveling to and from risk-areas receive it.

1.4.2 HUMAN IMMUNE RESPONSE TO YF-17D VACCINATION

While many vaccines in clinical practice are subunit or inactivated vaccines, the YF-17D vaccine is a live attenuated vaccine. Because of the process of attenuation, even live-attenuated viral strains (such as measles and oral polio vaccines) show usually only limited replication [109] [110]. However, the YF-17D vaccine causes a systemic viral infection [111]–[116]. This is thought to be the major reason for the strong CD8 T

cell responses seen with this vaccine, in contrast to most other vaccines that are inefficient activators of CD8 T cells [116].

The immune response to YD-17D vaccination has attracted high interest and several studies have revealed snapshots of the immune events and parameters that constitute such strong T cell immunogenicity (Figure 9, Table 9).

In vitro studies and mouse models showed that the YF-17D strain infects DCs for about one week without excessive multiplication, allowing immune stimulation for up to two weeks [112] [113] [115]. It delivers adequate antigen levels to the DC resulting in effective antigen processing and presentation to both CD4 and CD8 T cells [112] featuring multiple overlapping epitopes [117] [118]. Together with strong innate immune activation, this vaccine induces a strong adaptive response resulting into potent T cell responses [116]–[120] and protective antibody responses [94] [95] [98] [121].

The YF-17D vaccine is outstanding for the nAbs raised, which can persist for 30-40 years [94] [95] [98] [121]. A study showed that a protective humoral response (Plaque Reduction Neutralization Test, PRNT titers $\geq 1:20$) was detected in all vaccinees (238 healthy individuals tested) [117]. After vaccination, viremia reaches a peak within the first 10 days, after which it declines rapidly [118]. Recent studies showed a pivotal role of the innate immune system underlying specific immune activation induced by the YF-17D vaccine. It triggers multiple pattern recognition receptors, in particular Toll-like receptors, activating distinct subsets of dendritic cells (DC) that the virus can infect [111]–[113] [115]. Myeloid dendritic cells (mDCs defined as CD11c⁺ HLA-DR⁺ CD45⁺ CD19⁻ CD14⁻ CD56⁻ BDCA-2⁻; note: to our knowledge this gating includes CD14^{neg/lo} CD16⁺ monocytes, a point relevant later in my analyses) were reported to increase in number at day 7 after primary vaccination and up-regulated the activation marker HLA-DR [122]. In contrast, plasmacytoid DCs (pDCs) did not increase in number and did not get activated [122]. An other study showed that the frequencies of CD14⁺ CD16⁺, CD14⁺ CD16⁺⁺ and inflammatory (CD14⁺⁺ CD16⁺) monocytes were increased at day 7 after vaccination [123]. In addition, monocytes were activated upon YF-17D vaccination as shown by a higher percentage of CD14⁺ CD16⁺ cells expressing HLA-DR [123]. In contrast, the frequency of CD56⁺ natural killer (NK) cells slightly decreased at that time-point. The frequency of cytotoxic NK cells (CD56⁺ CD16⁺) was increased at day 7 after primary vaccination, whereas the percentage of cytokine-producing NK cells (CD56⁺ CD16⁻) was decreased [123]. NK cells showed an activated phenotype at day 6 and

proliferation at day 10 after vaccination [124]. Regarding the adaptive response, the YF-17D vaccine induces a mixed T helper type 1 (Th1)-Th2 CD4 T cell response which precedes the cytotoxic CD8 T cell response [120] [125]. In addition, the CD8 T cell response is robust, broad and polyfunctional [117] [118] [120]. Interestingly, the magnitude of the CD8 T cell response is determined by the initial viral load, highlighting the relevance of strong innate stimulation by a high viral load [119]. In particular, an HLA-A*02-restricted immunodominant epitope was found as the antigen for most reactive CD8 T cells and it mapped to the NS4b²¹⁴⁻²²² protein region of the virus: the nonamer epitope LLWNGPMAV (hereafter, A2/LLW) [97] [113] [118]. Our group and other studies showed that the A2/LLW-specific CD8 T cell response is highly prevalent. Already the naïve A2/LLW-specific CD8 T cells are present at high frequency, often detectable even directly ex vivo with tetramers in ca. 30% of unvaccinated HLA-A*02 positive individuals [97]. Studies on the B cell response showed that total circulating B cells decreased at day 7 after vaccination, followed by activation (CD69, IL-10R) after 2 weeks. In contrast, CD19^{low} CD27^{high} plasmablasts transiently increased at day 14 [122] [125].

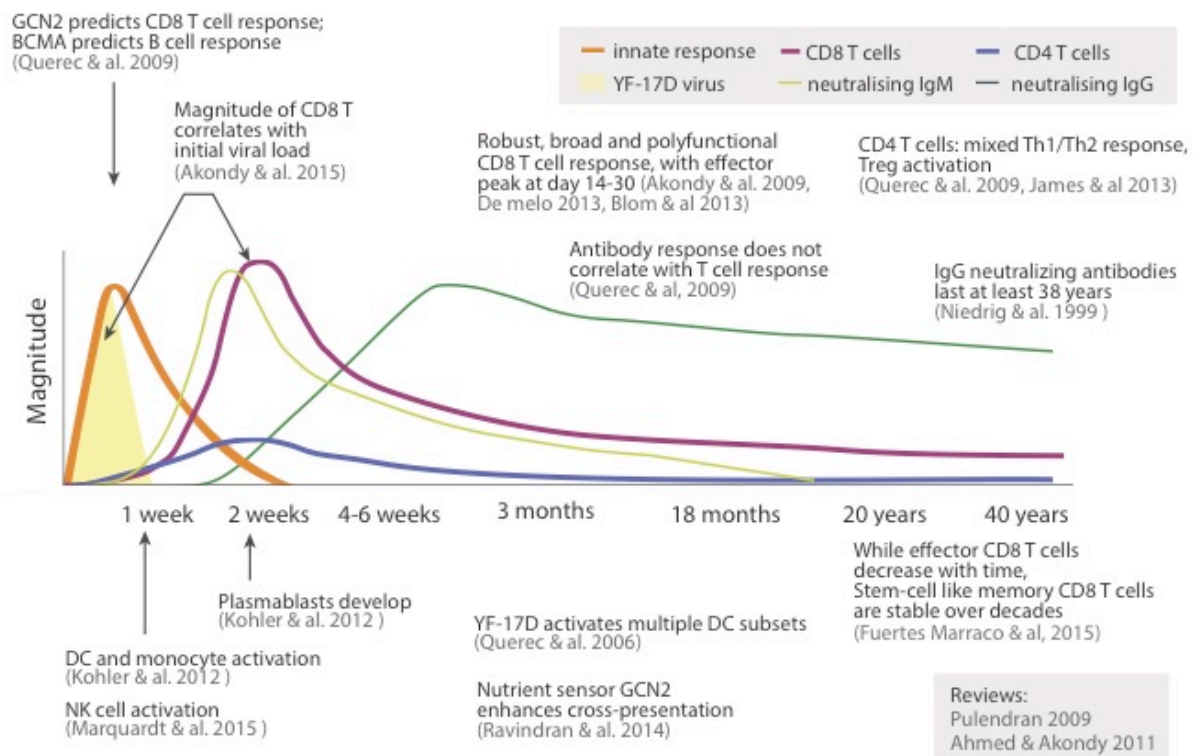


Figure 9 Major findings of the immune responses following YF-17D vaccination. Although the YF-17D vaccine was developed in 1937, studies highlighted mechanistic aspects only in the last decade. Figure courtesy of Silvia Fuertes- Marraco.

1.4.3 YELLOW FEVER AS A MODEL

Despite the major breakthroughs provided by immunotherapies, there is still a major and continuous need for further clinical improvements. Research in anti-viral immunity plays a central role in the comprehension of immune regulation in malignant disease as similar mechanisms may apply to the control of both infection and cancer. Furthermore, scientific principles of the optimal functioning of the immune system are often better determined in models of acute infection (transient and clearing back to healthy homeostasis) rather than tumor (chronic and pathological) models.

Recent advances have arisen from the use of vaccines as tools to investigate the immune responses in humans. Especially, live virus vaccines provide a unique

opportunity to study human immune responses in the context of a controlled immunological setting of a resolving acute infection [86] [114]. This, together with the possibility to acquire frequent blood samples over a span of several years after vaccination, allows characterizing the dynamics of the immune responses. Furthermore, vaccines are administered to large populations, and potentially allow for broader coverage of observations, in perspective and retrospective.

The YF-17D vaccine is widely accepted as an excellent model for human immunology research. Especially, the YF-17D strain causes a systemic viral infection, which leads to a robust CD8 T cell response in contrast to most other vaccines [111]–[116] [118].

While the YF-17D vaccine was developed in the 1930's, learning how it stimulates such robust and persistent immune responses has gained force especially only in the last decade. Despite the large number of studies and efforts already published (Figure 9, Table 9), the overall understanding of the immunogenicity and response to the YF-17D vaccine remains only partially defined. Furthermore, these studies focused mainly on the primary response to YF-17D vaccination and on the antibody response to booster vaccination, whereas there is a lack of evidence for the cellular responses following revaccination (Table 9).

The comparison of data originating from two groups of volunteers, receiving the vaccine for the first time or receiving a booster vaccine, might provide information regarding the effects of a recall response to YF-17D. In addition, the comparison of priming with booster vaccination represents a uniquely controlled experimental system in humans to assess whether and how the long-term memory immune cells react to antigen-specific re-challenge. The identification of key cellular and molecular components that sustain the potency and durability of immunity raised by YF-17D, will potentially improve the knowledge and the rationale for the design of more powerful immunotherapies in humans.

In the field of T cell-based therapies such as anti-cancer treatments, a more comprehensive knowledge of the mechanisms and dynamics governing the generation of T cell responses, including Stem Cell-like Memory (SCM) T cells as well as their relationship to other immune parameters, is needed in order to guide the design of new immunotherapies that can raise powerful and long-lasting T cell responses. The

argument that YF-17D vaccination is a particularly suitable and excellent model is justified because it generates life-long immune protection with a robust T cell compartment. In addition to the evidence on the robust acute CD8 T cell peak of effectors, our group discovered that SCM CD8 T cells persist for decades [97].

2. PROJECT NETWORK OVERVIEW AND AIMS OF THESIS

My PhD thesis work can be divided into two main axes (Figure 10). The first axis is centered on the so-called “TRAV12-2 bias” in the immunodominant CD8 T cell response to YFV. It arose from a first, cross-sectional study elaborated in our group (the “YF1” study), where a genome-wide analysis showed that A2/LLW-specific CD8 T cells are highly enriched for the T-cell receptor (TCR) alpha chain family TRAV12-2. The second axis focused on a second, longitudinal clinical protocol, the “YF2” study, in which we collected blood samples before and at several time-points after YF-17D vaccination in subjects receiving the vaccine either for the first time or as a booster vaccine.

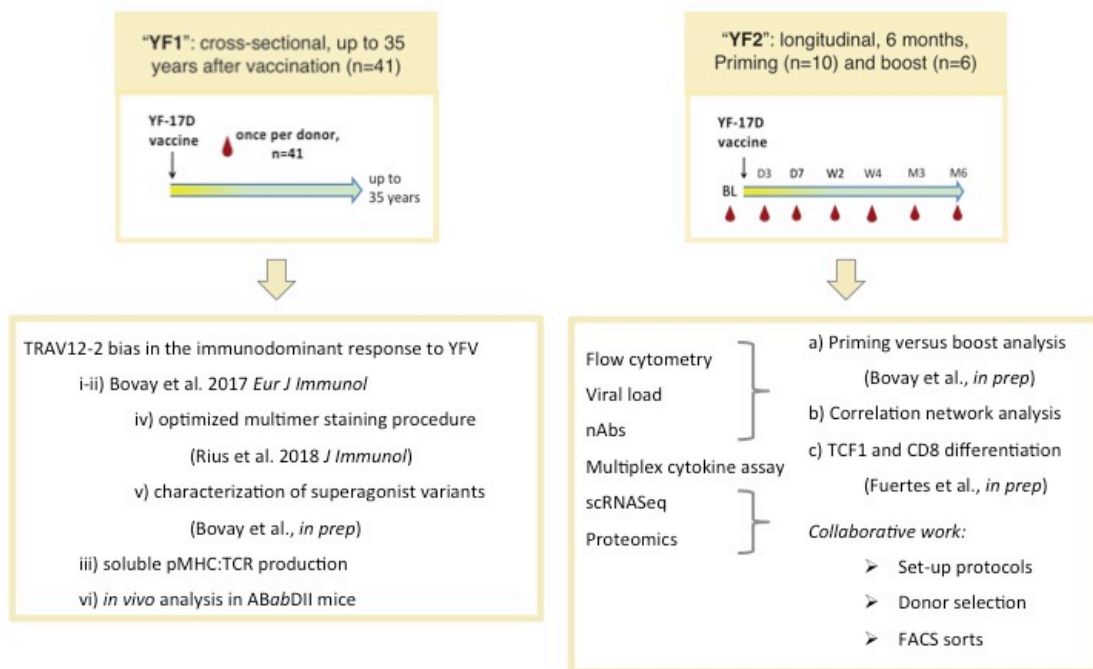


Figure 10 PhD project network overview. The aims of the two axes arising from the two clinical protocols “YF1” and “YF2” are detailed. The associated manuscripts are indicated.

The specific aims of my PhD project are the following:

Axis 1: TRAV12-2 bias and TCR:pMHC studies

i) Functionally and structurally characterize the TRAV12-2 bias in A2/LLW-specific CD8 T cells (3.1.1). *Is the TCR bias dependent on the epitope? Is the TCR bias already present in naïve CD8 T cells, before YF-17D vaccination? Are CD8 T cells expressing TRAV12-2 functionally superior? Is there a structural basis explaining the TRAV12-2 bias in A2/LLW-specific CD8 T cells?*

ii) Study the TCR diversity of these cells based on clonotyping (3.1.1). *Are A2/LLW-specific CD8 T cells indeed biased for particular α , and also potentially β - chains? What type of bias is it (TCR gene family, amino acid motif in the CDR3 sequence or exact same TCR sequence but different $\alpha - \beta$ pairing)?*

The points i-ii above were addressed and reported in my first author publication in the *European Journal of Immunology* [126].

In the development of this study [126], a major effort was directed to attempting the crystallization of the TCR:pMHC (YF5048), which I describe in:

iii) Detailed description of the soluble TCR:pMHC production process (3.1.3)

Within the work described above, two further aims were needed and led to corresponding projects:

iv) Optimize multimer staining protocol (3.1.2). *Is it possible to detect new A2/LLW-specific clonotypes using an optimized multimer staining protocol? What are the functional differences between the clones recovered from both protocols?*

v) Define and characterize potential superagonists of the A2/LLW epitope (in the context of crystallography work on a TRAV12-2+ TCR) (3.1.5). *Is it possible to enhance the response to an already potent viral antigen? What aspects of the TCR:pMHC interaction allow to achieve better functionality?*

Finally, a parallel project was to

vi) Analyze the TRAV12-2 bias and LLW immunodominance *in vivo* using a mouse model (ABabDII mice) (3.1.4). *Do these mice mount an A2/LLW-specific CD8 T cell*

response and does it recapitulate the human CD8 T cell response, in particular regarding the A2/LLW epitope (prevalence in naïve population and immunodominance, TCR usage, generation of SCM CD8 T cells)?

Axis 2: Longitudinal analysis of the human immune response to YF-17D vaccination, including prime versus boost

i) Uncovering the immune events in the acute immune response following primary and booster YF-17D vaccination. *What are the kinetics, dynamics and magnitudes of the main components of the immune system? What are the differences upon priming versus booster vaccination? To what extent are the innate and adaptive components mobilized upon boosting? Can we observe and study prominent recall responses? What is the impact of pre-existing antibodies on the recall responses? Is there a need for a booster dose after 10 years?*

ii) Identify the relationship between the various immune components using bioinformatics analyses. *What are the immune determinants that correlate with protection (measured by nAb titers and viral clearance) and with a strong T cell response? Are there any factors at baseline (before vaccination) that may predict the magnitude of the immune response or a subset of immune events after vaccination?*

iii) Characterize the generation of such remarkable SCM CD8 T cell population and pinpoint their relationship to other immune components. *When do they arise? How do they relate in activation and kinetic development to the other CD8 T cell subsets? What immune components do negatively / positively correlate with generation of stem cell-like memory CD8 T cells?*

3. RESULTS

3.1 AXIS 1: TRAV12-2 bias and TCR:pMHC studies

The first axis of my PhD work consisted in characterizing the molecular and functional aspects of the TCR:pMHC interaction in A2/LLW-specific CD8 T cells. First, we analyzed the TCR repertoire of A2/LLW-specific CD8 T cells. In particular, we discovered and characterized the genetic and structural basis of the TRAV12-2 bias in A2/LLW-specific TCR. This work was carried out between the groups of Prof. Daniel Speiser and Prof. Andrew Sewell (Cardiff University, Wales), including my scientific visit to Cardiff for 9 months with an SNF mobility grant (being myself the applicant and grantee). Also, A2/LLW-specific CD8 T cells were clonotyped using different multimer staining protocols.

We further investigated the TCR-pMHC interaction with peptide variants of the A2/LLW epitope.

Finally, we attempted to use an animal model to study the TCR bias in more details with the transgenic A*Bab*DII mouse model. The aim here was also to investigate whether a mouse model would recapitulate the events of the immune response to YF-17D vaccination as seen in the human system. This was done in collaboration with the group of Prof. Thomas Blankenstein (Max Delbrück Center for Molecular Medicine Berlin, Germany).

3.1.1 TRAV12-2 bias in the immunodominant response to YFV

3.1.1.1 Background

The YF-17D vaccine harbors an HLA-A*02-restricted NS4b²¹⁴⁻²²² epitope: LLWNGPMAV (hereafter, A2/LLW) that induces a highly prevalent and dominant CD8 T cell response [118]. Work from our group has revealed that YF-17D vaccination induces SCM specific for A2/LLW: these cells have a Naïve-like profile (CD45RA⁺ CCR7⁺) expressing SCM markers (CD95, CD58, CXCR3) and remarkably persist at stable frequencies for at least 25 years [97]. Incidentally, genome-wide analysis of A2/LLW-specific CD8 T SCM and various differentiation subsets in total CD8 T cells showed that A2/LLW-specific CD8 T cells are highly enriched for the T-cell receptor (TCR) alpha chain family TRAV12-2. This is highly reminiscent of the TRAV12-2 enrichment and immunodominance in CD8 T cells specific for the HLA-A*02-restricted Melan-A analog epitope ELAGIGILTV (A2/ELA) found in melanoma patients [127]–[129]. Remarkably, naïve A2/ELA-specific CD8 T cells in healthy individuals are also relatively frequent and heavily biased for TRAV12-2 [130]. TCR diversity and specificity is largely acquired through somatic gene rearrangements of the α and β chains. There is particularly high diversity in the complementarity determining region (CDR)-3 (hypervariable, unique to each TCR following somatic recombination) while CDR-1 is shared amongst TCR chain families (each family featuring a given fully germline-encoded segment) [51]. In an A2/ELA-specific TCR named MEL5 it was found that, unusually, the germline-encoded CDR1 α loop (instead of the hypervariable CDR3 loop) plays a major role in recognizing the epitope, conferring an “innate-like” pattern of antigen recognition [128]. This possibly explains the observations on relatively high precursor frequencies of naïve A2/ELA-specific CD8 T cells and immunodominance of this epitope based on advantageous thymic output of germline-encoded TCR [127]–[130].

At the beginning of my PhD thesis, I studied whether germline-encoded interactions operate in the recognition of the A2/LLW epitope of YF-17D by TCRs featuring the TRAV12-2 chain. I used structural and functional analyses to shed light on the high prevalence and immunodominance of the A2/LLW response, and to draw the parallel to

the CD8 T cell response to A2/ELA by the MEL5 TCR. We aimed at answering the following questions:

- *Is the TCR bias dependent on the epitope (only found for A2/LLW)?*
- *Is the TCR bias already present before YF-17D vaccination?*
- *Are A2/LLW-specific CD8 T cells expressing TRAV12-2 functionally superior to TRAV12-2-negative A2/LLW-specific counterparts?*
- *Is there a structural basis explaining the TRAV12-2 bias in A2/LLW-specific CD8 T cells (in the context of the TCR:pMHC interaction)?*
- *Are A2/LLW-specific CD8 T cells biased for particular β –chains also?*
- *What type of bias is the TRAV12-2 bias (TCR gene family, amino acid motif in the CDR3 sequence or exact same TCR sequence but different α – β pairing)*

This project resulted in a publication in the *European Journal of Immunology* in 2017 and this article was selected for the front cover of the journal [126] (Appendix 1). In this Chapter, I will summarize the main findings and discussion points while the full-length manuscript can be found in Appendix 2.

3.1.1.2 Results

A2/LLW-specific CD8 T cells are biased for the segment TRAV12-2, before and after vaccination

As mentioned above, our group has previously revealed a high enrichment in TRAV12-2 mRNA in A2/LLW-specific CD8 T SCM (Figure 11A). I confirmed this data using flow cytometry by analyzing TRAV12-2 protein levels on A2/LLW-specific CD8 T cells from eight YF-17D vaccines. Compared to total CD8 T cells (median 12.5%TRAV12-2⁺), the majority of A2/LLW-specific CD8 T cells expressed TRAV12-2, with a median of 55.5% TRAV12-2⁺ (Figure 11B). The TRAV12-2 bias reached a similar extent as in ELA-specific CD8 T cells from healthy donors (median 57.7%) (Figure 11B). The bias was further corroborated studying A2/LLW-specific clones isolated from four YF-17D vaccine donors, where PCR analysis detected that 45/57 clones were TRAV12-2⁺ (78.9%) (Figure 11C). In contrast, the V β usage showed rather broad diversity, with a preferential usage of certain V β families such as TRBV9 (16/57) and TRBV2 (10/57) (Figure 11D).

Taken together, I was able to confirm and quantify the bias towards TRAV12-2 in A2/LLW-specific CD8 T cells based on ex-vivo material and CD8 T cell clones from YF-17D vaccinees. This raised several questions: Is the TCR bias dependent on the epitope? Is the TCR bias already present before YF-17D vaccination? Are CD8 T cells expressing TRAV12-2 functionally superior?

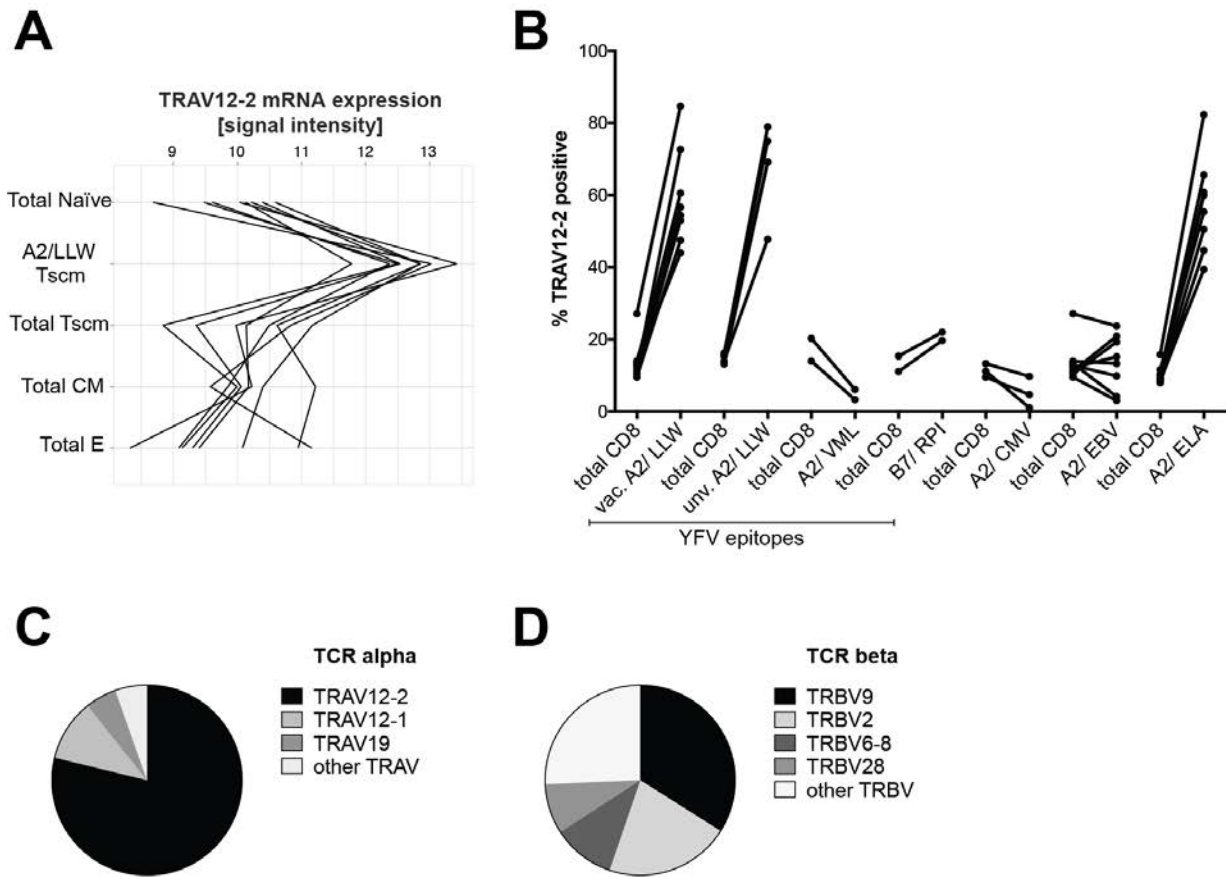


Figure 11 A2/LLW-specific CD8 T cells are strongly biased for TRAV12-2 similarly to A2/ELA-specific CD8 T cells. A, TRAV12-2 mRNA expression in A2/LLW-specific stem cell-like (SCM) CD8 T cells compared to reference differentiation subsets in total CD8 T cells (n = 8 YF-17D vaccines), including: Naïve, SCM, central memory (CM) and effectors (E). Samples were isolated from PBMCs by FACS and total RNA analyzed by microarray. B, Subject-paired comparison of TRAV12-2 expression by flow cytometry using an TRAV12-2-specific antibody between various antigen-specific and total CD8 T cells from YF-17D vaccines (“vac.”, n = 8) and unvaccinated individuals (“unv.”, n = 5), A2/VML (n= 2) and B7/RPI (n= 2) in YF-17D vaccines, as well as A2/CMV (n= 8, stars represent CMV-seronegative donors= 5/8), A2/EBV (n= 8) and A2/ELA (n= 8). C and D, TCR repertoire analysis of A2/LLW-specific CD8 T cell clones generated from 4 vaccinated donors. Total RNA was isolated from 57 A2/LLW-specific CD8 T cell clones, cDNA prepared, analyzed by PCR with primers specific for each TRAV (C) and TRBV (D) gene segment, and sequenced.

Therefore, I used other HLA multimers to detect CD8 T cells specific to alternative YF-17D epitopes. Only two other epitopes (the HLA-A*0201-restricted VMLFILAGL from NS4a protein, termed A2/VML, and HLA-B*07-restricted RPIDDRFGL from NS5 protein, termed B7/RPI) could be analyzed with sufficient positive events in flow cytometry and in HLA-corresponding donors (illustrating again the practical advantage of studying HLA-A*02-restricted epitopes with HLA-A*02 being highly frequent in the Caucasian population, and the comparatively high prevalence and immunodominance of the A2/LLW epitope *per se*). I also included other reference viral HLA-A*0201-

restricted specificities such as pp65 from cytomegalovirus (CMV) and BMFL1 from Epstein Barr Virus (EBV). TRAV12-2 analysis by flow cytometry revealed that, among the YFV epitopes, only the A2/LLW epitope response is biased for TRAV12-2 (Figure 11B).

Next, I analyzed the expression of TRAV12-2 in five unvaccinated HLA-A*0201⁺ donors. Interestingly, I found that the TRAV12-2 bias was already evident in naïve A2/LLW-specific CD8 T cells, prior to vaccination (median 69.2%) (Figure 11B).

On a per cell basis, TRAV12-2 does not confer functional advantages to A2/LLW-specific CD8 T cells

To address whether TRAV12-2 expression could potentiate T cell function, I analyzed various functional properties of TRAV12-2⁺ and TRAV12-2⁻ A2/LLW-specific CD8 T cell clones. First, I measured the functional sensitivity of 47 A2/LLW-specific CD8 T cell clones with a 51-chromium release assay (Figure 12A). Then, I measured the monomeric TCR:pMHC dissociation constant rates (k_{off}) in 33 A2/LLW-specific CD8 T cell clones using NTAmers (Figure 12B). In parallel, I examined cytokine production and degranulation by flow cytometry in 17 A2/LLW-specific CD8 T cell clones after 4 hours of stimulation with LLW-pulsed T2 cells (Figure 12C). These assays showed that TRAV12-2⁺ clones did not differ from TRAV12-2⁻ clones. Altogether, expression of TRAV12-2 did not confer a particular functional advantage to A2/LLW-specific CD8 T cells on a per cell basis.

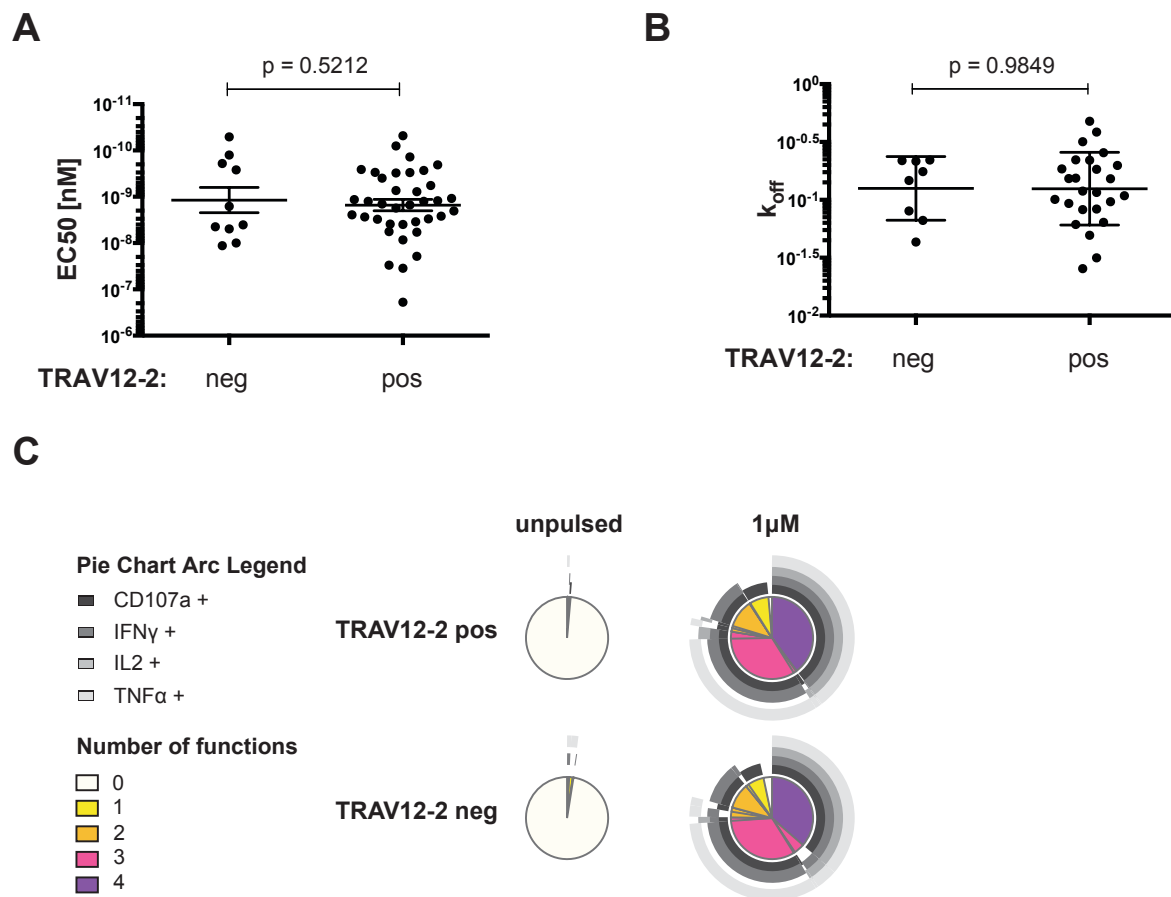


Figure 12 TRAV12-2 expression does not confer a functional advantage to A2/LLW-specific CD8 T cell clones. Functional properties of A2/LLW-specific CD8 T cells clones were assessed by various methods. A, Killing capacity (51-chromium release assay) of A2/LLW-specific CD8 T cell clones (TRAV12-2 positive n= 37, TRAV12-2 negative n= 10) stimulated with peptide-pulsed T2 cells. Data are representative of two independent experiments (mean and SEM; t-test p value). B, Monomeric dissociation constant (K_{off}) rates measured in CD8 T cell clones (TRAV12-2 positive n= 25, TRAV12-2 negative n= 8) using NTAmers (mean and SD; t-test p value). C, Intracellular cytokine staining of CD8 T cell clones (TRAV12-2 positive n= 11, TRAV12-2 negative n= 6) stimulated with peptide-pulsed T2 cells for 4h. Data are representative of two independent experiments.

The germline-encoded CDR1 α loop of TRAV12-2 contributes to pMHC binding

To determine whether a structural basis could explain the TRAV12-2 bias in A2/LLW-specific CD8 T cells, we initiated a collaboration with the group of Prof. Andrew Sewell at the University of Cardiff. Structural analysis can potentially reveal the critical and dominant contacts between the TCR chains, the LLW peptide and HLA-A*0201, determining differences and similarities to other TCRs, including whether this system has similar binding principles to the melanoma-specific MEL5 TCR. Thanks to a SNF Mobility grant, I had the opportunity to spend 9 months in the laboratory of Prof. Sewell

and to perform the experiments myself. The overall aims of my work in Cardiff were to:

- Construct, express and produce soluble A2/LLW-specific TCRs.
- Measure TCR affinity and binding kinetics using A2/LLW in real-time by surface plasmon resonance (SPR) on a BIAcore instrument.
- Solve a high-resolution crystal structure of a TRAV12-2⁺ TCR-A2/LLW complex.
- Detect potential cross-reactivity to other human epitopes and pathogens using *in silico* prediction and *in vitro* analyses.

Unfortunately, despite several attempts with different TCRs, I did not obtain refolding of a functional A2/LLW-specific TRAV12-2⁺ TCR. The troubleshooting to produce a soluble TCR is described in detail in section 3.1.3.

Nevertheless, I managed to solve the atomic structure of the A2/LLW pMHC complex at 1.59Å resolution. We could thus combine the data of this structure with the previously solved structure of the MEL5 TCR to perform *in silico* modeling of the A2/LLW-specific YF5048 TCR (TRAV12-2/TRBV9). This YF5048 TCR was chosen due to its closest similarity to the MEL5 TCR sequence for the α chain to facilitate the modeling (with only 3 amino acid differences in the CDR3 loop).

In this model, most of the interactions between the TCR and the peptide originated from the α chain encoded by TRAV12-2 (Figure 13A, Table 1). Five peptide residues are pointing toward the TCR: Leu1, Asn4, Gly5, Met7 and Ala8. These predominantly contact the CDR1α loop. In particular, Asn4 extends into a polar pocket of TRAV12-2, where its side chain is making a network of hydrogen bonds with the side chains of CDR1α Ser32 and CDR3α Asp92, as well as non-polar interactions with the CDR1α Gln31. The functional importance of Asn4 was highlighted by an alanine substitution scan. Indeed, it revealed that it is essential for TCR recognition as this substitution (LLW-4A) completely abrogated the response (Figure 13B). In order to understand the structural basis underlying this perturbation in TCR recognition, we solved the TCR-unbound structure of A2/LLW-4A. Comparison of the crystallographic structure of A2/LLW and A2/LLW-4A did not reveal major distortion in the overall peptide conformation. However, molecular modeling of the YF5048 TCR binding to the X-ray structure of the pMHC complex showed that the alanine at P4 is no longer in an optimal

position to be contacted by the TCR (Figure 14). Residue Asn4 of the peptide is making numerous favorable interactions with the TCR, including notably hydrogen bonds with Ser32 and Asp92 of TCR α . The lack of T cell response to A2/LLW-4A is therefore in line with the loss of critical TCR:pMHC interactions.

In conclusion, the modeling and functional assays revealed the key elements mediating the TRAV12-2⁺ YF5048 TCR interaction with the A2/LLW complex and support the hypothesis that the germline-encoded CDR1 α loop of TRAV12-2 makes critical contributions to cognate peptide recognition.

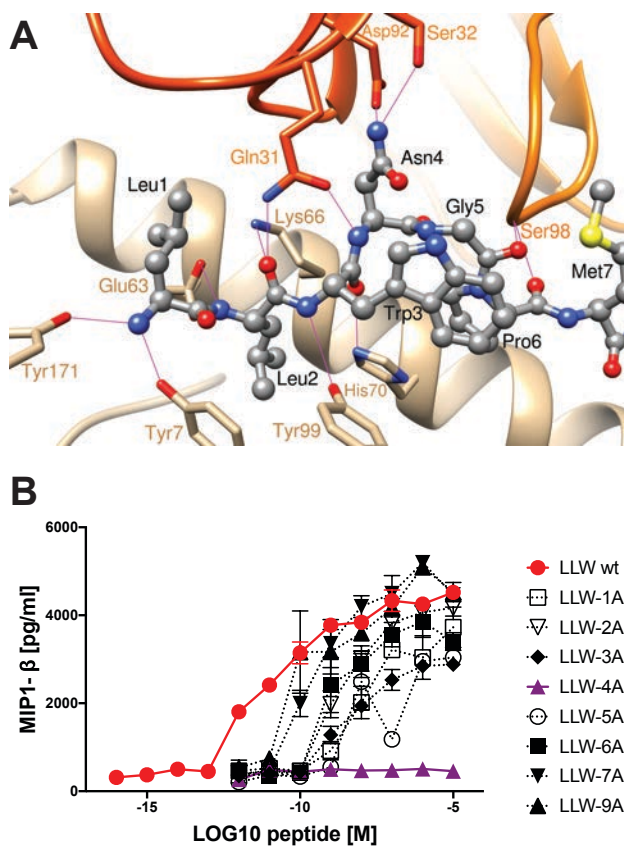


Figure 13 Molecular modeling indicates that the germline-encoded CDR1 alpha loop in TRAV12-2 makes major contributions to the binding with the A2/LLW complex. A, Calculated 3D structure of the YF5048 TRAV12-2/TRBV9 TCR bound to the HLA-A2/LLW peptide complex with ribbons representing α - and β - chains in dark and light orange, respectively; the MHC molecule in tan ribbon, and peptide in ball and stick representation. TCR and MHC side chains are shown in thick lines, with carbon atoms colored in orange and tan, respectively. Hydrogen bonds are displayed as magenta thin lines. B, Alanine-scan of the LLW peptide assessed by MIP-1 β ELISA with graded concentrations of the peptides (mean and SEM). Data are representative of two independent experiments.

CDR loop	TCR residue	Peptide residue	MHC residue	Bond type
CDR1 α	Arg28, N ϵ		Glu166, O ϵ 1/O ϵ 2	Electrostatic
	Arg28, NH2		Glu166, O ϵ 1/O ϵ 2	Electrostatic
	Arg28, O		Trp167, N ϵ 1	Electrostatic
	Gly29, C α		Trp167, CZ2	vdW
	Gly29, C α	Leu1, C δ 2		vdW
	Gln31, N ϵ 2	Leu2, O		Electrostatic
	Gln31, C β	Asn4, C β /C γ		vdW
	Gln31, C γ	Asn4, C γ		vdW
	Gln31, O ϵ 1	Asn4, N		Electrostatic
	Ser32, O γ	Asn4, N δ 2		Electrostatic
CDR2 α	Tyr51, OH		His151, O	Electrostatic
CDR3 α	Asn92, O δ 2	Asn4, N δ 2		Electrostatic
	Asn94, O		Arg65, NH2	Electrostatic
	Ala95, O		Arg65, N ϵ	Electrostatic
	Ala95, C β		Gly62, C α /O	vdW
CDR2 β	Ala95, C β		Lys66, C ϵ	vdW
	Asn48, O ϵ 1		Arg65, NH1	Electrostatic
	Tyr49, C ϵ 1		Arg65, C δ	vdW
CDR3 β	Arg55, NH2		Glu19, O ϵ 1	Electrostatic
	Gly97, C α		Thr73, C γ 2	vdW
CDR3 β	Ser98, N	Gly5, O		Electrostatic
	Ser98, N	Pro6, O		Electrostatic
	Ser98, C β	Met7, C ϵ		vdW

Table 1 Molecular interactions between TCR and pMHC in the structural 3D model. ("vdW"= van der Waals)

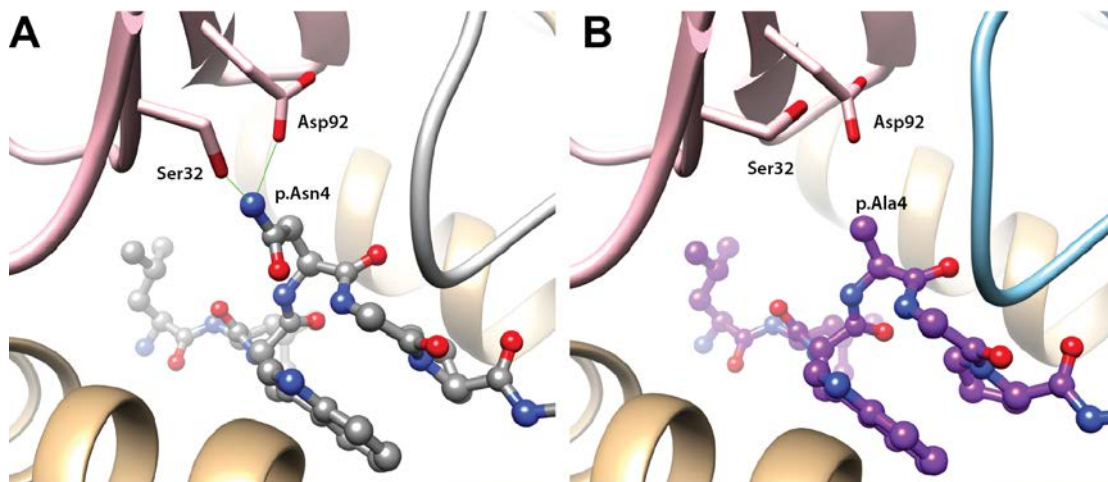


Figure 14 Conformation comparison of A2/LLW and A2/LLW-4A and modeling of the interaction with the YF5048 TCR explains the abrogation of the T-cell response in the alanine scan. A. Calculated 3D structure of the YF5048 TRAV12-2/TRBV9 TCR bound to the HLA-A2/LLW peptide complex with ribbons representing the α -chain; the MHC molecule in tan ribbon, and peptide in grey ball and stick representation. Hydrogen bonds are displayed as green thin lines. B. Calculated 3D structure of the YF5048 TRAV12-2/TRBV9 TCR bound to the HLA-A2/LLW-4A peptide complex with ribbons representing the α -chain; the MHC molecule in tan ribbon, and peptide in purple ball and stick representation. Hydrogen bonds are displayed as green thin lines.

A2/LLW and A2/ELA TRAV12-2 positive TCRs preserve their respective specificity

Given the germline nature of the CDR1 α loop of TRAV12-2 that is critical to peptide recognition of both A2/LLW and A2/ELA specificities, we addressed whether there is any cross-reactivity between T cells with these TRAV12-2-dominated biased specificities (Figure 15). The TRAV12-2⁺ A2/LLW-specific clones did not respond to the ELA peptide and conversely TRAV12-2 positive A2/ELA-specific clones did not respond to the LLW peptide. This indicates that there is no common, shared TRAV12-2-mediated mode of determining antigen recognition specificity. In addition to the contribution of germline-encoded segments in TCR:pMHC binding, this observation of no cross-reactivity between TRAV12-2⁺ A2/ELA and A2/LLW specific TCRs highlights the importance that the β chain plays in the effective TCR specificity (although the β chain's contribution to pMHC contact is minimal, it is determinant for specificity).

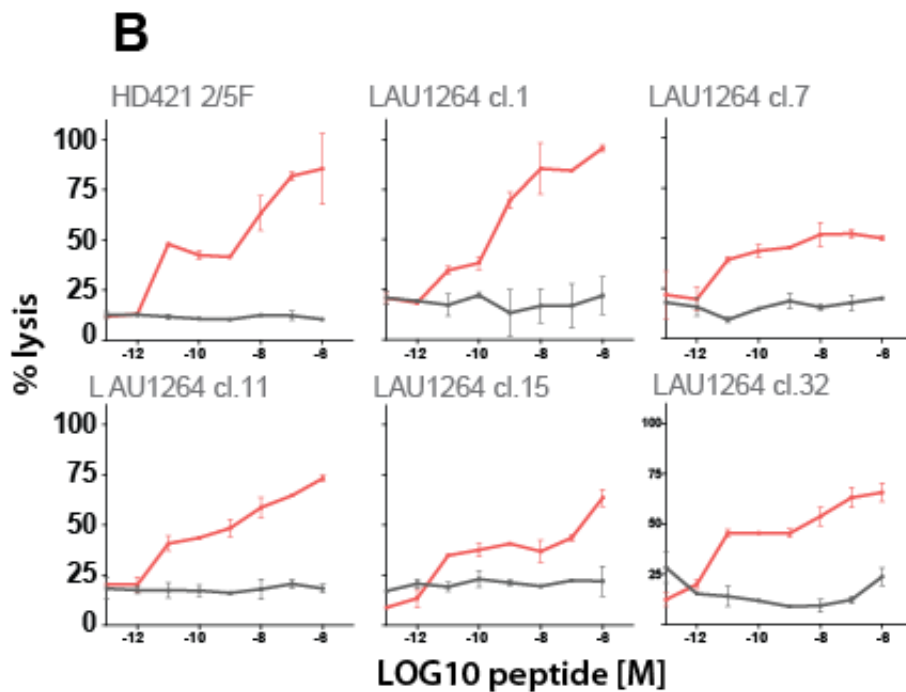
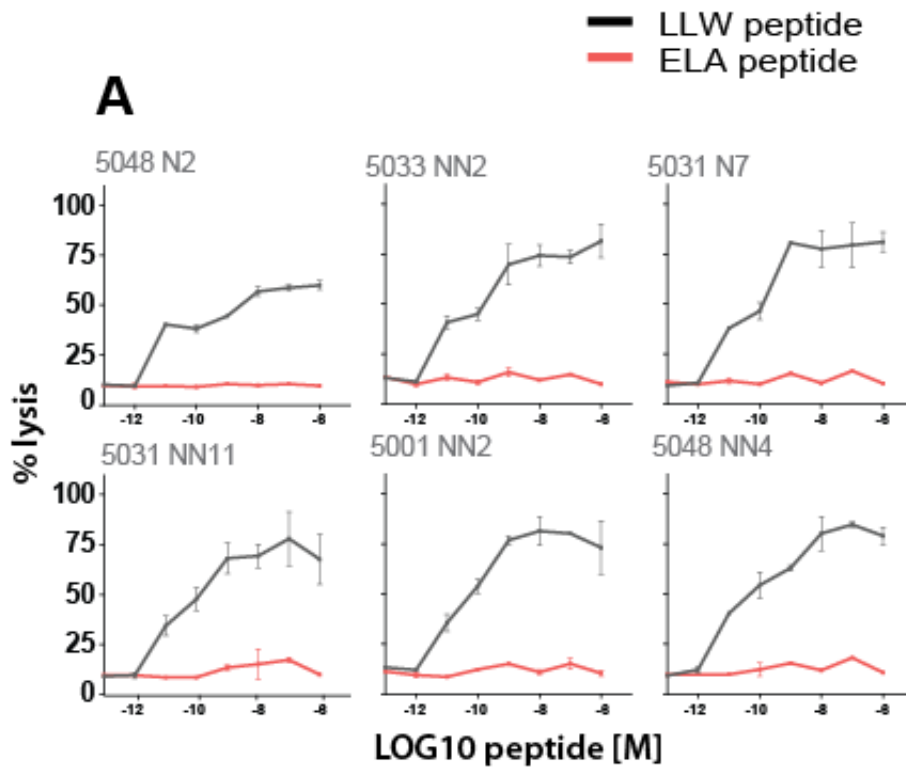


Figure 15 Absence of cross-reactivity between A2/LLW and A2/ELA epitopes. Recognition of the LLW and ELA peptides by A2/LLW-specific and A2/ELA-specific CD8 T cell clones was assessed by 51-chromium release assay using T2 cells as APCs. A, Cross-reactivity analysis of TRAV12-2 positive A2/LLW-specific CD8 T cell clones toward the LLWNGPMAV (LLW, black line) and ELAIGILTV (ELA, red line) peptides (mean and SD). B, Cross-reactivity analysis of TRAV12-2 positive A2/ELA-specific CD8 T cell clones toward the LLWNGPMAV (LLW, black line) and ELAIGILTV (ELA, red line) (mean and SD).

3.1.1.3 Discussion

In this study, we analyzed the TCR repertoire of CD8⁺ T cells specific for the immunodominant A2/LLW epitope in YF-17D vaccinees and controls. We revealed and quantified the TRAV12-2 bias in A2/LLW-specific CD8⁺ T cells. Various functional assays using T-cell clones demonstrated that TRAV12-2 does not provide a functional advantage on a per cell basis. Together with the fact that this strong TRAV12-2 bias was already present in naïve A2/LLW-specific CD8⁺ T cells before YF-17D vaccination, it rather suggests that TRAV12-2 might confer a selective advantage for high frequency and prevalence by favoring thymic output of naïve cells. We thus sought to investigate how TRAV12-2 may provide such advantage by investigating the mode of antigen binding and structural considerations of the TCR:pMHC complex.

The A2/ELA epitope represents a well-known model antigen for which T cells are biased for TRAV12-2 usage [130]–[134]. A2/ELA-specific CD8⁺ T cells exhibit high frequency and prevalence in HLA-A*0201 healthy individuals as well as melanoma patients, showing naïve (in healthy individuals) and [130]–[133] differentiated (in melanoma patients) phenotypes [131] [134]. Intriguingly, the binding between the MEL5 TCR expressing TRAV12-2 and the ELA peptide in complex with HLA-A*0201 occurs via dominant contacts with the CDR1 loop of TRAV12-2 [135]. The TRAV12-2 gene is also expressed by the A6 TCR, which is specific for the A2/Tax epitope of the human T-cell leukemia virus type 1 (HTLV-1) [28]. The CDR1 α and CDR2 α loops of the A6 TCR utilize an antigen-binding mode virtually identical to that seen in the MEL5-A2/ELA complex, making contacts between the CDR1 α loop and the Tax peptide. A study in HTLV-I-Associated Myelopathy/Tropical Spastic Paraparesis (HAM/TSP) patients revealed that TRAV12-2 transcripts are predominant [136] and the frequency of naïve cells with this specificity is very high [137]. Therefore, A2/Tax-specific CD8⁺ T cells constitute another documented example of high naïve frequency associated with TRAV12-2 bias.

Unfortunately, our extensive attempts to generate a TRAV12-2 TCR A2/LLW co-crystal structure failed. We resorted to molecular modeling of this interaction taking advantage of the high sequence similarity between the A2/LLW-specific TCR YF5048 and the A2/ELA-specific TCR MEL5. Conveniently, the LLW peptide in the free A2/LLW

structure we solved adopts a similar conformation to the ELA peptide in the A2/ELA/MEL5 TCR complex. Modeling showed that the YF5048 TCR α -chain positioned above the N-terminus of the peptide, making contacts predominantly with Asn4 in the middle of the peptide via the CDR1 α loop of TRAV12-2. The importance of this interaction is further supported by our results from the mutagenesis scan across the LLW peptide. Our modeling data suggests that the germline-encoded TRAV12-2 CDR1 α loop of A2/LLW-specific CD8⁺ T cells makes critical contacts with both MHC and peptide in a comparable manner to the CDR1 α loops in the MEL5 and A6 TRAV12-2⁺ TCRs [28] [135]. These three paralleled examples of TRAV12-2-biased responses endorse the concept that the interactions between the TCR and the antigen can rely substantially on TCR segments that already pre-exist in the germline rather than on somatic CDR3 rearrangement. However, it is important to note that this observation does not apply to all immunodominant T cell responses, as many public TCRs or immunodominant epitope-specific TCRs bind their cognate peptide predominantly via residues encoded in the rearranged CDR3 loops [138] [139].

Importantly, we showed that TCRs sharing this heritable TRAV12-2 CDR1 α component of antigen binding still preserve their respective antigen specificity. Indeed, we demonstrated that there is no cross-reactivity between the LLW and ELA specificities. Thus, even these examples of a TRAV germline-encoded antigen binding mode are still heavily relying on permissive sequences within the TRBV non-germline CDR3 loop to determine antigen specificity (beyond TCR:pMHC binding being largely contributed by germline TRAV segments).

It is intriguing that these three examples of TCRs binding their epitope with a germline component all involve the CDR1 α loop of TRAV12-2 and HLA*0201. It is conceivable that TCRs expressing the TRAV12-2 could have a selective advantage for binding to cognate antigen restricted by HLA-A*0201 or that other antigen specificities (not only restricted by HLA-A*0201) also harbor biases for certain germline-encoded TCR segments but that these have not yet been identified. In the HLA-A*0201 allele and its associated antigen specificities are the most studied because HLA-A*0201 is prevalent at 30-50% in Caucasian populations and is the most prevalent HLA subtype amongst the global human population, potentially inducing a research bias [140]. Indeed, the TCR:pMHC structural database is dominated by interactions with HLA A2. More

studies need to be conducted to appreciate the extent to which this phenomenon of germline-encoded TCR binding to pMHC applies to other specificities and TRAV/TRBV families.

Despite the tremendous theoretical genetic diversity of the TCR repertoire, most studies showed that the adult TCR repertoire is a consequence of a process that is far from random and TCR bias is commonly found in immune responses [51]. A specificity and/or TCR bias could reflect an evolutionary advantage during infection and other diseases. Several lines of evidence indicate that the germline-encoded TCR segments have features that promote binding to MHC molecules, suggesting co-evolution between TCR and MHC molecules [141]–[143]. Our data suggests that there is also co-evolution between the TCR and the cognate peptide. Indeed, we observed that TRAV12-2 TCR bias is present before YF-17D vaccination. In agreement with our functional studies on A2/LLW-specific clones, it was reported that TRAV12-2 usage in A2/ELA-specific CD8⁺ T cells was independent from functional avidity [133]. In fact, the origin of the large naïve A2/ELA-specific CD8⁺ T cell population was attributed to preferential thymic selection. First, the unusual frequency of the A2/ELA-specific population was shown to be generated by thymic output of higher number of precursors [144]. In addition, this large naïve pool might also result from the lack of antigen presentation by AIRE in the thymus of the natural EAA epitope. Indeed, it has been shown that AIRE-expressing cells in the thymus only present a truncated version of the Melan-A epitope due to misinitiation of its transcription [145]. Therefore, this leaky central tolerance might explain the abundance of these cells.

Given that antigen recognition features a germline-encoded component, there is presumably a genetic advantage that confers higher chances for thymic output of TCR constructions involving the CDR1 α of TRAV12-2. Thus, although TRAV12-2 does not confer a functional advantage on a per cell basis, it may provide an advantage at the level of the organism by skewing the naïve CD8⁺ T cell compartment towards these specificities recognized by TRAV12-2 CDR1 α . This possibly explains the high frequency and prevalence of specificities such as A2/LLW and A2/ELA.

In summary, we discovered the TCR bias for TRAV12-2 in A2/LLW-specific CD8⁺ T cells and demonstrated that there is no functional advantage in featuring TRAV12-2 on

a per cell basis. Rather, our structural modeling suggests that the germline-encoded CDR1 α loop centrally contributes to peptide binding similar to two other TRAV12-2 positive TCR specificities. We also demonstrated that TCRs sharing this TRAV12-2 CDR1 α – mediated mode of antigen binding still preserve their own antigen specificity.

3.1.1.4 Contributions

I cultured (restimulated and maintained) the library of clones used in this study, performed and analyzed the flow cytometry stainings, killing assays, combinatorial peptide library screens, ELISA and TCR sequencing. I also produced the pMHC complex for further X-ray and circular dichroism (CD) analysis. I solved its crystal structure with the help of Dr. Pierre Rizkallah. Dr. Konrad Beck performed and analyzed the CD experiment. The *in silico* modeling were performed by Dr. Vincent Zoete. I wrote the manuscript entitled “T cell Receptor Alpha Variable 12-2 bias in the immunodominant response to Yellow Fever virus” with the essential contribution of Dr. Silvia Fuertes, Prof. Daniel Speiser, Dr. Vincent Zoete, Dr. Konrad Beck, Prof. Andrew Sewell and Dr. Garry Dolton.

3.1.2 Fishing out new A2/LLW-specific clonotypes using an optimized multimer staining procedure

3.1.2.1 Background

In the previous Chapter, I highlighted the presence of a strong bias for the TRAV12-2 gene in A2/LLW-specific CD8 T cells before and after YF-17D vaccination. I also showed using A2/LLW-specific clones that most of the clonotypes were unique and that public clonotypes were infrequent. One major technical limitation in the study of antigen-specific CD8 T cells is their detection and discrimination from other specificities. In the present Chapter, I would like to further develop the clonotype analysis of A2/LLW-specific CD8 T cells and in particular show the experiments that we did to optimize the multimer staining procedure in the framework of my scientific visit in Cardiff.

In 1996, the development of fluorochrome-conjugated Class I pMHC tetramers enabled for the first time the visualization and analysis of antigen-specific T cells by flow cytometry [146]. These complexes consisted of four biotinylated pMHC molecules bound to fluorochrome-conjugated streptavidin [146]: as opposed to single pMHC molecules, such a “multimeric” form favors TCR aggregation and enhances binding, thus detection of cognate TCRs. Improvements to the pMHC multimer technology led to the production of dextramers in 2005 [147]. This allowed the detection of far more antigen-specific T cells than with tetramers [148]. In addition, an optimized protocol of multimer staining in combination with a protein kinase inhibitor (PKI) treatment and the addition of an anti-fluorochrome antibody was developed in the group of Prof. Andrew Sewell. The PKI Dasatinib treatment prevents the TCR downregulation during the staining, while the antibody crosslinking the pMHC multimer reduces its cell surface removal during washes [149] [150]. These two optimization steps led to a substantial increase in the number of detectable antigen-specific T cells [151] [152] (Figure 16). It was recently demonstrated by this group that tumor-specific T cells in tumor-infiltrating lymphocytes failed to be stained with tetramers although this population was fully functional. However, such T cells could be detected with this optimized protocol combining PKI Dasatinib and crosslinking antibody [150].

I tested this optimized multimer staining protocol in order to fish out new A2/LLW-specific clonotypes that could potentially be missed by the conventional multimer staining procedure. This data was included in a manuscript published in the *Journal of Immunology* in 2018 [153].

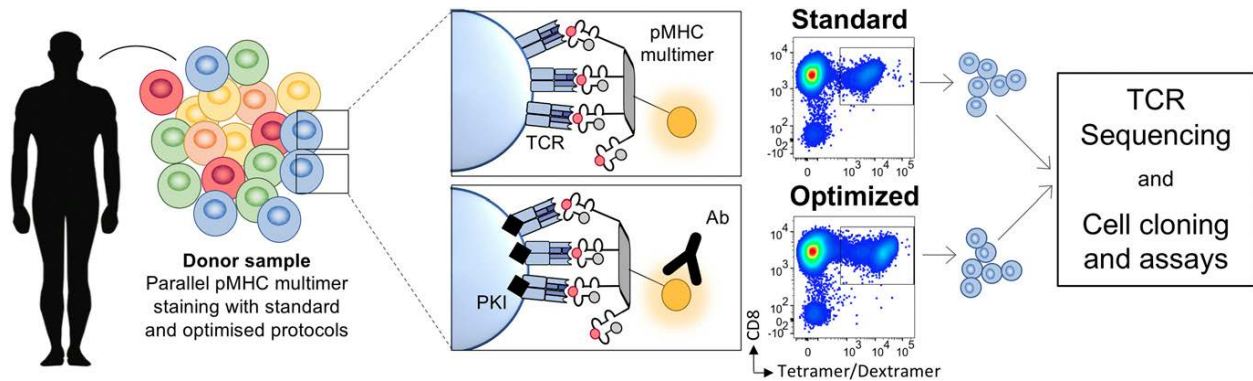


Figure 16 Study approach. Cell samples were stained in parallel using standard and optimized pMHC multimer staining protocols. The standard approaches used pMHC tetramer or dextramer while the optimized protocol further included the protein kinase inhibitor (PKI) Dasatinib and an anti-fluorochrome antibody (Ab). Multimer⁺ T cells were sorted by flow cytometry for TCR sequencing or cell cloning. This figure was taken from [153].

3.1.2.2 Results

First, a T cell line was generated from PBMCs of an HLA-A*02+ donor vaccinated with YF-17D. Briefly, PBMCs were cultured for 14 days in complete medium in presence of 10^{-5} M LLW peptide, 10 μ g/ml anti-CD28 antibody and 20U/ml of IL-2 [153]. Then, this T cell line was stained with the A2/LLW multimer using either the standard or optimized staining protocols. The standard staining procedure was performed as following: $2-3 \times 10^6$ cells of a T cell line were stained with PE-conjugated dextramer on ice for 30 mins in dextramer buffer (0.05M Tris-HCL, 15mM sodium azide, 1% bovine serum albumin, pH 7.2). The optimized protocol involved two additional steps: 1) cells were pre-treated with 50 nM Dasatinib (PKI) at 37°C for 10-30 minutes and without washing prior to staining with dextramer; 2) following dextramer staining, a second staining with a mouse anti-PE monoclonal antibody (binding the PE-conjugated dextramer) and washing was used [153].

Using the standard staining, 0.08% of CD8 T cells were detected with cognate pMHC dextramer. This A2/LLW-specific frequency rose to 0.16% of cells when the PKI

Dasatinib was included along with anti-fluorochrome antibody in the optimized staining protocol (Figure 17A).

In this vaccinated donor, TRAV chain usage was biased towards TRAV12-2 as expected from our own findings [126] (Figure 17B). The TRBV chain dominance was shared between TRBV20-1 and TRBV15 with similar distribution (Figure 17B).

TRAV chain repertoire analyses of sorted cells by high throughput sequencing revealed 9 CDR3s for the standard dextramer stained cells and 27 for the optimized staining, with 8 clonotypes shared between them (Figure 17C). Importantly, the optimized staining protocol revealed 19 sort-unique CDR3s compared to 1 from the standard protocol sort (Figure 17C and Table 2). Interestingly, a previously identified public TRAV sequence (CAVGDDKIIFG) was identified in this donor using both procedures (Table 2) [126]. Similar analyses of TRBV use gave 9 and 18 CDR3s for standard and optimized staining respectively with 6 shared sequences. Thus, TCR β -chain sequencing also showed more CDR3s for the optimized protocol (n=12) compared to the standard stained and sorted cells (n=3) (Figure 17C and Table 3).

Taken together, the pMHC multimer staining procedure optimized using the combination of PKI Dasatinib and multimer-crosslinking antibody revealed more and mainly unique A2/LLW-specific clonotypes compared to the standard multimer staining protocols.

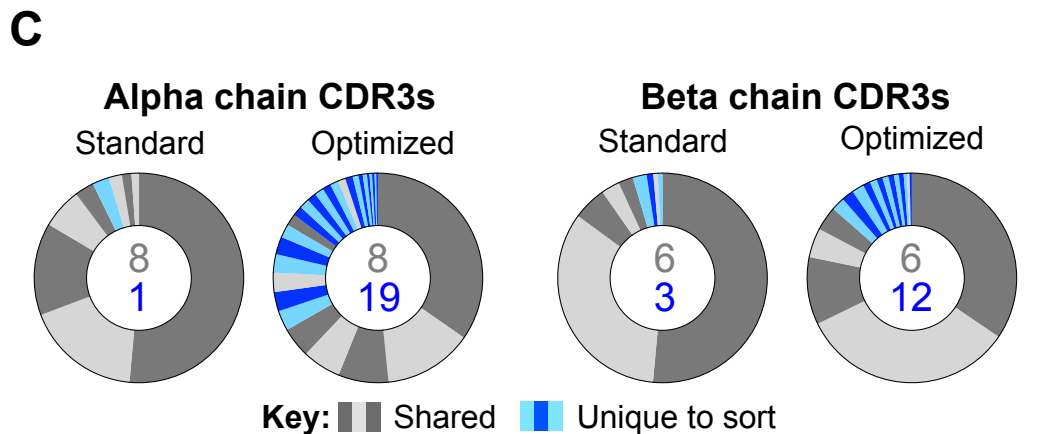
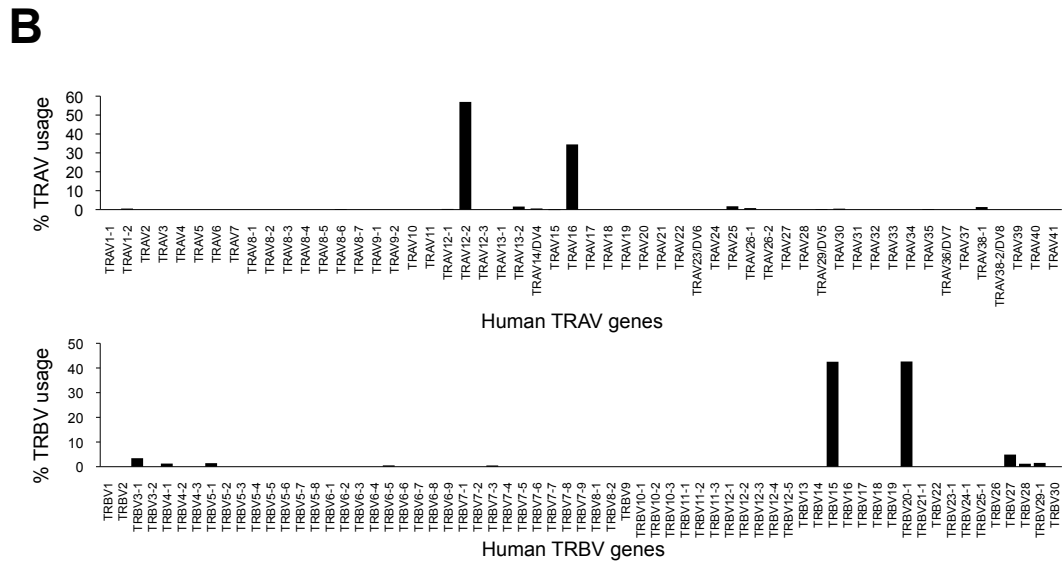
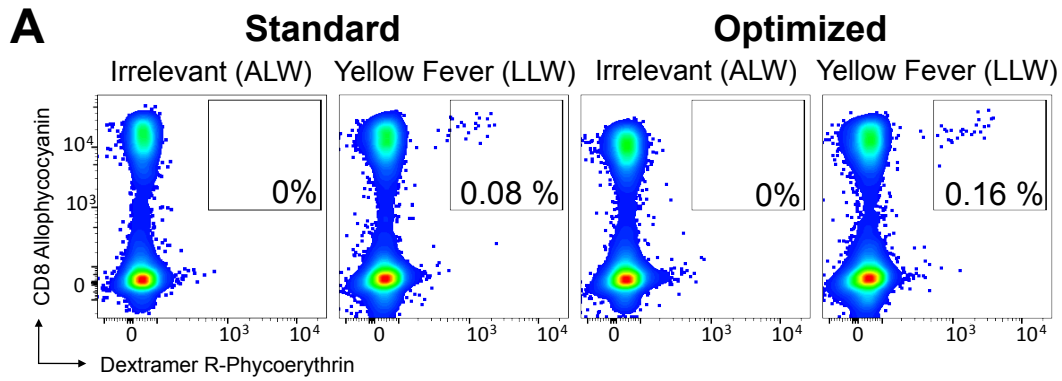


Figure 17 Optimized pMHC multimer staining revealed many more TCRs than standard staining. (A) A T-cell line from a yellow fever vaccinated HLA-A2⁺ donor was sorted by flow cytometry in parallel using either HLA A2-LLWNGPMAV dextramer alone (standard) or in combination with protein kinase inhibitor and anti-fluorochrome antibody (optimized). Percentage dextramer⁺ cells of CD8⁺ T cells is shown for each gate. Irrelevant dextramer made with HLA A2-ALWGPDPAAA was used to set the gates for sorting. (B) Cumulative TRAV (upper panel) and TRBV (lower panel) gene usage for standard and optimized staining protocols, with all human genes listed on the x-axis for completeness. (C) TCR sequencing and CDR3 analysis (Table 1 and 2) of alpha (left) and beta TCR chains (right) are displayed as sort-shared (grey) or sort-unique (blue) sections of a donut pie, with each section for each sort corresponding to a different CDR3. The number of shared (grey) and unique (blue) CDR3s for the respective sorts are shown in the center of each pie.

Alpha chain

Protocol	Frequency (%)	V segment	J segment	CDR3 α
Standard	51.44	TRAV16	TRAJ37	CALSPSGNTGKLIF
	17.81	TRAV12-2	TRAJ23	CAVGGGKLIF
	14.26	TRAV12-2	TRAJ33	CAVSNYQLIW
	6.27	TRAV12-2	TRAJ40	CVASGTYKYIF
	2.97	TRAV12-2	TRAJ30	CAVGNDKIIF
	2.64	TRAV13-2	TRAJ13	CAENSGGYQKVTF
	1.98	TRAV12-2	TRAJ16	CAVNSDGQKLLF
	1.48	TRAV38-1	TRAJ48	CAFPEsnFGNEKLTF
	1.15	TRAV12-2	TRAJ30	CAVGDDKIIF
Optimized	34.67	TRAV12-2	TRAJ33	CAVSNYQLIW
	13.71	TRAV12-2	TRAJ23	CAVGGGKLIF
	7.76	TRAV16	TRAJ37	CALSPSGNTGKLIF
	5.95	TRAV12-2	TRAJ30	CAVGNDKIIF
	3.10	TRAV12-2	TRAJ40	CVASGTYKYIF
	2.98	TRAV25	TRAJ5	CASIGGRRALTF
	2.98	TRAV12-2	TRAJ30	CAVIGDKIIF
	4.66	TRAV12-2	TRAJ30	CAVGDDKIIF
	2.85	TRAV12-2	TRAJ30	CATGDDKIIF
	2.72	TRAV12-2	TRAJ24	CAVNSGTDSWGKLF
	2.07	TRAV26-1	TRAJ24	CIVRGDSWGKLF
	1.81	TRAV12-2	TRAJ16	CAVNSDGQKLLF
	1.55	TRAV14DV4	TRAJ16	CAMRETTASDGQKLLF
	1.55	TRAV25	TRAJ16	CAADGQKLLF
	1.42	TRAV1-2	TRAJ33	CASMDSNYQLIW
	1.42	TRAV12-2	TRAJ34	CAVGTDKLIF
	1.29	TRAV30	TRAJ11	CGTDISGYSTLTF
	1.29	TRAV12-2	TRAJ27	CAVIAGKSTF
	1.16	TRAV38-1	TRAJ48	CAFPEsnFGNEKLTF
	1.16	TRAV12-2	TRAJ50	CAVNAAGTSYDKVIF
	0.91	TRAV12-1	TRAJ30	CVVADDKIIF
	0.65	TRAV29DV5	TRAJ52	CAASDTNAGGTSYGKLF
	0.65	TRAV12-2	TRAJ57	CAPSQGGSEKLVF
0.39	TRAV8-6	TRAJ41	CAVRWENSGYALNF	
0.39	TRAV35	TRAJ48	CAGRREKLTF	
0.39	TRAV12-2	TRAJ31	CAVNNARLMF	
0.26	TRAV12-2	TRAJ30	CAVSDDKIIF	

Key: Shared, Sort Unique

Table 2 A greater number of unique (in blue) Yellow fever-specific TCR α -chain clonotypes are revealed with the optimized pMHC multimer staining protocol (n=19) when compared to standard protocol (n=1). Frequency (%) of clonotypes is calculated as *Individual number of reads / Total number of reads x 100*. TRAV/TRAJ annotation is displayed according to the IMTG database [154].

Beta chain

Protocol	Frequency (%)	V segment	J segment	CDR3 β
Standard	51.46	TRBV20-1	TRBJ2-7	CSASHRAGNEQYF
	33.62	TRBV15	TRBJ2-1	CATGLAGGNEQFF
	5.21	TRBV15	TRBJ2-7	CATSRGQAYEQYF
	2.84	TRBV27	TRBJ2-7	CASSPGTGTYEQYF
	2.29	TRBV3-1	TRBJ2-7	CASSPGQAYEQYF
	2.13	TRBV5-1	TRBJ2-7	CASSLSDRVGEQYF
	1.03	TRBV27	TRBJ1-5	CASSERGSNQPQHF
	0.71	TRBV6-5	TRBJ1-1	CASRQQGGTEAFF
	0.71	TRBV20-1	TRBJ2-3	CSASAADTDTQYF
Optimized	34.50	TRBV15	TRBJ2-1	CATGLAGGNEQFF
	33.29	TRBV20-1	TRBJ2-7	CSASHRAGNEQYF
	10.41	TRBV15	TRBJ2-7	CATSRGQAYEQYF
	4.54	TRBV27	TRBJ2-7	CASSPGTGTYEQYF
	3.74	TRBV3-1	TRBJ2-7	CASSPGQAYEQYF
	2.07	TRBV28	TRBJ2-3	CASSLSSSTGPTDTQYF
	1.90	TRBV29-1	TRBJ2-7	CSVDVGAYEQYF
	1.84	TRBV4-1	TRBJ2-7	CASSQGGAYEQYF
	1.15	TRBV20-1	TRBJ2-7	CSAFRDFSQYEQYF
	1.09	TRBV27	TRBJ2-1	CASSQGLAGVHEQFF
	0.92	TRBV5-1	TRBJ1-6	CASSLDWRGADSPLHF
	0.92	TRBV20-1	TRBJ2-7	CSALAGAFYEQYF
	0.86	TRBV7-3	TRBJ1-4	CASSVLRGRQGAWGEKLF
	0.75	TRBV27	TRBJ1-5	CASSRGGTGDQPQHF
	0.75	TRBV29-1	TRBJ2-1	CSVDGRTGINEQFF
	0.52	TRBV3-1	TRBJ2-3	CASSPGLAGGLASTDTQYF
	0.40	TRBV6-5	TRBJ1-1	CASRQQGGTEAFF
	0.35	TRBV4-1	TRBJ2-1	CASSQGERFGNEQFF

Key: Shared, Sort Unique

Table 3 A greater number of unique (in blue) Yellow fever virus-specific TCR β - chain clonotypes are revealed with the optimized pMHC multimer staining protocol (n=12) when compared to standard protocol (n=3). Frequency (%) of clonotypes is calculated as *Individual number of reads / Total number of reads x 100*. TRBV/TRBJ annotation is displayed according to the IMTG database

3.1.2.3 Discussion

Several recent studies have suggested that the use of pMHC multimer staining may underestimate the size of antigen-specific T cell populations, in particular when low-affinity (but functional) TCRs predominate such as in cancer. Importantly, recent studies also indicate that these populations that go undetected by standard stainings can make important contributions to immune responses [155]–[157].

Here, we used an optimized staining protocol including a PKI Dasatinib treatment to prevent TCR internalization due to multimer binding to TCR and the addition of an anti-fluorochrome antibody to cross-link and thus stabilize the multimer. We compared standard and optimized staining protocols in combination with high-throughput TCR sequencing to characterize A2/LLW-specific CD8 T cells.

Class I-restricted antiviral TCRs bind their cognate antigen with high affinity compared to self-antigens or to the binding between class II-restricted TCRs and class II pMHC complexes [47] [158]. Therefore, it has been assumed that the standard class I pMHC tetramer staining is the prototype successful protocol at detecting antigen-specific cells. Unexpectedly, we found that the optimized staining (combination of PKI Dasatinib and antibody cross-link) identified a much larger population of A2/LLW-specific CD8 T cells in a vaccinated donor. Of note, the situation was similar for the EBV BMLF1 epitope GLCTLVAML [153]. Although we showed that specific viral populations could be underestimated by standard staining, this was not the case for all viral epitopes. For instance, both protocols revealed similar specific populations from the influenza M1 epitope GILGFVFTL, CMV pp65 epitope NLVPMVATV, and EBV LMP2A epitope CLGGLTMV. Nevertheless, the optimization steps led to a brighter staining of the Ag-specific T cells from these populations [153].

The present work was performed in the group of Prof. Andrew Sewell where the procedure was optimized starting from their own standard protocol of dextramer staining (“Cardiff”). The “Lausanne” protocol performed in the group of Prof. Daniel Speiser relies on the addition of sodium azide, a metabolic inhibitor, in the buffer to limit the internalization of the TCR/CD3 complex [159]. Direct comparison of the two standard protocols has not been performed. Table 4 considers side-by-side the two

standard protocols. Sodium azide is also present in the “Cardiff” buffer so one can expect that the two additional steps would also improve the recovery of antigen-specific CD8 T cells compared to the standard “Lausanne” staining. Nevertheless, I have not tested whether the optimization would also improve the number of antigen-specific CD8 T cells detected with the “Lausanne” standard staining protocol.

Lausanne	Cardiff
Phosphate-buffered saline	0.05M Tris-HCl
5mM EDTA	pH 7.2
0.2% BSA	1% BSA
20mM sodium azide	15mM sodium azide
40min at 4°C	30min on ice
PE-labeled multimer (TC Metrix)	PE-labeled dextramer (in house)
s	<u>Optimization:</u> - <i>PKI Dasatinib</i> - <i>Anti-fluorochrome Ab</i>

Table 4 Comparison of A2/LLW-specific CD8 T cells standard staining procedure from Lausanne and Cardiff laboratories.

It is important to mention that these stainings and TCR analysis were performed on T cell lines and not directly ex vivo on fresh PBMCs. This strategy was adopted because direct ex vivo analysis was close to detection limit. In my opinion, it is crucial to repeat this experiment *ex vivo*. Especially, it would be interesting to test these optimization steps on unvaccinated donors. The naïve pool of A2/LLW-specific CD8 T cells is surprisingly high and can be detected ex vivo directly in most of unvaccinated donors [97] [126]. However, the frequency of these naïve cells is very close to the detection limit of 0.01%. Therefore, such an improvement would be helpful to analyze and isolate the naïve population of unvaccinated donors. To ensure a correct gating of specific CD8 T cells and to phenotypically characterize these cells, markers of differentiation should be added to the FACS panel.

As the yellow fever epitope was not the main specificity of interest for this publication, I regret that no time was dedicated to isolate specific clones for further functional analysis. Furthermore, I am convinced that the expertise in the group of Prof. Daniel

Speiser would have enabled to analyze ex vivo material and led to a successful cloning.

In conclusion, this project highlights the importance of further optimization of multimer staining protocols to avoid underestimating the size of functional Ag-specific T cell populations and to maximize the brightness of the staining for a better signal:noise ratio. This is not only true for rare populations and epitopes recognized by low-affinity TCRs but also for strong viral epitopes. It would be interesting to test whether these additional steps lead to an improvement in the detection of Ag-specific T cells using the “Lausanne” staining protocol.

3.1.2.4 Contributions

This work contributed to the thesis of Cristina Rius Raphael, a PhD student from the group of Prof. Andrew Sewell in Cardiff, UK. I contributed in her project by producing the PE-labeled A2/LLW-specific multimer, performing the first tests of the optimized protocol on my previously generated A2/LLW-specific clones and then proceeded with the sort of the specific population from T cell lines derived from a vaccinated donor and took care of the first steps of the RNA extraction. Cristina and her collaborators then sequenced the TCRs using the SMARTer technology and analyzed the data. I participated to the preparation of the manuscript entitled “Peptide-MHC class I multimer staining can fail to detect relevant functional T-cell clonotypes and underestimate antigen-specific T cell populations”.

3.1.3 Detailed description of the soluble TCR:pMHC production process

3.1.3.1 Background

As mentioned in 3.1.1, I attempted multiple times without success to solve the crystal structure of a TRAV12-2⁺ TCR in complex with A2/LLW. The critical step that failed was to produce a soluble TCR, which is necessary to then mix with pMHC in solution and make the TCR:pMHC complex crystals. In this Chapter, I would like to describe in detail the procedure of TCR production that I used [160]. This work is not part of a manuscript. The aim of this chapter is to highlight the issues that I encountered during this process in parallel to the detailed description of the methodology – thus this methodological information is inserted here and not repeated in the Methods section for the purpose of clarity.

Briefly, the procedure to produce a soluble TCR involves cloning of the protein sequences into an expression vector, expression of protein chains as inclusion bodies (IB) in *E. Coli*, purification of IB, refolding by dilution of denaturing agents, an anion exchange purification step and several gel filtration purification steps in order to obtain enough pure proteins to perform experiments such as SPR and X-ray crystallography (Figure 18).

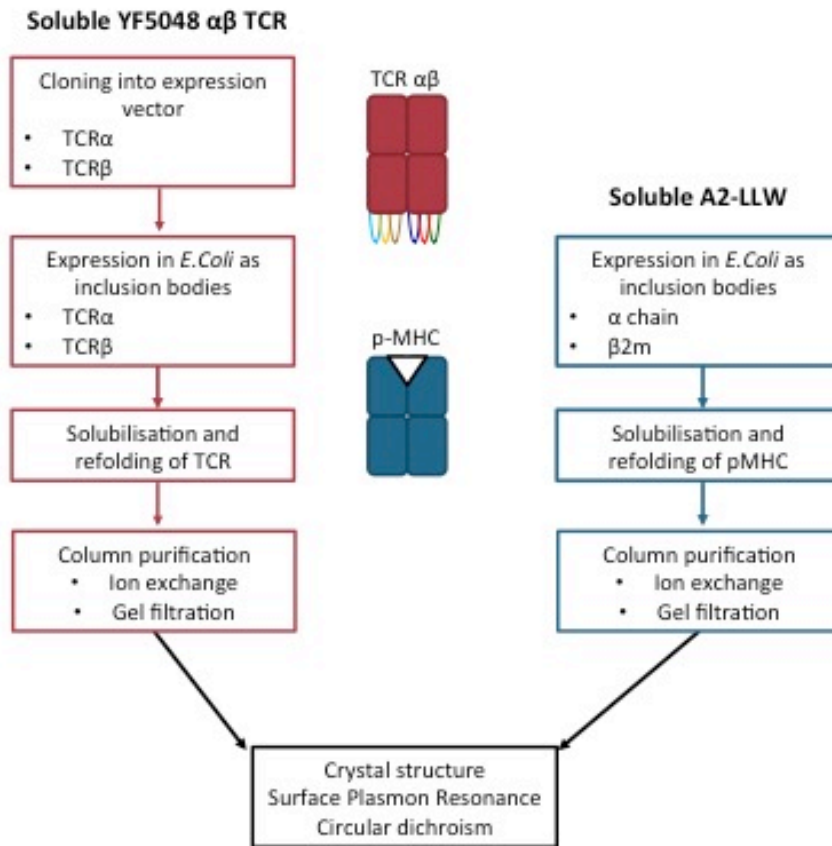


Figure 18 An overview of the process of soluble TCR:pMHC manufacture

3.1.3.2 Results

Cloning of the α and β TCR chains into pGMT7 expression vector

First, I chose five TRAV12-2⁺ TCR sequences from our library of A2/LLW-specific CD8 T cell clones. It is important to mention that the original sequences were modified in order to introduce a non-native disulfide bond into the interface between the TCR constant domains (Table 5). The introduction of these cysteine substitutions, known as “Boulter-disulfide”, improves the stability of the soluble TCR [161]. The selection of these clones was based on the functional assays and their fitness (expansion potential of the clones in culture upon restimulation). The sequences were then optimized for expression in *E. Coli* and restriction sites for cloning were added (Table 6). The sequences were synthesized by GeneWiz (USA) into the cloning plasmid pUC57. I processed all ten chains (α and β) in parallel but I will give only one example for each step.

YF1_alpha TRAV12-2
MQKEVEQNSGPLSVPEGAIASLNCTYSDRGSQSFFWYRQYSGKSPELIMFIYSNGDKEDGRFTAQLNKASQYVSLLRDSQPSSDA TYL CAVTDKIIIFG KGTRLHLPIQNPDPAVYQLRDSKSSDKSVCLFTDFDSQTNVSQSKSDVYITDKCVLDMRSMDFKSNSAVAW SNKSDFACANAFNNSIIPEDTFFPSPESS
YF1_beta TRBV6-8
MNAGVTQTPKFHILKTGQSMTLQCAQDMNHGYMSWYRQDPGMGLRLIYYSAAGTTDKEVPNGYNVSRNLNTEDFPLRLVSAAPS QTSVYL CASSYSRTGSYEQYFG PGTRLTVTEDLKNVFPPEVAVFEPSEAEISHTQKATLVCLATGFYDPDHVELSWWWNGKEVHSGV CTDPQLKEQPALNDSRYALSSRLRVSATFWQDPRNHFRQCQVQFYGLSENDEWTQDRAKPVTVQIVSAEAWGRAD
YF3_alpha TRAV12-2
MQKEVEQNSGPLSVPEGAIASLNCTYSDRGSQSFFWYRQYSGKSPELIMFIYSNGDKEDGRFTAQLNKASQYVSLLRDSQPSSDA TYL CAGGDDKIIFG KGTRLHLPIQNPDPAVYQLRDSKSSDKSVCLFTDFDSQTNVSQSKSDVYITDKCVLDMRSMDFKSNSAVAW SNKSDFACANAFNNSIIPEDTFFPSPESS
YF3_beta TRBV7-2
MGAGVSQSPSNKVTEKGDVELRCDPISGHTALYWYRQSLGQGLEFLIYFQGNAPDKSGLPSDRFSAERTGGSVSTLTIQRTQQE DSAVYL CASSQGLAYEQFFG PGTRLTVLEDLKNVFPPEVAVFEPSEAEISHTQKATLVCLATGFYDPDHVELSWWWNGKEVHSGVCT DPQPLKEQPALNDSRYALSSRLRVSATFWQDPRNHFRQCQVQFYGLSENDEWTQDRAKPVTVQIVSAEAWGRAD
YF4_alpha TRAV12-2
MQKEVEQNSGPLSVPEGAIASLNCTYSDRGSQSFFWYRQYSGKSPELIMFIYSNGDKEDGRFTAQLNKASQYVSLLRDSQPSSDA TYL CAVKDARLMFG DGTQLVVKPIQNPDPAVYQLRDSKSSDKSVCLFTDFDSQTNVSQSKSDVYITDKCVLDMRSMDFKSNSAV AWSNKSDFACANAFNNSIIPEDTFFPSPESS
YF4_beta TRBV9
MDSGVTQTPKHLITATGQRVTLRCSRSGDLSVYWYQQSLDQGLQFLIQQYNGEERAKGNILERFSAQQFPDLHSELNLSSLELGD SALYF CASSVEGPGELFFG EGSRLTVLEDLKNVFPPEVAVFEPSEAEISHTQKATLVCLATGFYDPDHVELSWWWNGKEVHSGVCTD PQPLKEQPALNDSRYALSSRLRVSATFWQDPRNHFRQCQVQFYGLSENDEWTQDRAKPVTVQIVSAEAWGRAD
YF6_alpha TRAV12-2
MQKEVEQNSGPLSVPEGAIASLNCTYSDRGSQSFFWYRQYSGKSPELIMFIYSNGDKEDGRFTAQLNKASQYVSLLRDSQPSSDA TYL CAVGSDKIIFG KGTRLHLPIQNPDPAVYQLRDSKSSDKSVCLFTDFDSQTNVSQSKSDVYITDKCVLDMRSMDFKSNSAVAW SNKSDFACANAFNNSIIPEDTFFPSPESS
YF6_beta TRBV2
MEPEVTQTPSHQVTQMGEVILRCVPISNHLFYWYRQILGQKVEFLVSFYNNSEIKSEIFDDQFSVERPDGSNFTLKIRSTKLEDS AMYF CASSEATGASYEQYFG PGTRLTVTEDLKNVFPPEVAVFEPSEAEISHTQKATLVCLATGFYDPDHVELSWWWNGKEVHSGVC TDPQPLKEQPALNDSRYALSSRLRVSATFWQDPRNHFRQCQVQFYGLSENDEWTQDRAKPVTVQIVSAEAWGRAD
YF15_alpha TRAV12-2
MQKEVEQNSGPLSVPEGAIASLNCTYSDRGSQSFFWYRQYSGKSPELIMFIYSNGDKEDGRFTAQLNKASQYVSLLRDSQPSSDA TYL CAVDTNAGKSTFG DGTTLTVKPIQNPDPAVYQLRDSKSSDKSVCLFTDFDSQTNVSQSKSDVYITDKCVLDMRSMDFKSNSA VAWSNKSDFACANAFNNSIIPEDTFFPSPESS
YF15_beta TRBV9
MDSGVTQTPKHLITATGQRVTLRCSRSGDLSVYWYQQSLDQGLQFLIQQYNGEERAKGNILERFSAQQFPDLHSELNLSSLELGD SALYF CASSVSGSSYEQYFG PGTRLTVTEDLKNVFPPEVAVFEPSEAEISHTQKATLVCLATGFYDPDHVELSWWWNGKEVHSGVCT DPQPLKEQPALNDSRYALSSRLRVSATFWQDPRNHFRQCQVQFYGLSENDEWTQDRAKPVTVQIVSAEAWGRAD

Table 5 Original amino acid sequences containing the Boulter-disulfide mutation. CDR3 sequences are highlighted in red.

YF1_alpha TRAV12-2

GGATCCATGCAGAAAGAGGTGGAACAGAATAGCGGCCCGCTGAGTGTGCCTGAAGGTGCCATTGCCAGCCTGAACTGCACCT
ATAGCGATCGCGGCAGCCAGAGCTTTTTCTGGTACCGCCAGTATAGCGGCAAGAGCCCGGAACTGATTATGTTTCATCTATAGT
AATGGCGATAAAGAGGACGGCCGCTTTACCGCCAGCTGAATAAGGCCAGCCAGTACGTTAGTCTGCTGATTTCGCGATAGCC
AGCCGAGCGATAGCGCCACCTATTTATGCGCCGTGACCGACGACAAGATCATCTTTGGCAAGGGTACCCGCCTGCATATTCT
GCCGATCCAGAATCCTGATCCTGCCGTTTATCAGCTGCGCGATAGCAAAAGCAGCGACAAGAGCGTGTGTCTGTTTACCGACT
TCGACAGCCAGACCAACGTGAGCCAGAGCAAAGACAGCGACGTGTACATCACCGACAAATGCGTGCTGGACATGCGCAGCAT
GGACTTCAAAGCAACAGCGCCGTGGCTGGAGCAACAAAGCGATTTTGCCTGCGCCAACGCATTCAACAACAGCATCATC
CCGGAAGACACCTTCTTCCGAGTCCGGAAGCAGCTAATAAGAATTC

YF1_beta TRBV6-8

GGATCCATGAATGCCGGTGTGACCCAGACACCGAAGTTCCACATTCTGAAGACCGGCCAGAGCATGACCCTGCAGTGCGCC
AGGATATGAACCATGGCTATATGAGCTGGTACCGCAAGATCCGGGTATGGGCCTGCGTCTGATCTACTATTCTGCAGCCGC
CGGTACCACCGATAAAGAAGTGCCGAACGGCTACAACGTTAGCCGCCTGAACACCGAGGATTTTCCGCTGCGCCTGGTGAGT
GCCGCACCGAGTCAAGACCAGCGTGTATCTGTGCGCCAGCAGCTATAGCCGACCGGCAGCTATGAGCAGTATTTTGGCCCG
GGTACCCGCTTAACCGTGACCGAGGATCTGAAGAATGTGTTTCCGCCGGAAGTGGCCGTGTTTGAACCTAGCGAAGCCGAGA
TCAGCCACACCCAGAAAGCCACACTGGTGTGTCTGGCCACCGGCTTTTACCCGGATCATGTGGAGCTGAGTTGGTGGTGAA
TGTTAAAGAGGTGCACAGCGGTGTGTACCGATCCGAGCCGCTGAAAGAACAGCCGGCACTGAATGATAGCCGTTATGCC
CTGAGCAGTGCCTGCGTGTGAGTGCCACCTTTTGGCAAGATCCTCGTAACCATTTCCGCTGCCAGGTGCAGTTCTACGGCC
TGAGTGAAAACGACGAATGGACCCAGGATCGCGCAAACCGGTGACCCAGATTGTGAGCGCAGAAGCATGGGGTGCAGCAG
ATAATAAGAATTC

YF3_alpha TRAV12-2

GGATCCATGCAGAAAGAGGTGGAACAGAATAGCGGCCCGCTGAGTGTGCCTGAAGGTGCCATTGCCAGCCTGAACTGCACCT
ATAGCGATCGCGGCAGCCAGAGCTTTTTCTGGTACCGCCAGTATAGCGGCAAGAGCCCGGAACTGATTATGTTTCATCTATAGT
AATGGCGATAAAGAGGACGGCCGCTTTACCGCCAGCTGAATAAGGCCAGCCAGTACGTTAGTCTGCTGATTTCGCGATAGCC
AGCCGAGCGATAGCGCCACCTATTTATGCGCCGGTGGTGACGACAAGATCATCTTTGGCAAGGGTACCCGCCTGCATATTCT
GCCGATCCAGAATCCTGATCCTGCCGTTTATCAGCTGCGCGATAGCAAAAGCAGCGACAAGAGCGTGTGTCTGTTTACCGACT
TCGACAGCCAGACCAACGTGAGCCAGAGCAAAGACAGCGACGTGTACATCACCGACAAATGCGTGCTGGACATGCGCAGCAT
GGACTTCAAAGCAACAGCGCCGTGGCTGGAGCAACAAAGCGATTTTGCCTGCGCCAACGCATTCAACAACAGCATCATC
CCGGAAGACACCTTCTTCCGAGTCCGGAAGCAGCTAATAAGAATTC

YF3_beta TRBV7-2

GGATCCATGGGCGCCGGCGTTAGTCAGAGCCCGAGCAATAAAGTGACCGAGAAGGGCAAAGACGTGGAAGTGCAGTGCAGT
CCGATTAGCGGCCATACCGCCCTGTATTGGTATCGCCAGAGTCTGGGCAAGGCCTGGAGTTTCTGATCTACTTCCAGGGCA
ACAGCGCCCCGATAAAAGCGGTCTGCCGAGCGATCGCTTTAGTGCCGAACGTACCGGTGGTAGCGTGAGCACCCTGACCA
TTCAGCGCACCCAGCAGGAAGACAGTGCCGTGTATTTATGCGCCAGCAGCCAGGGCCTGGCATATGAGCAGTCTTTTGGTCC
GGGCACACGCCTGACCGTGTGGAAGACCTGAAAACGTGTTCCCGCCGGAAGTGGCCGTGTTTGAACCGAGCGAGGCAGA
GATTAGCCATACAGAAAAGCCACCCTGGTGTGCCTGGCCACCGGCTTTTACCCGGATCATGTGGAAGTGCAGTGGTGGGTG
AACGGCAAAGAGTTTATAGCGGCGTGTGTACCGATCCGAGCCGCTGAAGGAACAACCGGCCCTGAATGATAGCCGCTATG
CACTGAGTAGCCGCTGCGCGTTAGTGCAACCTTCTGGCAAGATCCTCGTAACCATTTTTCGCTGTCAGGTGCAGTCTACGGC
CTGAGCGAAAACGATGAATGGACCCAGGACCGTGCCAAACCGGTGACCCAGATTGTGAGTGCAGAAGCCTGGGGCCGTGCC
GACTAATAAGAATTC

YF4_alpha TRAV12-2

GGATCCATGCAGAAGGAAGTGAACAGAATAGTGGTCCGCTGAGCGTTCCGGAGGGTGCCATCGCCAGCCTGAATTGCACCT
ATAGCGATCGCGGCAGCCAGAGTTTCTTCTGGTATCGCCAGTACAGCGGCAAAAGCCCGGAGCTGATCATGTTTCATCTACAG
CAATGGTGACAAAGAAGATGGCCGCTTTACCGCCAGCTGAACAAGGCAAGCCAGTATGTGAGCCTGCTGATTTCGATAGC
CAGCCGAGCGATAGCGCCACCTACCTGTGCGCCGTTAAAGATGCCCGCCTGATGTTCCGGCATGGTACCCAGCTGGTGGTG
AAACCGATTGAGAACCCTGATCCGGCCGTGTATCAGCTGCGCGATAGCAAAAGCAGCGACAAGAGCGTGTGCCTGTTACCG
ACTTTGATAGCCAGACCAACGTGAGCCAGAGCAAGGATAGCGACGTGTATATCACCGACAAGTGCCTGCTGGACATGCGCAG
CATGGACTTCAAAGTAACAGCGCCGTTGCCTGGAGCAATAAGAGCGACTTCGCTGCGCCAATGCCTTCAACAACAGCATCA

TCCCGGAGGACACCTTCTTTCCGAGTCCGGAAAGCAGC TAATAAGAATTC
YF4_beta TRBV9
GGATCC ATGGATAGTGGTGTACCCAGACCCCGAAACACCTGATCACCGCAACCGGTGACGCGTTACCCTGCGTTGCAGTC CGCGCAGCGGTGATCTGAGCGTGTACTGGTATCAGCAGAGCCTGGATCAGGGTCTGCAGTTTCTGATCCAGTACTATAACGG TGAAGAGCGCGCCAAAGGCAACATTCTGGAGCGCTTAGCGCCAGCAGTTCCCGGATCTGCATAGCGAGCTGAACCTGAGC AGCCTGGAAGTGGGCGATAGCGCCCTGTATTTTTGCGCAAGTAGCGTGGAGGGTCCGGGTGAAGTGTTTTTGGCGAAGGTA GCCGCCTGACCGTGCTGGAAGACCTGAAGAACGTGTTTCTCCGGAAGTTGCCGTGTTGAACCGAGCGAGGCCGAGATTAG CCATACCCAGAAAGCCACCCTGGTGTGTCTGGCCACCGGTTCTATCCGGATCATGTGGAAGTGAAGTGGTGGTGAACGGC AAGGAAGTGCACAGCGCGTGTGTACAGATCCGAGCCGCTGAAAGAACAGCCGGCACTGAATGATAGCCGCTATGCACTGA GCAGCCGCTGCGCGTTAGTGCCACCTTTGGCAAGATCCTCGCAACCATTTTCGCTGTGAGGTGCAGTTCTACGGCCTGAG CGAAAATGATGAGTGGACCAAGACCGCGCAAACCGGTGACCCAGATTGTTAGCGCCGAAGCATGGGGTGCAGCCGAT TAA TAA GAATTC
YF6_alpha TRAV12-2
GGATCC ATGCAGAAAGAGGTGGAACAGAATAGCGGCCCGCTGAGTGTGCCTGAAGGTGCCATTGCCAGCCTGAACTGCACCT ATAGCGATCGCGCAGCCAGAGCTTTTTCTGGTACCGCCAGTATAGCGGCAAGAGCCCGGAAGTGAATTATGTTTCATCTATAGT AATGGCGATAAAGAGGACGGCCGCTTACCGCCAGCTGAATAAGGCCAGCCAGTACGTTAGTCTGCTGATTCGCGATAGCC AGCCGAGCGATAGCGCCACCTATTTATGCGCCGTGGGTAGCGACAAGATCATCTTTGGCAAGGGTACCCGCCTGCATATTCT GCCGATCCAGAATCCTGATCCTGCCGTTTATCAGCTGCGCGATAGCAAAAGCAGCGACAAGAGCGTGTGTCTGTTACCGACT TCGACAGCCAGACCAACGTGAGCCAGAGCAAAGACAGCGACGTGTACATACCGACAATGCGTGCTGGACATGCGCAGCAT GGACTTCAAAGCAACAGCGCCGTGGCCTGGAGCAACAAAGCGATTTTGCCTGCGCCAACGCATTCAACAACAGCATCATC CCGGAAGACACCTTCTTTCCGAGTCCGGAAAGCAGC TAATAAGAATTC
YF6_beta TRBV2
GGATCC ATGGAACCGGAAGTGACACAGACCCCGAGCCATCAAGTGACCAGATGGGCCAGGAAGTGAATTCTGCGCTGCGTT CCGATCAGCAACCACCTGTACTTCTACTGGTATCGCCAGATCCTGGGCCAGAAAGTGAATTTCTGGTGAGCTTCTATAACAA TGAAATCAGCGAAAAGAGCGAGATCTTCGACGACCAGTTTAGCGTGAACGCCCGGACGGCAGTAATTTCACTGAAAATCC GCAGCACCAAACTGGAGGATAGCGCCATGATTTTTGCGCCAGCAGCGAGGCAACAGGTGCCAGCTACGAACAGTATTTCCG TCCGGGTACCCGTCTGACCGTGACCGAAGACCTGAAGAACGTGTTTCCGCCGGAAGTGGCCGTTTTGAACCGAGTGAAGCC GAGATTAGCCACACCCAGAAAGCCACCCTGGTGTGCCTGGCAACCGGTTTTTACC GGATCATGTGGAAGTGAAGTGGTGGG TTAACGGCAAAGAAGTTCACAGCGGCGTGTGCACCGACCCGACCGCTGAAAGAACAGCCGGCCCTGAATGACAGTCGTTA TGCCCTGAGCAGCCGTCTGCGCGTTAGCGCCACCTTTGGCAAGATCCTCGCAACCCTTTTCGCTGCCAGGTGCAGTTCTAT GGCCTGAGCGAGAACGACGAATGGACCCAGGATCGCGCAAACCGGTGACCCAAATTGTGAGTGCCGAAGCCTGGGGTCTG GCCGAT TAATAAGAATTC
YF15_alpha TRAV12-2
GGATCC ATGCAGAAAGAAGTGAACAGAATAGCGGCCCGCTGAGCGTTCCGGAAGGTGCAATTGCCAGCCTGAATTGCACCT ACAGCGATCGCGCAGCCAGAGCTTTTTCTGGTACCGCCAGTATAGCGGCAAAAGCCCGGAAGTGAATTATGTTTATTTATAGC AACGGCGATAAAGAGGATGGCCGCTTACCGCCAGCTGAATAAGGCCAGCCAGTACGTGAGCTTACTGATTCGCGATAGCC AGCCGAGCGATAGCGCCACCTATCTGTGCGCCGTGGATACCAATGCCGGTAAGAGCACCTTCGGCGATGGTACCACCCTGAC CGTGAAGCCGATCCAGAATCCTGATCCTGCCGTGTATCAGCTGCGCGACAGCAAAAGCAGCGATAAGAGCGTGTGCCTGTTT ACCGACTTCGACAGCCAGACCAATGTGAGCCAGAGCAAGGATAGCGACGTGTACATTACCGACAAGTGCCTGCTGGACATGC GCAGCATGGACTTCAAGAGCAATAGCGCCGTGGCCTGGAGCAACAAAGCGATTTTCGATGTGCCAACGCCTTCAACAACAG CATCATCCCGGAGGATACCTTCTTTCCGAGCCCGAGAGCAGT TAATAAGAATTC
YF15_beta TRBV9
GGATCC ATGGATAGCGCGTGACCCAGACCCCGAAACACCTGATCACCGCCACCGGTGACGCGTTACCCTGCGTTGTAGCC CGCGTAGCGGTGACCTGAGCGTGTATTGGTACCAGCAGAGCCTGGATCAGGGTCTGCAGTTTCTGATCCAGTACTACAACGG CGAAGAAGTGCCTGCAAGGCAACATCCTGGAACGCTTAGCGCCAGCAGTTTCCGGATCTGCACAGTGAAGTGAATCTGAGT AGCCTGGAGCTGGGTGATAGCGCCCTGTATTTTTGCGCCAGCAGCGTTAGCGGCAGCAGCTACGAACAGTATTTGGTCCGG GTACCCGCCTGACCGTGACCGAAGACCTGAAGAATGTGTTTCCGCCGAGGTGGCCGTGTTTGAACCGAGCGAAGCCGAGA TCAGTCATACCCAGAAAGCCACCCTGGTGTGCCTGGCAACCGGTTCTATCCGGATCATGTGGAAGTGAAGTGGTGGTGA

```

CGGCAAAGAAGTGCATAGCGGTGTGTGCACCGATCCGCAGCCGCTGAAAGAACAGCCGGCCCTGAACGATAGCCGCTATGC
CCTGAGCAGCCGTCTGCGTGTAGTGCCACCTTTTGCAAGATCCTCGCAATCATTTCGCTGCCAGGTGCAGTTTTACGGCC
TGAGCGAAAATGACGAGTGGACCCAGGATCGCGCCAAACCGTTACCCAGATTGTTAGCGCCGAGGCATGGGGTTCGCGCCG
ATTAATAAGAATTC

```

Table 6 Optimized nucleotide sequences for E.Coli. 5'BamHI restriction sites are highlighted in yellow, 3'EcoRI restriction sites in pink and 3'UTR in green. BamHI and EcoRI restriction sites are absent from all optimized sequences.

The TCR α and β chains were cloned into the expression vector pGMT7 (Figure 19). First, I digested the pUC57 plasmid containing our sequences and the pGMT7 plasmid using the enzymes BamHI and EcoRI for 2h at 37°C. I ran the digestion products on an agarose gel and cut the band of interest according to their lengths (Figure 20). DNA was purified from the agarose gel using the Wizard® SV Gel and PCR Clean-Up system (Promega).

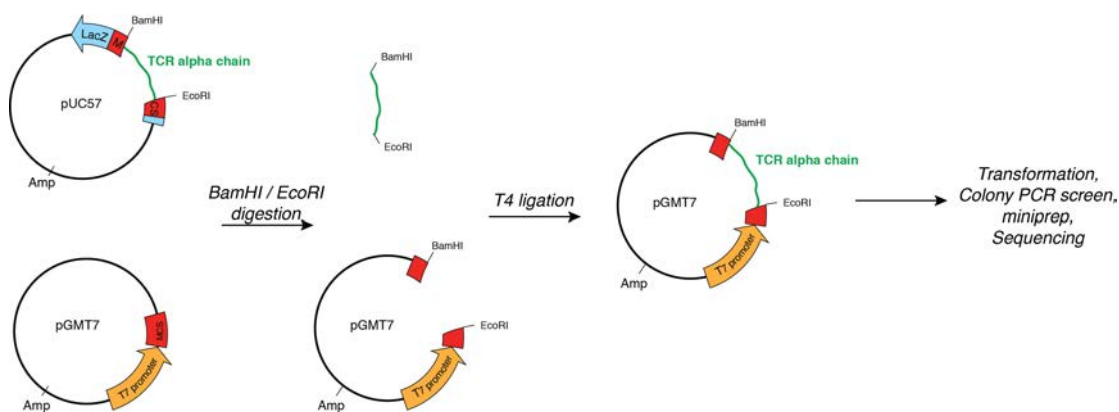


Figure 19 Overview of the cloning process of a TCR chain into the pGMT7 expression vector.

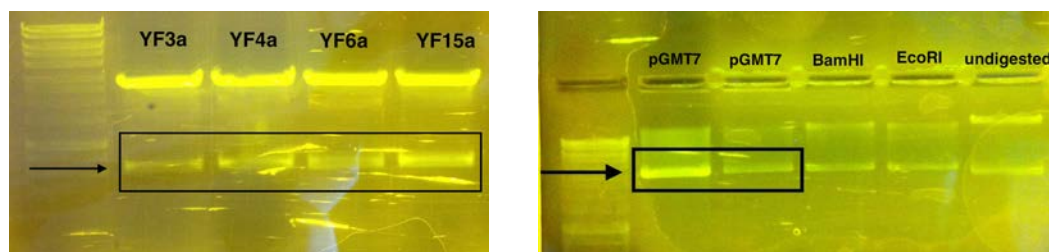


Figure 20 Example of plasmid digestion. Hyperladder™ 1kb Bioline. On the left panel, the inserts are released from the pUC57 plasmid after digestion by the restriction enzymes EcoRI and BamHI (black rectangle). On the right panel, the pGMT7 plasmid is opened up after digestion by the restriction enzymes EcoRI and BamHI (black rectangle).

Next, the digested TCR sequences were ligated to the digested pGMT7 plasmid following this equation:

For 100ng pGMT7:

$$\frac{100ng \times 500 \text{ (size of insert)}}{3000 \text{ (size of pGMT7)}} \times 3 = 50ng \text{ of insert}$$

After 2h at room temperature, we transformed the ligation products into One Shot™ chemically competent TOP10 bacteria (ThermoFisher) and plated the bacteria on CARB⁺ agar plates. Plates were left at 37°C overnight until colonies grew. I picked five colonies per chain and grew them in CARB⁺ LB medium overnight. DNA was isolated from bacteria using the PureLink® Quick Plasmid miniprep kit (Life Technologies). I sent two products per chain for sequencing (Central Biotechnology Services, Cardiff University, Wales). I confirmed that no mutation was introduced in the ligation products. The α and β TCR chains were then inserted into a vector that allows protein expression in *E. coli*.

Expression of TCR chains as inclusion bodies in *E. Coli*, purification and protein refolding

The DNA products were then transformed into BL21 star or Rosetta™ (DE3)pLysS competent bacteria (Promega or Novagen) and plated on CARB⁺ agar plates. The next day, three colonies were picked into 40 ml CARB⁺ TYP medium and shaken at 37°C until the optical density (OD) reached 0.5. These small cultures were transferred to 1L CARB⁺ TYP medium shaken at 37°C. At OD = 0.5, the protein expression as IB was induced by the addition of 1mM IPTG for 3 hours. An aliquot was taken to check the protein expression and purity of the IB (Figure 21). It is important to note that all α chains took longer to reach the expected OD compared to the β chain, suggesting that these constructs were somehow toxic to the bacterial cells. The cultures were then centrifuged for 20min at 4'000rpm and pellets were kept for IB purification. The Rosetta™ bacteria were growing very slowly compared to BL21 bacteria (data not shown). Furthermore, they led to sticky IB. Therefore, we decided to transform only BL21 star (DE3)pLysS competent bacteria (Promega) for the next experiments.

Purified IB of α and β chains were opened up with 20mM DTT at 37°C for 15min. The α and β chains were then added sequentially with a ratio 1:1 to the refold buffer (2.5M Urea) at 4°C. The next day, the refold buffer containing both chains were transferred to a dialysis tube into 20L of cold water for 10 hours and again into a fresh 20L of cold water overnight.

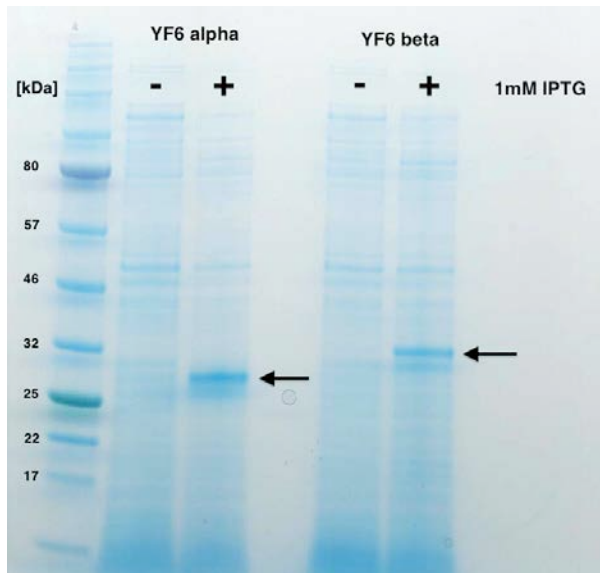


Figure 21 Example of inclusion bodies purity. YF6 α and β chains were produced as inclusion bodies in E.Coli. Although the protein of interest was overexpressed (arrow), several contaminants remained in the preparation, hence the need to purify the inclusion bodies before refolding the TCR.

Protein purification by anion exchange chromatography

The first step of protein purification involves anion exchange chromatography. It consists in the attraction of negatively charged molecules such as proteins to a positively charged ion exchange resin. The mobile phase has a low conductivity (10mM Tris), which favors the binding of the proteins to the column. The proteins are then eluted from the column by applying a linear salt gradient (NaCl).

I ran the various refolds on the anion exchange chromatography column (7.9ml POROS® 10/100 HQ 50 μ m). Figure 22 shows an example of the YF6_5001 TCR (YF6) as well as the α 11 β 6 TCR which serves as a positive control. The fractions eluted in the main peak were analyzed by SDS-PAGE followed by Coomassie staining. Under non-reducing conditions, this staining revealed that some fractions contained a

potential refolded TCR at a high molecular weight (55kb). However, under reducing conditions, only a band at the size of the β chain was visible. This suggests that the band of high molecular weight might be a homodimer of β chains (35kb). On the contrary, the positive control that was performed side-by-side with the YF6 TCR refold worked as expected: under non-reducing conditions, I observed a band at the size of the refolded $\alpha 11\beta 6$ TCR (55kb), whereas both α and β chains are visible under reducing conditions (28kb and 35kb, respectively). None of the other YF TCR refolds led to the production of a soluble refolded TCR. The results of the analysis of the Coomassie gel after anion exchange purification are summarized in Table 7.

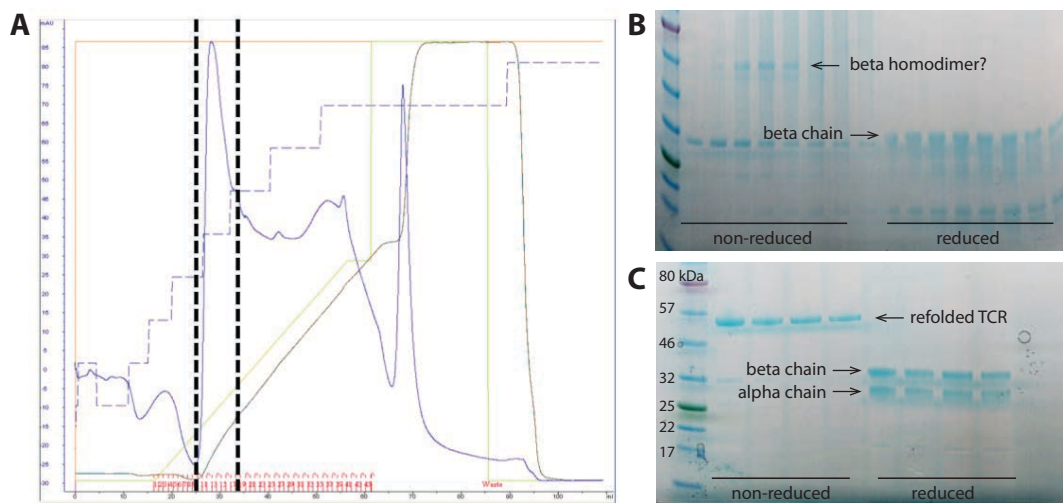


Figure 22 Example of anion exchange chromatography purification step. A, Trace of an anion exchange purification after refolding of the YF6 TCR shows a main peak between the two dotted lines. The TCR and potential contaminants from the IB preparation are eluted by gradually increasing the NaCl gradient (green line) from 0mM to 500mM and all the proteins bound on the column are eventually eluted into the waste fraction with 1M NaCl to regenerate the column. Analysis of the fractions comprised in the main peak of elution by SDS-PAGE under non-reducing and reducing conditions followed by Coomassie staining allows the discrimination of the fractions containing the protein of interest. The YF6 TCR is shown in B, whereas the $\alpha 11\beta 6$ TCR is shown in C as a positive control.

TCR	Reducing conditions	Non-reducing conditions
YF1	Aggregation (smear on the gel)	α and β chains visible
YF3	no visible band at the expected size	only β chain visible
YF4	no visible band at the expected size	only β chain visible
YF6	β chains homodimer	only β chain visible
YF15	Aggregation (smear on the gel)	only β chain visible

Table 7 Summary of anion exchange chromatography purification.

Troubleshooting

To minimizing the aggregation, I added arginine to the refold buffer (2.5M Urea + 400mM arginine). Arginine is one of the most commonly used folding helps for the recovery of soluble proteins from IBs [162] [163]. However, I did not observe any improvement in terms of aggregation upon addition of arginine in the buffer. Nevertheless, to maximize chances, I still decided to use the arginine-containing buffer for all refolding experiments (data not shown).

As it seemed that the issue comes mainly from the α chain, I increased the ratio of α and β chains (Figure 23):

- For the YF1, YF3, YF4, and YF15 TCRs, increasing the α : β ratio allowed to observe two visible bands (α and β chains) on the Coomassie gel under reducing conditions. However, only a smear could be detected under non-reducing conditions, suggesting aggregation of the TCR.
- For the YF6 TCR, increasing the α : β ratio allowed to see a faint band corresponding to the α chain in addition to the β chain under reducing conditions. It prevented the formation of the β chains homodimer but rather led to aggregation.

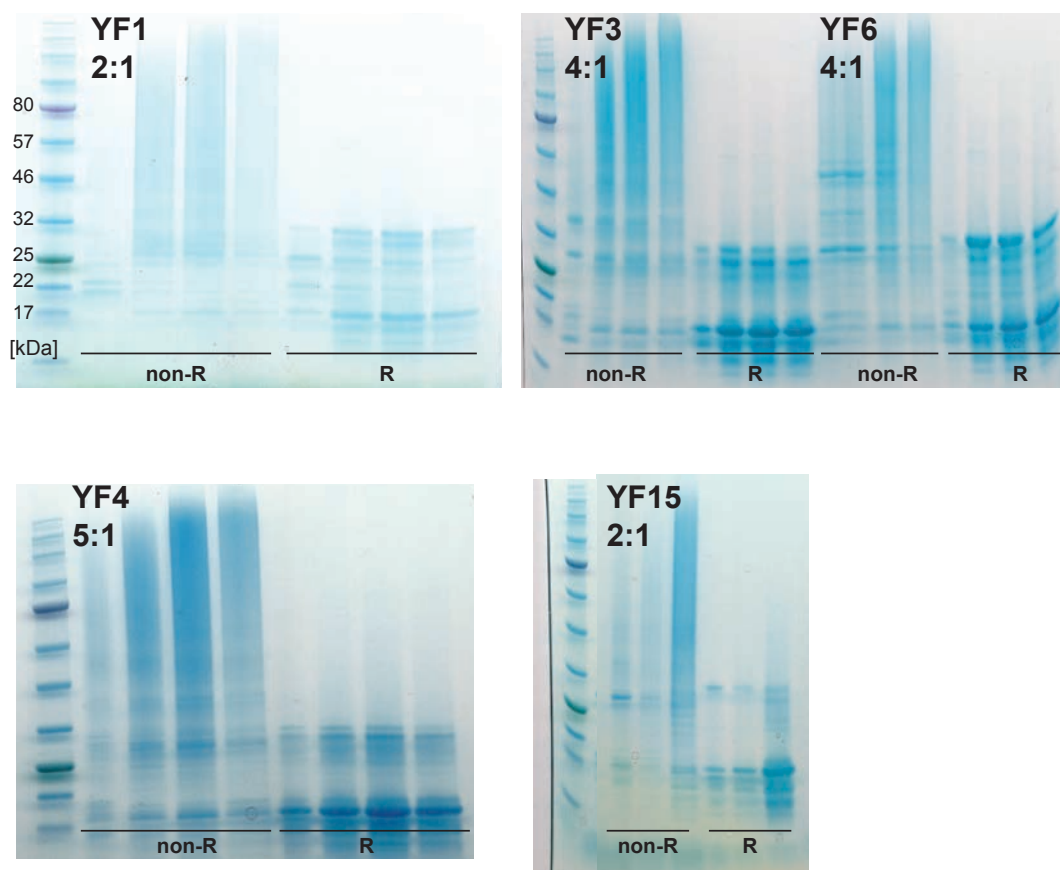


Figure 23 Analysis of the fractions comprised in the main peak of elution after anion exchange chromatography by SDS-PAGE under non-reducing and reducing conditions followed by Coomassie staining. TCR identities and α : β chains ratios are indicated on the figure. “R” stands for “reducing conditions” and “non-R” for “non-reducing conditions.

To confirm that the trouble came from the α chain, we attempted to refold the β chains of our YF TCRs together with the α chain of the MEL5 TCR, which is very similar to ours (all of them are TRAV12-2 positive). The refold of chimeric TCRs worked for the β chain of the YF3, YF4 and YF15 TCRs. An example is shown in Figure 24A. The β chain of the YF6 TCR only aggregated with the α chain of the MEL5 TCR (data not shown). We did not test the β chain of the YF1 TCR.

After anion exchange chromatography, fractions containing the chimeric TCRs were pooled, concentrated and purified by several steps of gel filtration (24ml Superdex 200 10/300 GL column) (Figure 24B). Gel filtration chromatography columns separate proteins on the basis of their size. Proteins move through a stationary phase composed of porous beads. Molecules that are too large to enter the pores stay in the mobile

phase move through the column more quickly and elute first, while smaller molecules diffuse further into the pores and therefore move more slowly. Several steps of gel filtration purification allow having a pure product of refolded TCR that could be further used to solve the crystal structure and perform binding affinity assays and thermodynamics by SPR.

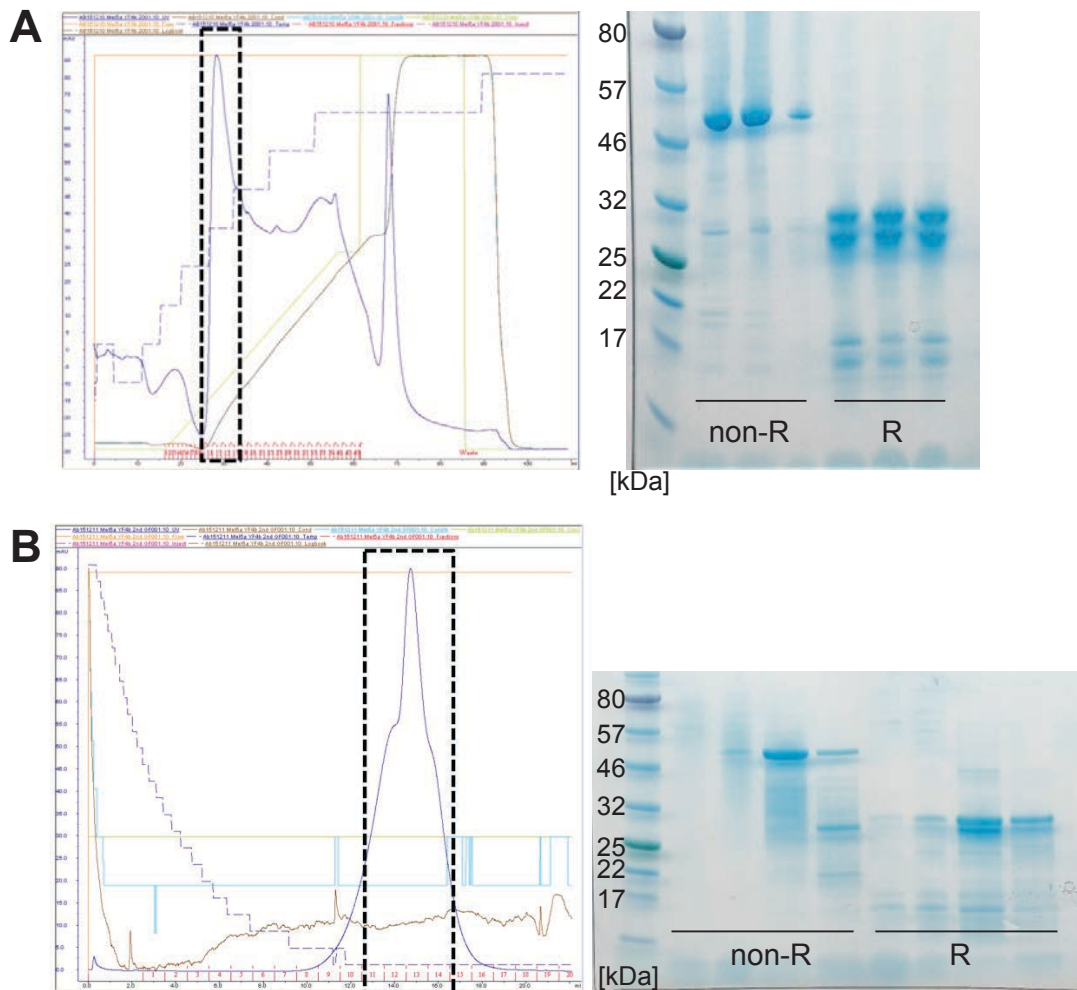


Figure 24 Example of a chimeric TCR containing the α chain of the MEL5 TCR and the β chain of the YF4 TCR. A, Trace of an anion exchange purification after refolding and analysis of the fractions comprised in the main peak of elution highlighted by the dotted rectangle by SDS-PAGE under non-reducing (“non-R”) and reducing (“R”) conditions followed by Coomassie staining. B, Trace of the second step of gel filtration and analysis of the fractions comprised in the dotted rectangle by SDS-PAGE under non-reducing (“non-R”) and reducing (“R”) conditions followed by Coomassie staining. The third analyzed fraction contains pure refolded TCR as no contaminants were detectable.

IBs are the results of cytoplasmic accumulation of recombinant proteins in *E. Coli*. They offer a high level of protein expression. However, they are often present as insoluble aggregates devoid of biological activity [164]. As the conventional method of refolding insoluble IBs by dialysis did not work, I tried to extract the insoluble proteins from *E. Coli*. This involves a purification step on a HiTrap Q HP anion exchange chromatography column (GE Healthcare). Regrettably, the starting material was not sufficient enough to recover any protein from the purification as revealed by the SDS-PAGE (data not shown).

3.1.3.3 Discussion

Before 1987, it was not imagined that pMHC could be successfully produced starting from empty MHC molecules produced in the laboratory (bypassing the restriction of isolating from the naturally bound pMHC) because of the failure of empty MHC to refold, until it was discovered that the MHC heavy chain and the b2m actually pair quite easily when refolded in presence of the cognate peptide [165]. Unlike pMHC complexes, α and β TCR chains hardly refold correctly *in vitro* and are therefore rather insoluble when obtained from expression in *E. Coli*. The first structures of a human and mouse $\alpha\beta$ TCRs were solved in 1996 [28] [29]. Since then, the recovered yield of stable TCR chains has been improved by the introduction of the Boulter disulfide bond as it was used in our experiments [166]. To date, *E. Coli* still makes up for the main system for TCR production as it has the advantages of low cost, higher protein yield and greater procedure speed. Here, I would like to discuss the alternative systems that we could have tested for the production of our YF TCRs.

Eukaryote expression platforms have also been extensively explored. Insect cells have the machinery for folding of mammalian proteins, increasing the chances to obtain a soluble protein. However, these systems are also able to carry out complex post-translational modifications such as glycosylation, which might be then challenging for further crystallization [167].

Human cells can be used for the generation of proteins. It allows transfecting bicistronic vectors encoding both TCR chains separated by a 2A sequence making the ribosome

skip the synthesis [168]. When the 2A sequence is fused in frame between two cistrons, it triggers co-translational “ribosomal skipping”. This contributes to the equimolar expression of the α and β chains and more efficient folding [169]. As for insect cells, human cells induce post-translational modifications to the protein of interest, yet in this case (the human expression context for a human protein) this might provide a proper refolding as the proteins are in their species context. TCRs possess up to seven N-linked glycosylation sites [170]. However, post-translational modifications are often considered as a nuisance in protein crystallography. Especially, glycans, a larger chemical modification, increase surface entropy and reduce favorable crystal contacts [167]. A way to overcome the issue of N-glycosylation is to use an expression system with intact folding and initial glycosylation, but restricted processing of the N-glycans in order to permit subsequent removal by the endoglycosidase H [167] [171]. The development of this strategy was initiated in the lab at a time close before I left, so I did not have the change to test it, knowing that the establishment of such method can take several months (it is still ongoing).

I spent already several months on troubleshooting and alternative methods were not available directly in the lab, thus we decided not to pursue our attempts to refold a YF TCR. Meanwhile, we decided to perform an *in silico* modeling of the YF TCR that had the closest sequence to MEL5 together with the X-ray structure of the cognate pMHC complex as described in the previous Chapter [126].

3.1.3.4 Contributions

I performed all the work presented in the “Results” section after being introduced to the various techniques by Dr. Anna Bulek. Conclusions and troubleshooting were discussed with both Dr. Anna Bulek and Dr. David Cole.

3.1.4 in vivo analysis of the TRAV12-2 bias using the transgenic ABabDII mouse model

3.1.4.1 Background

In order to overcome the limitations of working with human material, we sought whether an appropriate mouse model could be used for YF-17D vaccination. In particular, we considered the importance of recapitulating our observations in the mouse, and sought the model that would allow us to study A2/LLW-specific CD8 T cells, including the TRAV12-2⁺ TCR bias of A2/LLW-specific CD8 T cells and the impact of this bias on the immune response to YF-17D. The group of Prof. Thomas Blankenstein from the Max-Delbrück-Center for Molecular Medicine in Berlin (Germany) has a unique mouse model, the ABabDII transgenic mice, which carry human $\alpha\beta$ TCRs and a single human MHC-I gene: HLA-A*0201 [172]. It was shown that A2/ELA-specific CD8 T cells in ABabDII mice use uniquely TRAV12-2 and have a limited V β repertoire, validating the TRAV12-2 bias observed in human A2/ELA-specific CD8 T cells [172]. Therefore, we could likely use ABabDII to model the TRAV12-2 bias in A2/LLW responses during YF-17D vaccination.

In a collaborative agreement with us, this group performed pilot immunizations with the LLWNGPMAV peptide in their animal facility and shipped to us frozen blood, spleen and thymus. We first needed to address whether the observations in humans after YF-17D vaccination can be validated in the ABabDII mouse model. The initial questions were :

- *Do ABabDII mice mount an A2/LLW-specific CD8 T cell response?*
- *Is the A2/LLW epitope already detectable in the naïve population?*
- *Is this epitope immunodominant in these mice?*
- *Is the TCR usage in these mice similar to that in humans?*
- *Does an SCM CD8 T cell subset also develop in A2/LLW-specific cells in these mice?*

3.1.4.2 Results

A2/LLW-specific CD8 T cell response in ABAbDII mice

ABAbDII mice received subcutaneous injections of 100ug of LLWNGPMAV peptide + 50ug CpG + IFA (Incomplete Freund's adjuvant). Blood samples from 6 naïve and 6 immunized mice were collected and analyzed by flow cytometry at day 7. One part of each sample was used for tetramer staining using a PE-labeled chimeric A2/LLW-specific tetramer enabling mouse CD8 binding (H2-Kb/ LLW). The other part was used for *in vitro* LLW peptide stimulation and subsequent intracellular staining for IFN γ . Immunization with peptide did not induce a response that could be detected by tetramer staining (Figure 25). It is important to note that we deplore a positive control for this experiment.

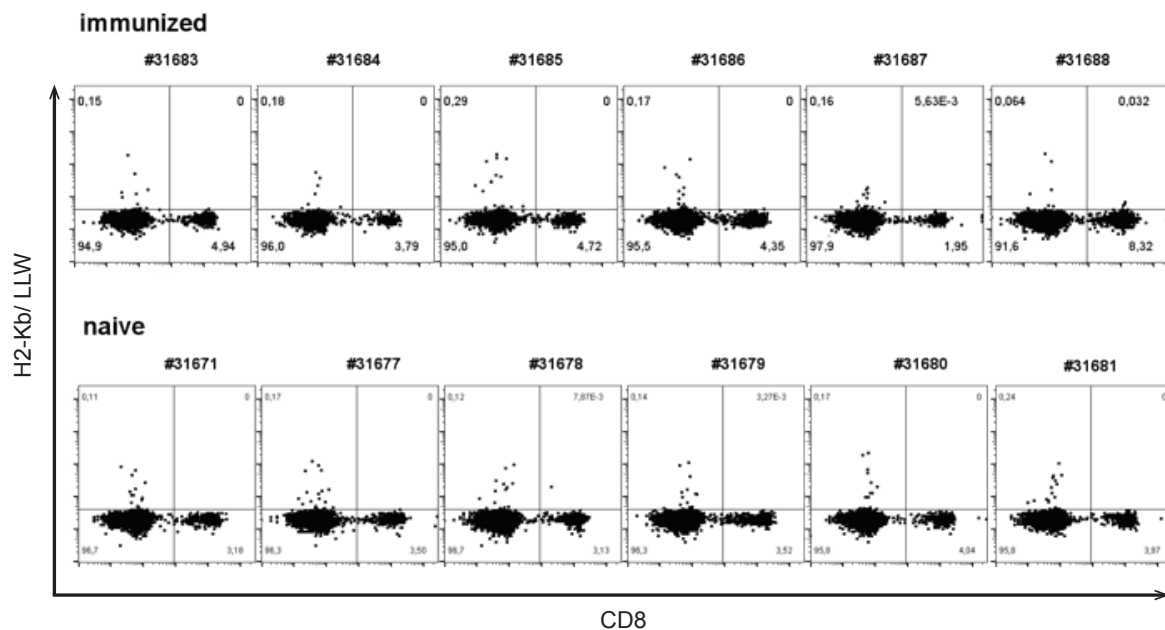


Figure 25 Lack of peripheral A2/LLW-specific CD8 T cell response in ABAbDII mice after first *in vivo* injection of the LLW peptide. Staining of CD8 T cells with PE-labeled H2/Kb/LLW chimeric tetramer and anti-mouse CD8 after gating on CD3-positive lymphocytes from either immunized or naïve mice.

However, 4 out of 6 immunized mice showed a moderate and close to be significant ($p = 0.0545$) specific response to peptide restimulation as demonstrated by the production of IFN γ (Figure 26). This suggests that the peptide is indeed immunogenic in these mice.

expand in splenocytes from the immunized mouse, as shown by the IFN γ production (Figure 27). Detectable tetramer staining was also achieved, however, this tetramer staining intensity was not prominent (Figure 27).

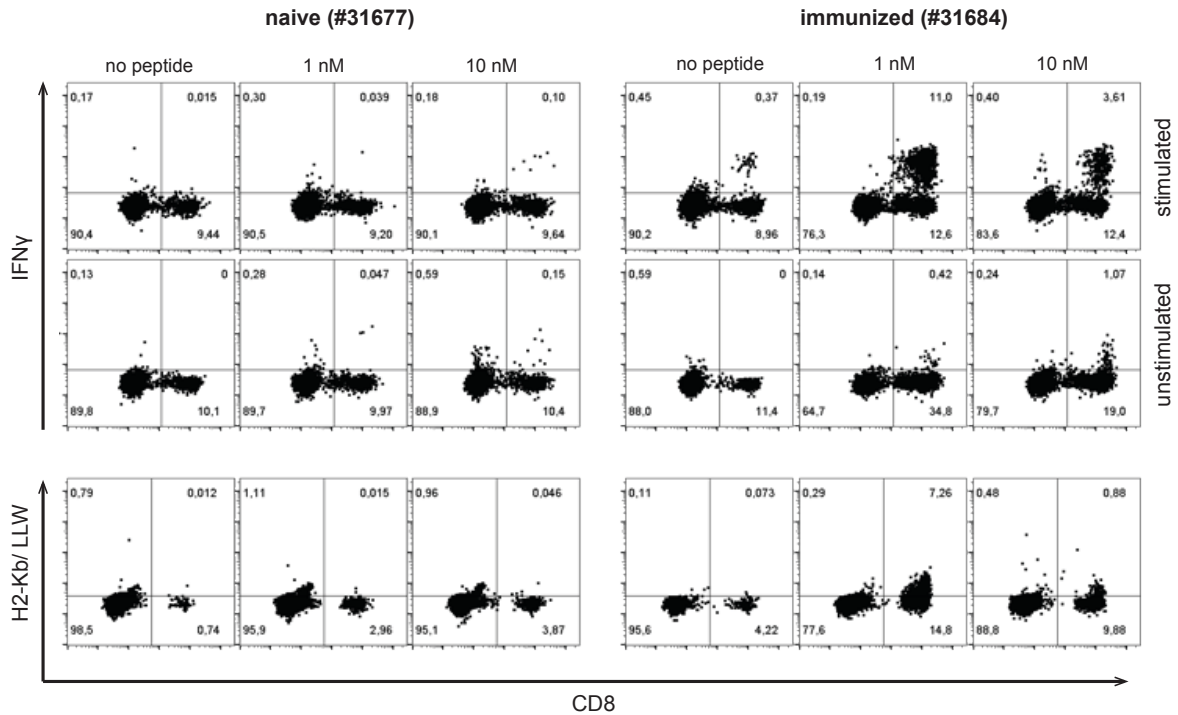


Figure 27 IFN γ production and tetramer staining were monitored in CD8 T cells from splenocytes at day 11 after injection followed by *in vitro* expansion with the LLW peptide for 7 days. Two concentrations were used for expansion: 1nM, 10nM, and a “no peptide” control.

We therefore decided to inject the remaining mice with a booster dose of the peptide (or vehicle for naïve mice) 3 weeks after the first injection (Figure 28). Blood samples were analyzed 7 days after the booster injection. A2/LLW-specific CD8 T cells were detected in all immunized mice (Figure 29).

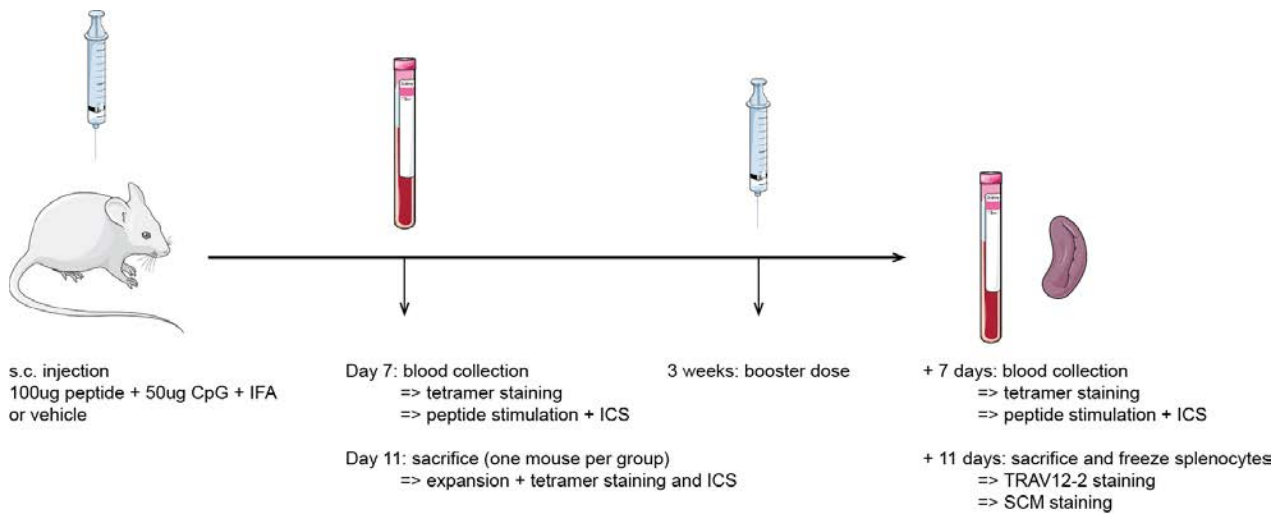


Figure 28 Schematic representing the experimental timeline of LLW peptide injection and samples collection

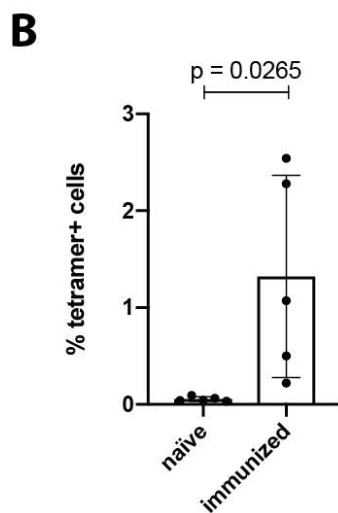
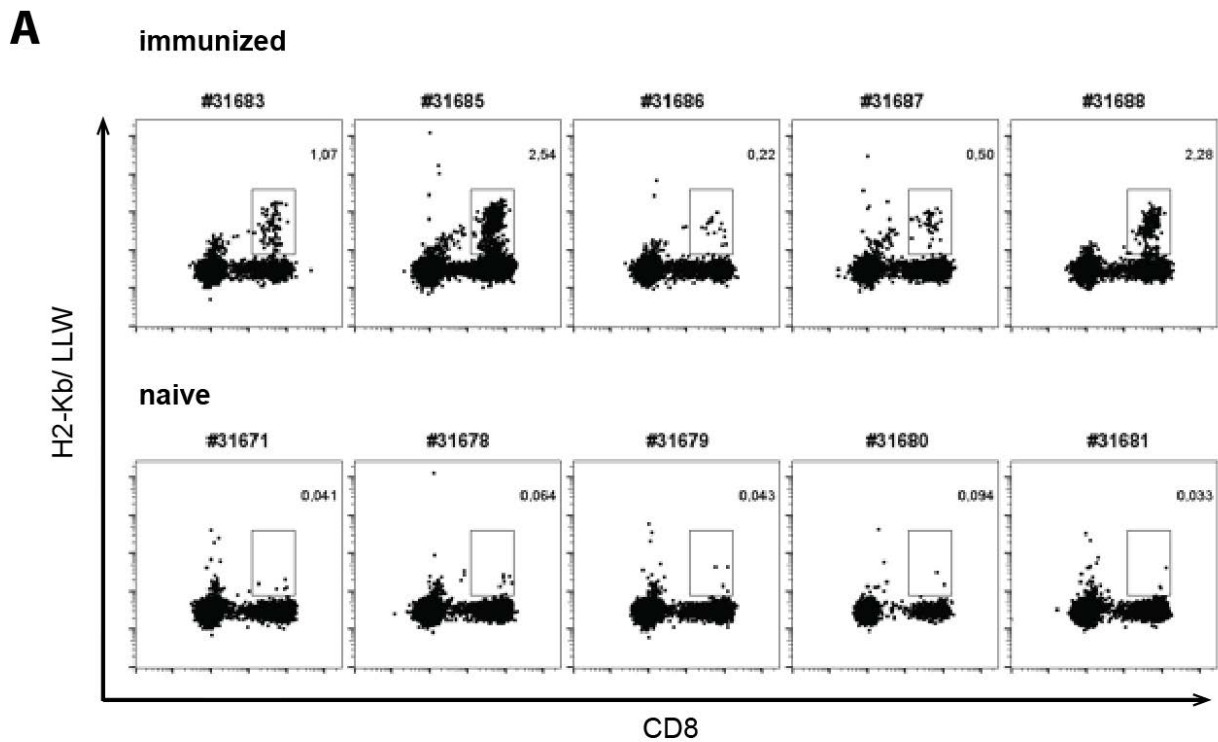


Figure 29 Peripheral A2/LLW-specific CD8 T cell response in ABA_BDII mice after the second in vivo injection of the LLW peptide. Staining of CD8 T cells with PE-labeled H2/Kb/LLW chimeric tetramer after gating on CD3-positive lymphocytes from either immunized or naïve mice. (n = 5 per group). A, Individual dot plots. B, Quantification of tetramer-positive cells and statistical analysis (t-test, p-value is indicated on the graph).

It seems that the intracellular staining for IFN γ after peptide stimulation was not very strong this time (Figure 30). However, the IFN γ production reflects the tetramer response to the peptide.

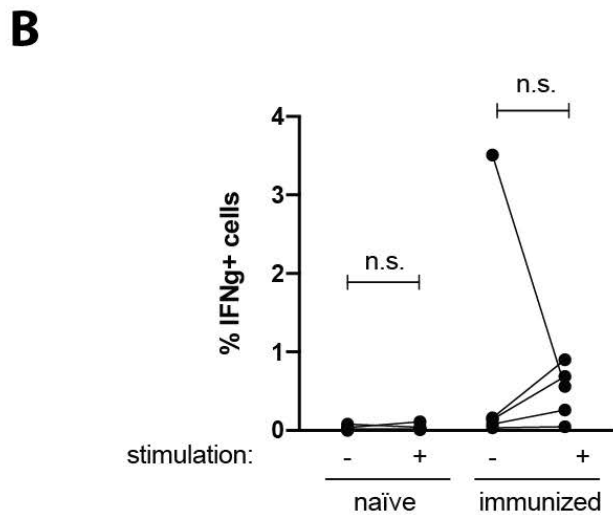
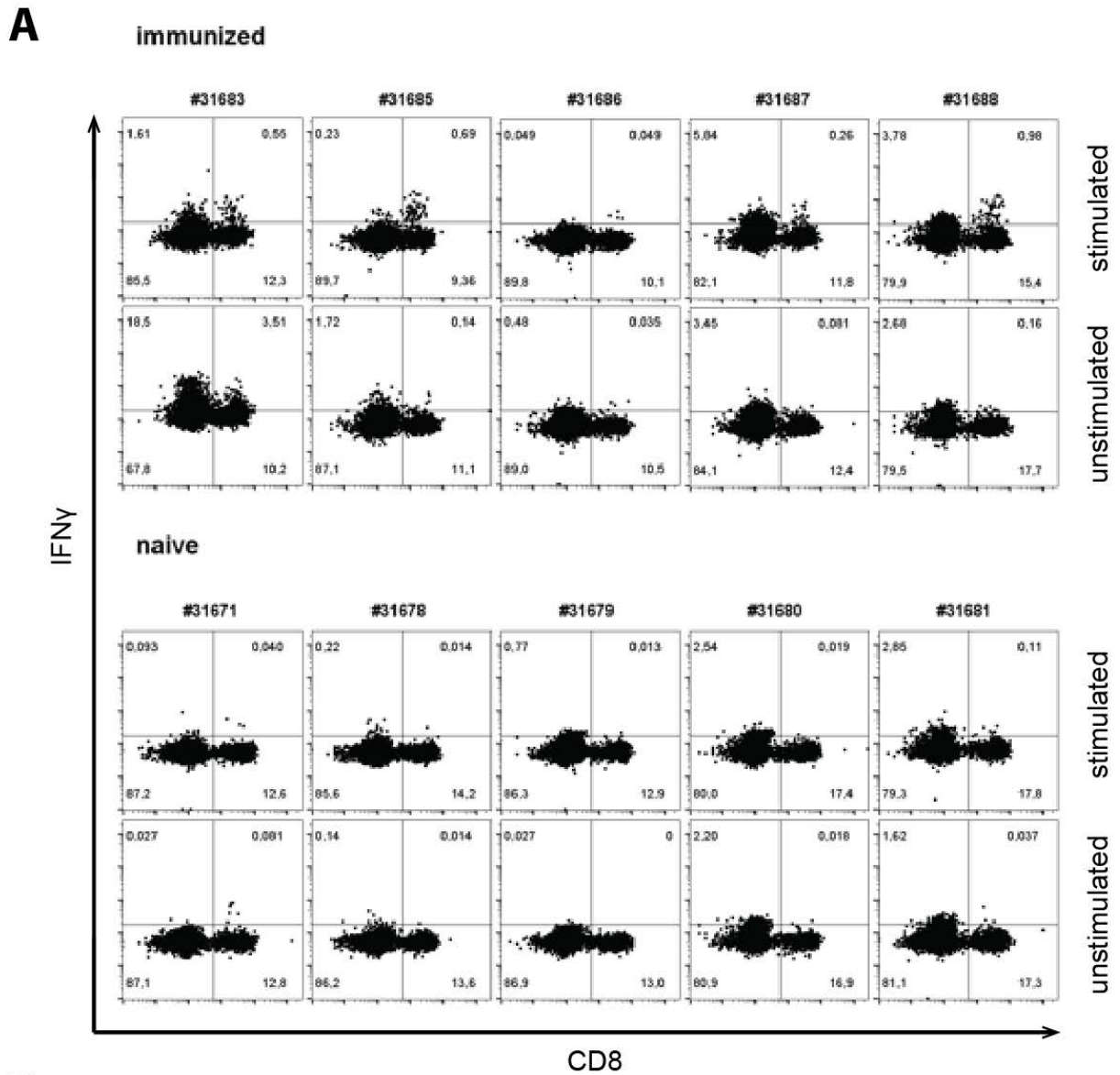


Figure 30 Peripheral IFN γ production after second *in vivo* injection of the LLW peptide in ABA₂DII mice followed by *in vitro* peptide stimulation. Intracellular staining of CD8 T cells after gating on CD3-positive lymphocytes from either immunized or naïve mice ($n = 5$ per group). A, Individual dot plots. B, Quantification of IFN γ -positive cells and statistical analysis (paired t-test, "n.s." = not significant).

Altogether, we concluded that two injections of the LLW peptide are required to induce a detectable A2/LLW-specific CD8 T cell response *ex vivo* in AB*ab*DII mice. Of note, this epitope could not be detected in naïve mice.

TRAV12-2 usage of A2/LLW-specific CD8 T cells in AB*ab*DII mice

We next wondered whether A2/LLW-specific CD8 T cells in AB*ab*DII mice would show a TRAV12-2 bias, similarly to human A2/LLW-specific CD8 T cells [126]. The analysis was carried out directly on frozen splenocytes from immunized mice (in 10%DSMO-90% FCS). We quantified by flow cytometry the TRAV12-2 usage in A2/LLW-specific CD8 T cells compared to total CD8 T cells (Table 8 and Figure 31). The gate of TRAV12-2- positive cells was set according to the staining of the “primary antibody only” sample. The TRAV12-2 segment was already highly expressed by the majority of total CD8 T cells. We did not observe any further enrichment in TRAV12-2 usage in A2/LLW-specific CD8 T cells (median 48.0%) compared to total CD8 T cells (median 54.8%). Actually, the percentage of TRAV12-2- positive cells was even lower in A2/LLW-specific CD8 T cells compared to total CD8 T cells (Figure 31B). This result does not reflect the human TCR bias of A2/LLW-specific CD8 T cells which express TRAV12-2 with a median of 55.5% compared to 12.5% in total CD8 T cells [126]. Alternatively, the fact that AB*ab*DII mice already express high levels of TRAV12-2 might reflect a global bias for TRAV12-2 in this model and mask TRAV12-2 biases in given antigen-specificities.

Marker	Fluorochrome	Company
CD8	Alexa Fluor 700	“in house” LICR
CD44	FITC	“in house” LICR
CD62L	PE-Cy7	eBioscience
CD122	eFluor450	eBioscience
Sca-1	PerCP-Cy5.5	eBioscience
H2-Kb/LLW	PE	TC Metrix
Va2.1	-	Beckman Coulter
Secondary goat anti-rat	APC	BD Bioscience
Live/dead	VIVID-AQUA	Life Technologies

Table 8 Flow cytometry panel used for TRAV12-2 usage and SCM phenotype

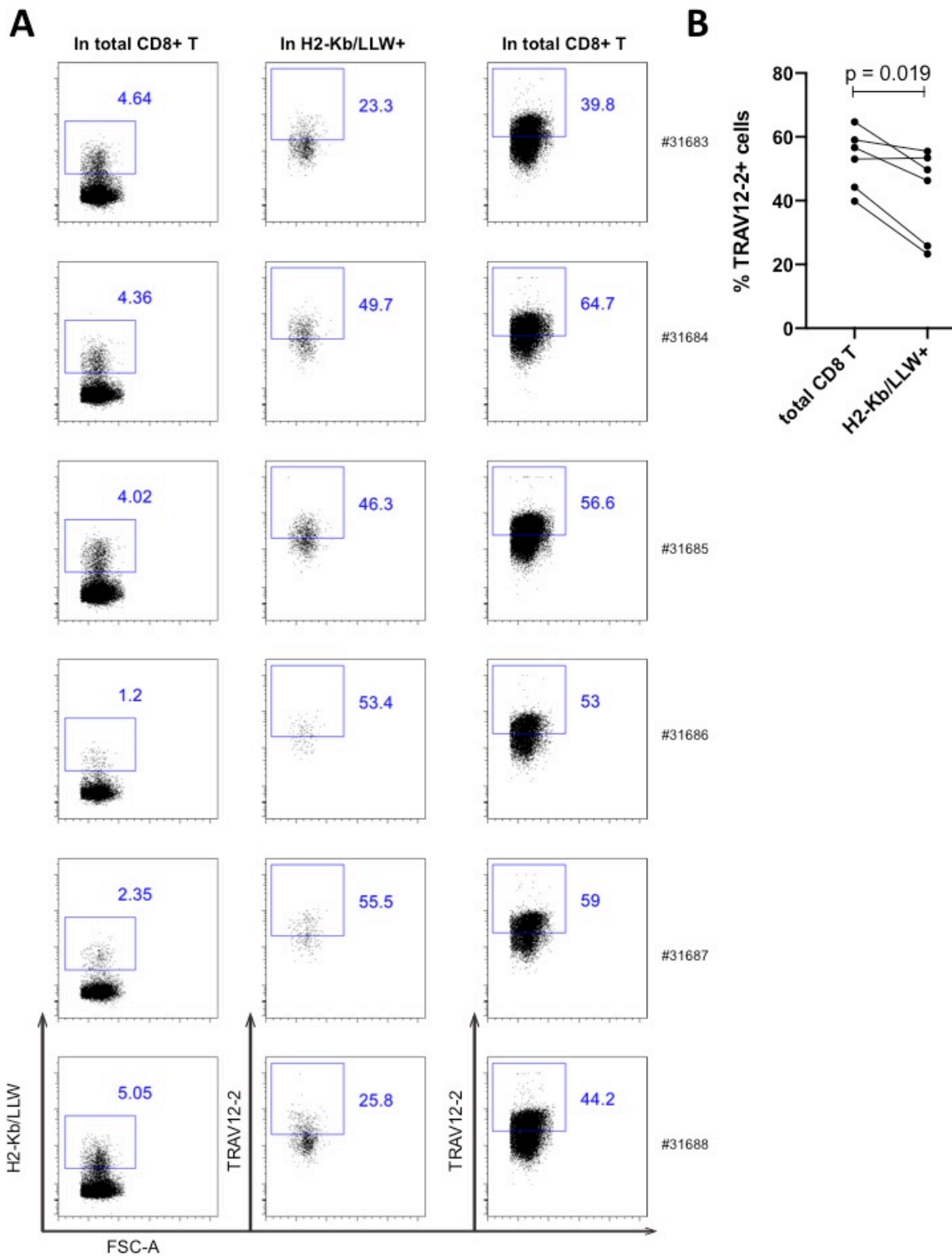


Figure 31 TRAV12-2 usage in splenocytes from immunized *ABAbDI* mice at day 11 after the second injection of the LLW peptide. A, Tetramer staining (left panel) was monitored in total CD8 T cells. TRAV12-2 usage was monitored either in total CD8 T cells (middle panel) or in H2-Lb/LLW-specific CD8 T cells (right panel). (n = 6). B, Quantification of TRAV12-2 expression (paired t-test, p-value is indicated on the graph).

SCM subset in A2/LLW-specific CD8 T cells in ABAbDII mice

The SCM subset was previously described in mice as a CD44^{low} CD62L^{high} population expressing high cell surface levels of stem cell antigen-1 (Sca-1), B cell lymphoma protein-2 (Bcl-2) and common IL-2 and IL-15 receptor β chain (CD122) [173] [174]. Mouse SCM cells were phenotypically defined *in vivo* following allogeneic transplantation [173] or following *in vitro* manipulation with drugs [174] [175]. However, there is no evidence of antigen-specific SCM responses to viral or bacterial antigens in mice. Here we characterized by flow cytometry the surface expression of Sca-1 and CD122 in the naïve compartment (CD44^{low} CD62L^{high}) of A2/LLW-specific CD8 T cells compared to total CD8 T cells (Figure 32). There was no difference in terms of expression levels for both markers, suggesting that immunized mice do not develop an SCM subset in A2/LLW-specific CD8 T cells. This phenotype does not align with the one seen in human studies: A2/LLW-specific CD8 T cells in humans expressed high levels of the SCM markers CD95 and CXCR3 compared to total CD8 T cells in vaccinated individuals [97].

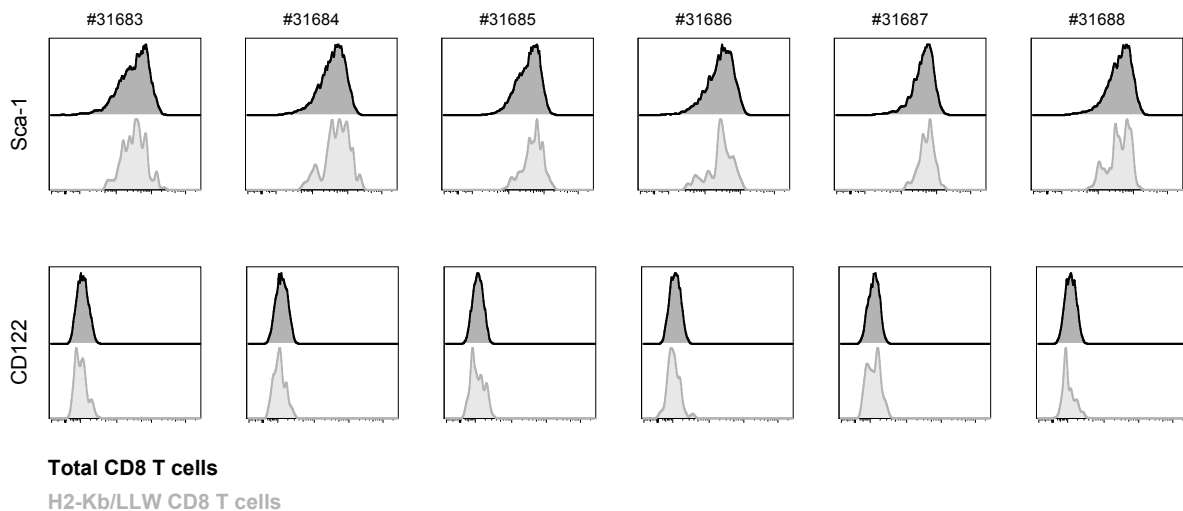


Figure 32 SCM phenotype of splenocytes from immunized ABAbDII mice at day 11 after the second injection of the LLW peptide. Histograms of Sca-1 and CD122 expression after gating on CD44^{low} CD62L^{high} CD8 T cells.

3.1.4.3 Discussion

Compared to mouse models, questions about mechanisms of protection, ontogeny and development of the immune response after YF-17D vaccination and after wild-type YFV infection cannot be readily addressed in humans. We therefore sought of an appropriate mouse model and investigated the CD8 T cell responses specific to YF-17D in ABabDII mice.

Unfortunately, this mouse model turned out to be unsuitable. First, the mice needed 2 doses in order to develop a response that could be detected using a chimeric A2/LLW-specific tetramer enabling mouse CD8 binding. The tetramer positive population could not be detected in unvaccinated (naïve) mice as opposed to the achievable direct *ex vivo* detection of naïve A2/LLW-specific CD8 T cells in humans. Then, we could not observe a TRAV12-2 bias in these mouse A2/LLW-specific CD8 T cells, as opposed to human counterparts. In addition, we could not observe a murine SCM phenotype in of A2/LLW-specific CD8 T cells with the immunization protocol used in these mice. Finally, the mice could not be physically shared with us (only tissue was shipped), making experiments and logistics difficult.

To date, the most relevant animal models to study the YFV are non-human primates (NHP) due to their close relationship to humans and their natural susceptibility to infection. They develop a disease very similar to (yet more severe than) the disease in humans [176]. However, NHP are logistically, costly and ethically challenging to work with. In addition, NHP are outbred leading to a large variability of MHC haplotypes. Therefore, only a few YF-17D studies have been conducted using these models [177]–[180].

Mice are naturally resilient to YFV infection: when the virus is introduced subcutaneously to mimic vaccination, little or no replication is detected [181]. This is mainly due to restriction by type-I interferon [182] [183]. YFV can replicate after SC injection in type-I interferon receptor knockout mice (IFNAR^{-/-}), which lack all type-I interferon responses. However, the IFNAR^{-/-} model is not ideal for the study of T cell responses as the innate immunity is compromised in these mice and this could potentially lead to an impaired activation and proliferation of T cells [184] [185]. Furthermore, type-I interferon is produced by human cells when infected with YF-17D

in vitro [115] [186] [187]. Nevertheless, the effector phenotypes of the YFV-specific T cells induced in these mice appear to be similar to those effectors seen in human studies [181]. More recently, the Syrian golden hamster appeared to model the disease well, although it requires an adapted virus strain [188] [189]. The main disadvantage is the current lack of reagents available for this species.

Thus, there is still an obvious need for an optimal animal model in order to study the mechanisms of protection and the development of the immune response after YF-17D vaccination and after wild-type YFV infection.

3.1.4.4 Contributions

As the ABabDII mice could not be shared with us, Dr. Ioannis Gavvovidis from the group of Prof. Thomas Blankenstein injected the mice at the Max-Delbrücke Center for Molecular Medicine in Berlin. He also performed the initial tetramer and intracellular stainings. He also carried out the freezing of the spleen samples for shipment to Switzerland. A previous PhD student from our lab, Dr. Tim Murray, compared the viability of mouse CD8 T cells after direct or overnight rest staining (data not shown). I optimized and performed the TRAV12-2 and SCM panels stainings.

3.1.5 Characterization of potential superagonist variants of the A2/LLW epitope

3.1.5.1 Background

As presented in 3.1.1, we aimed to examine the TCR:pMHC interface and T-cell functionality using CPL screens to determine the relative TCR-binding strength of the LLW epitope, whether stronger altered versions of the epitope exist. The CPL screen involves the creation of synthetic peptides libraries featuring all possible combinations of amino acids in the nonamer, which are divided into peptide mixtures where one amino acid residue is always fixed at a given position – this pools and greatly diminishes the numbers of tests needed, avoiding to screen all possible peptide combinations individually. Deconvolution allows then discovering individual agonist peptides from the mixture. Usually, a reduced number of candidate peptides are pinpointed from this analysis, which can then be individually tested in further peptide stimulations [190]–[192].

This technique enables the identification of peptide preferences of A2/LLW-specific TCRs and optimal peptide derivatives. In addition, during our attempts to solve a TCR:pMHC complex, super-agonist peptides potentially identified would have been particularly helpful in determining the optimal conditions for crystallization as it is known that crystallization is favored by the use of the strongest TCR-binding peptide.

CPL screens were performed on several A2/LLW-specific TCRs, as reported in our publication on the TRAV12-2 [126]. We decided to focus on and further investigate the YF5048 TCR in the context of the master project of the student that I supervised in 2017/2018, Philippe Delbreil. The aim of his work was to characterize the properties of the agonist variants identified from the CPL screening, focusing on the impact in functionality of the A2/LLW specific CD8 T cell clone LAU5048 NN4 carrying the YF5048 TCR. We wanted to determine whether it is possible to enhance the response to an already potent viral antigen and what are the aspects of the TCR:pMHC interaction that could allow to achieve a better functionality. For this, we studied the influence of the different mutations based on various assays to measure functional avidity, TCR:pMHC molecular interaction, and pMHC stability (Figure 33).

In contrast to tumor antigens, the A2/LLW epitope was shown to be highly potent in terms of functional and magnitude of response [97] [117] [118] [120] [126].

Nevertheless, our work attests that altered peptides improving T cell function exist even for a strongly immunogenic viral epitope. Interestingly, this enhancement was not due to a higher TCR avidity (longer off-rates of binding) but rather to a more rigid pMHC complex relating to lower entropy loss upon TCR:pMHC binding.

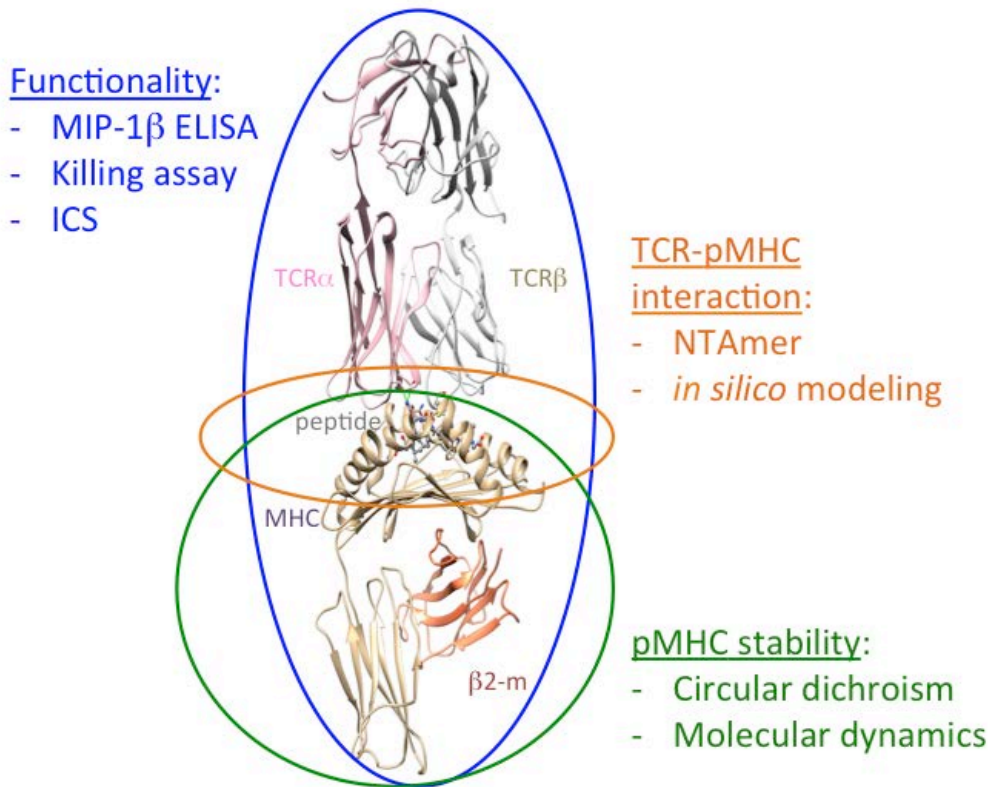


Figure 33 Overview of the parameters analyzed in this section. Influence of the different peptide variants on overall CD8 T cell functionality was examined through an intracellular cytokine staining (ICS) and a flow cytometry analysis measuring CD8 T cell cytokine production, a ^{51}Cr release assay measuring killing capacity, as well as an ELISA measuring the production of the MIP-1b cytokine. The avidity of the TCR-pMHC complex was determined by the monomeric dissociation for each peptide with NTAmer staining. In addition, an *in silico* analysis of the TCR-pMHC interaction was performed to shed some light on the molecular interactions of the complex. Finally, various aspects of pMHC complex stability were examined by circular dichroism and *in silico* analysis of molecular dynamics.

3.1.5.2 Results

Identification of superagonist peptides for the A2/LLW-specific CD8 T cell clone YF5048

The initial phase was to identify candidate superagonist peptides for the A2/LLW epitope binding to YF5048 TCR by performing a CPL screen on the YF5048 clone [126].

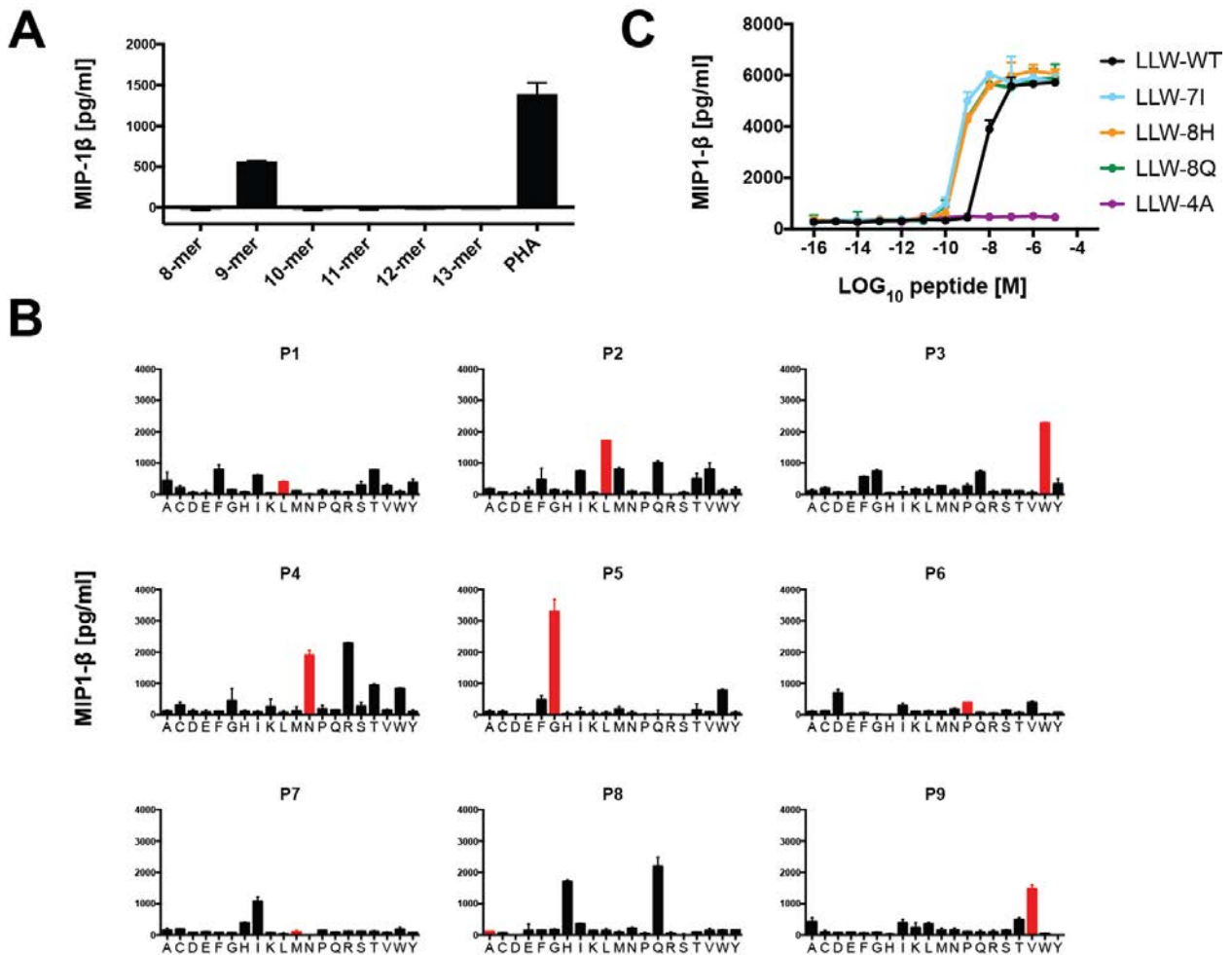


Figure 34 Peptide recognition signature of an individual TCR derived from clone YF5048. A, Peptide length preference is determined by examining functional recognition of a sizing scan comprising random peptide mixtures of different lengths. Values are expressed as the concentration of MIP-1 β secreted in the supernatant measured by ELISA in duplicate (mean and SD). B, Nonamer CPL scan for clone YF5048 assayed by MIP-1 β activation in duplicate (mean and SD). Index peptide residues are represented as red bars. Data are representative of 3 independent experiments. C, Recognition of 3 individual peptides chosen from the CPL assessed by MIP-1 β activation in duplicate with graded concentrations of the peptides (mean and SD).

First, we assessed the peptide length preference of the YF5048 clone by the functional recognition of a custom-built “sizing scan” comprising random peptide libraries of different lengths (8 to 13-mer) [193]. Previous data suggest that CD8 T cell clones exhibit preference for the length of the index peptide [193]: as expected, we validated that the YF5048 clone exhibited a preference for the length of the index peptide (i.e. a 9-mer) (Figure 34A). We thus performed a nonamer CPL screening to assess potential superagonists. Only a few non-index residues at positions 7 and 8 could increase the response compared to the index peptide (Figure 34B). In particular, the CPL results suggested that LLW-7I (LLWNGPIAV), LLW-8H (LLWNGPMHV) and LLW-8Q (LLWNGPMQV) are optimal peptides (Figure 34B). As previously reported, LLW-4R (LLWRGPMAV) failed to activate the TCR [126].

Next, we tested the peptide sequences revealed by the nonamer CPL screening by stimulating with peptides individually (Figure 34C). Indeed, the ELISA confirmed that all three mutant peptides (LLW-7I, -8H and -8Q) induced the expression of the cytokine MIP-1 β at superior levels than stimulation with LLW-WT. The LLW-4A (LLWAGPMAV) peptide served as a negative control (according to our previous report [126]).

We further investigated the functional sensitivity to the mutant peptides revealed by the CPL screening. First, we assessed the killing capacity of the YF5048 clone using a chromium release assay after stimulation with these peptides (Figure 35A and B). Upon titration, the LLW-7I peptide led to an approximately 1-log higher functional sensitivity than LLW-WT (Figure 35A), although only a tendency decrease was observed in EC50 (Figure 2B, data from three independent experiments) (unpaired t-test LLW-WT vs LLW-7I: $p = 0.0384$). The response to the LLW-8H and -8Q peptides were comparable to the LLW-WT peptide (unpaired t-test: $p = 0.0735$ and $p = 0.1700$, respectively).

Second, we compared the degranulation and secretion of cytokines upon stimulation with the various peptides by flow cytometry. Stimulation with titrating amounts of the LLW-7I peptide led to an approximate 1-log increased secretion of all measured cytokines compared to LLW-WT titration (Figure 35C and Figure 36). The calculated EC50 of the LLW-7I peptide titration was approximately 10-fold better than LLW-WT for IFN γ , TNF α and IL-2 (unpaired t-test: $p = 0.0211$, $p = 0.0543$, $p = 0.2186$, respectively) (Figure 35D). Similar effects were observed for the degranulation marker CD107a (unpaired t-test: $p = 0.131$) (Figure 35C and D). The peptides LLW-8H and LLW-8Q did

not improve substantially the functional sensitivity compared to LLW-WT. Also, the LLW-7I peptide induced a higher polyfunctionality at low peptide concentrations compared to the LLW-WT (Figure 37).

Altogether, we showed that the substitution to an isoleucine at P7 in the LLWNGPMAV nonamer results in improved sensitivity (functional avidity) in the YF5048 clone.

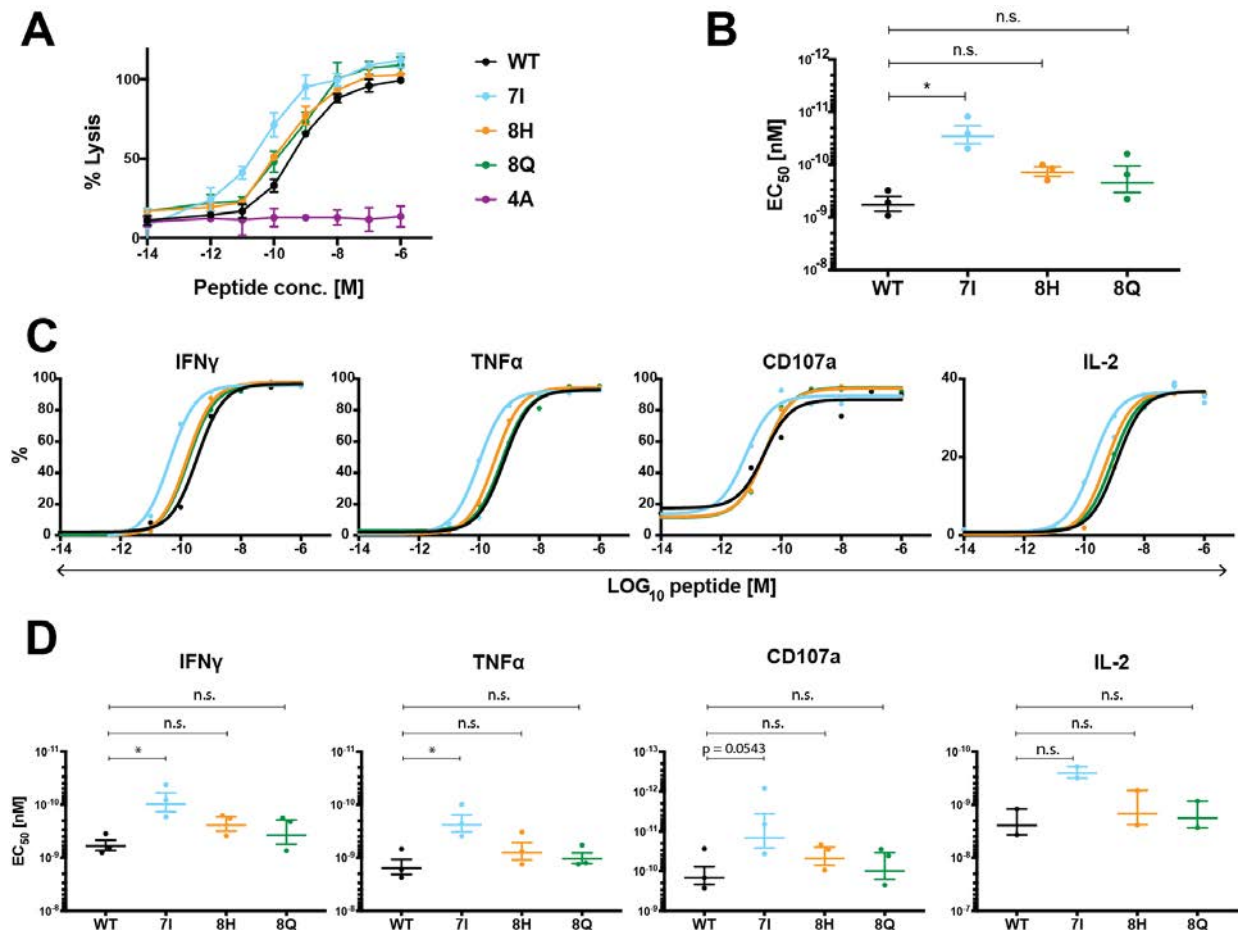


Figure 35 Functional properties of the YF5048 clone following stimulation with mutant peptides identified by the CPL. A, Killing capacity (51-chromium release assay) with titration of the different peptides as indicated. Data are the combination of 3 independent experiments (mean and SEM). B, The EC₅₀ values of the 3 independent 51-chromium release assays shown in A (mean and SEM). Statistical values were obtained from a t-test, * = $p < 0.05$, n.s. = not significant. C, Intracellular cytokine staining following peptides stimulation for 4 hours. Data are the combination of 3 independent experiments (mean and SEM). IL-2 expression was assessed in only 2 independent experiments. D, Values of the 3 independent intracellular cytokine staining are expressed as EC₅₀ (mean and SEM). Statistical values were obtained from a t-test, * = $p < 0.05$, n.s. = not significant.

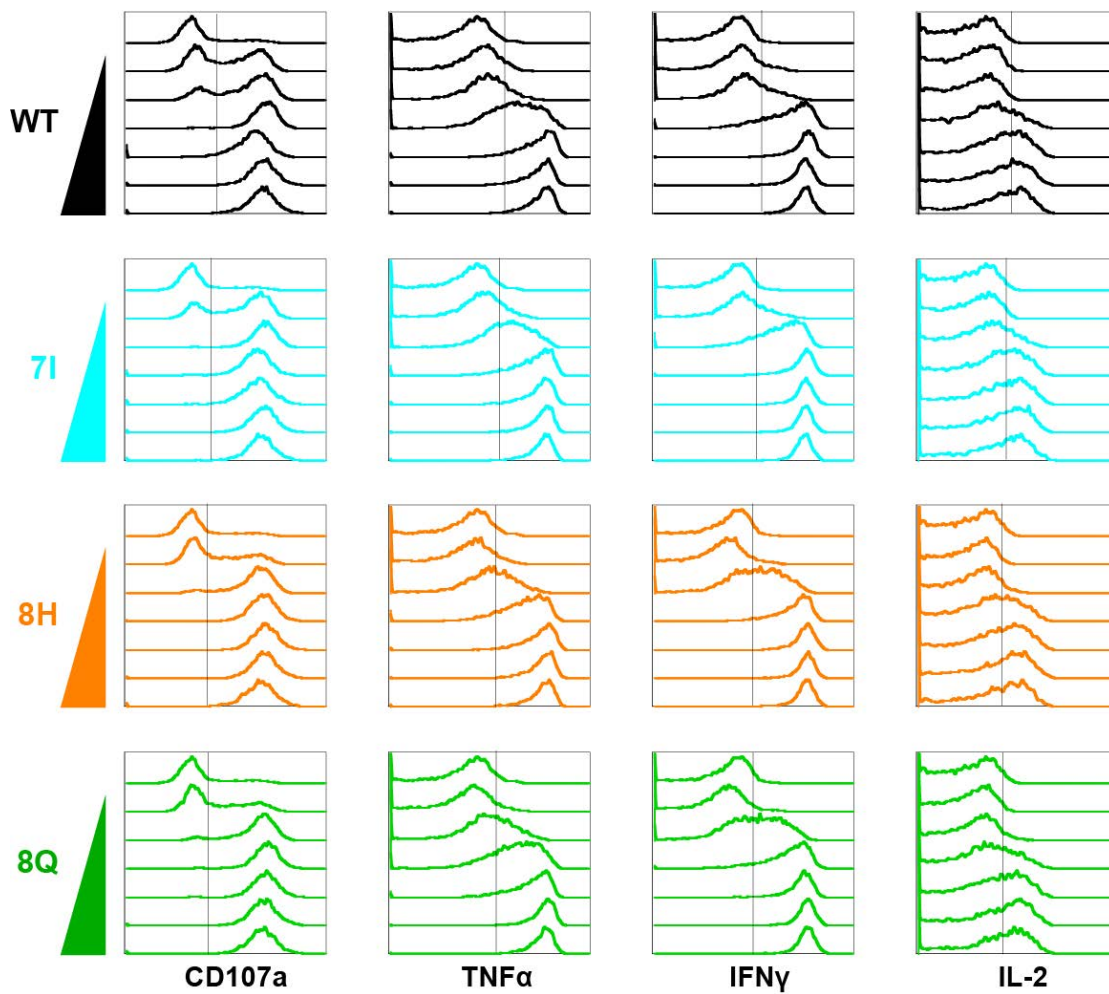


Figure 36 Gating strategy for the intracellular cytokine staining. Staining was performed on the YF5048 NN4 clone following stimulation with T2 cells pulsed with the indicated peptides at concentrations ranging between 10^{-11} and 10^{-6} M. Unpulsed T cell clone is used as negative control. A representative flow cytometry experiment is shown.

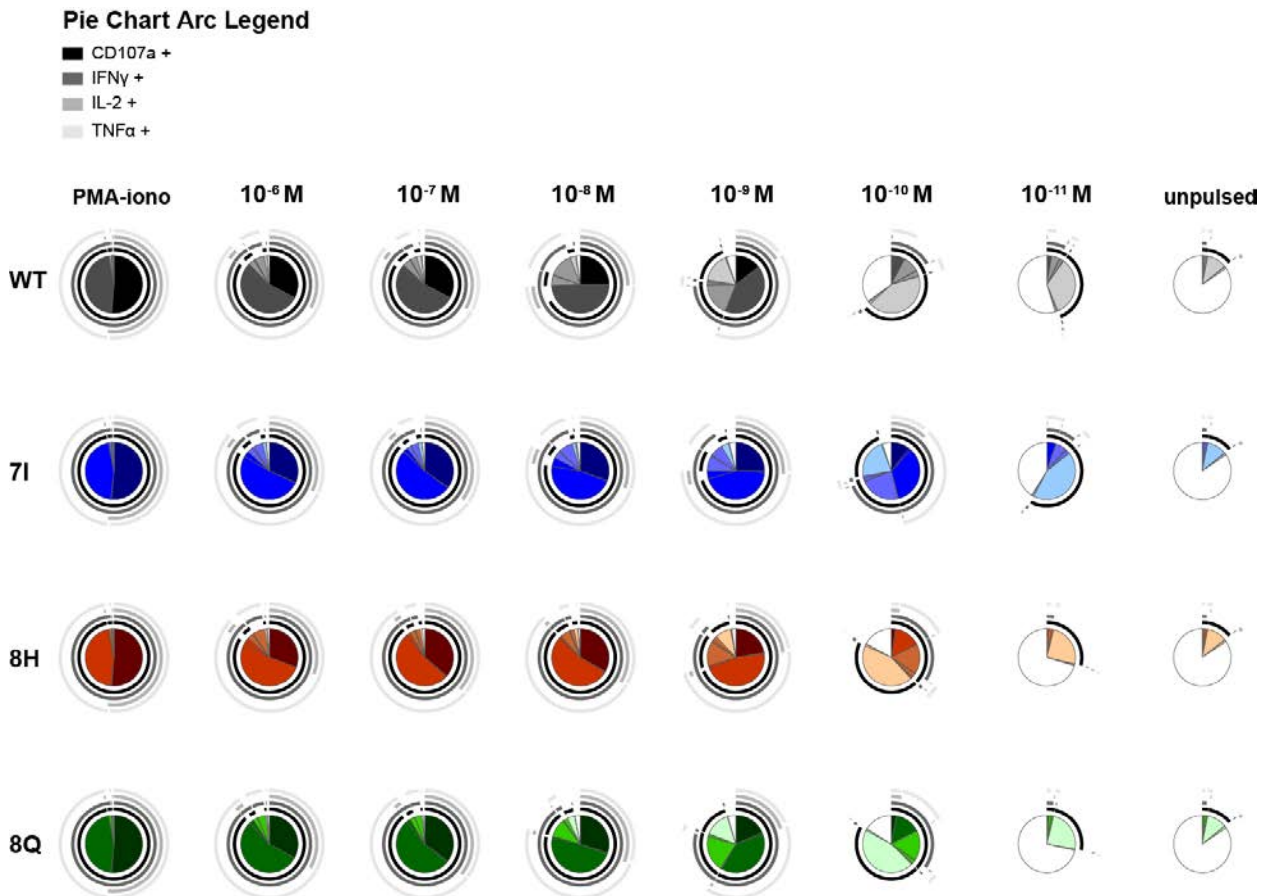


Figure 37 SPICE analysis of a representative intracellular cytokine staining. Pie charts showing frequencies of the combinatorial expression of the indicated cytokines and degranulation marker following stimulation of the YF5048 clone with various peptides at concentrations ranging between 10^{-11} and 10^{-6} M. Color graduation corresponds to the number of simultaneous functions.

The 7I mutation in LLW does not impact the TCR:pMHC off-rate, in contrast to the 8Q and 8H mutations

We hypothesized that the enhanced functional sensitivity of the LLW-7I mutant could be a consequence of a stronger TCR:pMHC interaction. In order to characterize the interaction between the TCR and the agonist pMHC complexes, we first used fluorescently-labeled pMHC multimers at equivalent concentrations and calculated the fluorescence intensity upon staining of the YF5048 clone (Figure 38A) [151] [194]. The A2/LLW-8H and -8Q multimers stained the YF5048 NN4 clone with a slightly stronger intensity (Figure 38A).

Previous reports have linked higher functional avidity specifically to longer TCR:pMHC off-rates [43]–[45] [195] [196]). We next measured the monomeric dissociation constant

rates (k_{off}) using dually labeled pMHC multimers built on NTA-Ni²⁺-His-tag interactions called NTAmers (Figure 39 and Figure 40) [197] [198]. We found that the off-rate k_{off} was highly decreased for A2/LLW-8H and -8Q compared to A2/LLW-WT (unpaired t-test: $p < 0.0001$ and $p < 0.0001$, respectively) (Figure 38B). Rather unexpectedly, no significant difference was observed for the $t_{1/2}$ of A2/LLW-7I compared to A2/LLW-WT (unpaired t-test: $p = 0.1274$), such that changes in off-rates would not explain increased sensitivity of the LLW-7I peptide.

We did not observe changes in PD1 expression (a potential regulator of TCR:pMHC signaling) but we did not examine the expression of other inhibitory receptors or the phosphatase SHP-1 [199] (Figure 41). We think that the relatively short (4h) stimulation used in this experiment does not allow to detect effect on the expression of these regulatory markers.

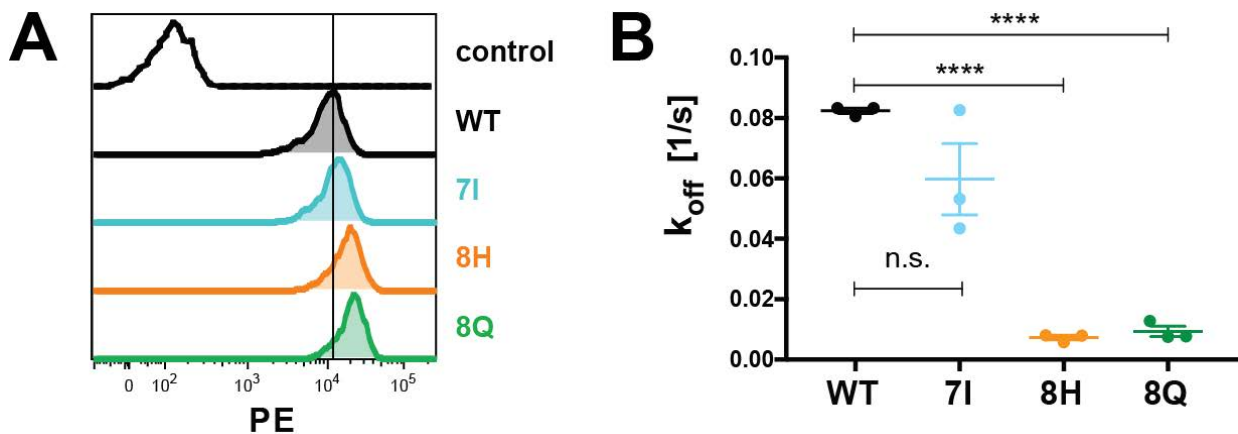
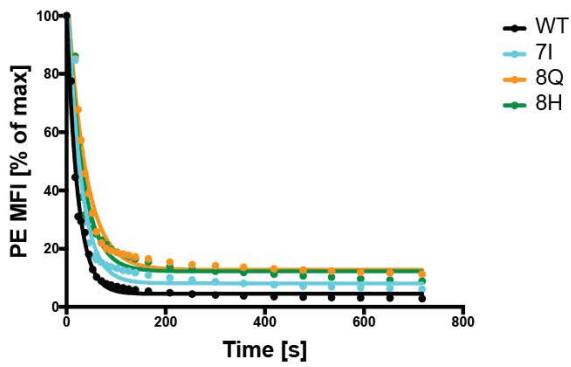
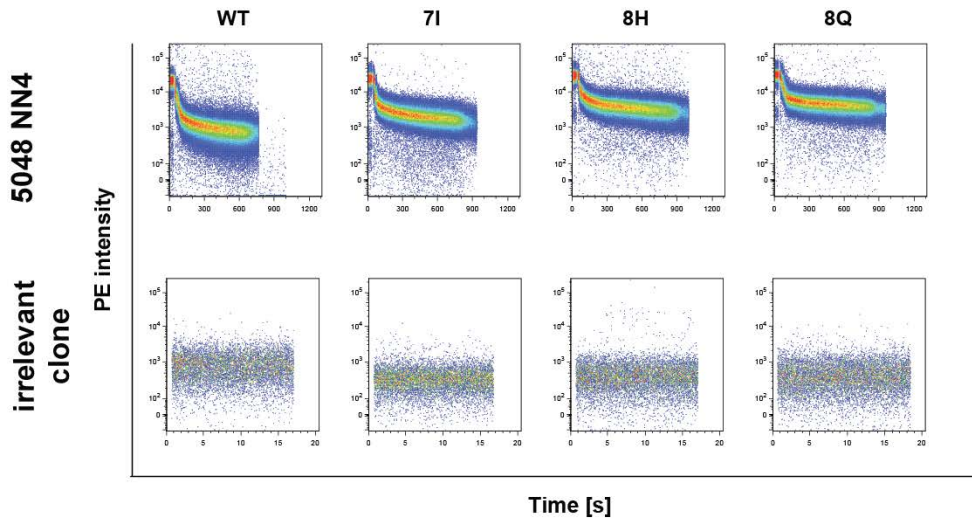
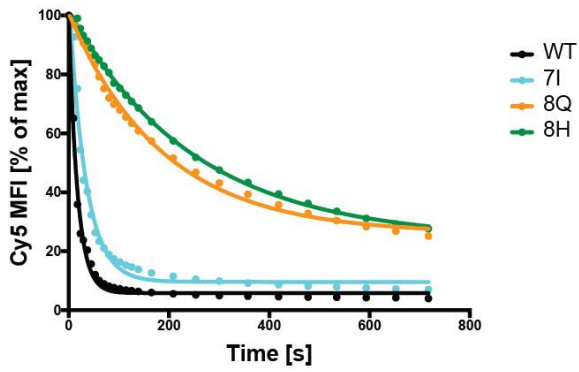
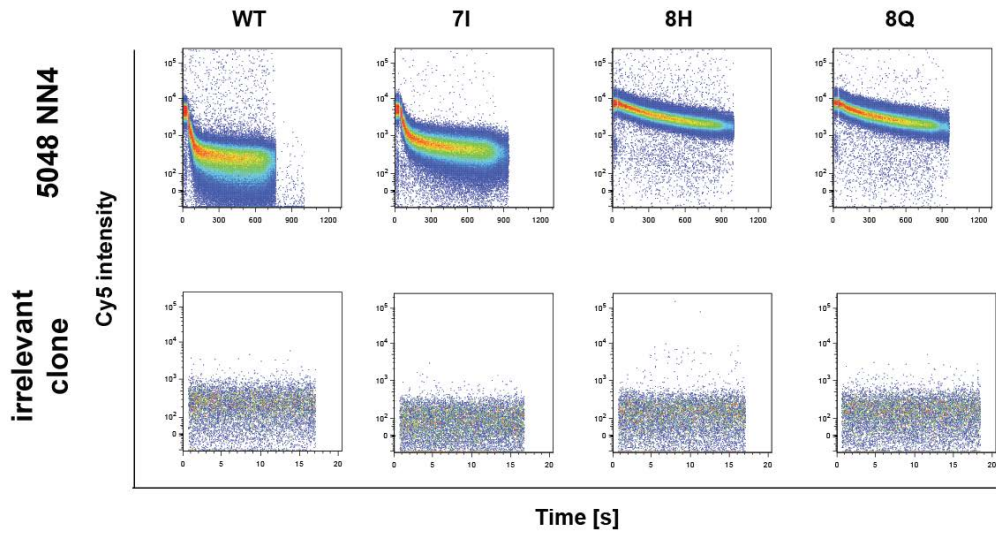


Figure 38 TCR affinity of the YF5048 clone towards mutant peptides. A, Wild-type and mutant pMHC multimer staining intensities (Y axis labels) of the YF5048 clone. B, TCR dissociation rates (k_{off}) of the NTamer Cy5 decay normalized to PE background, calculated from the data of the 3 independent experiments (mean and SEM; t-test).



	WT	7I	8H	8Q
HalfLife	15.01	18.35	20.85	24.93

Figure 39 PE-NTA fluorescence decay. Dot plot from a representative flow cytometry experiment is shown. Half lives were analyzed in Prism with a first-order monomeric decay function after subtraction of non-specific background from an irrelevant clone.



	WT	7I	8H	8Q
HalfLife	12.03	22.96	173.1	130.2

Figure 40 Cy5- pMHC fluorescence decay. Dot plot from a representative flow cytometry experiment is shown. Half lives were analyzed in Prism with a first-order monomeric decay function after subtraction of non-specific background from an irrelevant clone.

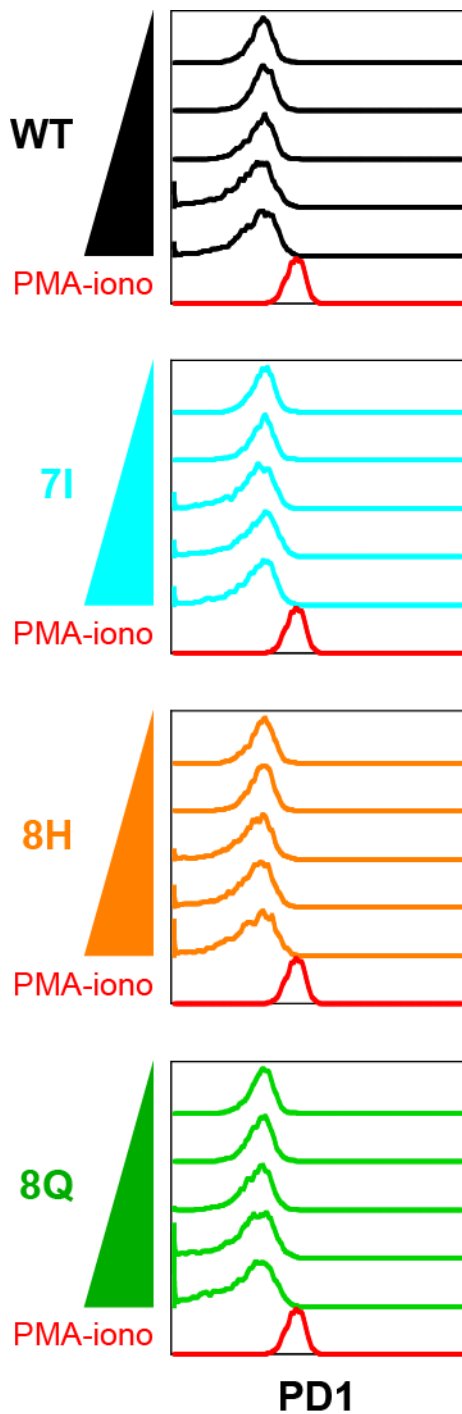


Figure 41 PD1 expression in the YF5048 clone after stimulation with T2 cells pulsed with the indicated peptides at concentrations ranging between 10^{-11} and 10^{-6} M. Unpulsed T2 cells were used as a negative control (not shown) and treatment with PMA-ionomycin (“PMA-iono”) was used as a positive control and. A representative flow cytometry experiment is shown

***In silico* modeling shows no particular structural advantage in the 7I mutation of LLW, while the 8Q and 8H mutations show favorable contacts with the TCR**

In order to address structural determinants of the TCR:pMHC interaction, we solved the atomic structure of the A2/LLW-7I, A2/LLW-8H and A2/LLW-8Q pMHC complexes (Figure 42).

Unfortunately, we could not determine the structural parameters that govern the TCR binding to the pMHC complex due to the failure to obtain a crystal of the YF5048 TCR [126]. Instead, we performed *in silico* modeling based on our crystal structures of the three mutant pMHC complexes and the previously solved structure of the MEL5 TCR [128], which has a TCR α chain that is very close in sequence to the TCR α chain of YF5048 [126]. In these modeled structures, the LLW-8H and -8Q mutant peptides made favorable contacts with the TCR (Figure 43A and B), which would explain the higher TCR avidity measured by NTAmer. In contrast, the 7I substitution (isoleucine at P7) did not introduce additional favorable contact with the TCR (Fig 4C). This is in line with the lack of a particular advantage in TCR:pMHC k_{off} as measured by NTAmer for the 7I mutation (Figure 38), but still did not explain the increased functional avidity based on immunoassays upon titration with the 7I peptide (Figure 35).

In conclusion, our data shows that a substitution to an isoleucine at P7 does not change the TCR k_{off} . This was further supported by our *in silico* model which shows that the 7I mutant peptide does not make more favorable contacts with the TCR compared to the WT peptide. The superior T cell function induced by the LLW-7I mutant peptide is therefore not due to increased structural TCR:pMHC interactions.

In contrast, our data suggest that the LLW-8H and -8Q mutant peptides make favorable contacts with the TCR, supporting the significantly longer off-rates and higher TCR avidity compared to the WT peptide.

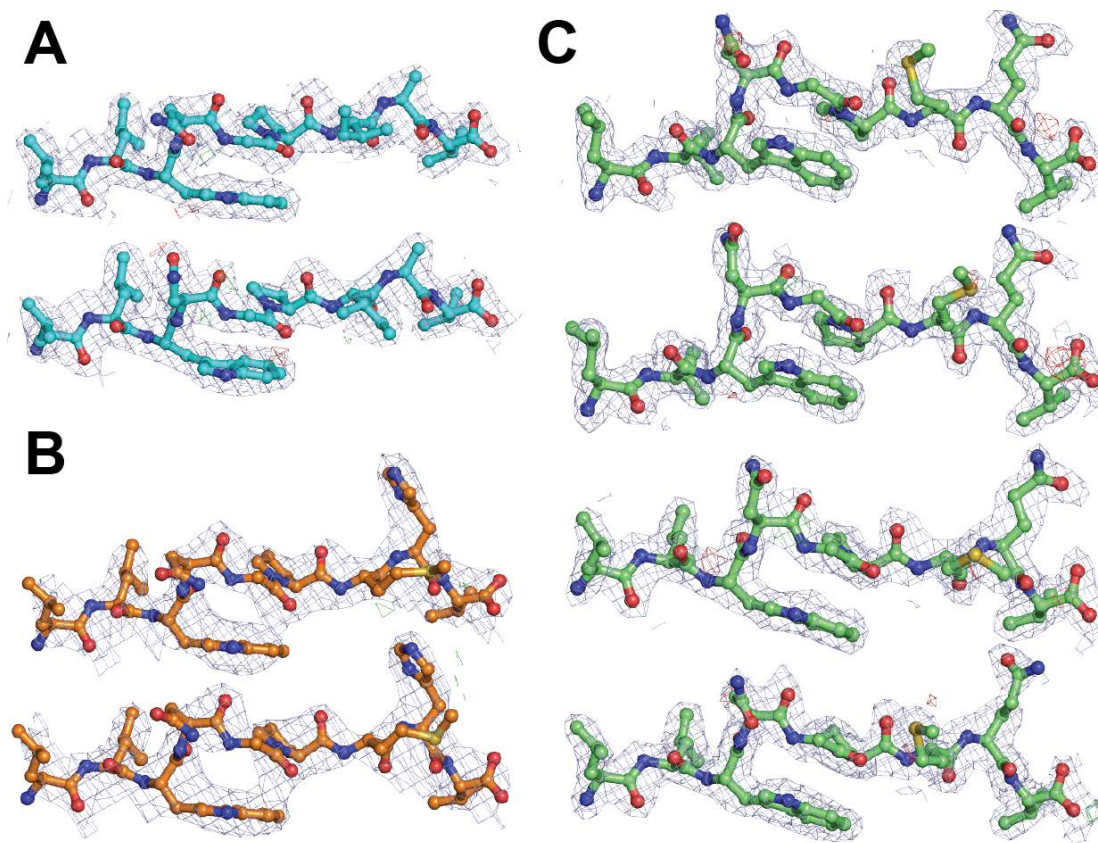


Figure 42 Observed electron density around the peptide copies in complex with HLA-A2 showing the overall conformation of the peptides. A, LLW-7I (LLWNGPIAV), B, LLW-8H (LLWNGPMHV), C, LLW-8Q (LLWNGPMQV).

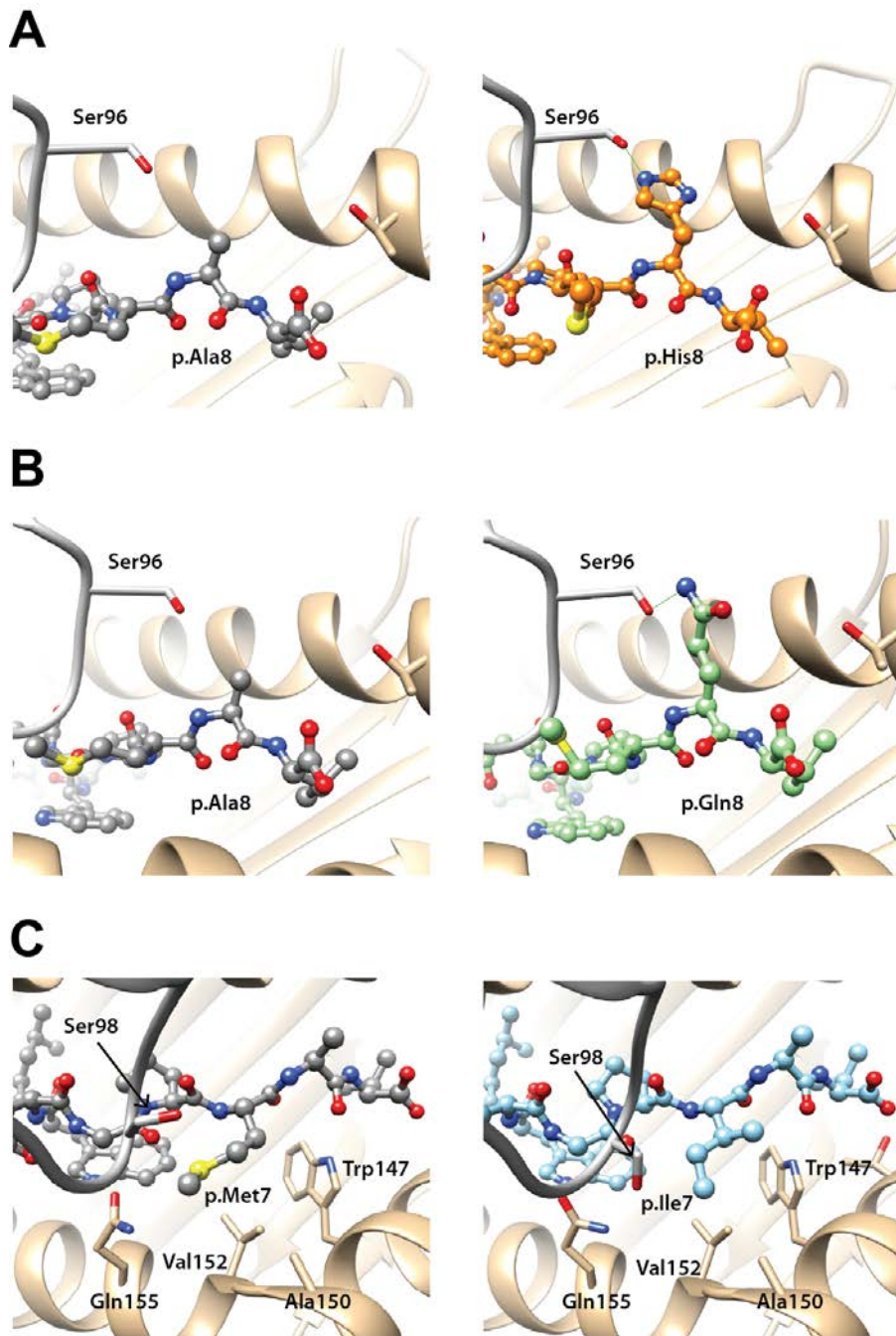


Figure 43 Molecular modeling of the YF5048 TCR bound to the various mutant peptides in complex with HLA-A2. Ribbons represent TCR β -chain in grey; the MHC molecule in tan ribbon, and peptides in ball and stick representation. A) WT peptide on left (in grey) and 8H peptide on the right (in orange). B) WT peptide on left (in grey) and 8Q peptide on the right (in green), C) WT peptide on left (in grey) and 7I peptide on the right (in light blue).

The 7I mutant peptide shows higher entropy loss and rigidity in complex with HLA-A*02

Another potential mechanism by which the 7I mutant peptide could lead to an enhanced T cell function is that the peptide binds the MHC molecule with higher affinity. To assess this, we expressed, refolded and purified HLA-A*0201 in complex with the mutant and WT peptides. To assay the peptide binding affinity to the MHC molecule, we performed circular dichroism (CD) temperature melting experiments (Figure 44A). The A2/LLW-7I, A2/LLW-8H and A2/LLW-8Q complexes showed a melting temperature T_m of 66.2, 65.2, 65.3 °C, respectively. Thus, the stability of the mutant complexes is not significantly different from the A2/LLW-WT complex (T_m of 66.5 °C, ΔH_{vH} of -488 kJ/mol).

The values of transition enthalpies ΔH_{vH} were also calculated in the same experiment (Figure 44B). The binding of the LLW-7I peptide to the MHC shows a lower (favorable) ΔH_{vH} than the other peptides, suggesting that the entropy loss upon binding is greater and that the resultant LLW-7I mutant pMHC complex is more rigid than the LLW-WT pMHC complex.

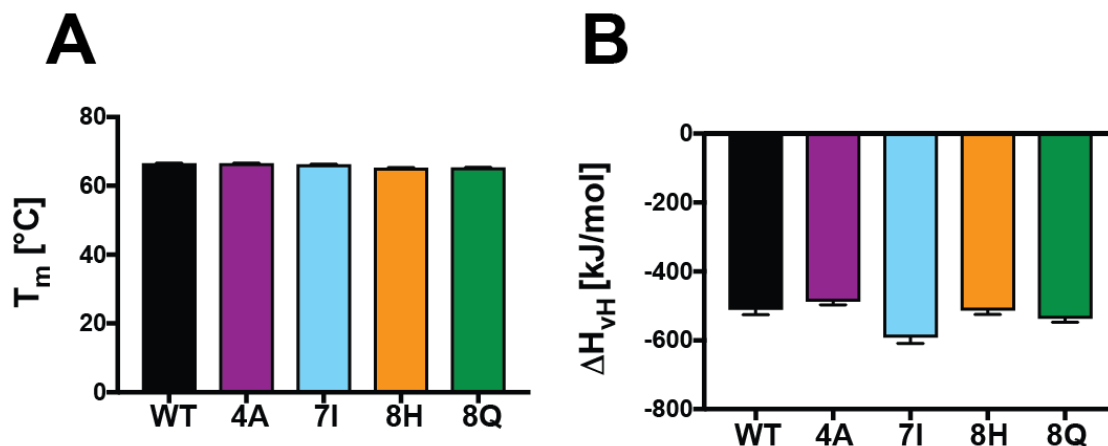


Figure 44 Stability of the mutant peptides binding to HLA-A*0201. A, Apparent melting temperature T_m assayed by circular dichroism spectroscopy (mean and SD). B, van't Hoff's enthalpy of unfolding ΔH_{vH} assayed by circular dichroism spectroscopy (mean and SD).

In order to investigate pMHC rigidity further, we performed molecular dynamics (MD) simulations of the A2/LLW pMHC complex variants starting from the crystal structures of the A2/LLW-7I, A2/LLW-8H and A2/LLW-8Q complexes. The Root Mean Square Fluctuations (RMSF) of the different peptide and MHC residues were calculated. The

latter constitute a measure of the vibration intensity of the residues around their average position: a residue is more flexible if its RMSF value is higher. In the A2/LLW-WT complex, the peptide residues Leu1, Asn4 and Met7, which are facing the solvent in the absence of TCR, are the most flexible residues, while the peptide residues Leu2, Trp3 and Val9, which are buried into the MHC pockets, are less flexible (Figure 45A).

Interestingly, the isoleucine substitution at P7 of the LLW-7I mutant peptide in the pMHC complex shows a significantly decreased flexibility compared to Met7 in the LLW-WT pMHC complex (Figure 45A, $p = 0.0006$).

Of note, the difference between the RMSF of the other peptide residues between the LLW-WT and -7I mutant are not significant (Figure 45A). Also, the flexibility of Met7 in the LLW-8H and LLW-8Q mutants is similar to that of the WT peptide.

His8 and Gln8 contain more dihedral angles than the Ala8 residue in the WT system, and can be expected to display more flexibility when they face the solvent, in absence of TCR. This is indeed what is observed in the MD simulations for residues His8 and Gln8, in the MD simulations of the A2/LLW-8H and -8Q complexes, compared to Ala8 of the WT complex. However, this increase in flexibility compared to Ala8 is limited and not statistically significant (Figure 45A, $p=0.03$ and 0.2 for LLW-8H and -8Q, respectively). The corresponding small entropy penalty upon binding for the mutated systems is compensated by the additional interactions made between the His8 or Gln8 side chains and TCR, compared to Ala8 in the WT system as suggested by our *in silico* model (Figure 43B and C).

The peptide substitutions could potentially modify the MHC flexibility. To control for this, the RMSF of the MHC residues were calculated from the same MD simulations (Figure 45B). No significant difference could be observed in the flexibility of the MHC residues upon peptide mutation. Glu154 shows a higher flexibility in the A2/LLW-7I complex compared to the WT pMHC. However, this residue is not in contact with the mutation site, and the difference in the RMSF is not statistically significant ($p=0.07$). The only exception is the higher flexibility of Thr73, in the A2/LLW-7I and -8H complexes, which is statistically significant with p values of 0.01 and 0.009 , respectively. This MHC residue is close to residues 7 and 8 of the peptide, explaining that its flexibility could be a function of mutations at these positions of the peptide. However, the absolute values and the differences in the RMSF remain small.

The larger binding avidity of the A2/LLW-7I complex for the TCR compared to the A2/LLW-WT complex can be explained by the more limited flexibility of the isoleucine side chain before binding the TCR (i.e. in absence of the TCR) which translates into a lower entropy penalty upon TCR binding [200]. The A2/LLW-7I complex seems to be enthalpically favorable and more rigid than the A2/LLW-WT complex. This is supporting a better recognition of the interface by the TCR as less induced fit is required.

In conclusion, the superior functional sensitivity of the LLW-7I mutant peptide is not provided by an optimal interaction with the TCR but rather by an increased pMHC complex rigidity.

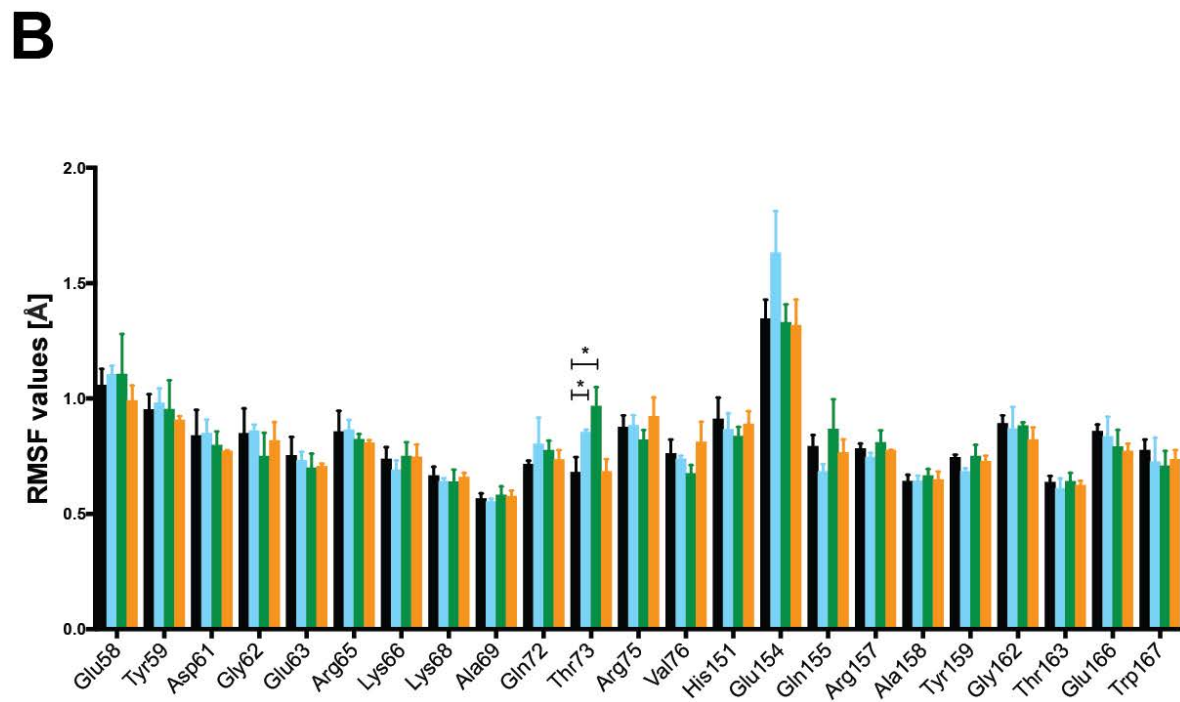
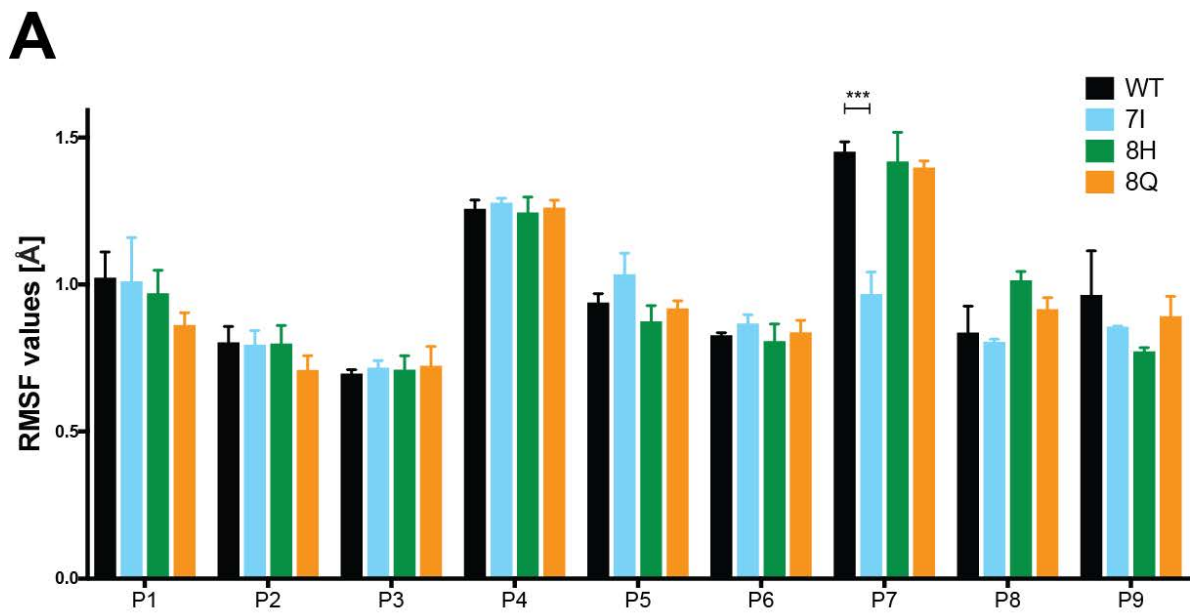


Figure 45 Flexibility of the peptide and MHC residues. Root Mean Square Fluctuations (RMSF in Å) calculated for the peptide (A) and MHC (B) residues, averaged over 3 independent MD simulations of the LLW-WT, -7I, -8H and -8Q complexes, each 140 ns in length. Standard deviations are reported. Of note, the MD simulations were performed for the pMHC complex, in absence of the TCR.

3.1.5.3 Discussion

Using a CPL screening, we identified 3 superagonist peptides: the LLW-7I mutant peptide confers a higher functionality sensitivity compared to the natural WT sequence, whereas the LLW-8H and LLW-8Q mutant peptides moderately increase functional sensitivity. The data presented in this chapter are summarized in Figure 46.

	assay	read-out		peptides			
				WT	7I	8H	8Q
functional sensitivity	ELISA	MIP-1b	EC50	6.4E-09	3.4E-10	5.9E-10	4.6E-10
	51Cr	lysis	EC50	2.1E+09	4.7E+10	7.9E+09	8.3E+09
	ICS	INFg	EC50	6E-10	9.8E-11	2.4E-10	3.8E-10
		TNFa	EC50	1.6E-09	2.4E-10	8E-10	1E-09
		CD107a	EC50	1.5E-10	1.5E-11	4.9E-11	9.9E-11
		IL-2	EC50	2.5E-09	2.5E-10	1.5E-09	1.8E-09
TCR avidity	NTAmer	dissociation rate	t1/2	12.1333	17.9667	141	113.633
pMHC binding	CD	stability	Tm	66.5	66.2	65.2	65.3
		rigidity	dHvH	-511	-592	-514	-537
	MD	flexibility at P7	RMSF	1.4503	0.9656	1.4167	1.3961

Figure 46 Table summarizing the data sets of the various mutant peptides

The LLW-8H and LLW-8Q substitutions showed modest enhancement of the functional sensitivity compared to LLW-WT. In that case, the mechanism explaining this slight improvement is relatively clear as we found that the TCR dissociation rate (k_{off} measured by NTAmer) was significantly lower compared to A2/LLW-WT. This was further supported by our *in silico* modeling suggesting that the TCR makes favorable interactions with the mutated residues. This is in agreement with several reports that have positively correlated functional avidity specifically to longer TCR:pMHC off-rates [43]–[45] [195] [196].

However, our data shows that a substitution to an isoleucine at P7 does not change the TCR:pMHC off-rates. This was further supported by our *in silico* model which shows that the 7I mutant and wild type peptides make similar interactions with the TCR. The superior T cell function induced by the LLW-7I mutant peptide is therefore not due to an increased interface with the TCR. In contrast, the LLW-8H and -8Q mutant peptides display longer TCR:pMHC off-rates and the *in silico* modeling suggests these peptides

make more favorable contacts with the TCR, supporting the significantly higher TCR avidity compared to the WT peptide.

Position 7 of a nonamer peptide is not usually considered as a primary MHC anchor residue, we indeed did not find any significant change in thermal stability for A2/LLW-7I compared to the WT complex. However, supported by experimental ΔH_{vH} values and *in silico* molecular dynamics simulations, our results suggest that the LLW-7I mutant peptide binds the MHC molecule with higher rigidity. It has been shown that peptide motion, which also impacts MHC motion, affects recognition by the TCR [200]. Along these lines, the LLW-7I mutant peptide may therefore be presented by the MHC to the TCR more efficiently compared to the WT peptide – a phenomenon related to k_{on} - given that the more rigid isoleucine side-chain in the A2/LLW-7I pMHC complex might require less induced fit and might lead to lower entropy penalty upon TCR binding. We may hypothesize that this 7I substitution leads to a more favorable pMHC-TCR binding, decreasing the related binding constant (K_D , which is described as $K_D = k_{off}/k_{on}$), which translates into a higher affinity of the TCR:pMHC complex [201].

While our experimental data shows that the 7I mutation does not alter the TCR dissociation rate (k_{off}) measured using the NTamer technology, we hypothesize it improves the TCR association rate (k_{on}) of the TCR:pMHC complex, consequently explaining the 1-log higher functional avidity observed with immunoassays (killing and cytokine secretion) on the YF5048 clone. To answer this question, we will perform an on and off-rate analysis with tetramers [202]. Briefly, tetramer binding kinetics is measured by flow cytometry at different time-points during tetramer staining until equilibrium is reached (k_{on}). Addition of an HLA-blocking antibody leads to the tetramer dissociation (k_{off}). These measurements will be performed at 4°C to inhibit tetramer internalization. For this experiment, it is useful to use a tetramer consisting of CD8 null binding monomers to ensure that we consider effects from the TCR only.

Another technical pitfall relates to the assessment of the pMHC rigidity. Indeed, our conclusions are mainly based on *in silico* data from the molecular dynamics analysis. We also have some experimental data regarding the values of transition enthalpies ΔH_{vH} measured by CD but it would have been important to investigate the peptide:MHC interaction in more detail. Isothermal titration calorimetry (ITC) allows to

determine the thermodynamics parameters of binding interactions by measuring changes in enthalpy when two molecules interact. However, such technique requires the molecules to interact in solution. This is not possible for pMHC complexes as they do not dynamically interact in solution.

However, we could assess pMHC stability by measuring the on- and off-rates using a cellular peptide-binding assay. This involves pulsing HLA-A2-carrying T2 cells with the peptide followed by anti-HLA-A2 staining and fixation. For peptide on-rates, T2 cells are monitored by flow cytometry at several time points for 22 hours. For peptide off-rates, T2 cells are pulsed overnight. Part of the cells are stained with anti-HLA-A2 and fixed, while the remaining cells being washed and incubated at 37°C and 5% CO₂ for peptide dissociation, then stained with anti-HLA-A2 and fixed. Dissociation is measured by flow cytometry at several time points to calculate the off-rate [203].

One hypothesis would be that the LLW-71 peptide is better presented to the T cell. It is complex to assess experimentally the extent of the peptide presentation at the cell surface of APCs but we could monitor HLA-A2 levels in presence of the different peptides by flow cytometry. In addition, we could pulse APCs with the LLW-71 peptide and perform functional experiments at different time-points to determine whether this mutant peptide has a longer half-life at the cell surface and whether the antigen density would consequently be higher [203].

Another scenario could be that the TCR signal transduction is improved after stimulation with the LLW-71 peptide compared to the WT peptide. To test this hypothesis, T cell activation could be measured with a calcium (Ca²⁺) flux experiment, and the phosphorylation of the key players in the signal transduction pathways could be examined by phospho-flow cytometry.

It is important to note that the mutant peptides identified by CPL are specific to the TCR carried by the clone tested (i.e. YF5048). Therefore, we do not necessarily expect that the mutant peptides would generally improve functional sensitivity at the polyclonal, population level. To confirm this, we will stimulate PBMCs from the donor LAU5048 that was used for the cloning with the different peptides and monitor the cytokine response by flow cytometry in the total A2/LLW-specific CD8 T cell population (including TRAV12-2⁺ and TRAV12-2⁻ cells).

We are also interested in assessing the functional sensitivity (killing assay and cytokine production) of the double-mutant peptides LLWNGPIHV (LLW-7I8H) and LLWNGPIQV (LLW-7I8Q).

In conclusion, in contrast to tumor antigens, the A2/LLW epitope was showed to be highly potent [97] [117] [118] [120] [126]. Nevertheless, our work attests that altered peptides improving T cell function exist even for a strong viral epitope. Interestingly, the enhancement induced by the LLW-7I substitution was not due to a higher TCR avidity but rather to a more rigid pMHC complex.

3.1.5.4 Contributions

I performed and analyzed the killing assays, ELISA and NTAmer stainings. The ICS data were produced by Philippe Delbreil and analyzed by myself. The *in silico* TCR:pMHC modeling and molecular dynamics were performed by Dr. Vincent Zoete. Dr. Konrad Beck performed and analyzed the CD experiment. From this project, I am currently preparing a manuscript entitled “Functionally optimized peptide rigidity in a novel superagonist mutant of the immunodominant Yellow Fever Virus epitope NS4b₂₁₄₋₂₂₂” with the essential contribution of Dr. Silvia Fuertes and Dr. David Cole.

3.1.6 CONCLUDING REMARKS

In this chapter, I addressed several aspects of the TRAV12-2 bias in A2/LLW-specific CD8 T cells, including the functional and structural analysis of the TCR:pMHC interaction and finding a suitable mouse model.

Several questions remain open. However, we could not find appropriate and/or immediately available models to answer them:

- We attempted to use the *ABabDII* transgenic mice as a mouse model to study the YF-17D vaccination, including the TCR bias of A2/LLW-specific CD8 T cells. Unfortunately, this mouse model turned out unsuitable for the biological and logistic reasons mentioned in section 3.1.4.3.

- In order to test our hypothesis that TRAV12-2 would favor thymic output, we could have used a fetal thymus organ culture (FTOC). This is a culture system that allows intrathymic T cell development *in vitro*. However, we cannot do this because we do not have the *ABabDII* transgenic mice.

- In the absence of a crystal structure of an A2/LLW-specific TRAV12-2 positive TCR in complex with A2/LLW, mutational analysis of the TCR would be required to support our *in silico* model and determine which residues are critical for antigen binding. We could measure functional avidity of TCR mutants with transfection into the TCR $\alpha\beta$ J76/CD8 T cell line. T cell signaling responses following stimulation with LLW-pulsed targets would provide a functional map of the TCR binding site, in particular the contribution of the germline-encoded CDR1 loop of TRAV12-2 compared to the somatically recombined CDR3 loops. However, these experiments are technically challenging: it is possible that some of the mutants would not express well at the cell surface, requiring careful validation that the expression level is similar for wild-type and mutant TCRs.

- Given the immunodominance and prevalence of A2/LLW-specific CD8 T cells, another interesting question is whether there is any advantage in having the HLA*02 type. We could establish a new clinical protocol to assess whether HLA-A*02 positive individuals are better protected and/or raise better innate/adaptive responses than non-HLA-A*02 individuals. However, it would not be feasible during the time of my PhD. An alternative is to seek for published reports of clinical studies on YF-17D vaccination with large numbers of volunteers or cases that may have HLA data – at first sight, we did not find such studies.

3.2 AXIS 2: Longitudinal analysis of the human immune responses to YF-17D vaccination

When I joined the laboratory of Prof. Speiser, the recruitment of a clinical study (“YF2 study”) was ongoing, in which we collected blood samples longitudinally before and several time-points after YF-17D vaccination (Figure 47). The study involved healthy volunteers receiving a dose either for the first time (“priming” group, n= 10) or after at least 10 years of previous vaccination (“boost” group, n= 6). By the time I concluded the major experiments in Axis 1, the “YF2” study cohort biobank was ready for analysis.

The main aims of my work on the YF2 study were (Figure 47):

- a) Characterize the dynamics, proportions and profiles of all major immune cell populations following primary and booster YF-17D vaccination.
- b) Interrogate correlations and identify the key determinants of immunogenicity using bioinformatics analyses (based on the parameters in a).
- c) Uncover the activation and differentiation of A2/LLW-specific effector and long-lasting memory CD8 T cells.

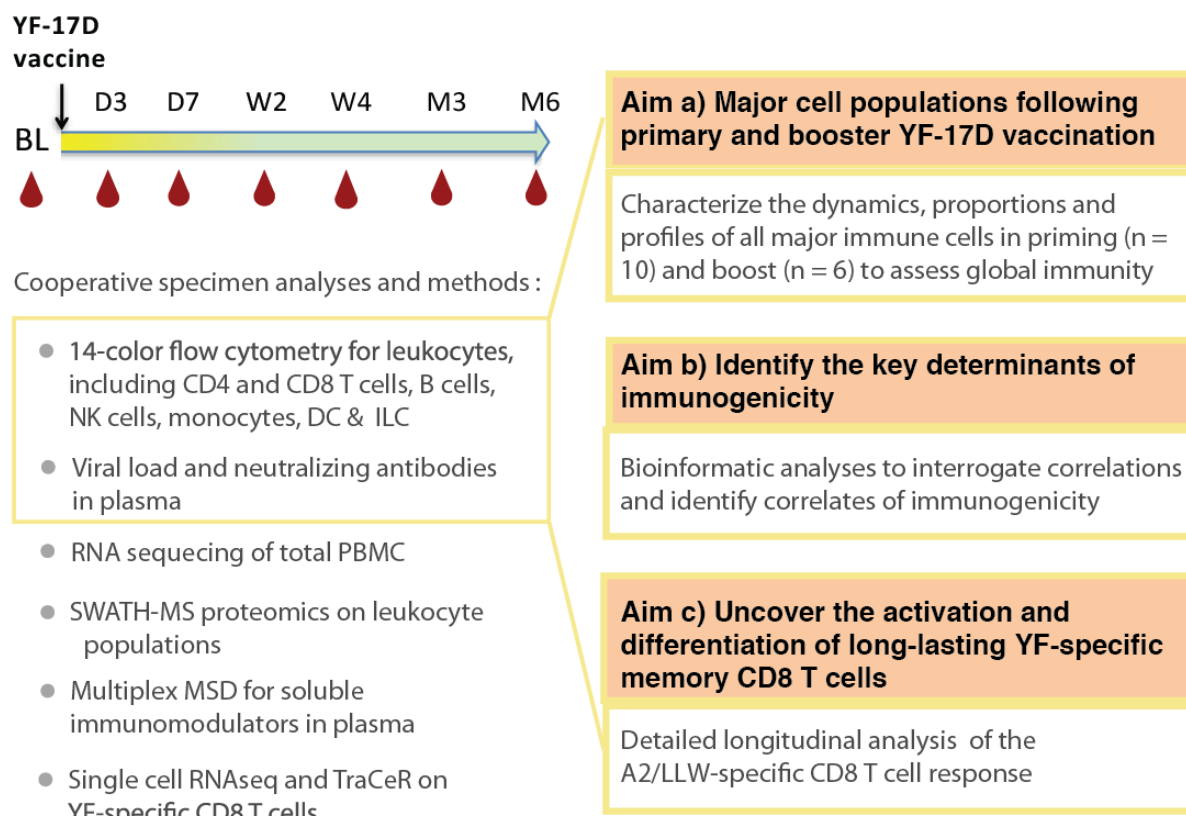


Figure 47 Overview of the longitudinal YF2 study. Blood samples were collected at several time-points before vaccination (“BL”) and after vaccination (days “D”, weeks “W”, months “M”) with various purposes (as depicted by specific experimental methods).

We have designed multiple, complementary and parallel analyses using comprehensive and cutting-edge technology, sustained by a solid and collaborative network of world-leading experts that have agreed to participate in this project.

I characterized the proportion, number and activation state of all major immune cell populations by flow cytometry. Only these data alongside nAbs and viral titers will be shown in my PhD thesis.

In a preliminary phase, I made major efforts to establish quality-controlled and optimized flow cytometry panels with at least 14 colors using an LSR-II SORP cytometer (Figure 48). Next, I investigated the PBMCs from all 16 donors and time-points of the YF2 study (112 samples per panel) for:

- Adaptive immune cell types: CD8 T cells (including YFV-specific T cells with tetramers), CD4 T cells, B cells.
- Innate immune cell types: monocytes and dendritic cells (DC), Innate Lymphoid Cells (ILC), Natural killer (NK) cells.

Of note, PBMCs were isolated by Ficoll gradient for freezing and subsequent grouped analysis of multiple sample dates per volunteer in the same experiment. Therefore, erythrocytes, platelets and granulocytes (neutrophils, basophils, and eosinophils) could not be analyzed as these cell types are excluded by Ficoll gradient isolation. All samples were cryopreserved during the longitudinal collection from donors and while awaiting experimental use, thus certain cell types such as DC are also likely more negatively affected by this experimental design.

All these cell types bulleted listed above were studied for their composition of differentiation subsets and activation status. I obtained frequencies as well absolute numbers based on the information that we obtain from complete blood cell counts also performed at each blood sample collection from the donors.

LSRII - SORP	Whole PBMCs					CD8+ fraction	
	T		B	Mono/DC	ILC/NK	Yellow Fever-specific	
	T1	T2				Tet	TCF1
FITC	HLA-DR	CD58	CD19	Dump: CD3, CD19, CD20, CD56, FcER1	Dump: CD3, CD14, CD15, CD19, CD20, CD33, CD34, CD203c, FcER1	CD58	TCF1
PerCP-Cy5.5	PD1 PerCPef710	CD38	CD38	CD123	CD38	CXCR3	PD1 PerCPef710
PE	CD58	Ki67	IgD	peIF2S1 (aRab)	ckit	tetramer	tetramer
ECD	CD45RA	CD15S PE-CF594	HLA-DR	CD16	HLA-DR	HLA-DR	HLA-DR
PE-Cy7	CD95	CD95	BCMA	HLA-DR	CD56	CD95	CD95
APC	CCR10	Foxp3	CD83	CD83	Nkp44 (CD336)	Ki67 A647	CD58
A700	CD38	CD3	CD86	CD86	CD137	CD38	CD38
APC-A750	CD8	CD8	CD40 APC-H7	CD1c AC7	-	CD8	CD8
BrV421	CCR7	CCR7	CD20 PaB	CD141 VioBlue	CRTH2	CCR7	CCR7
Krome Orange	CD3	CD45RA BV510	CD3	CD14	CD16	CD45RA BV510	CD45RA BV510
BV605	CXCR5	CD25	CD27	-	CD127	CD127	CXCR5
BV650	CD69	CXCR3	CD69	CD40	CD69	CD69	CD69
BV785	CD4	CD4	CD138 BV711	CD303	PD1 BV711	PD1 BV711	CD127
DAPI / UV	FVD-eF455	FVD-eF455	FVD-eF455	FVD-eF455	FVD-eF455	FVD-eF455	FVD-eF455

FcR Block 20% without pre-incubation

All samples were fixed overnight with the Foxp3 kit (eBioscience)

Figure 48 Flow cytometry panels used for the YF2 study.

Obviously, I could not run all 112 samples per panel (with multiple panels) on the same day. Therefore, I paid special attention to use the same lot of antibodies throughout the experiments. Importantly, I performed Cytometer Set-up and Tracking (CSnT) settings

before each flow cytometry acquisition in order to quality control the performance of the machine and to calibrate the voltages such that we normalize the sensitivity of the machine across experiments [204]. Thus, inter-experimental variability is minimized.

In this chapter, I will describe the data in two parallel ways: one conventional analysis and one functional data analysis, for reasons that will be outlined.

For the conventional analysis of our flow cytometry data, we applied the traditional method involving visual inspection and manual gating using serial 2D dot plots with FlowJo software, to then generate tabulated counts and frequencies of the populations of interest.

In parallel, functional data analysis (FDA) was applied to analyze and interpret our longitudinal study. Although time course studies hold great potential in deciphering the temporal dynamic of continuous immunological processes, analyzing the resulting time-series data remains challenging in part due to small sample sizes, uneven time-points, natural heterogeneity and multi-dimensionality of immunological data. In addition, the temporal order and dependence of repeated measures from the same individual introduce complex correlation structure in the data, which if ignored can lead to loss of information and reduced statistical power.

In order to make the results description succinct, in this section, I jointly address aims a and b, which interrogate the same data series.

3.2.1 Characterization of all major immune cell populations following primary and booster YF-17D vaccination (aims a and b)

3.2.1.1 Background

Despite the accumulating knowledge about the highly effective YF-17D vaccine, it is clear that a better comprehension of the immune correlates of protection is needed in order to gain insight into the mechanisms by which the vaccine induces such optimal immune responses. There is an inadequacy in the global characterization of all arms of the immune response (Table 9). Most studies focused on the primary adaptive response of YF-17D vaccination. Especially, these studies pinpoint only on few aspects

at the time. In addition, studying the immune response to YF-17D vaccination should include the early phase shortly after vaccination, and also the comparison to baseline.

	Prime	Boost
CD8 T cells	Dos Santos et al 2005 Martins et al 2007 Miller et al 2008 Querec et al 2009 Luiza et al 2011 Kohler et al 2012 Muyaja et al 2014 Akondy et al 2015 Campi et al 2015 De Witt et al 2015 Fuertes et al 2015 Konsgaard et al 2017	Dos Santos et al 2005 Konsgaard et al 2017
CD4 T cells	Dos Santos et al 2005 Martins et al 2007 Kohler et al 2012 Blom et al 2013 Muyaja et al 2014 Campi et al 2015 De Wolf et al 2017 Konsgaard et al 2017	Dos Santos et al 2005 Konsgaard et al 2017
Ag-specific CD8 T cells	Co et al 2002 Miller et al 2008 Akondy et al 2009 Co et al 2009 Querec et al 2009 Blom et al 2013 Melo et al 2013 Muyaja et al 2014 Akondy et al 2015 Fuertes et al 2015 Wieten et al 2016 Akondy et al 2017 Konsgaard et al 2017	Muyaja et al 2014 Wieten et al 2016 Konsgaard et al 2017
Ag-specific CD4 T cells	Kohler et al 2012 De Melo et al 2013 James et al 2013 Koblitschke et al 2017	no report
B cells	Martins et al 2007 Silva et al 2011 Kohler et al 2012 Muyaja et al 2014 Campi et al 2015	no report

nAbs	Rosenzweig et al 1963 Poland et al 1981 Niedrig et al 1999 Dos Santos et al 2005 Hepburn et al 2006 Querec et al 2009 Luiza et al 2011 Collaborative group 2014 Muyaja et al 2014 Campi et al 2015 Wieten et al 2016 Kongaard et al 2017	Dos Santos et al 2005 Hepburn et al 2006 Muyaja et al 2014 Wieten et al 2016 Kongaard et al 2017 Miyaji et al 2017
virus	Miller et al 2008 Akondy et al 2009 Muyaja et al 2014 Akondy et al 2015 Akondy et al 2017	Muyanja et al 2014
monocytes	Martins et al 2008 Luiza et al 2011 Kohler et al 2012 Hou et al 2017	no report
NK cells	Martins et al 2008 Da Costa Neves et al 2009 Luiza et al 2011 Muyanja et al 2014 Marquardt et al 2015 Hou et al 2017	no report
DCs	Kohler et al 2012 Hou et al 2017	no report
ILCs	no report	no report
Neutrophils/ eosinophils	Martins et al 2008 Luiza et al 2011	no report

Table 9. Reports of immune responses to vaccination with YF-17D in humans

The comparison between primary and booster vaccination will determine how the presence of pre-existing antibodies influence the reactivity to YF-17D. Furthermore, our study provides more insights of the importance of re-vaccination for the duration of immunity as it is still debated.

To our knowledge, it is the first study that compares in details primary and booster vaccinations side-by-side, including the global and specific adaptive and innate parameters in parallel to antibodies and viral load after priming and booster YF-17D vaccination. Therefore we can expect that our approach provides a more

comprehensive insight into the various immune parameters involved in the YF-17D vaccination.

3.2.1.2 Results

Of note, apart from nAbs and virus, I have added the fitted population means (popMean) derived from the FDA to the classical raw data and average. Data was first normalized by log- and logit-transformation of raw counts and frequency measures, respectively. Having treated measurements prior to vaccination as baseline (day 0), we next fit a linear spline model with 4 internal knots located at days 3, 7, 14, and 28 (Figure 49A). Visually, fitting a linear spline with 4 internal knots is equivalent to fitting a piecewise linear regression with 4 breakpoints and 5 segments. We chose the location of internal knots based on the observation that most features showed temporal fluctuations up to 4 weeks post vaccination, and reached a steady state from 28 days onward. Broadly speaking, the heterogeneity of individual profiles can be explained by either variability at the baseline (random intercepts) or variability in the slopes (random slopes). Given our sample size, we could not afford the most flexible model (by incorporating both random intercepts and random slopes). Instead, we opted for a random intercept model. Intuitively, our random intercept model assumes that individual profiles exhibit a consistent temporal dynamic, and that differences among individual profiles can be explained by variability at the baseline. Once the model was fit and unknown parameters were estimated/predicted for each feature, individual profiles were extracted for visualization and downstream analyses. It is important to note that popMean did not differ much from the average of raw data but were used for the global network analysis (Figure 49B, aim b).

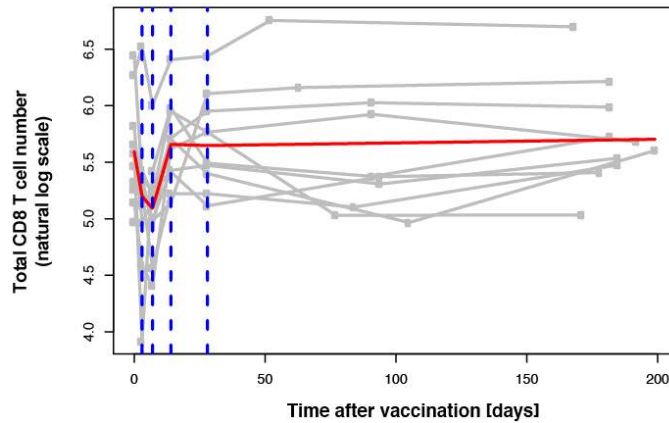
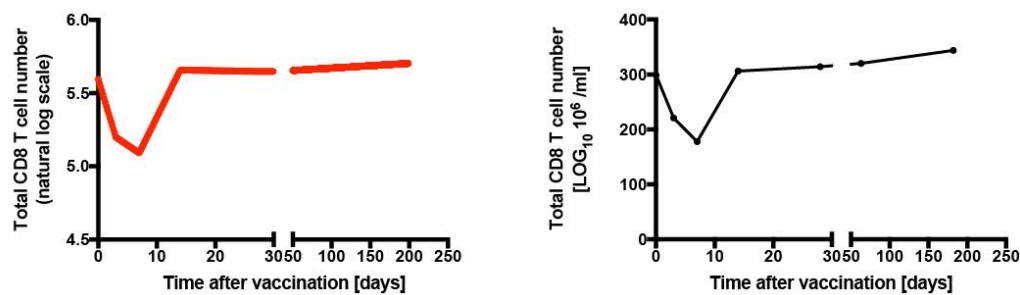
A**B**

Figure 49 Example of the functional data analysis. A, Total CD8 absolute numbers fitted into linear spline model with 4 nodes at days 3, 7, 14, and 28 (dotted blue bars). Grey lines represent the fitted individual profiles and the red line is the fitted population mean. B, Comparison of the fitted population mean (red line, left panel) and the mean of raw data (black line, right panel) of total CD8 absolute numbers.

Higher titers of neutralizing antibodies after primary than booster vaccination

The level of nAbs is generally considered as the main correlate of protection to assess the protective efficacy of the YF-17D vaccine [177] [205] [206]. In 6/6 individuals that had previously been vaccinated (booster group), nAbs could be detected already at baseline at levels > 1:20 titer (the titer considered protective [177] [207]) (Figure 50A and B). Following study vaccination, all the donors from the boost group showed a modest increase in nAbs titer with a peak at day 14 after booster vaccination (Figure 50A and B). The nAbs increase upon booster was below 4-fold in 5/6 donors, which is commonly considered as significant [99]. Upon priming, 10/10 individuals generated nAbs peaking at 28 days after vaccination (Figure 50A and B). The peak in nAbs titer was statistically significantly higher after primary vaccination compared to the peak in the booster vaccination (Figure 50B). This confirms the observations in previous

studies showing that YF-17D booster vaccination induces a limited increase in nAbs compared to primary vaccination [98] [99] [208] [209].

Interestingly, there was a trend towards an increase between the pre-booster nAbs titers and the levels of nAbs after 6 months (Figure 50C).

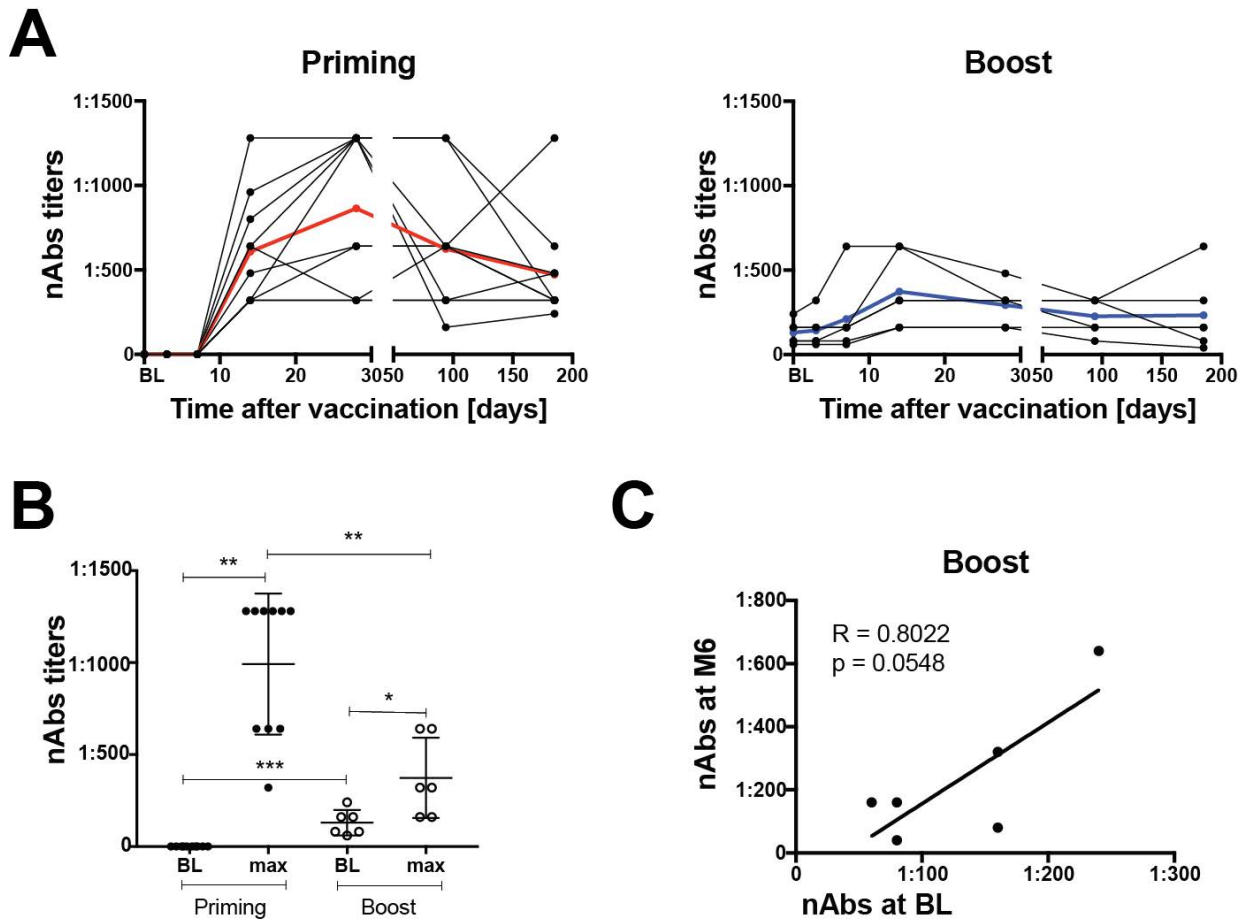


Figure 50 Neutralizing antibody titers in the plasma in response to primary and booster YF-17D vaccination.

A, Dynamics of YFV-specific neutralizing antibody (“nAbs”) titers during the course of primary YF-17D vaccination (right panel, $n = 10$) and booster vaccination (left panel, $n = 6$). The average of individuals within each group is shown in red and blue, respectively. B, YFV-specific neutralizing antibodies in sera of healthy volunteers before (“BL”) and after primary vaccination (“Priming”, $n = 10$) or booster vaccination (“Boost”, $n = 6$); “D28” = 28 days after primary vaccination, “D14” = 14 days after revaccination. Paired or unpaired t-tests. C, Linear correlation between the pre-existing neutralizing antibodies and long-term neutralizing antibodies level in sera of healthy volunteers after booster vaccination ($n = 6$).

The B cell activation upon booster vaccination is reduced compared to primary vaccination

Next, we studied the detailed B cell response during the course of primary and booster YF-17D vaccinations (Figure 51A, Figure 52A). As expected from the seroconversion period, the number and frequency of total B cells is transiently reduced at day 7 after primary YF-17D vaccination [88]. This observation has been hypothesized to be a consequence of the compartmentalization of B cell activation, which precedes plasma cell differentiation and antibody production [122] [125]. In contrast to primary vaccination, booster vaccination did not induce a reduction in B cell numbers (Figure 52A). The same opposing trends of total B cells was observed in terms of frequency (data not shown).

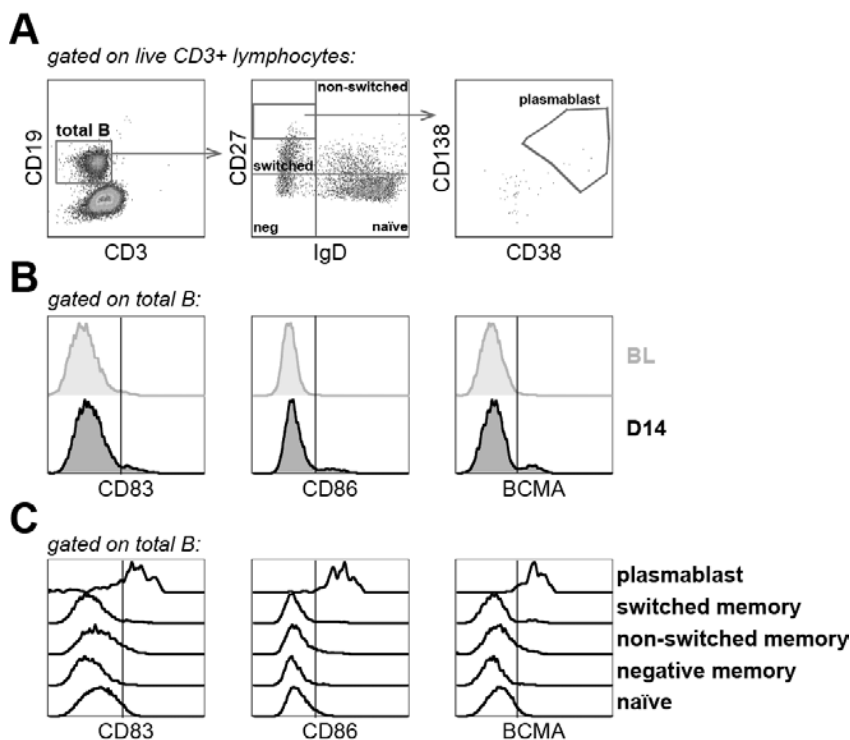


Figure 51 Representative FlowJo gating strategy for the B cells analysis A, Total B cells (CD19+ CD3-) were gated on live lymphocytes using forward/sideward scatter properties. Singlets were selected using forward/side ward scatter width/height characteristics. B cell subsets distribution was based on IgD and CD27 expression to determine naïve (IgD+ CD27-), negative memory (IgD-CD27-), non-switched memory (IgD+ CD27+), switched memory (IgD-CD27+), and plasmablasts (IgD- CD27++ CD38+ CD138+). B, The indicated activation markers were analyzed in total B cells (CD19+ CD3-) at baseline (BL) and day 14 after YF-17D vaccination (D14). They are represented in off-set overlay histograms. C, The indicated activation markers were analyzed in various B cell subsets. The expression at baseline (BL) and at day 14 after YF-17D vaccination (D14) are represented in off-set overlay histograms.

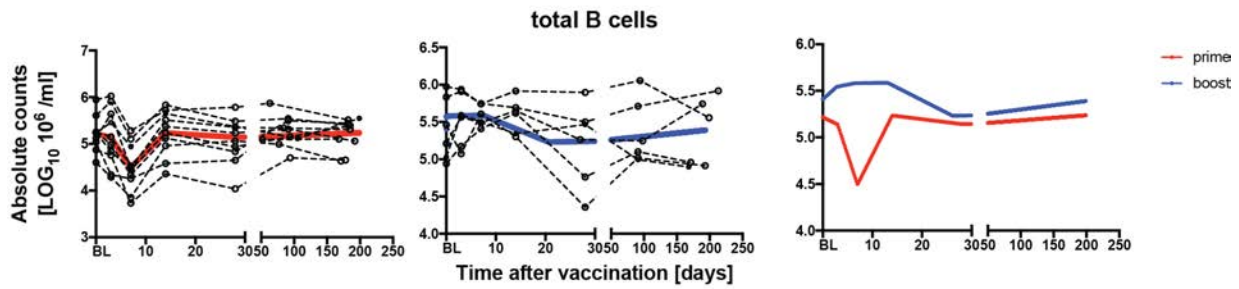
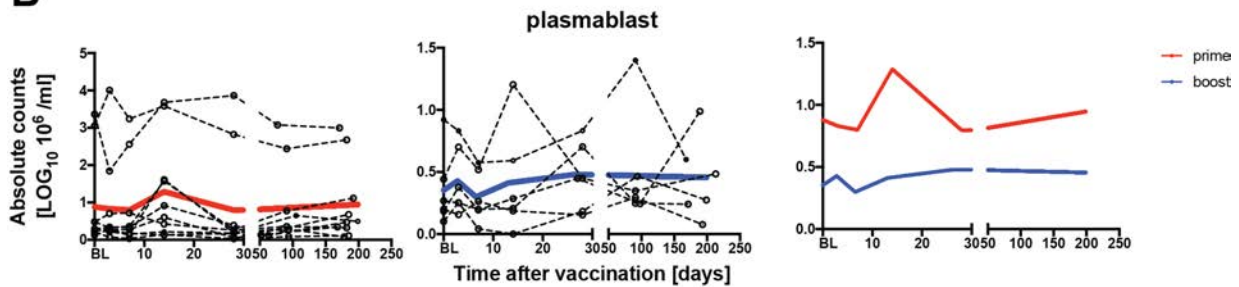
A**B**

Figure 52 Kinetics of total B cells and plasmablasts in response to primary and booster YF-17D vaccination.

A, Absolute number of total B cells (CD19+CD3⁻) in healthy volunteers after primary vaccination (left panel, n = 10) and booster vaccination (middle panel, n = 6). The fitted population mean is represented in red for the priming group and in blue for the booster group (right panel). B, Absolute number of plasmablasts (CD19+IgD⁻CD27⁺⁺CD38⁺CD138⁺) in healthy volunteers after primary vaccination (left panel, n = 10) and booster vaccination (middle panel, n = 6). The fitted population mean is represented in red for the priming group and in blue for the booster group (right panel). C, Heat map showing the absolute number of plasmablasts among healthy volunteers after primary vaccination for each time point (n = 10). D, Linear correlation between the neutralizing antibody titers (“nAbs”) at D28 and the absolute number of plasmablasts at D14 after primary vaccination (n = 10)

The dynamics of B cell subset numbers followed the one of total B cells, except for plasmablasts (IgD⁻ CD27⁺⁺ CD38⁺ CD138⁺) (Figure 51A). In contrast to other B cell subsets, which also transiently decreased, the number and percentage of plasmablasts increased after primary YF-17D vaccination, reaching a maximum at day 14 and subsequently returned to baseline level (Figure 52B). Booster dose of YF-17D vaccine induced a slight increase of plasmablasts but the peak occurred very early on at day 3 (Figure 52B).

B cell maturation antigen (BCMA), also known as TNFRSF17, is a receptor for the B cell growth factor BLyS-BAFF [210] [211]. It is essential for the maintenance of long-live plasma cells [212]–[214]. BCMA was therefore highly expressed only by plasmablasts and not by other B cell subsets (Figure 53A). BCMA maximal expression

was observed at day 14 after primary YF-17D vaccination, whereas it took place at day 3 after booster vaccination (Figure 53B).

A systems biology approach revealed that BCMA mRNA level in PBMCs collected at day 7 after primary YF-17D vaccination predicted the magnitude of nAb titers. [113]. However, we did not find that the percentage of B cells expressing BCMA at day 7 after primary vaccination correlated with the nAbs titers after 28 days ($p = 0.1137$) (Figure 53E).

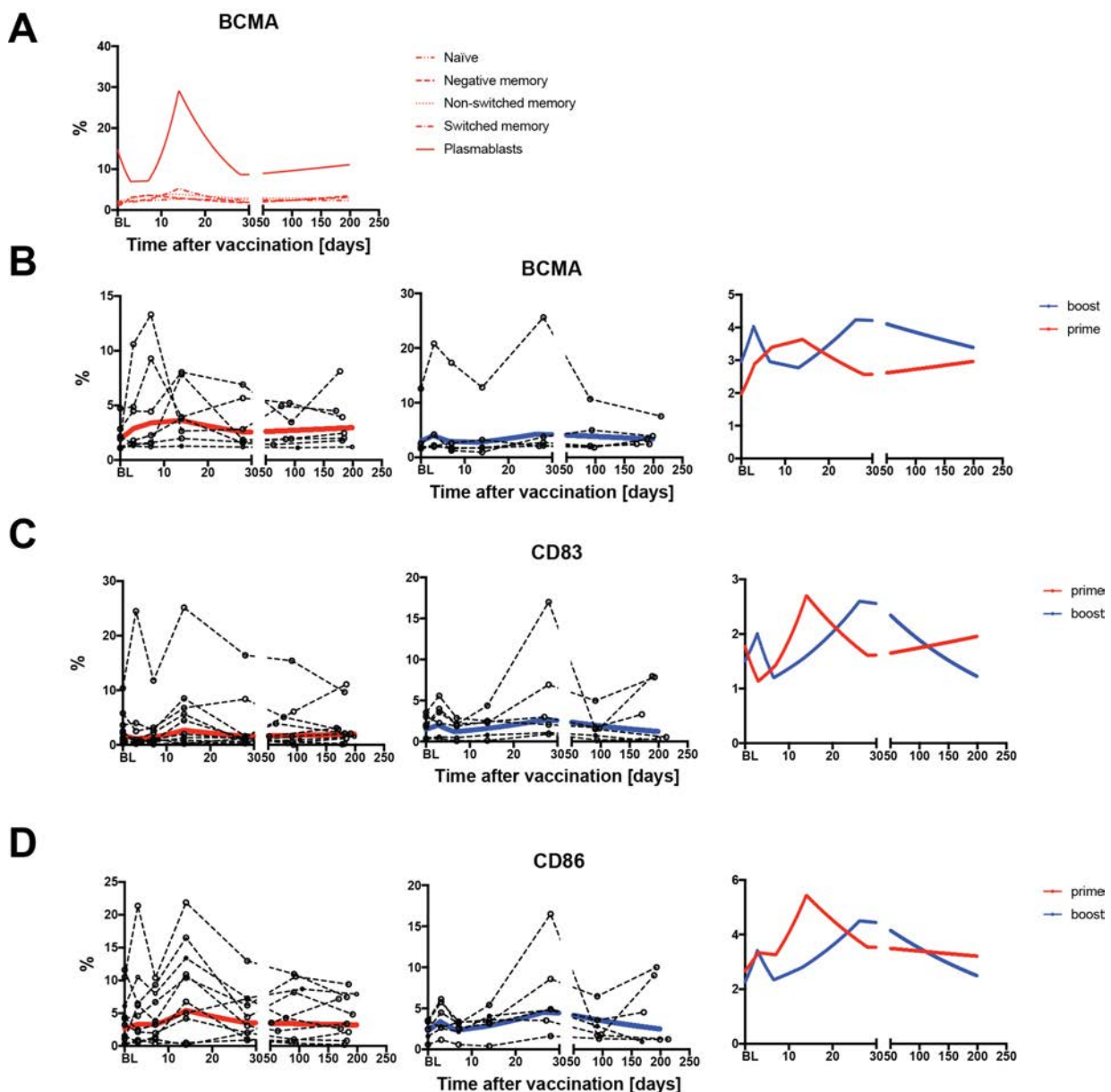


Figure 53 Kinetics of activation in B cells in response to primary and booster YF-17D vaccination. A, Percentages of cells positive for BCMA within the various B cell subsets in healthy volunteers after primary vaccination ($n = 10$). B, Percentages of cells positive for BCMA within total B cells subsets in healthy volunteers after primary vaccination (left panel, $n = 10$) and booster vaccination (middle panel, $n = 6$). The fitted population mean is represented in red for the priming group and in blue for the booster group (right panel). C, Percentages of cells

positive for CD83 within total B cells subsets in healthy volunteers after primary vaccination (left panel, n = 10) and booster vaccination (middle panel, n = 6). The fitted population mean is represented in red for the priming group and in blue for the booster group (right panel). D, Percentages of cells positive for CD86 within total B cells subsets in healthy volunteers after primary vaccination (left panel, n = 10) and booster vaccination (middle panel, n = 6). The fitted population mean is represented in red for the priming group and in blue for the booster group (right panel). E, Linear correlation between the percentage of B cells positive for BCMA and the level of neutralizing antibodies at D28 after primary vaccination (n = 10).

In order to analyze activation of B cells in response to YF-17D vaccination, we studied the expression of CD83 and CD86 [215]–[217] (Figure 51B and C). Analysis of B cell activation status revealed an increase in the percentage of CD83⁺ and CD86⁺ cells within total B cells at day 14 after primary YF-17D vaccination (Figure 53C and D). In contrast, up-regulation of CD83⁺ and CD86⁺ B cells after booster vaccination precedes the one after primary vaccination and occurred at day 3 (Figure 53C and D). Mainly the plasmablast subset among total B cells showed an activated status (Figure 51C).

Altogether, the plasmablast population increases and gets activated in both vaccination groups. The peak of these events occurs at day 14 after primary vaccination, while a booster vaccination induces a much earlier response peaking at day 3.

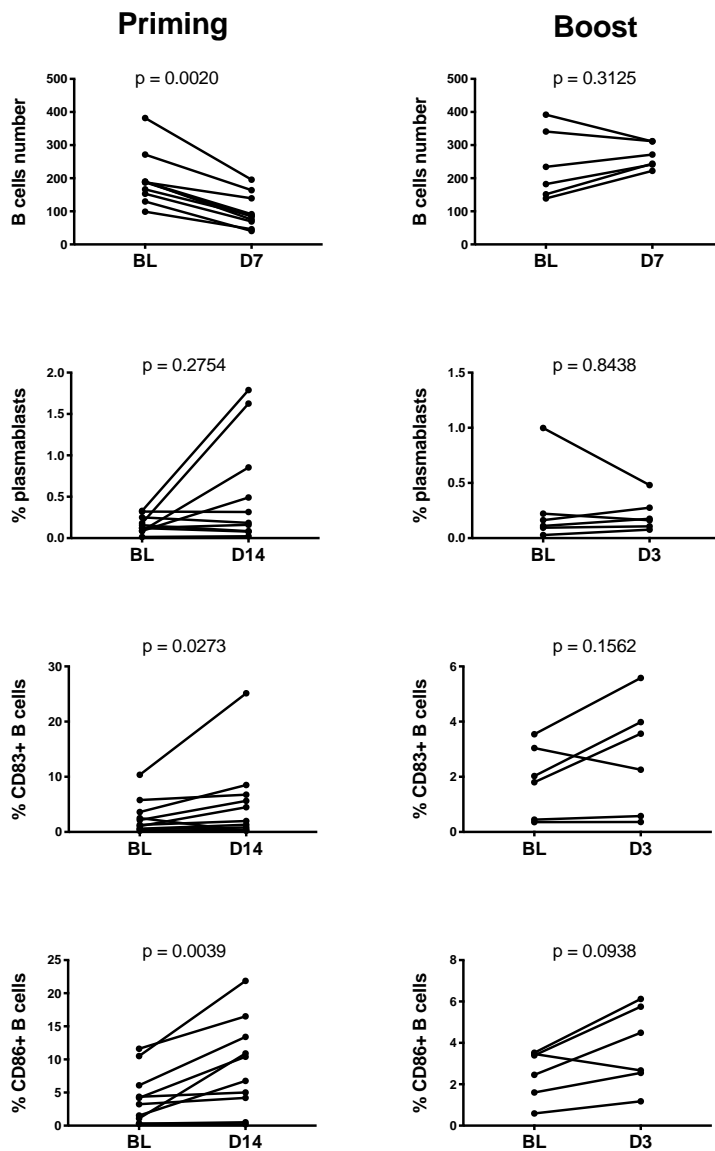


Figure 54 Changes of B cell-related parameters after primary or boost vaccination. Changes are calculated from baseline “BL” to the peak at either day 3 “D3”, day 7 “D7” or day 14 “D14” after vaccination. P-values of Wilcoxon test are indicated in the graphs.

YF-17D viral replication is detectable after primary but not after booster vaccination

The live-attenuated YFV-17D virus can be detected in blood circulation within the first week after vaccination [118]. We assessed viral replication after primary and booster YF-17D vaccination, for two reasons: first, because this viral load is positively correlated with a stronger immune response and in particular with the magnitude of the CD8 T cell activation [119]; second, if a subject is immune to Yellow Fever, we

hypothesized that virus would be rapidly neutralized and less capable to replicate. Viral load would thus be a measure of pre-existing immunity as well as predictive of subsequent T cell activation.

We found that most individuals of the priming group showed detectable viremia, with a peak at day 3 (n = 4/10) or day 7 (n = 2/10), after which it dropped rapidly (Figure 55A). In 4/10 individuals of the priming group there was no detectable virus (n= 4/10) (Figure 55A). None of the individuals in the booster group (n=0/6) showed detectable viremia (Figure 55B).

By directly comparing the nAbs titers versus viremia, we found a positive correlation between the absence of detectable viral copies after booster vaccination and pre-existing positive nAbs titers (Figure 55D). These observations provide supporting evidence to the hypothesis that pre-existing humoral immunity to the virus precludes replication of the YF-17D vaccine virus [99].

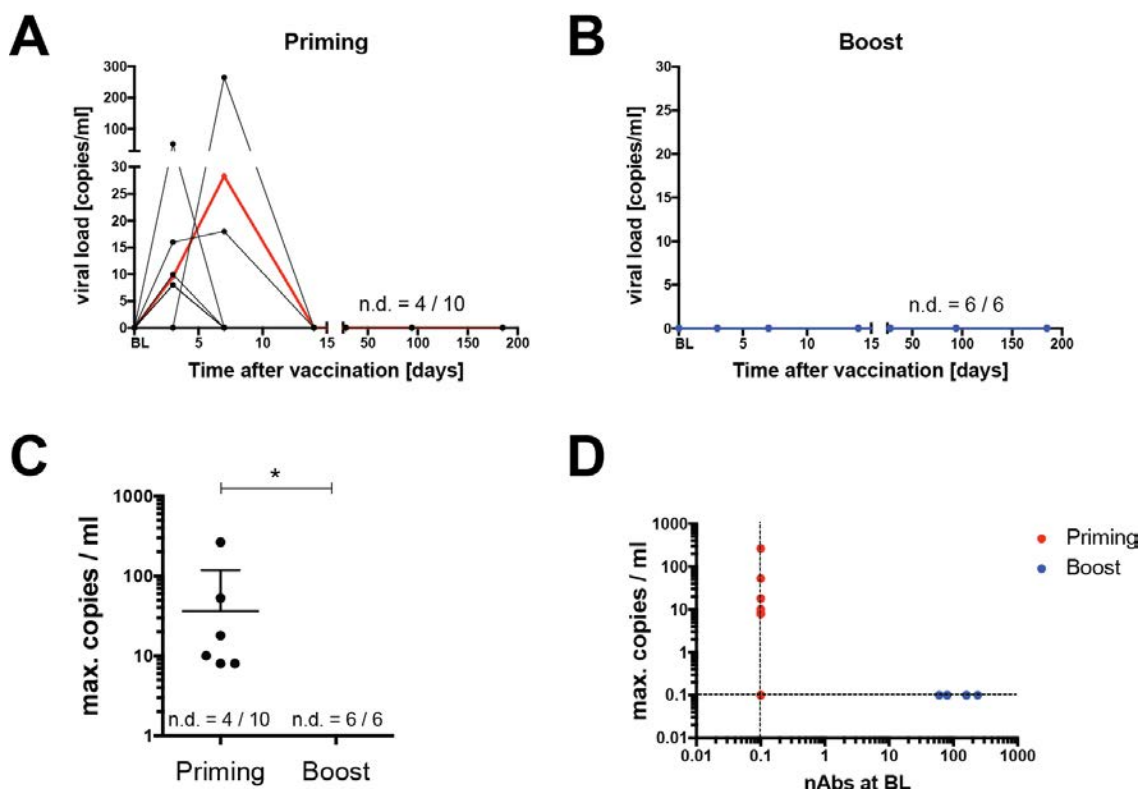


Figure 55 Viral load in the plasma in response to primary and booster YF-17D vaccination. A, Dynamics of viral load during the course of primary YF-17D vaccination (left panel, n = 10) and booster vaccination (right panel, n = 6). The average of individuals within each group is shown in red and blue, respectively. B, Comparison of maximal copies of viral RNA per ml assessed in sera of healthy volunteers after primary vaccination (“priming”, n = 10) and booster vaccination (“boost”, n = 6); “n.d.” = not detectable. Mann-Whitney test, p = 0.0395. C, Relationship between maximal copies of viral RNA per ml and the neutralizing antibodies titers before primary or booster vaccination.

Booster YF-17D vaccination induces minor T cell activation compared to primary vaccination

In order to assess T cell activation, we measured modulations of the activation markers CD69, CD38 and HLA-DR as well as the proliferation marker ki67, in CD8 and CD4 T cells (Figure 56). In analogy to previous studies, CD38 and HLA-DR expression reached their maximal up-regulation in CD8 T cells at day 14 after primary YF-17D vaccination and decreases back to baseline level around day 28 (Figure 57A and B) [99] [120] [122]. The expression of the early activation marker CD69 increased before the peak of the response, at day 7 after primary YF-17D vaccination (Figure 57C). However, we did not observe an up-regulation of these activation markers in CD8 T cells after a booster dose of YF-17D (Figure 57, Figure 58).

Within the priming group, we expected a link between viral load and T cell activation [119]. When the maximal viral load is comprised between 0 and 60 copies / ml, we found a positive linear correlation between the maximal viral load and the frequencies of activated CD8 T cells (defined as HLA-DR+ CD38+) at day 14 after YF-17D vaccination ($p = 0.0152$) (Figure 59). Above this range, the correlation was not linear any more. This is in accordance with previously published data [119].

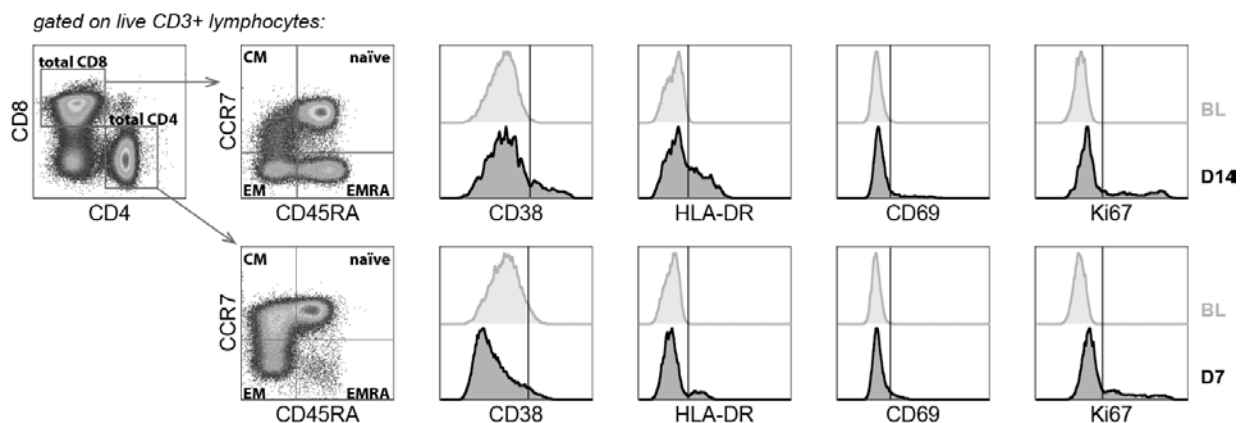


Figure 56 Representative FlowJo gating strategy for the total T cells analysis. CD8 versus CD4 distinction were gated on live CD3+ CD16- lymphocytes. Subsets distribution in CD8 and CD4 T cells was based on the conventional differentiation markers CCR7 and CD45RA to determine naïve (CCR7+ CD45RA+), CM (CCR7+ CD45RA-), EM (CCR7- CD45RA-), and EMRA (CCR7- CD45RA+). The indicated activation markers were analyzed in total CD4 and CD8 T cells. The expression at baseline (BL) and at day 14 after vaccination (D14) are represented in off-set overlay histogram

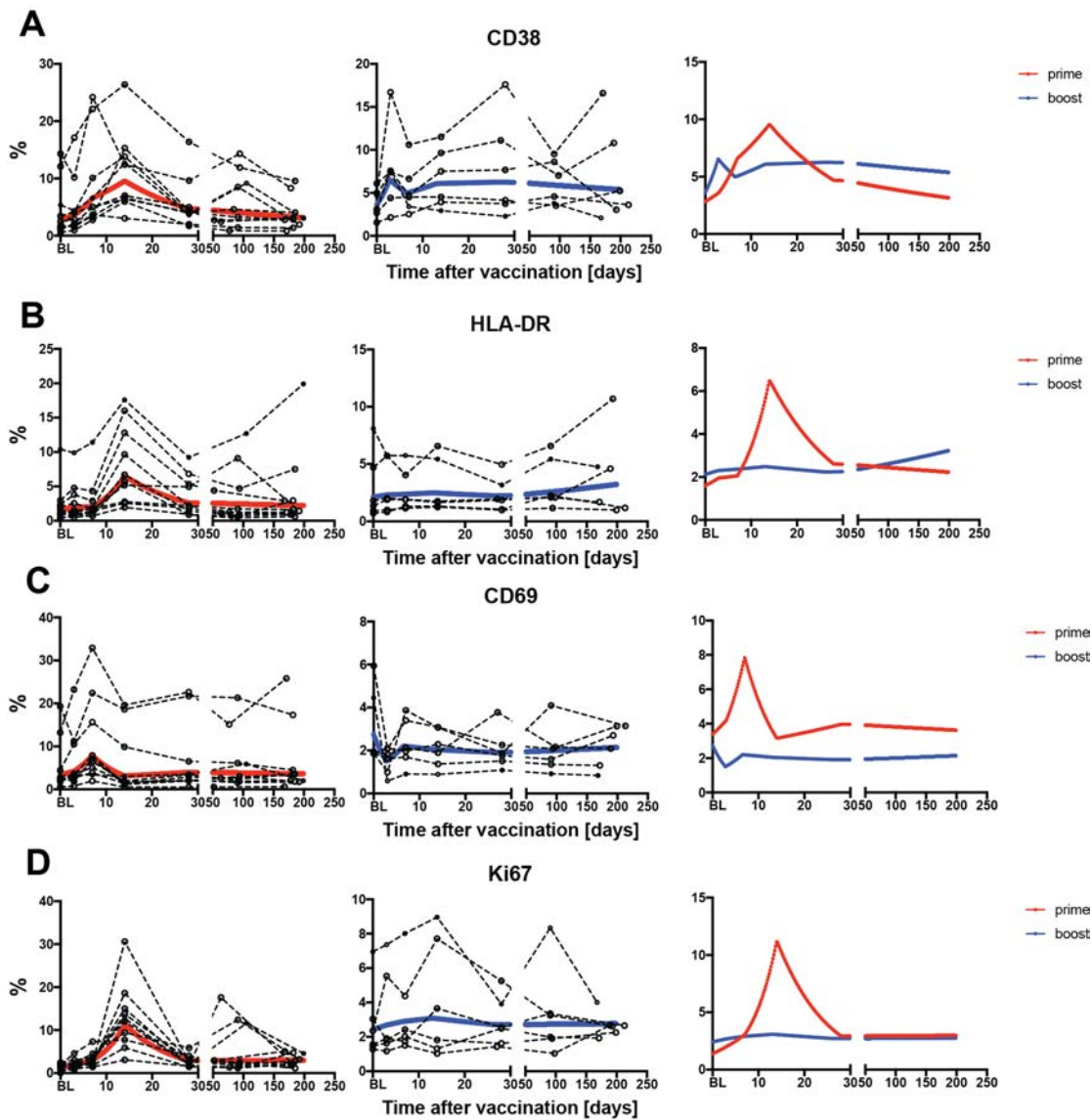


Figure 57 Kinetics of activation and proliferation in total CD8 T cells in response to primary and booster YF-17D vaccination. A, Percentages of cells positive for CD38 within total CD8 T cells in healthy volunteers after primary vaccination (left panel, $n = 10$) and booster vaccination (middle panel, $n = 6$). The fitted population mean is represented in red for the priming group and in blue for the booster group (right panel). B, Percentages of cells positive for HLA-DR within total CD8 T cells in healthy volunteers after primary vaccination (left panel, $n = 10$) and booster vaccination (middle panel, $n = 6$). The fitted population mean is represented in red for the priming group and in blue for the booster group (right panel).

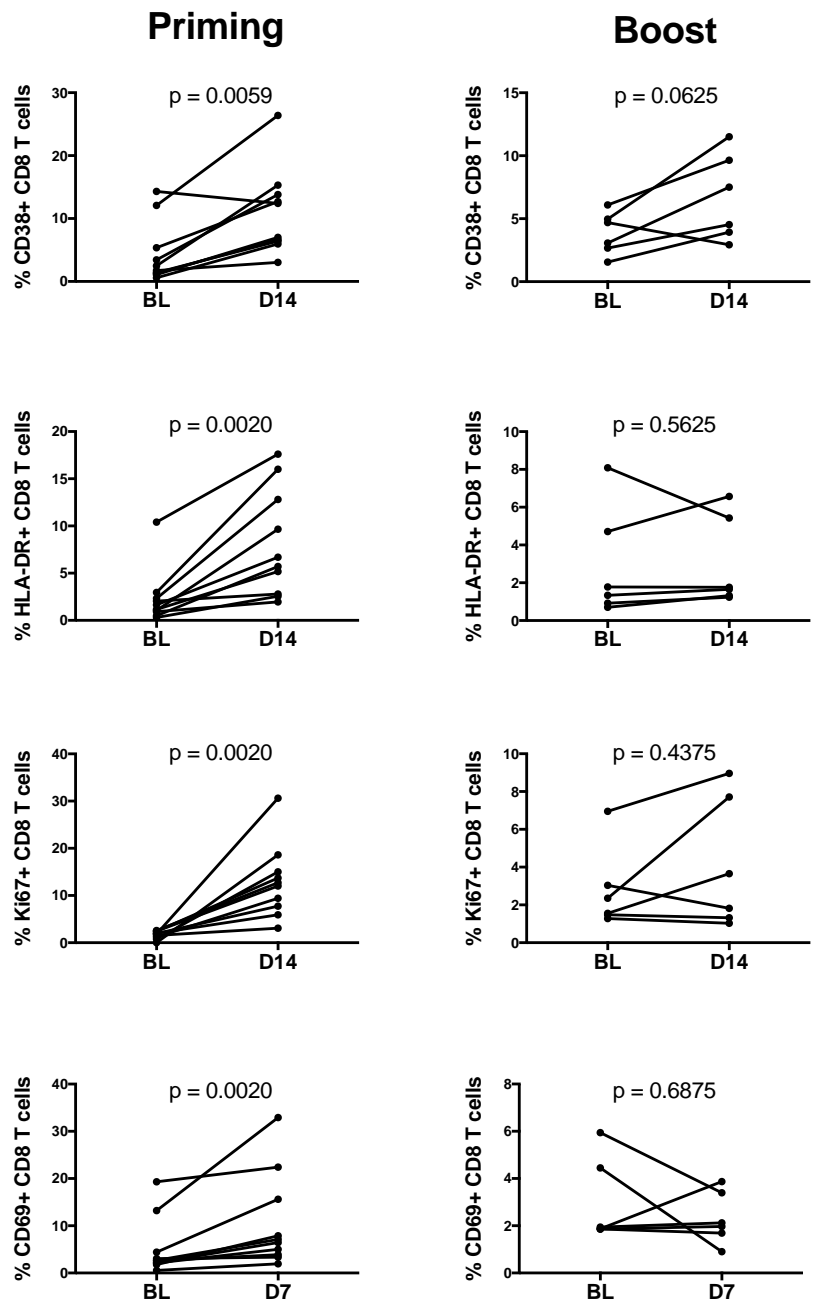


Figure 58 Expression changes of the activation and proliferation markers in CD8 T cells after primary or boost vaccination. P-values of Wilcoxon test are indicated in the graphs.

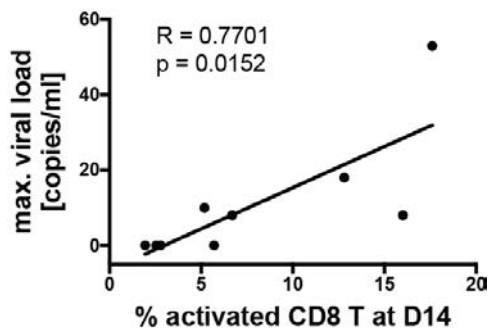


Figure 59 Linear correlation between the percentage of activated CD8 T cells at day 14 after primary YF-17D vaccination and maximal viral load. “activated CD8 T cells at D14” defined as CD38+ HLADR+ CD8 T cells at day 14 (n=9).

Concerning CD4 T cells, the overall activation induced by the YF-17D vaccine was more modest (significant increase in HLA-DR and Ki67), even after primary vaccination (Figure 60, Figure 61). The CD4 T cell responses that could be detected in the priming group preceded the CD8 T cell response, peaking at day 7 after vaccination (Figure 60).

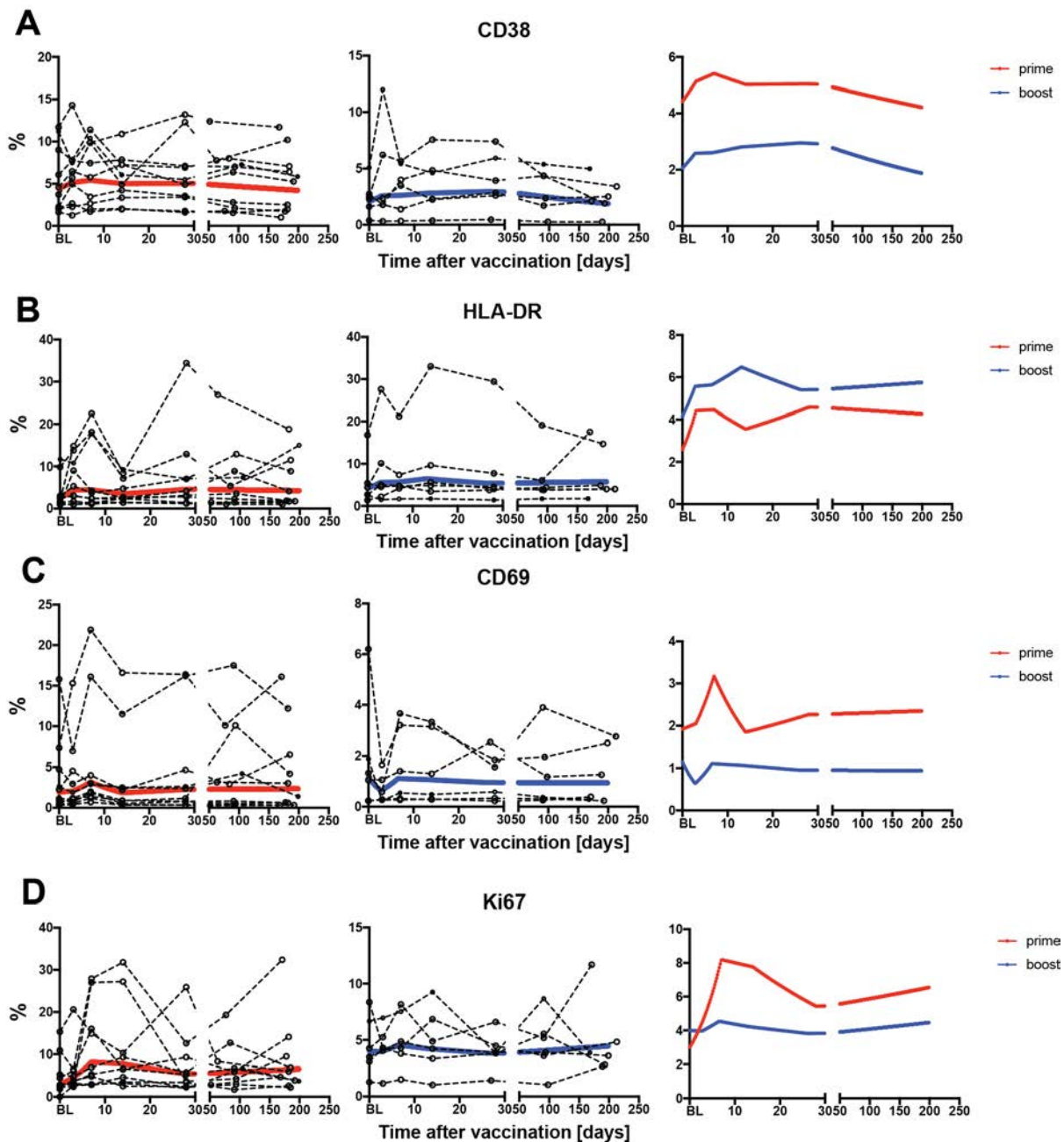


Figure 60 Kinetics of activation and proliferation in total CD4 T cells in response to primary and booster YF-17D vaccination. A, Percentages of cells positive for CD38 within total CD4 T cells in healthy volunteers after primary vaccination (left panel, $n = 10$) and booster vaccination (middle panel, $n = 6$). The fitted population mean is represented in red for the priming group and in blue for the booster group (right panel). B, Percentages of cells positive for HLA-DR within total CD4 T cells in healthy volunteers after primary vaccination (left panel, $n = 10$) and booster vaccination (middle panel, $n = 6$). The fitted population mean is represented in red for the priming group and in blue for the booster group (right panel). C, Percentages of cells positive for CD69 within total CD4 T cells in healthy volunteers after primary vaccination (left panel, $n = 10$) and booster vaccination (middle panel, $n = 6$). The fitted population mean is represented in red for the priming group and in blue for the booster group (right panel). D, Percentages of cells positive for Ki-67 within total CD4 T cells in healthy volunteers after primary vaccination (left panel, $n = 10$) and booster vaccination (middle panel, $n = 6$). The fitted population mean is represented in red for the priming group and in blue for the booster group (right panel).

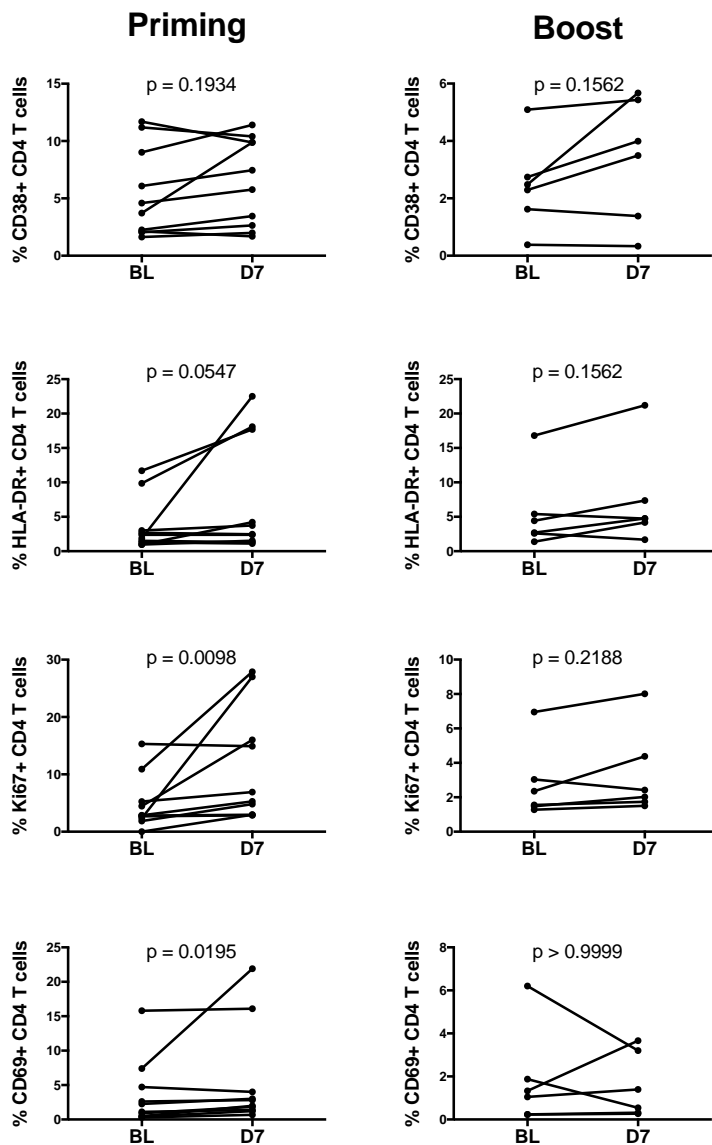


Figure 61 Expression changes of the activation and proliferation markers in CD4 T cells after primary or boost vaccination. P-values of Wilcoxon test are indicated in the graphs.

The absence of detectable virus in the plasma of booster vaccinees suggests that the low degree of T cell activation was due to the neutralization of antigen when there is pre-existing humoral immunity. This dichotomy between primary and secondary vaccination regarding T cell activation is consistent with a recent report [99].

The magnitude of the re-call response of antigen-specific T cells is reduced compared to primary YF-17D vaccination

To further investigate the CD8 T cell response, we focused on the magnitude and kinetics of the antigen-specific response to the YF-17D vaccine. Using an A2/LLW-specific fluorescent multimer, we analyzed by flow cytometry the CD8-enriched fraction of PBMCs during the course of primary and booster vaccination (Figure 62). Following the peak of the viral replication at day 3/7 after primary vaccination, the A2/LLW-specific response culminated at day 14, which is in line with previous studies (Fig 8A) [98] [99] [118] [120]. A2/LLW-specific CD8 T cells showed an activated phenotype indicated by the up-regulation of the activation markers CD38 and HLA-DR at day 14 after primary vaccination (Figure 63A and B). The expression of the proliferation marker Ki67 was also increased at the peak of the primary response (Figure 63D).

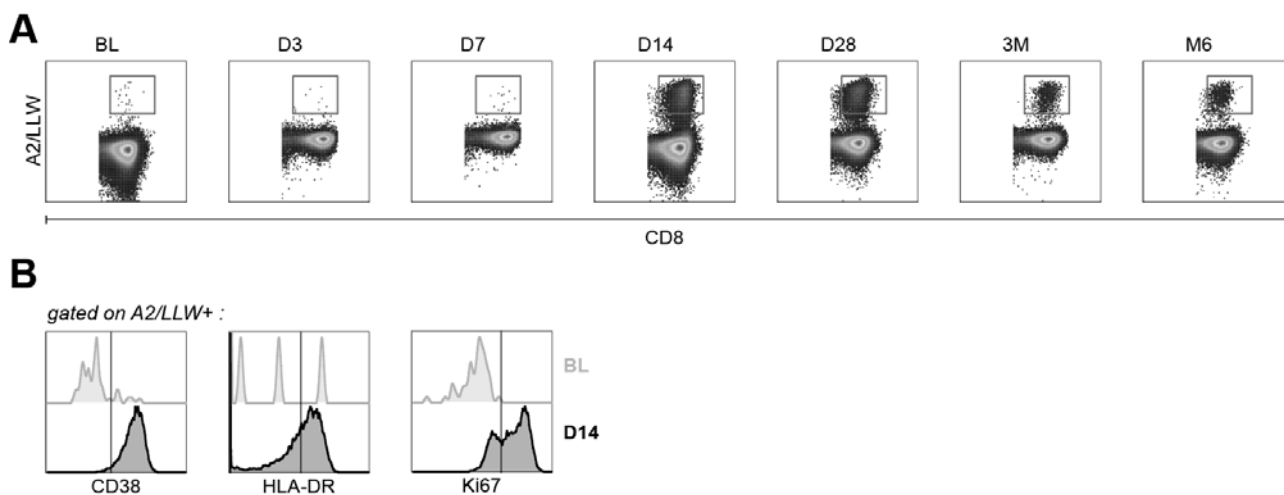


Figure 62 Representative FlowJo gating strategy for the analysis of A2/LLW-specific CD8 T cells. A, Frequency of tetramer positive CD8 T cells (A2/LLW) is represented in dot plots at baseline (BL) and several time points after YF-17D vaccination (D = days, M = months). B, The indicated markers were analyzed in tetramer positive CD8 T cells. The expression at baseline (BL) and at day 14 after vaccination (D14) are represented in offset overlay histograms.

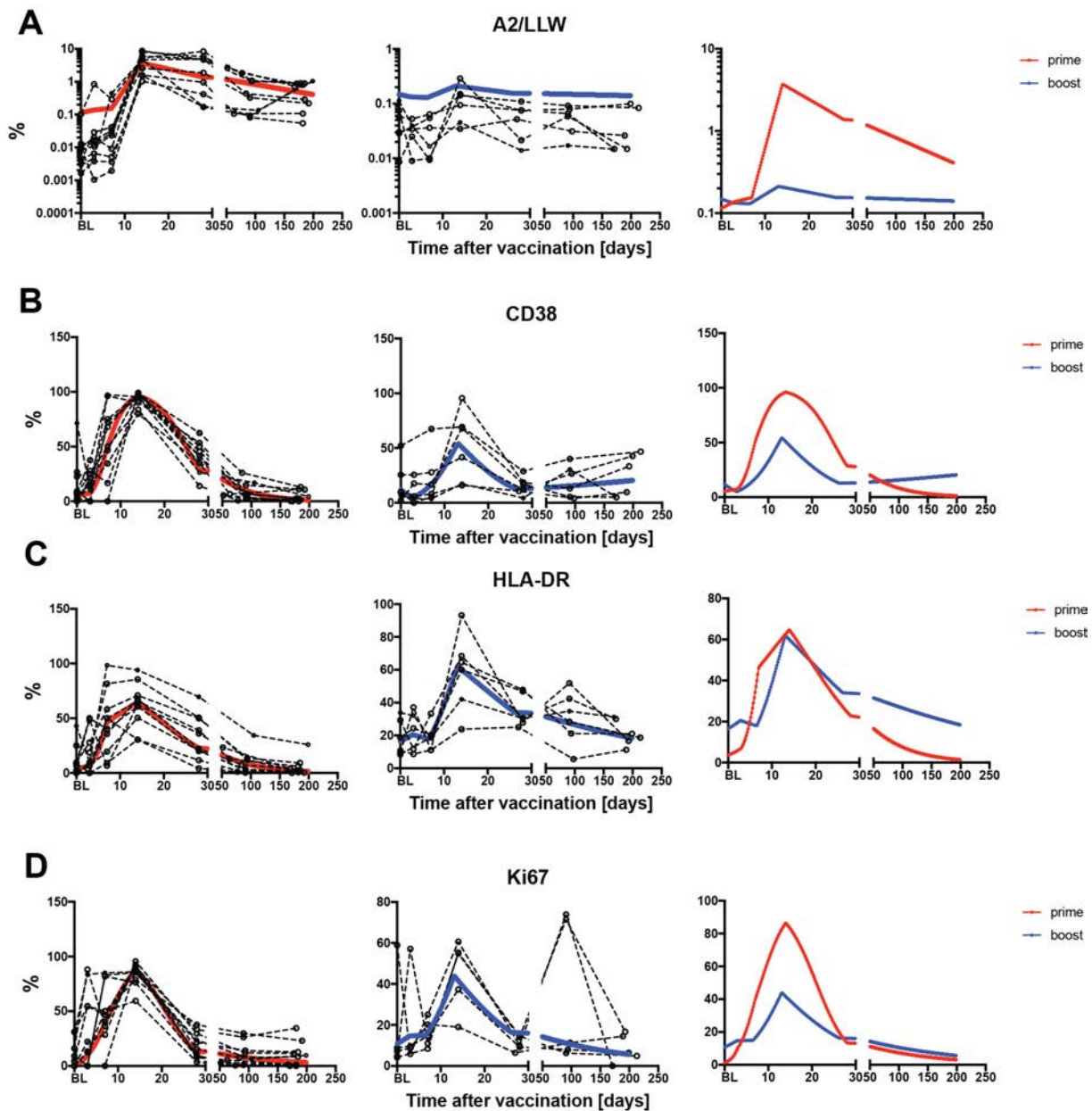


Figure 63 Kinetics of A2/LLW-specific CD8 T cells in response to primary and booster YF-17D vaccination. A, Percentage of tetramer positive CD8 T cells (A2/LLW) expressed as percentage in total CD8 T cells in healthy volunteers after primary vaccination (left panel, $n = 10$) and booster vaccination (middle panel, $n = 6$). The fitted population mean is represented in red for the priming group and in blue for the booster group (right panel). B, Percentages of cells positive for CD38 within total tetramer positive CD8 T cells in healthy volunteers after primary vaccination (left panel, $n = 10$) and booster vaccination (middle panel, $n = 6$). The fitted population mean is represented in red for the priming group and in blue for the booster group (right panel). C, Percentages of cells positive for HLA-DR within total tetramer positive CD8 T cells in healthy volunteers after primary vaccination (left panel, $n = 10$) and booster vaccination (middle panel, $n = 6$). The fitted population mean is represented in red for the priming group and in blue for the booster group (right panel). D, Percentages of cells positive for Ki67 within total tetramer positive CD8 T cells in healthy volunteers after primary vaccination (left panel, $n = 10$) and booster vaccination (middle panel, $n = 6$). The fitted population mean is represented in red for the priming group and in blue for the booster group (right panel).

Booster vaccinees showed higher detectable frequencies of A2/LLW-specific CD8 T cells at baseline compared to pre-boost frequencies (Mann-Whitney test, $p = 0.0312$) (Figure 64). Following booster vaccination, a modest increase of the antigen-specific population frequency was observed (Figure 63A). Supporting this observation, booster vaccinees showed similar up-regulation of activation marker but decreased Ki67 expression compared to the priming group (Figure 63D).

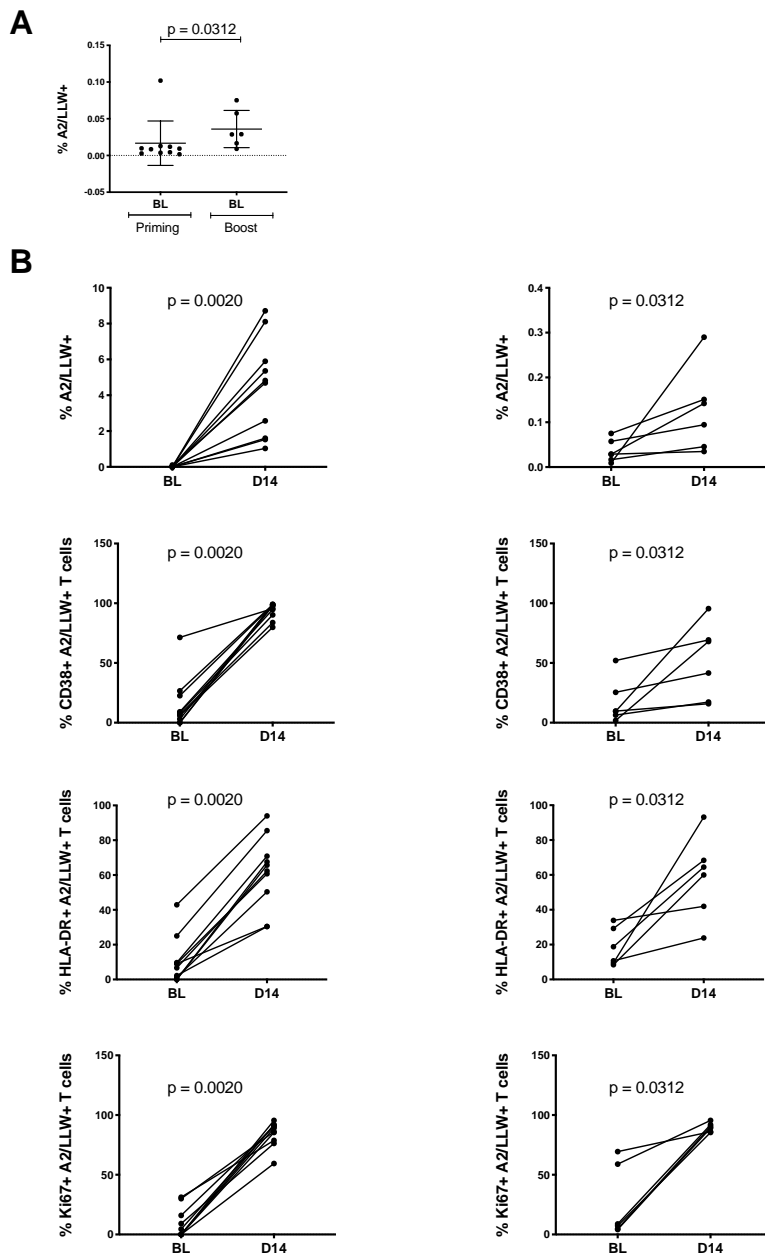


Figure 64 Changes of A2/LLW-related parameters. A, Comparison of the frequencies of tetramer positive CD8 T cells (A2/LLW) at baseline (BL) in healthy volunteers from the priming (n = 10) and boost (n = 6) groups. P-value of Mann-Whitney test is indicated on the graph. B, P-values of Wilcoxon test are indicated on the graphs.

Taken together, a booster dose of the YF-17D vaccine does not substantially induce the proliferation of A2/LLW-specific CD8 T cells found in blood.

T cells transiently drop immediately after YF-17D primary vaccination

Given the established correlation between viral load and the magnitude of the CD8 T cell response [119], we analyzed the number of total CD8 and CD4 T cells based on flow cytometry analyses and the complete blood counts (Figure 56). Intriguingly, the numbers of both CD8 and CD4 T cells in the blood transiently declined immediately after primary YF-17D vaccination and expanded back to baseline level after 14 days (Figure 65A and B). The same was true in terms of frequencies (data not shown). This observation had already been made by Kohler et al [122]. Notably, the drop of total CD8 T cells in the peripheral blood preceded this increase in A2/LLW-specific CD8 T cells. In contrast, we did not observe such a decrease of CD8 or CD4 T cell numbers in individuals of the booster group (Figure 65A and B).

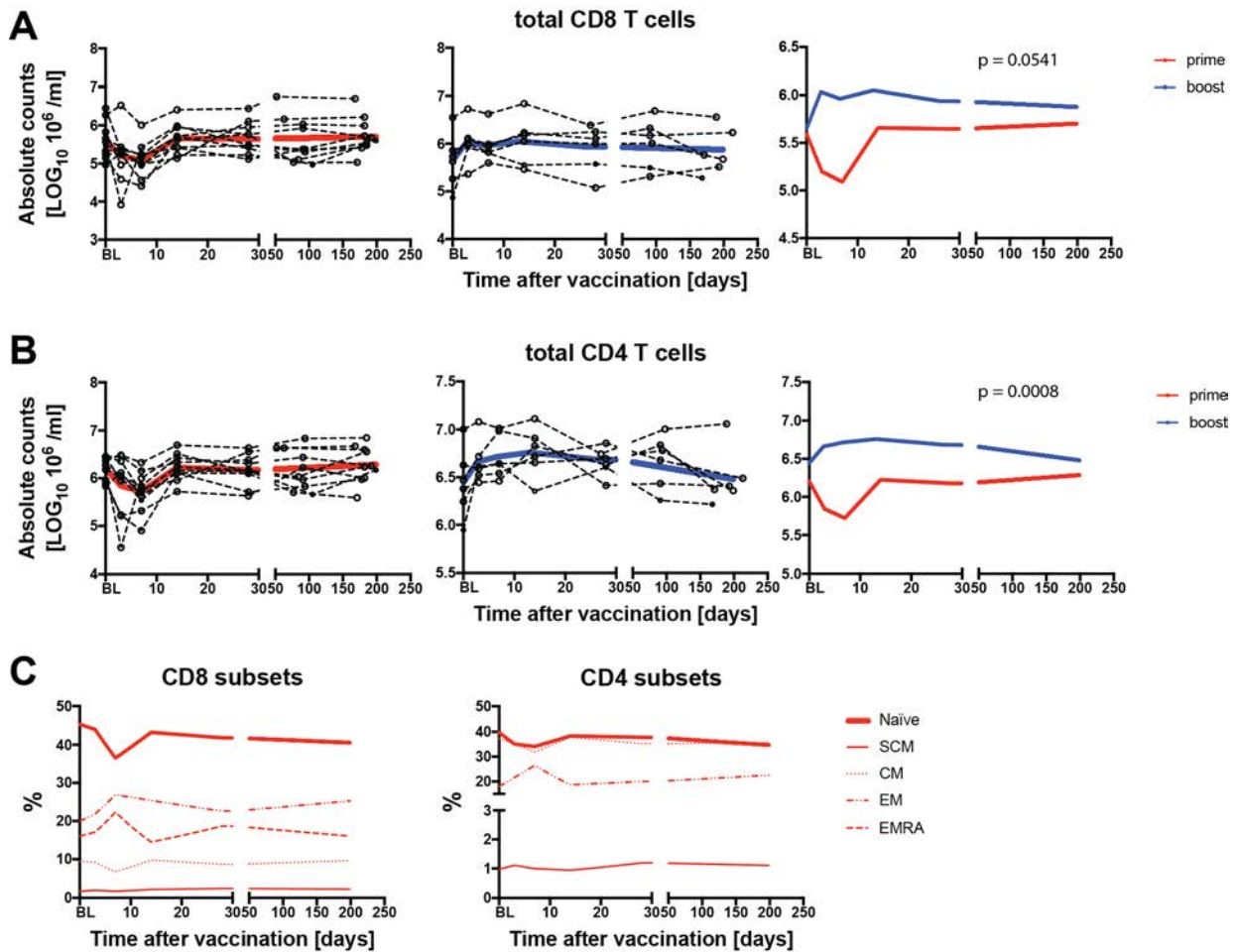


Figure 65 Kinetics of total CD8 and CD4 T cells in response to primary and booster YF-17D vaccination. A, Absolute number of total CD8 T cells in healthy volunteers after primary vaccination (left panel, $n = 10$) and booster vaccination (middle panel, $n = 6$). The fitted population mean is represented in red for the priming group and in blue for the booster group (right panel). B, Absolute number of total CD4 T cells in healthy volunteers after primary vaccination (left panel, $n = 10$) and booster vaccination (middle panel, $n = 6$). The fitted population mean is represented in red for the priming group and in blue for the booster group (right panel). C, Percentages of various CD8 (right panel) and CD4 (left panel) T cell subsets in healthy volunteers after primary vaccination ($n = 10$).

Interestingly, the reduction of CD8 and CD4 T cells after primary vaccination was restricted to the central memory (CM; $\text{CCR7}^+ \text{CD45RA}^-$) and naïve ($\text{CCR7}^+ \text{CD45RA}^+$) subsets (Figure 65C). Both these subsets express the chemokine receptor CCR7. This molecule is critical for naïve CD8 T cell migration to lymph nodes and splenic white pulp, and memory CD8 T cell localization into secondary lymphoid organs. The CM population that expresses CCR7 is able to enter lymph nodes, whereas effector memory cells (EM; $\text{CCR7}^- \text{CD45RA}^-$ and EMRA; $\text{CCR7}^- \text{CD45RA}^+$) that lack expression of this receptor cannot enter lymph nodes and therefore localize preferentially in the periphery [218]–[220].

In addition to chemotaxis, another important aspect of T cell homing and subsequent priming is the retention in the lymph nodes. Upon peptide-MHC encounter on dendritic cells, T cells get activated and up-regulate the early activation marker CD69 on their surface. CD69 binds to the egress mediator Sphingosine 1-Phosphate Receptor 1 (S1PR1), which leads to the internalization of the receptor and consequently to T cell retention in the lymph node [221]–[227]. Along these lines, we found a positive correlation between CD69 expression level in T cells at baseline and the fold change in CD8 and CD4 T cell numbers ($p = 0.036$ and $p < 0.0001$, respectively) (Figure 66A). Curiously, we did not find a significant correlation between the fold change in CD8 T cell numbers and the peak frequency of CD69 at day 7 ($p = 0.3177$) (Figure 66B). This correlation was significant for CD4 T cell though ($p = 0.0162$). This would suggest that individuals with high CD69 expression before vaccination might have a pre-disposition to a better recruitment of CD8 T cells.

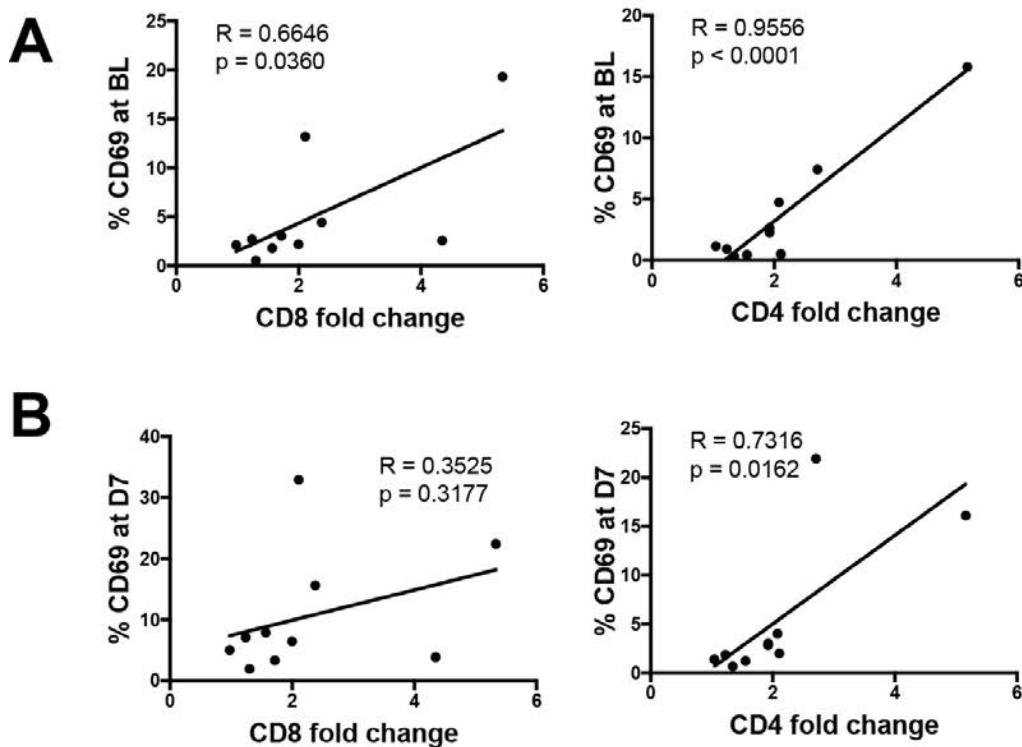


Figure 66 Correlation of the T cell drop with retention in the lymph node. A, Linear correlation between the fold change of total CD8 (left) and CD4 (right) T cell numbers in the blood after primary vaccination and the percentage of CD69+ CD8 T cells at baseline ($n = 10$). B, Linear correlation between the fold change of CD8 (left) and CD4 (right) T cell numbers after primary vaccination and the percentage of CD69+ CD4 T cells at day 7 ($n = 10$).

We next wondered whether T cells migrate to the skin after subcutaneous injection of the YF-17D vaccine. We therefore analyzed in some individuals the chemokine receptor CCR10, which is conventionally known as a skin homing marker (n = 6) [228]–[230]. Only a small proportion of CD8 and CD4 T cells in the periphery expressed this marker at baseline (Figure 67A). However, we noted that the increase of CCR10⁺ cells after primary vaccination correlated with the drop of CD8 T cells but not the drop of CD4 T cells (raw data: p = 0.0506 and p = 0.8851) (Figure 67B).

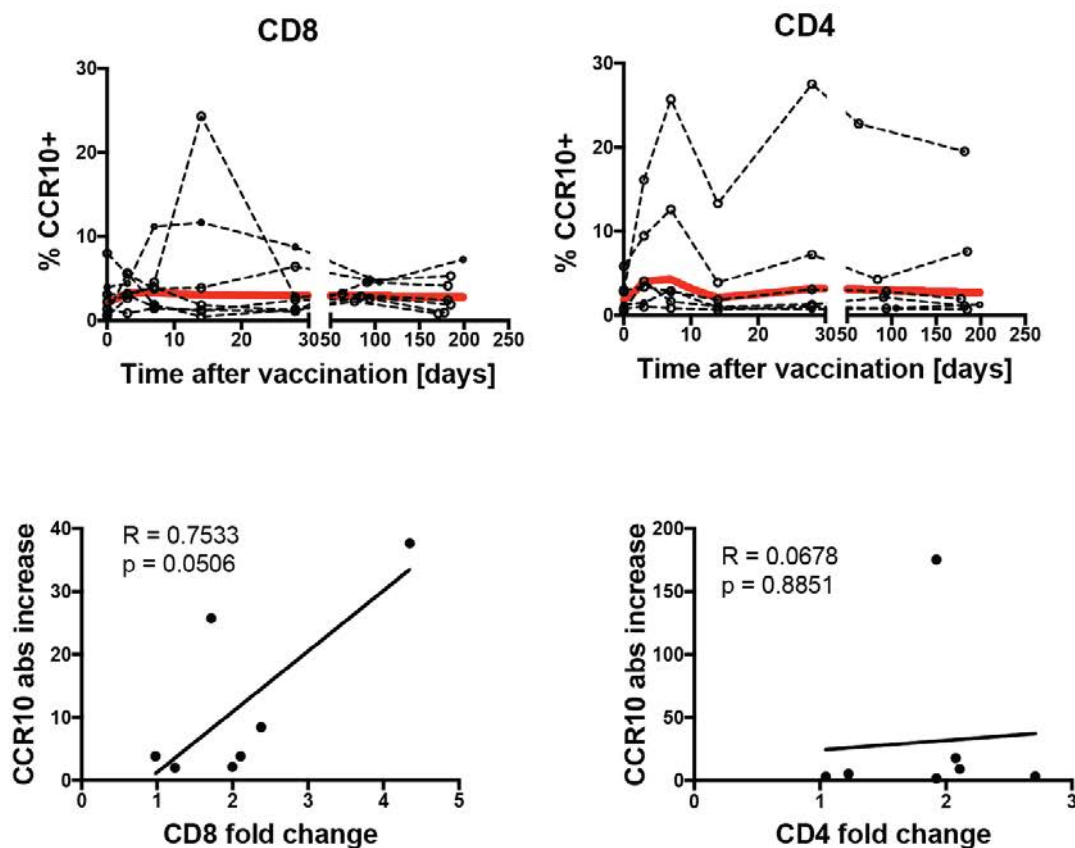


Figure 67 Correlation of the T cell drop with migration. A, Frequency of CCR10-positive CD8 and CD4 T cells following YF-17D primary vaccination. B, Linear correlation between the fold change of CD8 (left) and CD4 (right) T cell numbers after primary vaccination and the increase of CCR10 expression at day 7 (n = 7).

These findings indicate that the T cell drop observed after primary YF-17D vaccination results from the migration and trapping of T cells from the periphery into secondary lymphoid organs.

Innate immune activation is detectable in primary and not in booster vaccination

In agreement with recent findings, we hypothesized that the reduction in T cell responses observed in the booster versus the priming group is linked to pre-existing immunity (nAbs at baseline), which eliminates the vaccine virus, precludes viral replication and precludes antigen availability for T cell activation. This would also suggest that the innate response in the booster vaccination is not substantially triggered. To address innate activation, we studied NK cells, Innate-lymphoid cells (ILCs) and monocytes.

In our study, the number of total monocytes were slightly increased after primary vaccination, yet not significantly (Figure 69, Figure 69 and Figure 71). Previous work did not show much changes in monocytes number neither [122]. The same was observed in terms of frequencies (data not shown). The “classical” (CD14⁺⁺ CD16⁻) and “inflammatory” (CD14⁺⁺ CD16⁺) subsets were increased in terms of numbers and frequencies after primary vaccination (Figure 69 and Figure 71). In addition, activation of monocytes occurred at day 7 after primary vaccination, as shown by the up-regulation of the activation markers CD40, CD83 and CD86 (Figure 70). This was true for all monocyte subsets (Figure 72). In contrast, booster vaccination did not induce any significant change of any monocyte populations at day 3 and failed to activate these cells (Figure 69, Figure 70 and Figure 71).

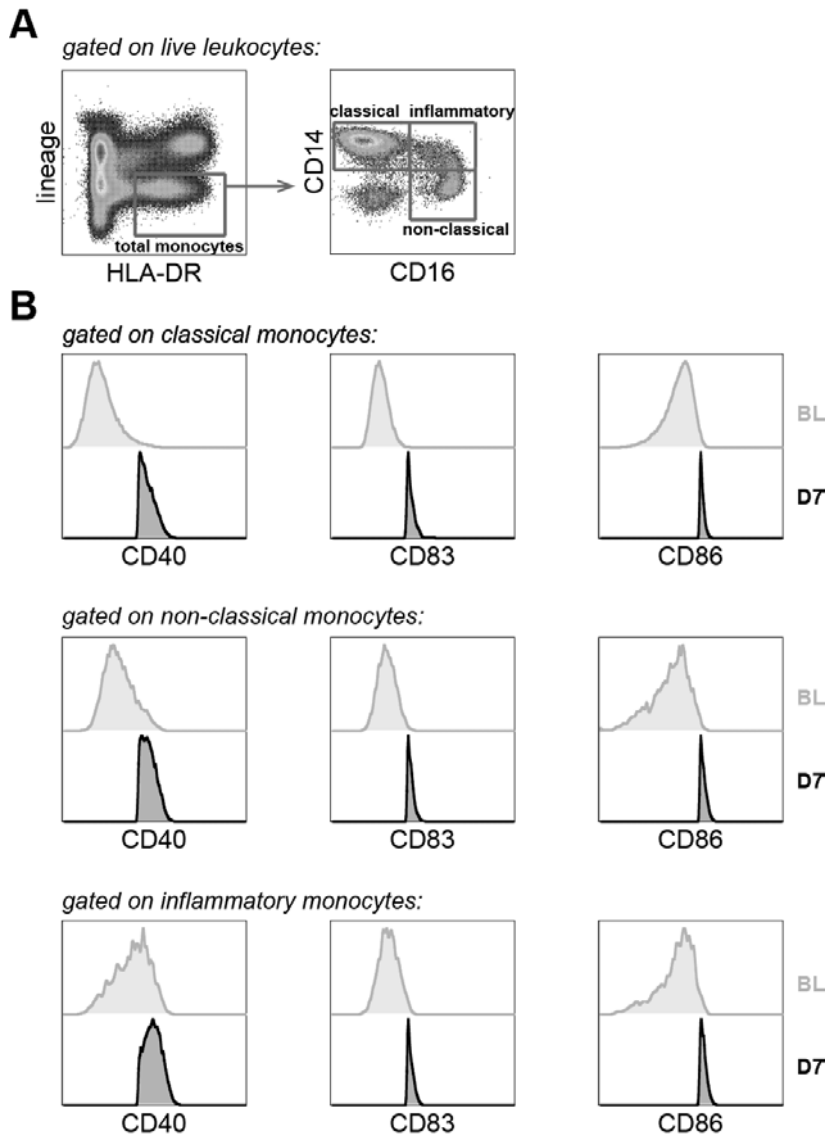


Figure 68 Representative FlowJo gating strategy for the monocytes analysis. A, Total monocytes (lineage- HLA-DR^+) were gated on live leukocytes using forward/sideward scatter properties. Singlets were selected using forward/side ward scatter width/height characteristics. Monocyte subsets distribution was based on CD14 and CD16 expression to determine classical ($\text{CD14}^{++} \text{CD16}^-$), non- classical ($\text{CD14}^+ \text{CD16}^{++}$), and intermediate ($\text{CD14}^{++} \text{CD16}^+$) monocytes. *Lineage:* CD3 , CD19 , CD20 , CD56 , FcER1 . B, The indicated activation markers were analyzed in all monocytes subsets at baseline (BL) and day 7 after YF-17D vaccination (D7). They are represented in off-set overlay histograms.

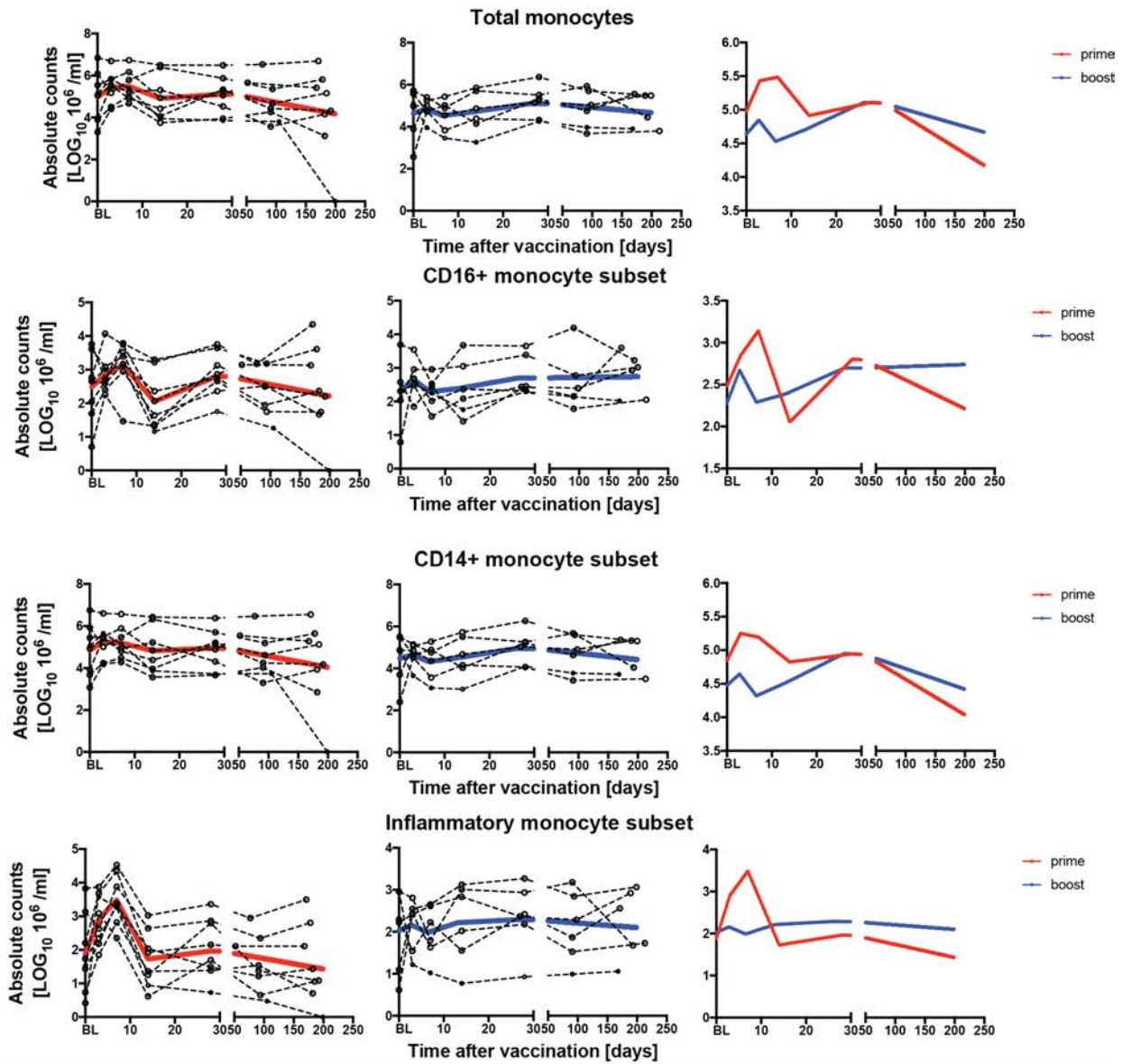


Figure 69 Kinetics of the monocytes response to primary and booster YF-17D vaccination. A, Absolute number of total monocytes in healthy volunteers after primary vaccination (left panel, $n = 7$) and booster vaccination (middle panel, $n = 6$). The fitted population mean is represented in red for the priming group and in blue for the booster group (right panel). B, Absolute number of the CD16+ monocyte subset in healthy volunteers after primary vaccination (left panel, $n = 7$) and booster vaccination (middle panel, $n = 6$). The fitted population mean is represented in red for the priming group and in blue for the booster group (right panel). C, Absolute number of the CD14+ monocyte subset in healthy volunteers after primary vaccination (left panel, $n = 7$) and booster vaccination (middle panel, $n = 6$). The fitted population mean is represented in red for the priming group and in blue for the booster group (right panel). D, Absolute number of the inflammatory CD14+CD16+ monocyte subset in healthy volunteers after primary vaccination (left panel, $n = 7$) and booster vaccination (middle panel, $n = 6$). The fitted population mean is represented in red for the priming group and in blue for the booster group (right panel).

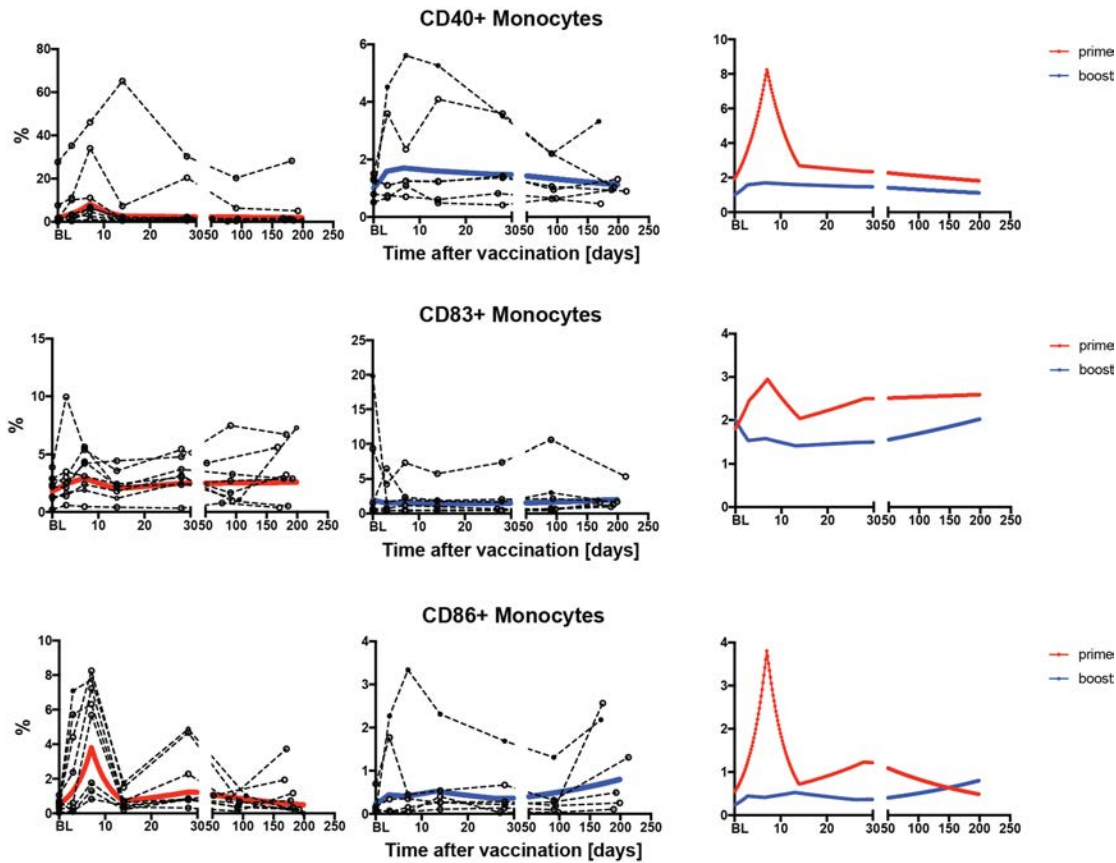


Figure 70 Kinetics of activation in total monocytes in response to primary and booster YF-17D vaccination. A, Percentages of cells positive for CD40 within total monocytes in healthy volunteers after primary vaccination (left panel, n = 7) and booster vaccination (middle panel, n = 6). The fitted population mean is represented in red for the priming group and in blue for the booster group (right panel). B, Percentages of cells positive for CD83 within total monocytes in healthy volunteers after primary vaccination (left panel, n = 7) and booster vaccination (middle panel, n = 6). The fitted population mean is represented in red for the priming group and in blue for the booster group (right panel). C, Percentages of cells positive for CD86 within total monocytes in healthy volunteers after primary vaccination (left panel, n = 7) and booster vaccination (middle panel, n = 6). The fitted population mean is represented in red for the priming group and in blue for the booster group (right panel).

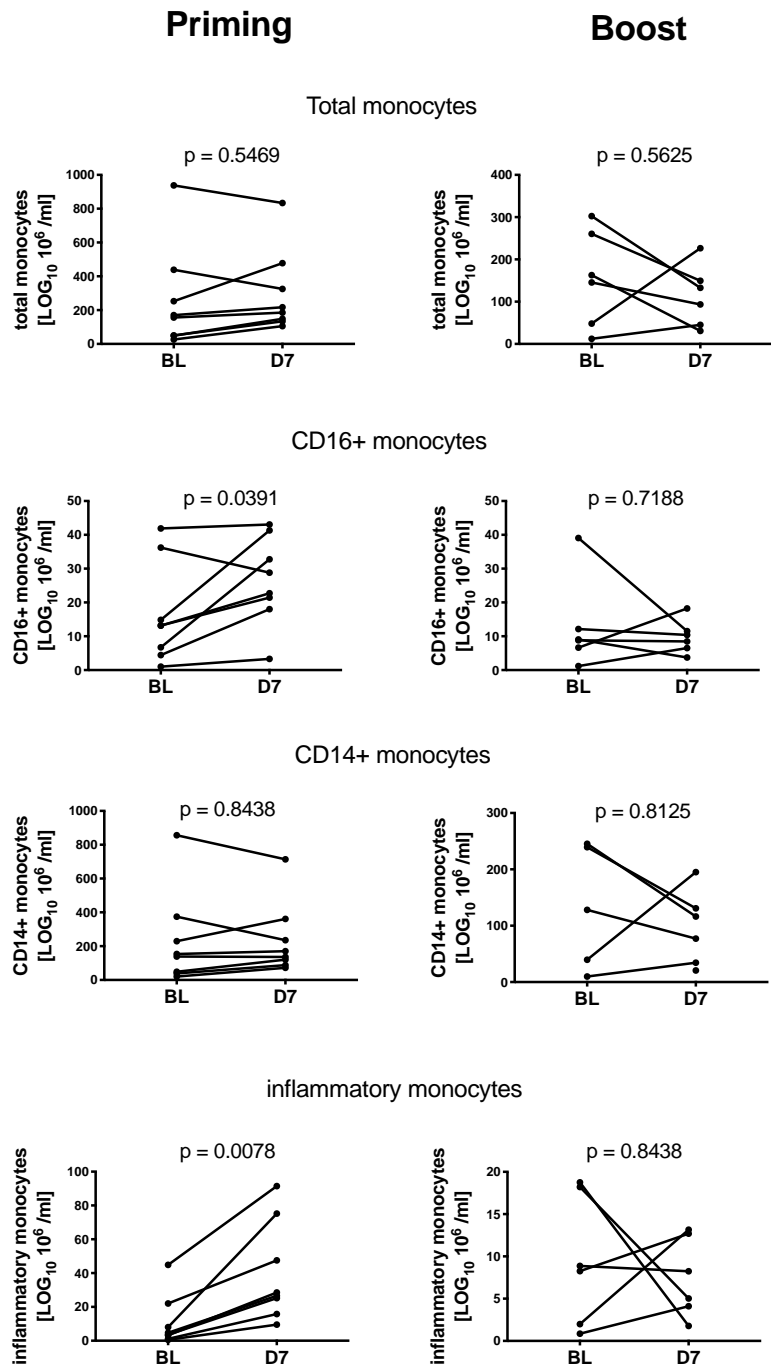


Figure 71 Changes of total monocytes and monocyte subsets number after primary or boost vaccination. P-values of Wilcoxon test are indicated in the graphs.

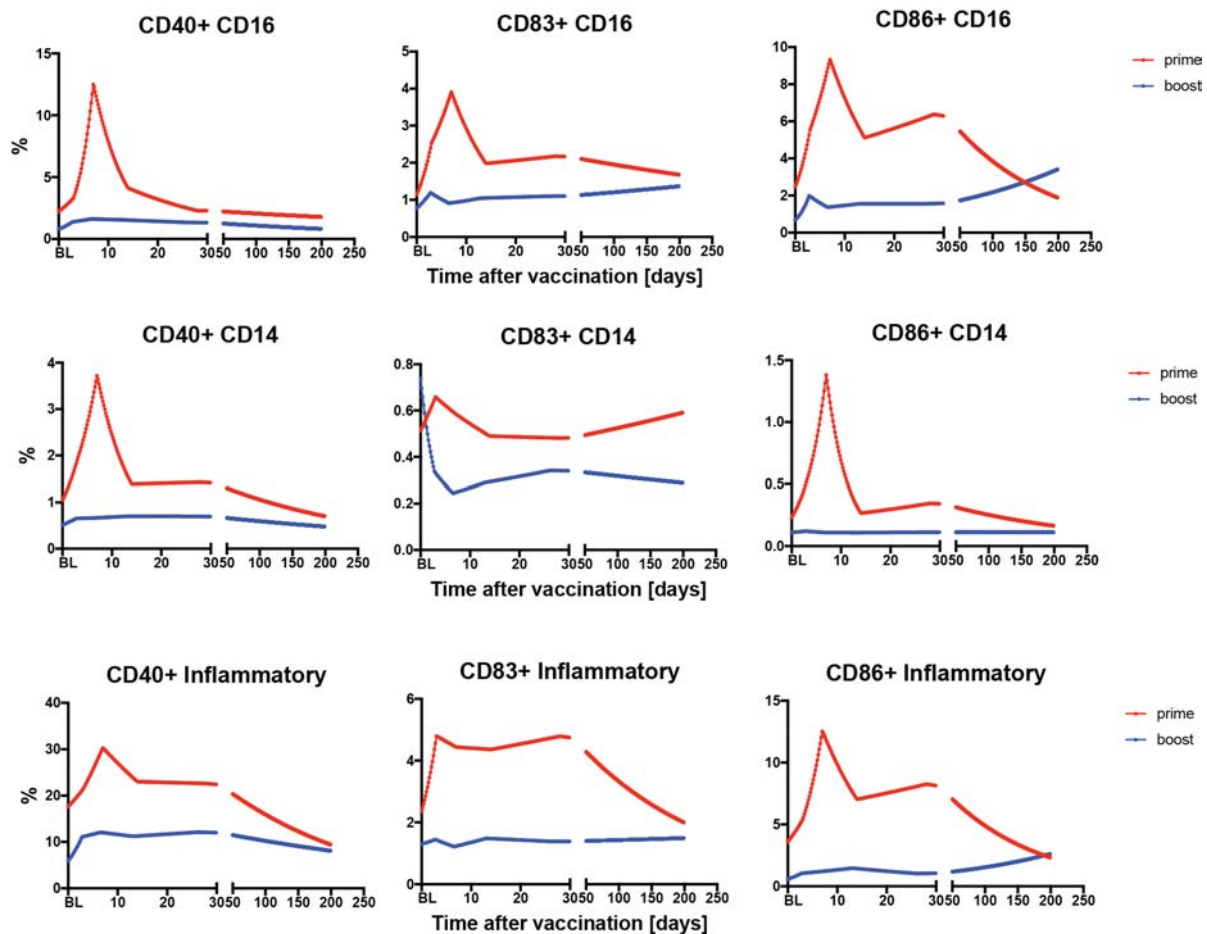


Figure 72 Kinetics of activation in monocyte subsets in response to primary and booster YF-17D vaccination. A, Frequencies of cells positive for the indicated markers within CD16⁺ monocytes in healthy volunteers after primary vaccination (left panel, n = 7) and booster vaccination (middle panel, n = 6). B, Frequencies of cells positive for the indicated markers within CD14⁺ monocytes in healthy volunteers after primary vaccination (left panel, n = 7) and booster vaccination (middle panel, n = 6). C, Frequencies of cells positive for the indicated markers within inflammatory CD14⁺ CD16⁺ monocytes in healthy volunteers after primary vaccination (left panel, n = 7) and booster vaccination (middle panel, n = 6). The fitted population mean is represented in red for the priming group and in blue for the booster group.

We also investigated the dynamics of dendritic cells (DCs) in the course of YF-17D vaccination. Total DCs did not show much changes in cell numbers both after priming and booster vaccination (Figure 73). The various myeloid and plasmacytoid DC subsets (mDC and pDC, respectively) did not show remarkable changes in terms of numbers but we observed a reduced number of cells at day 7 compared to baseline in both priming and booster groups (Figure 73).

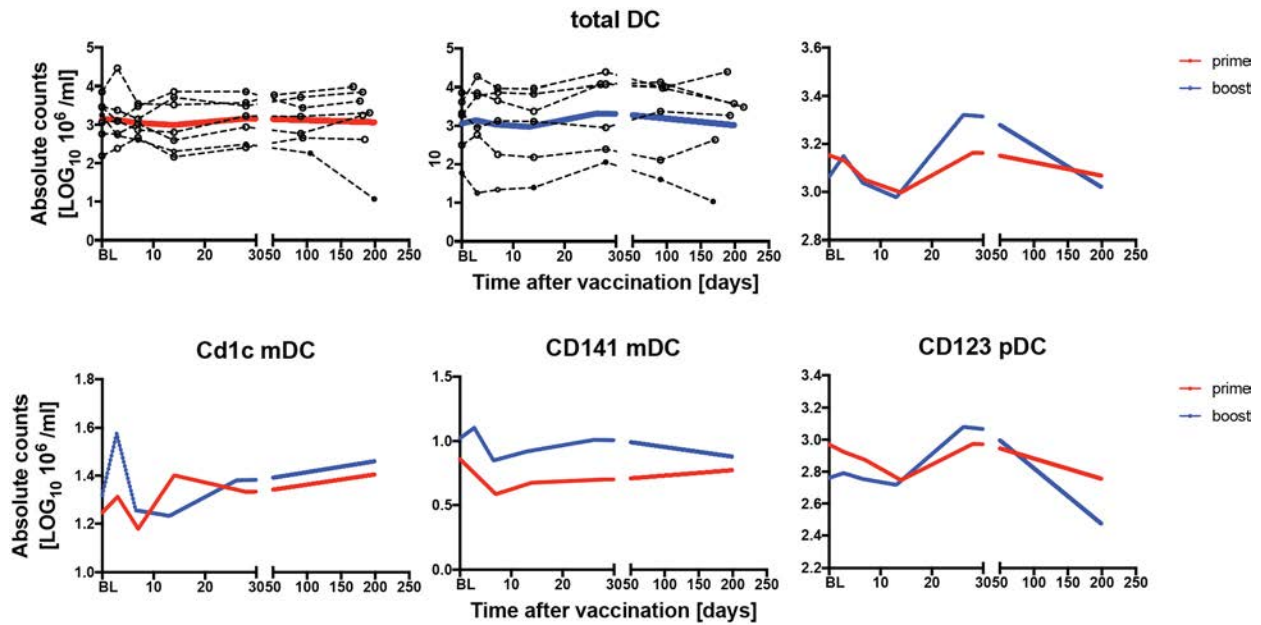


Figure 73 Kinetics of the dendritic cells response to primary and booster YF-17D vaccination. A, Absolute number of total dendritic cells (DC) in healthy volunteers after primary vaccination (left panel, $n = 7$) and booster vaccination (middle panel, $n = 6$). The fitted population mean is represented in red for the priming group and in blue for the booster group (right panel). B, Fitted population mean of absolute numbers of Cd1c mDC (left panel), CD141mDC (middle panel) and CD123 pDC (right panel) in healthy volunteers after primary vaccination (red line, $n = 7$) and booster vaccination (blue line, $n = 6$).

We next analyzed natural killer cells (NK; $CD56^+ CD3^- CD14^- CD15^- CD19^- CD20^- Fc\epsilon R1^-$) (Figure 74). It was previously shown that YF-17D induced a robust NK cell response with increased expression of Ki-67 and CD69 [124]. There was no substantial change in NK cell numbers after primary or booster vaccination but we observed an opposite trend between the two groups with a slight decrease and increase, respectively (Figure 75A). The analysis of NK subsets also revealed opposite dynamics between donors from the priming and boost groups (Figure 75B and C). On one hand, the number of NK dim cells ($CD56^+ CD16^+$), referred to as cytotoxic NK cells, was moderately decreased after primary vaccination, whereas it was slightly increased after booster vaccination (Figure 75B). On the other hand, the number of NK bright cells ($CD56^{++} CD16^-$), known as cytokine-secreting NK cells, was decreased after primary vaccination, whereas it was increased after booster vaccination (Figure 75C). As reported in a past study, the expression of several activation markers (4-1BB, CD69, Nkp44, PD-1) was increased at day 7 after primary vaccination (Figure 77) [123]. No increased expression of these markers was observed after booster vaccination (Figure 77).

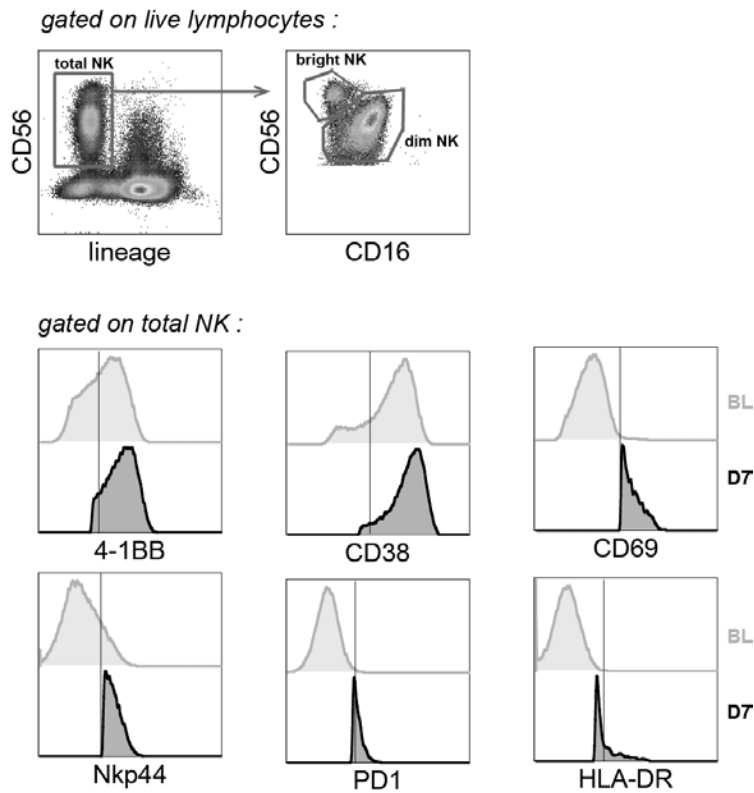


Figure 74 Representative FlowJo gating strategy for the NK cells analysis (A) Total monocytes (lineage-*HLA-DR+*) were gated on live lymphocytes using forward/sideward scatter properties. Singlets were selected using forward/side ward scatter width/height characteristics. Monocyte subsets distribution was based on CD14 and CD16 expression to determine classical (CD14⁺⁺ CD16⁻), non- classical (CD14⁺ CD16⁺⁺), and intermediate (CD14⁺⁺ CD16⁺) monocytes. *Lineage: CD3, CD19, CD20, CD56, FcER1.* (B) The indicated activation markers were analyzed in all monocytes subsets at baseline (BL) and day 7 after YF-17D vaccination (D7). They are represented in off-set overlay histograms.

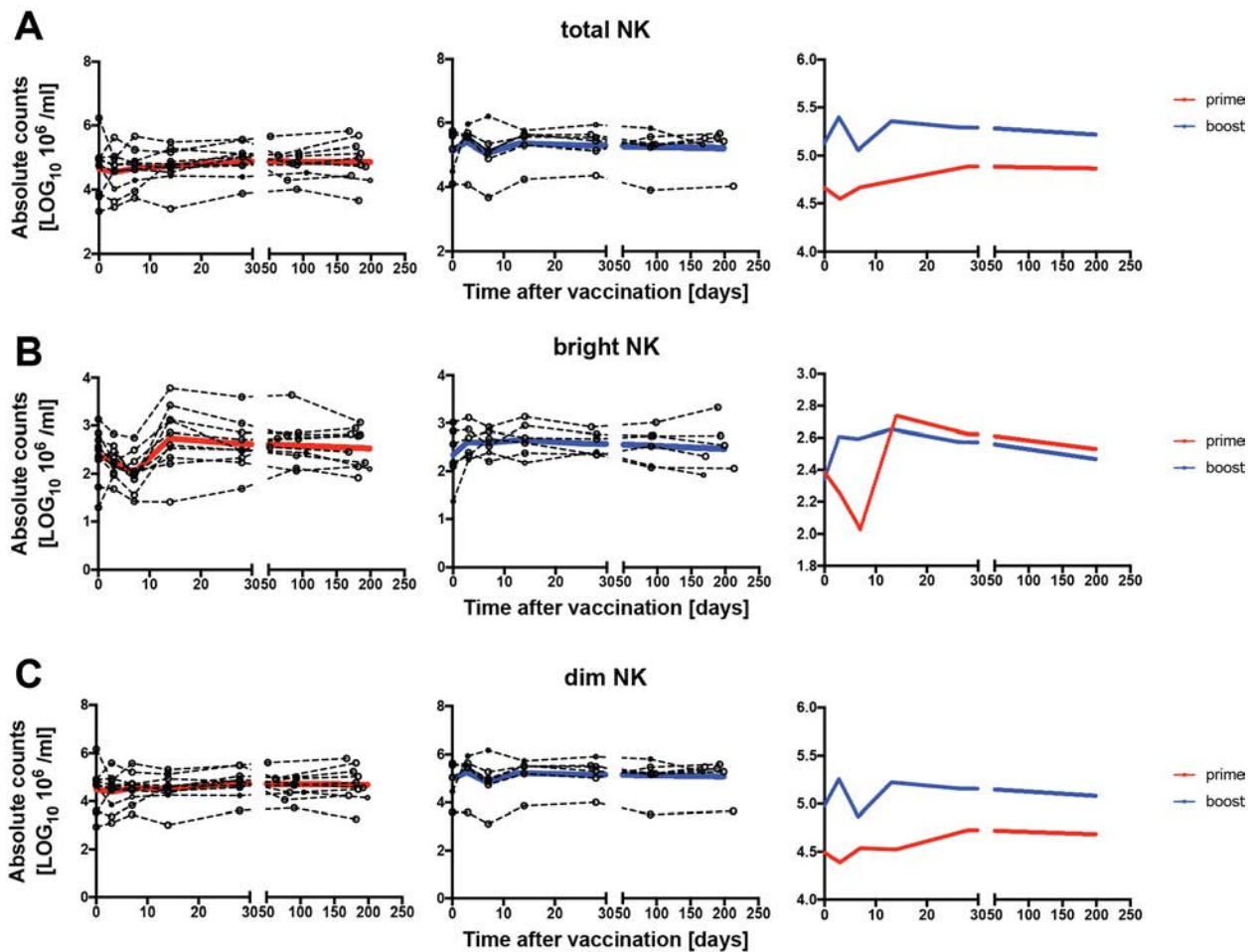


Figure 75 Kinetics of NK cells response to primary and booster YF-17D vaccination. A, Absolute number of total natural killer cells (NK) in healthy volunteers after primary vaccination (left panel, $n = 10$) and booster vaccination (middle panel, $n = 6$). The fitted population mean is represented in red for the priming group and in blue for the booster group (right panel). B, Absolute number of bright NK cells (CD56++ CD16-) in healthy volunteers after primary vaccination (left panel, $n = 10$) and booster vaccination (middle panel, $n = 6$). The fitted population mean is represented in red for the priming group and in blue for the booster group (right panel). C, Absolute number of dim NK cells (CD56+ CD16+) in healthy volunteers after primary vaccination (left panel, $n = 10$) and booster vaccination (middle panel, $n = 6$). The fitted population mean is represented in red for the priming group and in blue for the booster group (right panel).

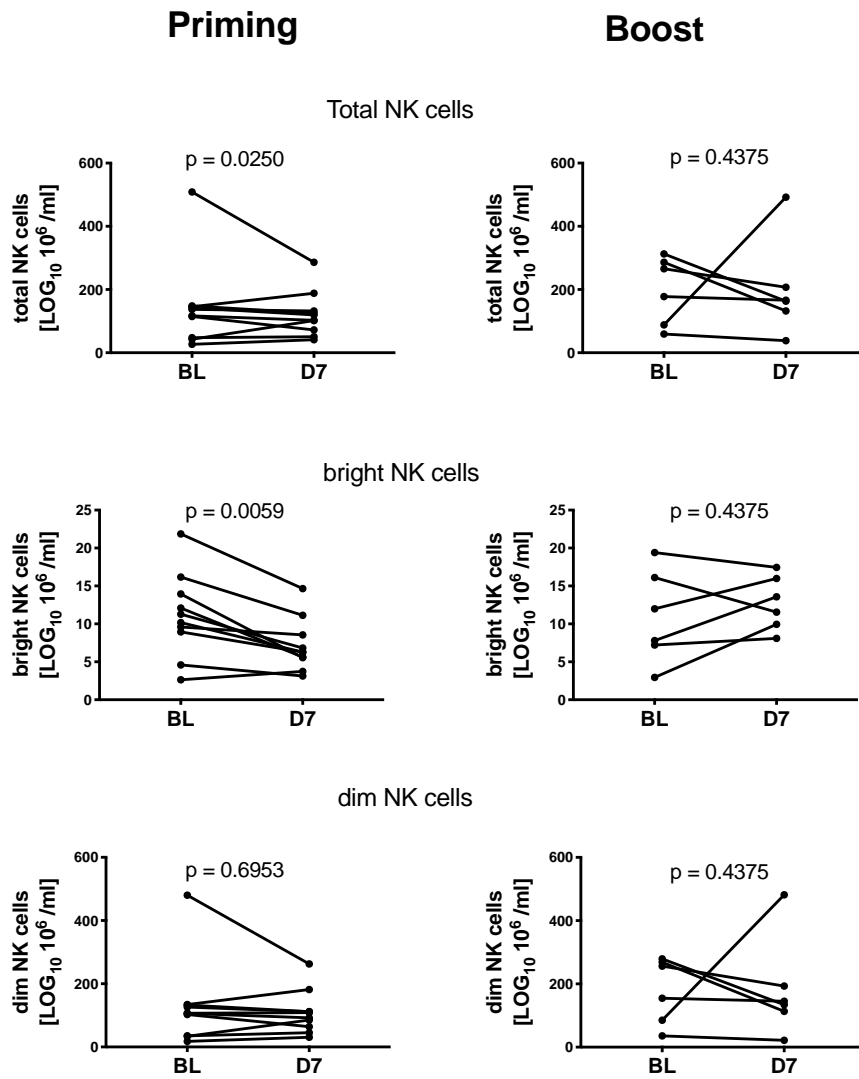


Figure 76 Changes of total Natural killer (NK) cells and their subsets number after primary or boost vaccination. P-values of Wilcoxon test are indicated in the graphs.

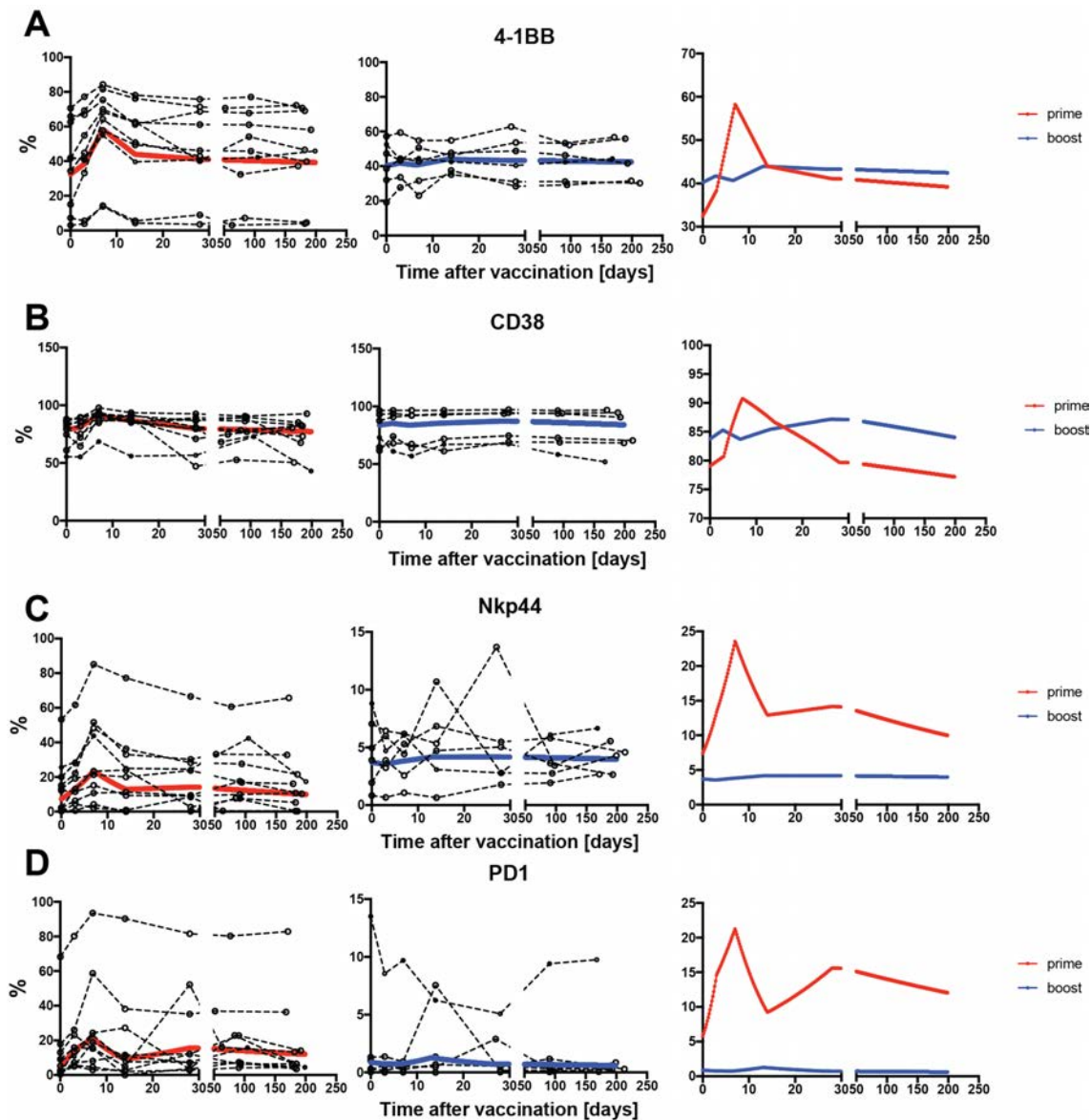


Figure 77 Kinetics of activation in total NK cells in response to primary and booster YF-17D vaccination. A, Percentages of cells positive for 4-1BB within total NK cells in healthy volunteers after primary vaccination (left panel, $n = 10$) and booster vaccination (middle panel, $n = 6$). The fitted population mean is represented in red for the priming group and in blue for the booster group (right panel). B, Percentages of cells positive for CD38 within total NK cells in healthy volunteers after primary vaccination (left panel, $n = 10$) and booster vaccination (middle panel, $n = 6$). The fitted population mean is represented in red for the priming group and in blue for the booster group (right panel). C, Percentages of cells positive for Nkp44 within total NK cells in healthy volunteers after primary vaccination (left panel, $n = 10$) and booster vaccination (middle panel, $n = 6$). The fitted population mean is represented in red for the priming group and in blue for the booster group (right panel). D, Percentages of cells positive for PD1 within total NK cells in healthy volunteers after primary vaccination (left panel, $n = 10$) and booster vaccination (middle panel, $n = 6$). The fitted population mean is represented in red for the priming group and in blue for the booster group (right panel).

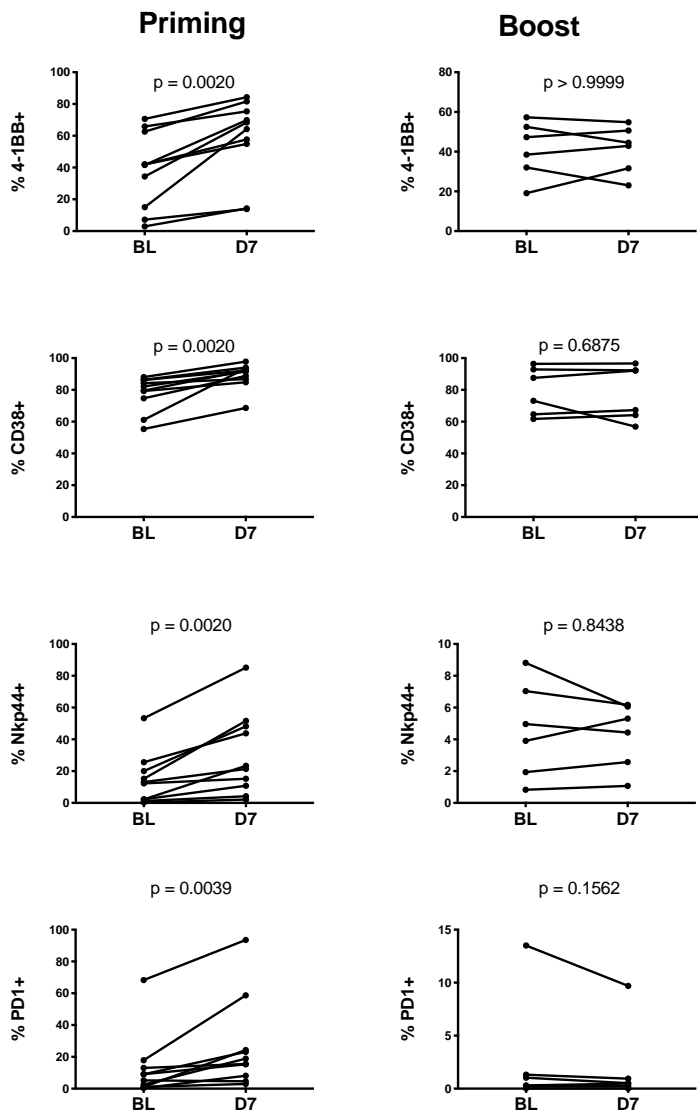


Figure 78 Changes in expression of the indicated activation markers in total Natural killer cells after primary or boost vaccination. P-values of Wilcoxon test are indicated in the graphs.

The innate lymphoid cell (ILC) response has not yet been described in the context of YF-17D vaccination. Therefore, we looked into the dynamics of total ILCs (CD127⁺ CD3⁻ CD14⁻ CD15⁻ CD19⁻ CD20⁻ CD33⁻ CD34⁻ CD203c⁻ FcER1⁻, CD16⁻) after primary and booster vaccination (Figure 79). On one hand our analysis revealed that the number of total ILCs transiently decreased 7 days after primary vaccination (Figure 80A). On the other hand, the number of total ILCs modestly increased after booster vaccination (Figure 80A, Figure 81). The dynamics of the ILC subsets also showed an opposite trend depending on the vaccination group. Immediately after primary vaccination, the number of ILC3 (c-kit⁺ CRTH2⁻) decreased transiently whereas the number of ILC2 (c-kit^{+/-} CRTH2⁺) transiently increased (Figure 80C and D). On the contrary, the number of ILC3 increased shortly after booster vaccination, whereas the

ILC2 subset modestly decreased (Figure 80C and D). The number of ILC1 (c-kit⁺ CRTH2⁻) did not show any particular trend neither after primary nor booster vaccination (Figure 80B). Despite the lack of known conventional ILC activation receptor, we attempted to analyze the expression of CD69 in total ILCs after primary and booster vaccination (Figure 79). Interestingly, we observed a sharp increase in CD69-positive ILCs after primary vaccination but not after a boost dose of the vaccine (Figure 82).

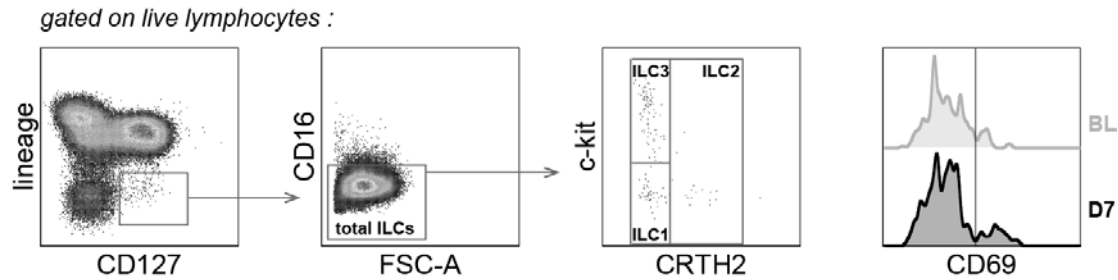


Figure 79 Representative FlowJo gating strategy for the ILCs analysis. Total ILCs (lineage⁻ CD127⁺ CD16⁺) were gated on live lymphocytes using forward/sideward scatter properties. Singlets were selected using forward/sideward scatter width/height characteristics. ILC subsets distribution was based on c-kit and CRTH2 expression to determine ILC1 (c-kit⁺ CRTH2⁻), ILC2 (c-kit⁺ CRTH2⁺), and ILC3 (c-kit⁺ CRTH2⁻). *Lineage:* CD3, CD14, CD15, CD19, CD20, CD33, CD34, CD203c, FcER1. The early activation marker CD69 was analyzed in total ILCs at baseline (BL) and day 7 after YF-17D vaccination (D7). They are represented in off-set overlay histograms.

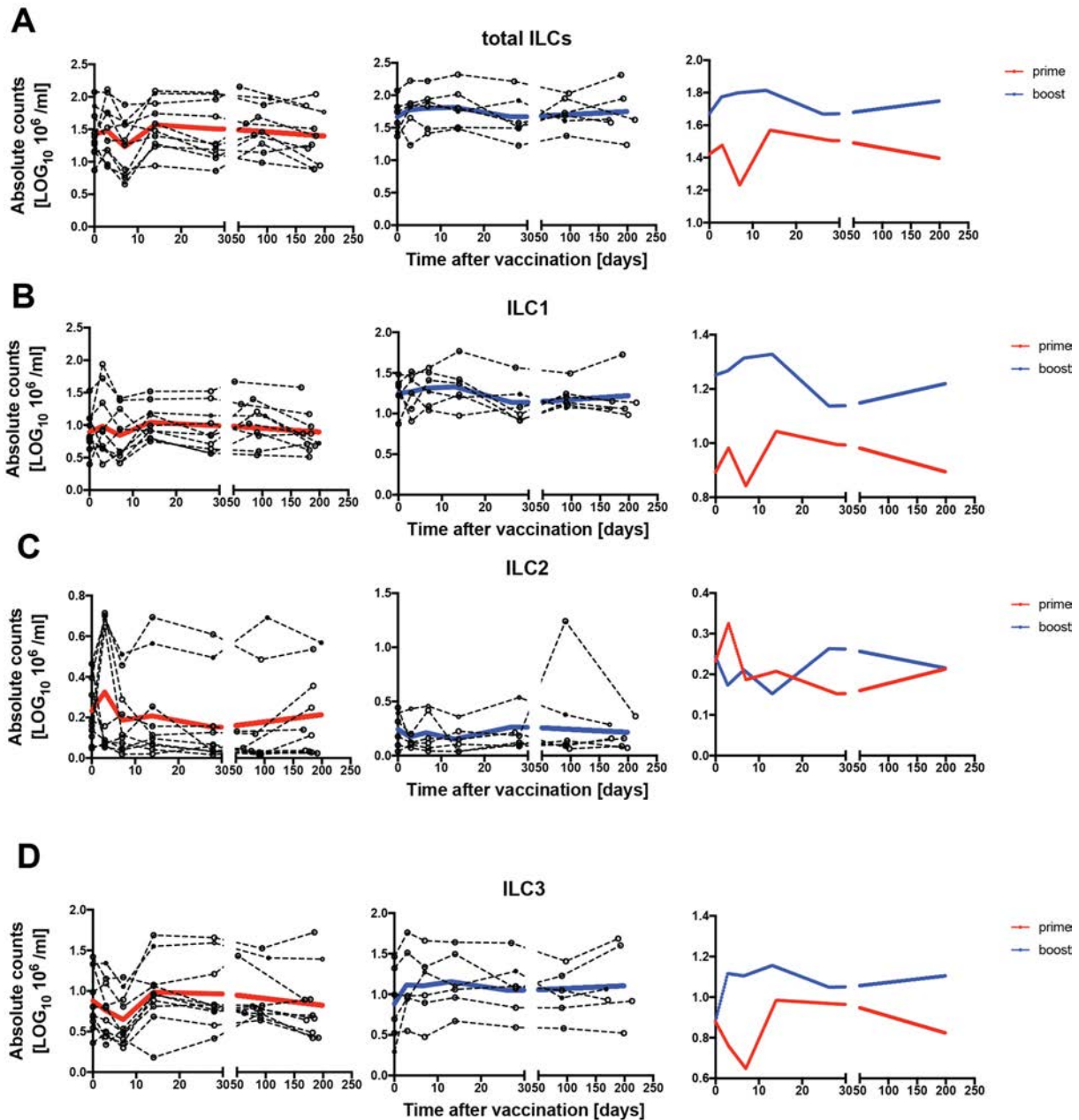


Figure 80 Kinetics of the ILC response to primary and booster YF-17D vaccination. A, Absolute number of total ILCs ($CD127^+ CD3^- CD14^- CD15^- CD19^- CD20^- CD33^- CD34^- CD203c^- FcER1^- CD16^-$) in healthy volunteers after primary vaccination (left panel, $n = 10$) and booster vaccination (middle panel, $n = 6$). The fitted population mean is represented in red for the priming group and in blue for the booster group (right panel). B, Absolute number of the ILC1 subset ($c-kit^- CRTH2^-$) in healthy volunteers after primary vaccination (left panel, $n = 10$) and booster vaccination (middle panel, $n = 6$). The fitted population mean is represented in red for the priming group and in blue for the booster group (right panel). C, Absolute number of the ILC2 subset ($c-kit^{+/+} CRTH2^+$) in healthy volunteers after primary vaccination (left panel, $n = 10$) and booster vaccination (middle panel, $n = 6$). The fitted population mean is represented in red for the priming group and in blue for the booster group (right panel). D, Absolute number of the ILC3 subset ($c-kit^+ CRTH2^-$) in healthy volunteers after primary vaccination (left panel, $n = 10$) and booster vaccination (middle panel, $n = 6$). The fitted population mean is represented in red for the priming group and in blue for the booster group (right panel).

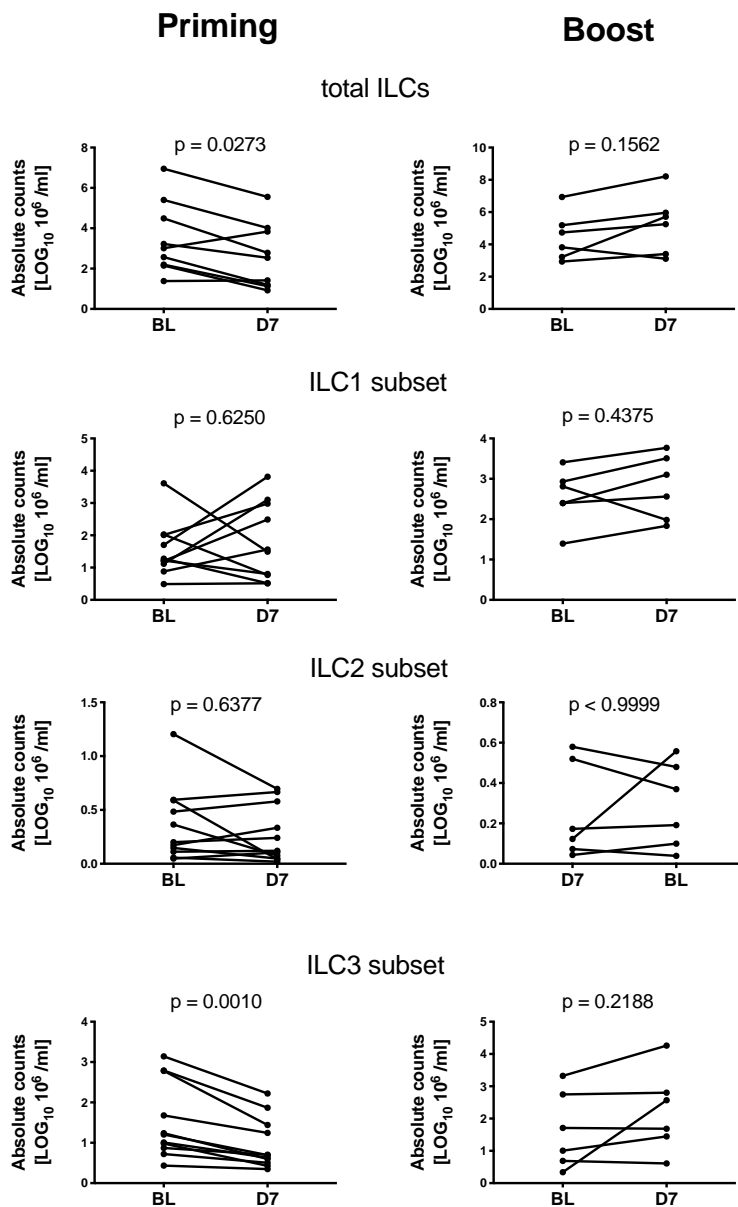


Figure 81 Changes of total ILCs and ILC subsets number after primary or boost vaccination. P-values of Wilcoxon test are indicated in the graphs.

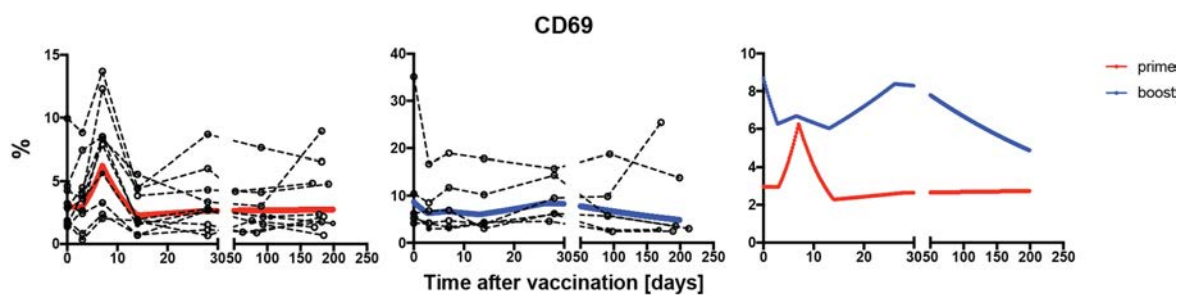


Figure 82 Kinetics of activation in total ILCs in response to primary and booster YF-17D vaccination. Percentages of cells positive for CD69 within total ILCs in healthy volunteers after primary vaccination (left panel, n = 10) and booster vaccination (middle panel, n = 6). The fitted population mean is represented in red for the priming group and in blue for the booster group (right panel).

The global immune response pattern is substantially reduced in booster compared to primary YF-17D vaccination

We aimed to assess and compare the global pattern of response to primary versus booster YF-17D vaccination by applying principal component analysis (PCA) and hierarchical clustering based on the immune observations detailed above. First, we controlled for potential age and gender bias due to study volunteer recruitment: while age was not significantly different between the two groups, the gender distribution was biased for females (5/6) in the booster group (Figure 83).

Comparing each immune feature between males and females at baseline, we found no significant gender-related bias (including no difference for the nAbs which are known to differ at baseline comparing priming or booster groups) (Figure 84). To further control for potential age-effects, we plotted each immune feature versus age and found that the frequency of CD38+ CD8 T cells significantly increased with age, while no other parameter showed age correlation (Figure 85). Since the age distribution in the two groups is not different we did not expect any age bias in the study either. Finally, we controlled each immune feature at baseline comparing the two groups and found that a few parameters significantly differed (Figure 86). As expected, nAbs titers were significantly higher at baseline in the booster group ($p = 0.006$). Significant differences were also found for the frequencies of CD38-positive CD4 T cells and CD86-positive monocytes ($p = 0.049$ and $p = 0.042$, respectively), which are not due to age (Figure 84) nor gender (Figure 85) effects.

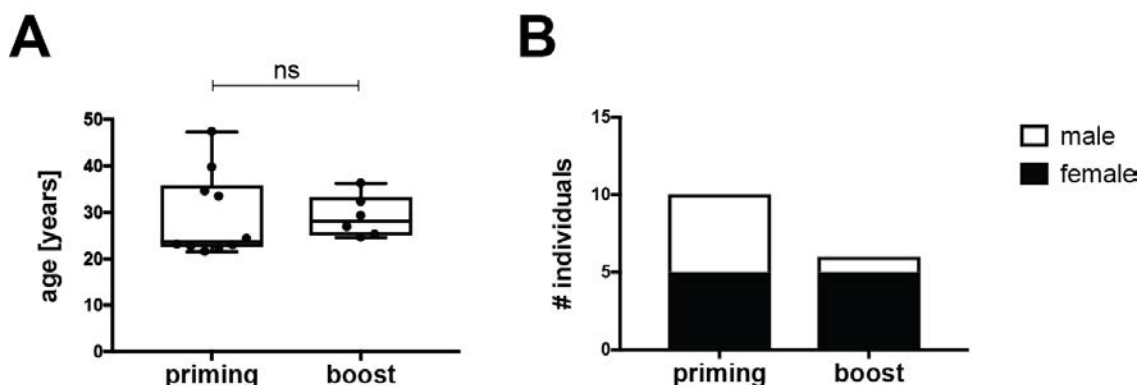


Figure 83 Age and gender composition of individuals from the priming and booster groups. P values (Chi square test and Mann-Whitney test, respectively), $n = 16$.

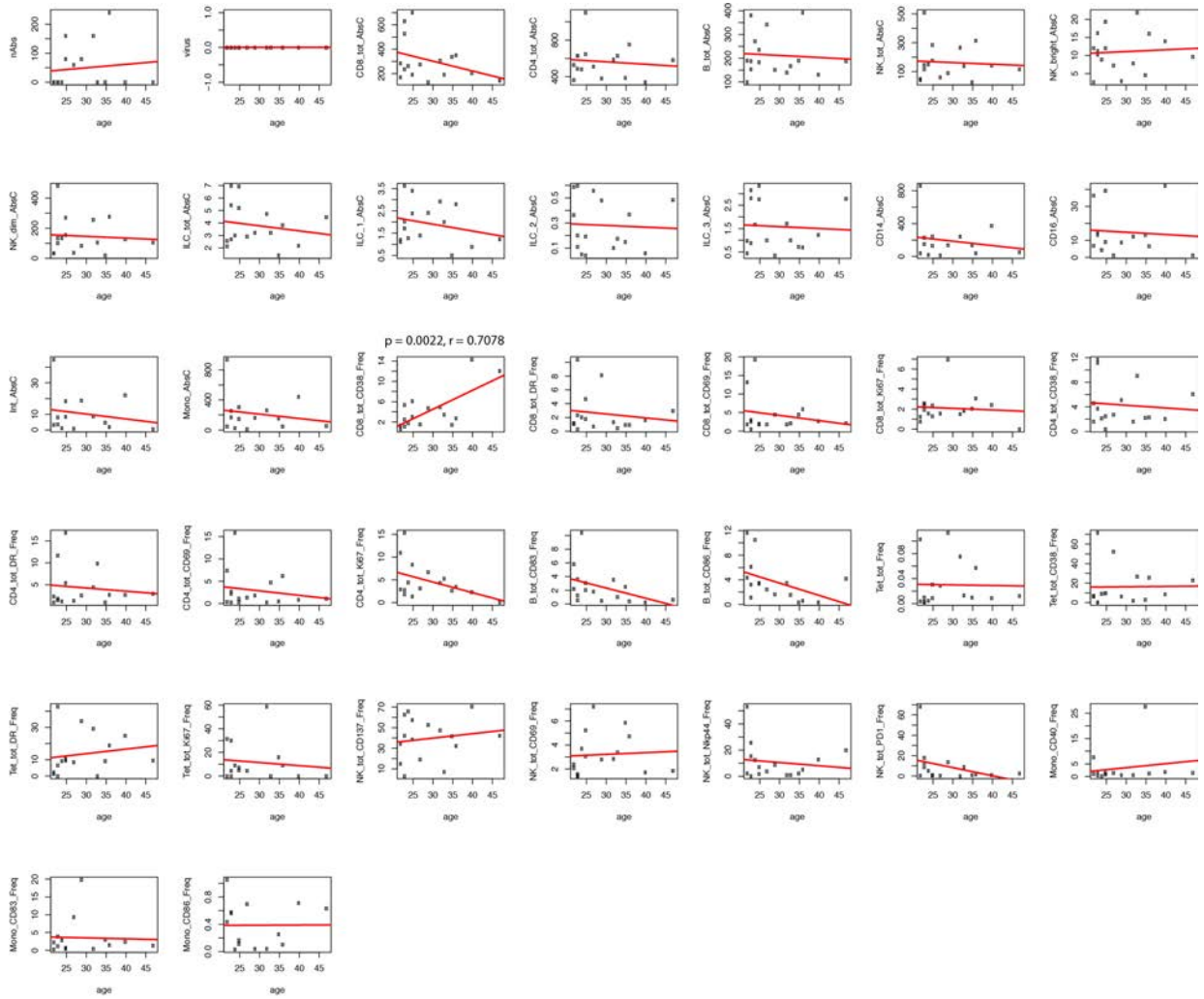


Figure 84 Correlation between age and the various immune parameters. Pearson r and p-values are indicated for significant correlation, n = 16.

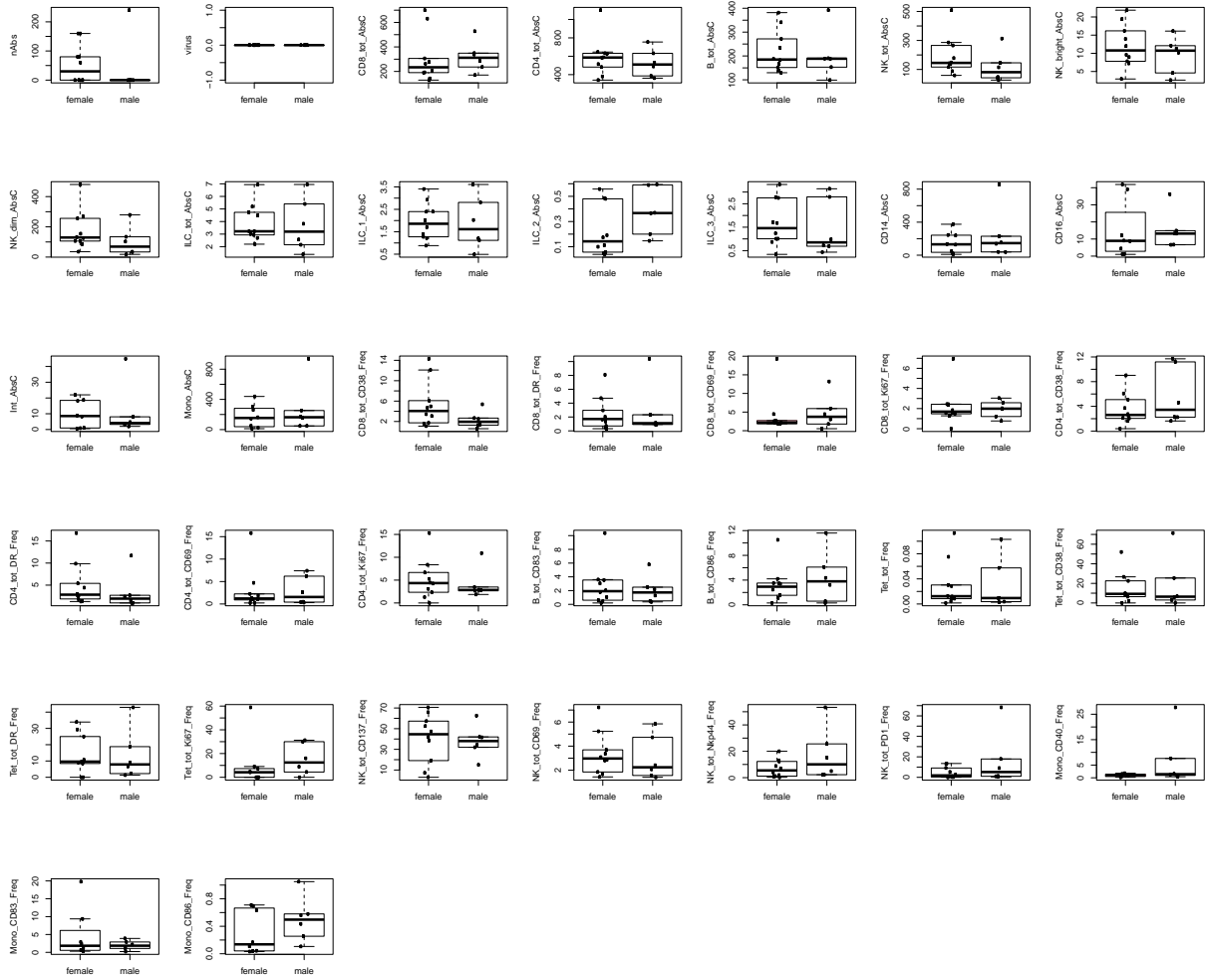


Figure 85 Comparison of the various immune parameters at baseline between male and female. None of the p-values (Mann-Whitney test) showed significance, n =16.

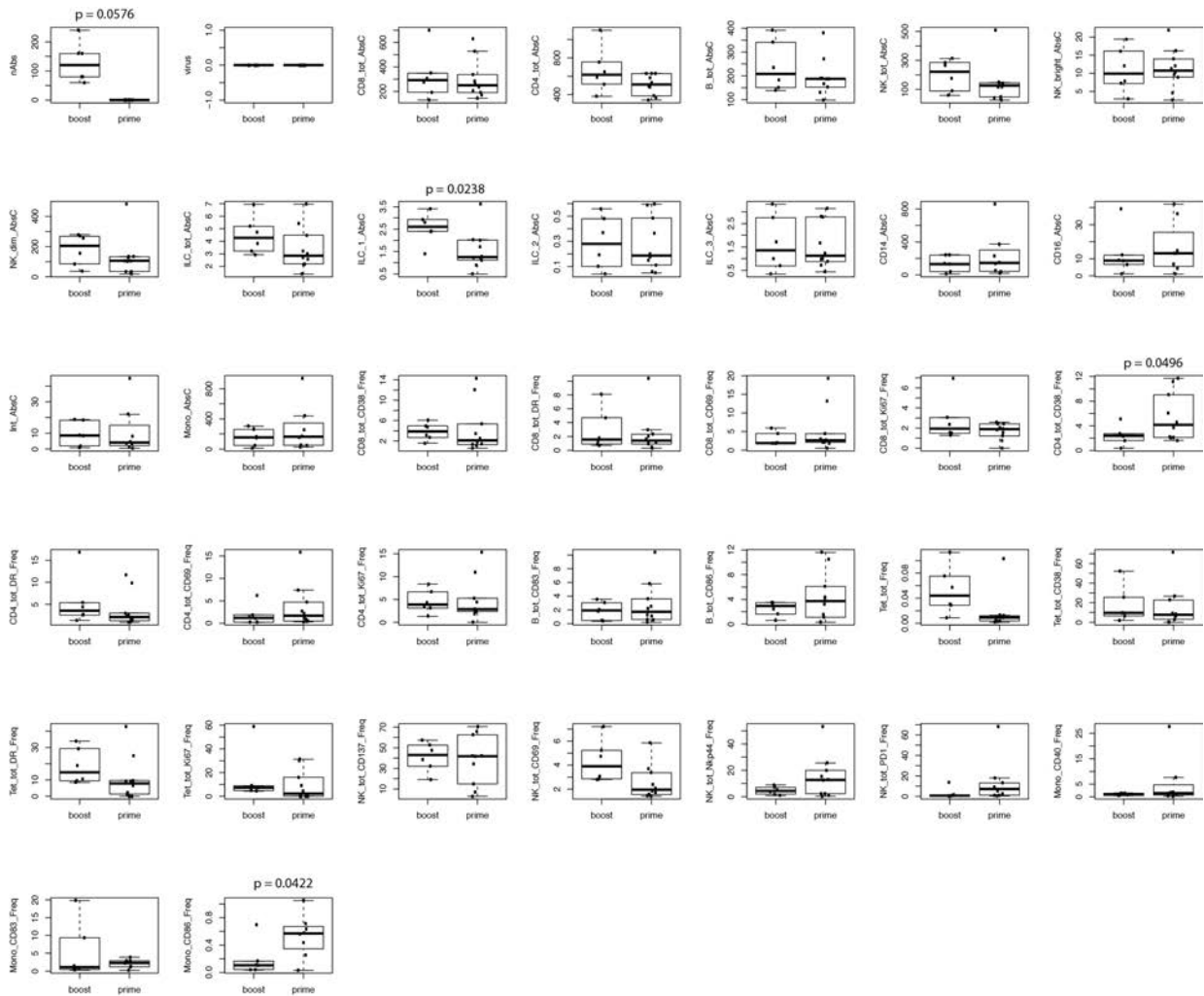


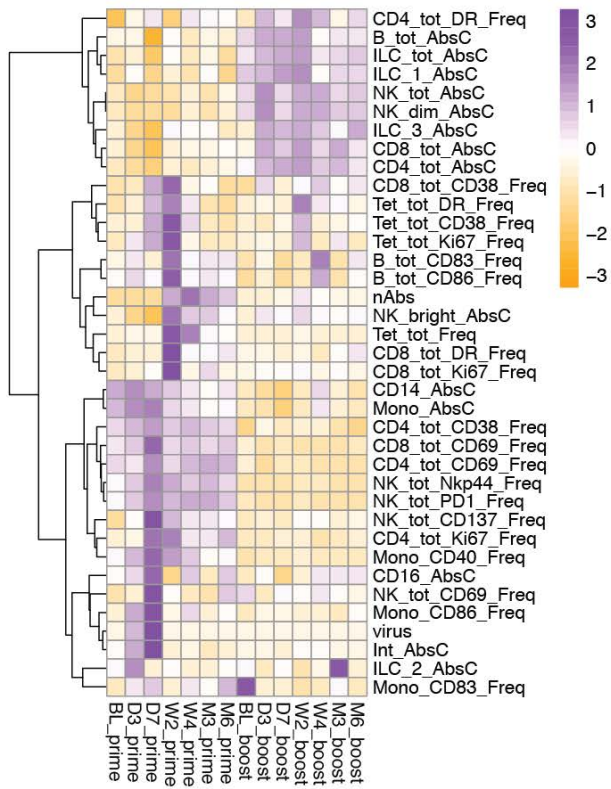
Figure 86 Comparison of the various immune parameters at baseline between priming and boost groups. P-values (Mann-Whitney test) are indicated for each comparison, $n = 16$.

Using a hierarchical clustering algorithm, we interrogated the relatedness of 37 immune features. This analysis was based on the frequencies and absolute counts from the flow cytometry data, the viral load, and the neutralizing antibody titers. We found 4 main clusters that reflected varying kinetics (Figure 87A) particularly in the priming group: i) early events peaking at day 7 such as monocyte, NK and CD4 T cell activation, together with CD69 in CD8 T cells (early clusters 1 and 2), followed by ii) events peaking at day 14 to 28 (cluster 3: adaptive activation in B and CD8 T cells and nAbs), and iii) events that drop at day 7 (B, CD4 and CD8 T cells in cluster 4). The resulting heatmap clearly illustrates that the pattern of immune reactivity is globally distinct in priming versus the booster vaccination, with the large majority of immune features peaking or dropping in priming but not in booster vaccination. We further performed a multidimensional scaling of all parameters to underline the differences

between the two vaccination groups and observed that i) the two groups cluster separately, and ii) it is particularly the day 7 and day 14 time-points upon priming which are isolated from each other and all the remaining samples (Figure 87B).

Altogether, the global pattern of immune responses is clearly distinct following primary and booster vaccination. While the innate and adaptive responses are robustly mobilized at day 7 and/or 14 after primary vaccination, the magnitude of the response is minor after booster vaccination.

A



B

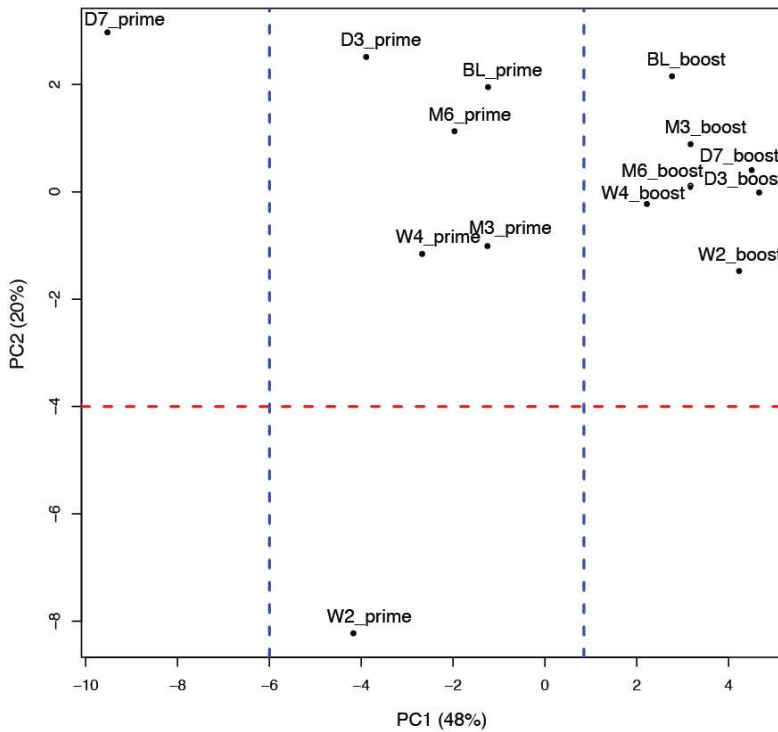


Figure 87 Global comparison of the flow cytometry data, viral load, and neutralizing antibody titers between primary and booster vaccination. A, heatmap based on median expression of the indicated markers. B. PCA analysis based on the expression of the same markers.

3.2.1.3 Discussion

Characterization of all major immune cell populations following primary and booster YF-17D vaccination

To our knowledge, our YF2 study is the first to compare longitudinally and side-by-side the innate and adaptive parameters (including viral load and neutralizing antibodies) after primary and booster YF-17D vaccination. As stated throughout the results, our work generally confirmed previous data revealed by several individual studies.

For instance, we validated a reduced antibody response to revaccination compared to primary vaccination [98] [99] [208] [209]. Furthermore, our study allowed us to reveal that the maximal nAbs titers is reached faster after booster than priming (day 14 vs. day 28) (Figure 50A and B). This is corroborated by the timing of B cell activation (Figure 53). However, we could not reproduce the correlation between BCMA expression at day 7 and the magnitude of nAbs titers after YF-17D priming [113]. This could be explained by the type of sample analyzed. Querec and colleagues analyzed the genomic signature of the TNFRSF17 gene (encoding BCMA) by RT-PCR, whereas we measured the surface expression of BCMA protein level by flow cytometry.

No previous study assessed the viral load after booster vaccination with YF-17D. We found no detectable virus in re-vaccinees (Figure 55B). However, it is questionable whether the virus could not replicate or the load was simply below our detection limit. For instance, it is surprising that 4 out of 10 individuals from the priming group showed no viral copies (Figure 55A). Nevertheless, these donors showed a diminished activation as quantified by the frequency of CD38-positive CD8 T cells. This relationship was highlighted by the positive correlation between viral load and the frequency of activated CD8 T cells (Figure 59).

The magnitude and timing of the total CD4 and CD8 T cell responses are in accordance with previous studies [112] [120] [122]. The T cell drop was already mentioned by Kohler and colleagues but has not been further investigated [122]. We found a correlation between the T cell drop and CD69 expression at baseline (Figure 66). Studies on CD4 T cells in mice suggested that CD69 expression promotes T cell

retention in the lymph nodes by downregulating the migratory response to S1P1 and that the modulation of CD69 expression is important for the migration of naïve CD4 T cells [231]. In addition, we showed that the T cell drop precedes the activation of T cells and the increase of antigen-specific CD8 T cells. Therefore, we hypothesize that these cells disappear from the periphery to migrate to lymph nodes for activation. However, antigen-specific CD8 T cells still increased significantly in the booster group although no T cell drop is observed. It would be interesting to further investigate into this mechanism. In addition to the retention marker CD69, we could analyze the adhesion markers CD62L and LFA-1, which allow to bind and enter the lymph node [232].

We analyzed the antigen-specific CD8 T cell response using the epitope A2/LLW because it is an immunodominant epitope and HLA-A*0201 is a prevalent allele in the Caucasian population [118] [140]. Other CD8 epitopes were described in the literature with other HLA-restriction [99] [117] [118] [233]. The kinetics and activation of A2/LLW-specific CD8 T cells are consistent across other YFV specificities. We did not address antigen-specific CD4 responses during my PhD thesis but we are planning to monitor the antigen-specific CD4 response following YF-17D vaccination in the near future. Two screenings identified CD4 epitopes [117] [234] [235]. Based on these and on the HLA typing of our donors, we selected some epitopes to be tested for immunogenicity. The epitopes giving the strongest response will be used for tetramer production. Of note, MHC Class II tetramers are more difficult to produce but scientists on site are experienced and already produced successfully such molecules. We intend to investigate the kinetics, subset distribution and activation of these cells. In particular, we would like to find out whether a population of antigen-specific SCM CD4 T cells is induced upon YF-17D vaccination.

In contrast to total CD8 T cells, we found that A2/LLW-specific CD8 T cells are activated at the same level by both primary and booster vaccination. However, we observed that the proliferation of these cells was lower after booster compared to primary vaccination, resulting in a lower magnitude of the A2/LLW-specific response.

Concerning the innate response, we did not find an overall decrease in the frequency of NK cells as previously published [123]. This could be explained by the variability among the donors of NK cells at baseline and their dynamics. We confirmed the

expansion and activation of monocytes at day 7 after primary vaccination [123]. We did not observe the increase of mDC numbers at day 7 as determined by Kohler and colleagues [122]. In this study however, mDCs are defined as CD11c⁺ HLA-DR⁺ CD45⁺ CD19⁻ CD14⁻ CD56⁻ BDCA-2⁻ CD16⁺ cells are not excluded from these cells. Therefore, it may be possible that the increase in mDCs that is described in this study can be imputed to the increase of monocytes. Indeed, we observed an increase in total monocytes and in particular in CD16⁺ monocytes.

For the first time, ILCs were investigated in the context of YF-17D vaccination. As the ILC3 was the only subset to show a drop after primary vaccination, it indicates that they are implicated in the response to the vaccine. We used CD69 as a potential activation marker although activation of ILCs is conventionally monitored by cytokine production.

Overall, our longitudinal study revealed the systemic and detailed dynamics of the immune response following YF-17D vaccination in humans.

Comparison between primary and booster YF-17D vaccination

The YF2 study allowed us to compare side-by side and in detail the innate and adaptive parameters after priming and boosting with YF-17D. We addressed the underlying questions:

i) What is the difference in the dynamics, proportions and profiles of the major cellular populations upon priming versus booster vaccination? To what extent are the innate and adaptive components mobilized upon boosting and can we observe and study prominent recall responses?

Our YF2 longitudinal study of primary and booster responses to YF-17D vaccination offers a unique opportunity to analyze human immune responses during an acute viral infection in a controlled experimental system (knowing the exact time of antigen exposure). To our knowledge, the study we report is the first to globally compare primary and booster vaccinations side-by-side, including specific adaptive and innate features in parallel to nAb titers and viral load.

As expected, at baseline, all the booster individuals showed detectable levels of nAbs (induced by their first vaccination 10 years prior), while primary vaccinees had no

detectable nAbs. We confirmed the observations in previous studies showing that YF-17D booster vaccination induces a limited further increase in nAbs, compared to the strong induction of nAbs upon primary vaccination [98] [99] [208] [209].

Following primary vaccine injection, the live-attenuated virus replicated with a peak of viremia detectable in circulating blood within the first 10 days for most of the donors. In contrast, no viral copy could be detected upon revaccination.

Regarding the cellular responses, our work and prior studies have shown that booster dose of YF-17D does not substantially re-activate the immune system [98] [99] [236]. We observed a modest adaptive response (CD8, CD4, B cells). Only the A2/NS4b-specific CD8 T cells showed high reactivation frequencies, while showing no profound amplification in terms of relative or absolute total A2/NS4b-specific CD8 T cells counts. The innate response in the booster vaccination was not substantially triggered neither. We faced some limitations that are inherent to human studies. For instance, accessible biomaterial is primarily limited to blood samples and to the secondary lymphoid organs or the skin. Another drawback is that we were limited in terms of frequency and amount of blood sampling in our volunteers (based on the volumes per period of time that are allowed for standard blood donations). Therefore, we analyzed few and specific time-points, providing snapshots of the response.

ii) What is the impact of pre-existing antibodies on the recall responses?

Titers of neutralizing antibodies (nAbs) are commonly examined as the most appropriate surrogate marker of protection. In mice, it is now clear that the presence of nAbs correlate with efficient protection against viral reinfection. Numerous studies on mouse models established that the residual titers of antibodies present at time of secondary infection and the amount of antigen expressed influence the strength of the immune response [237] [238]. Whether this relationship holds true in humans remains an essential question.

By comparing the nAbs titers versus viremia, we found direct relationship between the absence of detectable viral copies after booster vaccination and pre-existing positive nAbs titers, as we could not detect any viral copies in the sera of booster vaccinees. These observations provide supporting evidence to the hypothesis that pre-existing humoral immunity to the virus limits replication of the YF-17D vaccine virus. Therefore, the dichotomy between primary and secondary vaccination can be explained by the

presence of pre-existing nAbs, which rapidly shield the virus. Consequently, the virus fails to massively replicate and cellular responses are weakly primed.

In conclusion, our data indicate that the presence of pre-existing nAbs curtails viral replication and therefore might diminish the subsequent reactivity and magnitude of innate and adaptive immune responses after revaccination.

iii) Is there a need for a booster dose after 10 years?

Until recently, the World Health Organization (WHO) recommended a booster dose of the YF-17D vaccine. However, in 2013, the Strategic Advisory Group of Experts (SAGE) workgroup of the WHO proposed that revaccination every 10 years is not necessary and considered that a single dose of YF-17D provides life-long protection in healthy individuals [239].

The change in vaccination strategy stipulated by the WHO has elicited debate because there is limited clinical evidence on the incidence of YFV infections in vaccinated individuals, as it is not ethically possible to study YFV vaccine efficacy in humans. Antibodies are conventionally examined as the most appropriate surrogate correlate of protection, although innate and cellular adaptive immunity may contribute to sustaining the immune memory to YF-17D vaccination [240].

The humoral immunological response to a booster dose of the YF-17D vaccine has been addressed by several studies. Early studies from the '60s suggested that the magnitude of nAbs titers induced by booster vaccination was reduced compared to primary vaccination [208] [241]. Several studies highlighted the importance of the pre-booster serology, indicating that booster vaccination did not provide additional benefit if the primary vaccination was effective [98] [99] [209]. The impact of pre-vaccination serology on the outcome of YF-17D booster vaccination has been shown in that individuals with low titers had a strong humoral response to booster vaccination, whereas donors with high pre-vaccination titers did not increase their nAbs titers [96]. This latter observation has also been reported for vaccination with attenuated measles [242].

Regarding the cellular responses, our work and prior studies have shown that booster dose of YF-17D does not substantially re-activate the immune system [98] [99] [236].

We observed a modest response for CD8, CD4, B cells as well as the innate compartment at selected time-points in the blood.

In addition to the response to boost, it is important to consider the duration of immunity after primary immunization. Several studies assessed the long-term protection induced by primary YF-17D vaccination. Although the nAbs titers decrease with time, these studies showed that nAbs titers persist at protective level in most individuals (74.5-100%) [92] [94] [95] [121] [208] [209] [243]–[245].

Our YF2 study examined the response only until 6 months after vaccination. However, a previous study conducted by our laboratory showed that LLW-specific SCM CD8 T cells are detected several decades after primary vaccination with YF-17D [97]. These cells were fully functional and showed IL-15-driven homeostatic proliferation [97].

Despite the accumulating amount of evidence in favor of the WHO's decision, endemic countries do not follow this recommendation. For instance, the Brazilian national immunization policy guidelines still recommend a booster dose 10 years after primary YF-17D vaccination. The different conclusions drawn by the Brazilian authorities cannot be imputed to the different vaccine strains used (YF-17DD instead of YF-17D-204) as it presents only subtle nucleotide differences and similar immunogenicity [246]. Critically, Brazil has suffered recent massive outbreaks of Yellow Fever [247] [248]. The YFV has been extending from the previously known endemic area (Amazon region) into Southern and Southeastern regions in Brazil. Between December 2016 and July 2017, 777 cases of YF disease were confirmed leading to 261 deaths [248]. The Brazilian authorities rely on a study conducted in Brazil concluding that a booster dose is recommended as they found that nAbs titers decrease with time [101]. In addition, this decision is supported by a study on the duration of immunity in individuals living in endemic (Africa) or non-endemic areas (Switzerland) suggesting that endemic African populations might need a booster dose to achieve efficient immunity [249].

Here we report that a booster dose of the YF-17D vaccine in 6 healthy volunteers living in a non-endemic area (Switzerland) induces only modest increase in nAbs titers. In addition, compared to the robust global immune reaction upon priming, only few of the 37 innate or adaptive features (36 features in parallel to viremia) studied were slightly activated after booster vaccination. In spite of the limited number of individuals in our

study, our readouts provide evidence in support of the reduced magnitude and strength of the response conferred by booster YF-17D vaccination for already seropositive adults living in non-endemic areas. Our YF2 study spans up to 6 months after re-vaccination, but it would be interesting to have more long-term samples to monitor the duration of the secondary response in terms of persistence of neutralizing antibodies. Also, as already mentioned above, we cannot assess the protective efficacy of the vaccine.

It is important to emphasize the fact that our report only provides immunological data for the discussion as to whether a booster dose is needed after 10 years. Furthermore, one major limitation of our study is the small size of our cohort (n= 6 in boost group), especially given the heterogeneity observed in humans. Other perspectives need to be taken into consideration: epidemiology, public health (including risk/benefit), financial, and operational aspects.

Identification of key determinants of immunogenicity

The correlations that I presented above are based on conventional analytical strategies. This approach is not only labor intensive but also highly subjective. Given the large number of possible pairs of parameters to analyze, we might neglect information present in the data that is not visible at first sight and clearly give a direction to the analysis. This obstacle could be overcome by unsupervised learning algorithms enabling the identification of patterns that have not been previously considered [250]. An additional bias in our study comes from the limitation of the number of markers and their selection based on the literature. Nevertheless, flow cytometry remains a powerful tool for single-cell analysis at the cellular level.

Given the tremendous high number of parameters to consider in the YF2 study (several markers in various cell types and their subsets at 7 time-points, both frequencies and absolute numbers), it is not advisable to analyze their correlation “by hand”. We therefore received assistance from a bioinformatician to perform a global network analysis comprising all the analyzed parameters. Dr. Sina Nassiri performed the FDA and global network correlation analysis. In FDA, discrete observations are viewed as

noisy realizations of an underlying function over time. By treating the entire sequence of observations as a single functional entity, FDA directly utilizes the temporal structure and potential dependence of measurements to borrow information across observations. My main contribution was to explain and translate our biological questions so that they could be modeled bioinformatically. Dr. Silvia-Fuertes-Marraco and I are currently interpreting the data.

As discussed later (cf 4. Ongoing work and Perspectives), we are planning to analyze YF2 blood samples by single-cell RNA Sequencing, which will allow to analyze the whole transcriptome. The increased complexity of the resulting data will be analyzed by an unsupervised algorithm.

3.2.1.3 Contributions

Dr. Silvia Fuertes-Marraco and I designed the flow cytometry panels. I performed and analyzed the flow cytometry data. The viral load was measured by the group of Benton Lawson (Emory Center, Atlanta USA). The nAbs titers were quantified by Dr. Rama Akondy (Emory Center). Dr. Sina Nassiri performed the FDA and global network correlation analysis. I am preparing a manuscript entitled “Restricted adaptive and innate immune responses to Yellow Fever virus YF-17D vaccination in individuals with pre-existing neutralizing antibodies” with the essential contribution of Dr. Silvia Fuertes and Prof. Daniel Speiser.

3.2.2 Analysis of A2/LLW-specific effector and long-lasting memory CD8 T cells in the early response to YF-17D (aim c)

3.2.2.1 Background

The most recently and newly described subset of memory T cells is termed stem cell-like memory T cells (SCM) and has brought major fascination and promise in T cell-based therapies relying on long-lasting memory cells [52] [97] [173] [174] [251]–[256]. Constituting 2-4% of total CD4 and CD8 T cells in the periphery [52], SCM cells express CCR7 and CD45RA like Naïve cells (they are sometimes referred to as “Naïve-like” since they express most classically naïve markers) but distinctly (in contrast to Naïve) also express high levels of CXCR3, CD95, CD58, CD11a, IL-2 β and LFA-1 [52] [257]. They embrace the capacity of both IL-7- and IL-15-driven homeostatic proliferation and highest progeny potential, with the capacity to regenerate (self-renewal) and generate multiple memory and effector subsets. They are considered as the longest lasting memory T cell subset. Amongst others, our group has shown that they exhibit a gene expression profile which is between naïve and CM cells [52] [97]. TCR rearrangement excision circles analysis indicate that SCM have undergone several steps of division [52]. SCM T cells are antigen-experienced and can secrete various cytokines (TNF α , IFN γ , IL-2) [52]. Antigen-specific SCM cells have been identified for CMV, Flu, HIV, EBV, HCV, YFV and melanoma [52] [97] [251]–[255]. Our group identified SCM induced by YF-17D that last for decades [97]. However, this first clinical study did not cover the early, acute response, which occurs within the first few weeks (peaking at 2 weeks). The YF2 study thus allows us to analyze the distribution and dynamics of human CD8 T cell subsets in the early acute response to YF-17D vaccination.

This project was mainly led by my supervisor Dr. Silvia Fuertes and only the data I contributed to produce is presented below. The project is detailed in a manuscript in preparation in Appendix 3.

3.2.2.2 Results

A2/LLW-specific SCM CD8 T cells appear early after priming with YF-17D vaccination

The frequencies of the various A2/LLW-specific subsets were determined by flow cytometry following primary YF-17D vaccination (Figure 88A). While the naïve compartment remained fairly stable over time, memory cells (CM and SCM) appeared and expanded along with effector cells (EM and EMRA) (Figure 88B). After the peak of the response, effector cells entered a phase of contraction. To a lesser extent, the frequency of memory cells also gradually decreased (Figure 88B). After 6 months, it became obvious that EMRA and SCM persist while EM and CM kept contracting (Figure 88B).

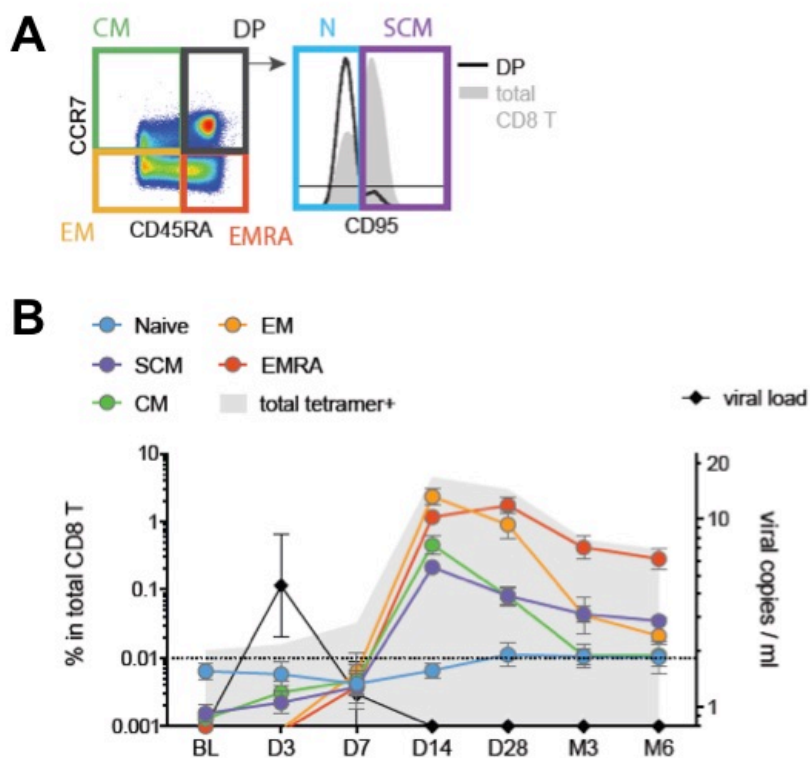


Figure 88 Analysis of A2/LLW-specific CD8 T cells subsets after YF-17D vaccination. A, Representative gating strategy to define CD8 T cell subsets: Central memory (CM: CCR+ CD45RA-), Effector memory (EM: CCR7-, CD45RA-), Effector memory CD45RA+ (EMRA: CCR7- CD45RA+), CCR7+ CD45RA+ cells are further subdivided into Naïve (CD95-) and stem cell-like(SCM: CD95+). B, Frequency of total or subsets of A2/LLW-specific CD8 T cells. The lines represent the average and standard error of the mean (n = 8) per subset as indicated; viral load data is complemented (right y-axis).

A2/LLW-specific SCM CD8 T cells are activated at the peak of the response

Next, we analyzed the expression of activation markers (CD69, CD38, HLA-DR and PD1) among the CD8 differentiation subsets. While CD69 expression was increased between day 3 and 7 after vaccination, it was evident that all other activation markers were up regulated at the peak of the response in memory subsets (CM and SCM), at the same level as the effector subsets (EM and EMRA) (Figure 89).

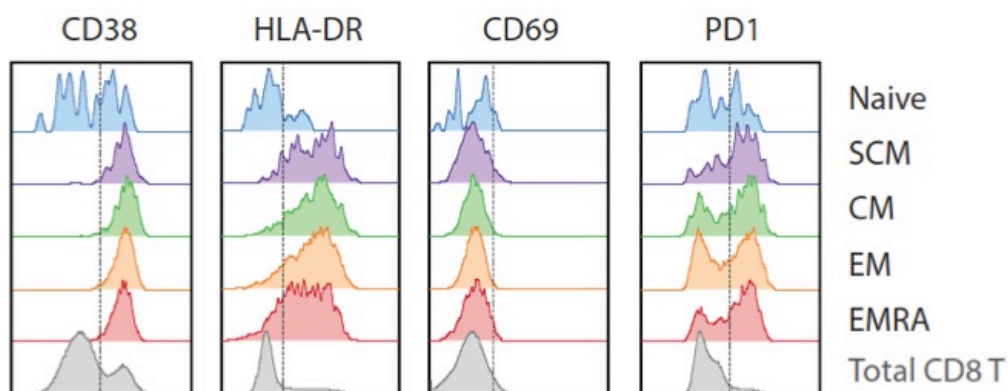


Figure 89 Activation of A2/LLW-specific CD8 T cells subsets at day 14 after YF-17D vaccination. Flow cytometry profiles showing each activation marker and subset, as indicated. Total CD8 T cells are shown as a reference. Data come from one representative donor.

SCM CD8 T cells retain proximity to the Naïve baseline during YF-17D vaccination

In order to visualize globally the dynamics of CD8 T cell differentiation, we applied multidimensionality reduction and t-stochastic neighbor embedding (tSNE) to the flow cytometry. tSNE analysis comprising 9 differentiation and activation markers was ran individually on 7 donors, 2 out of which are shown in Figure 90 (cf 6. Material and Methods). The differentiation subsets were gated “classically” based on the expression of CCR7, CD45RA and CD95 in order to identify them in the tSNE plots.

We observed that the SCM subset appeared and remained very close to the location of baseline Naïve cells. In contrast, effector populations burst out of the baseline Naïve location, peaking their distance at day 14, and gradually contracting closer to baseline.

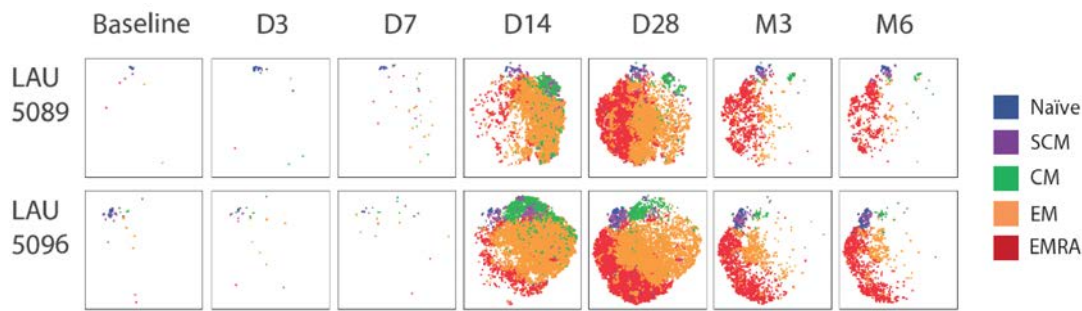


Figure 90 individual tSNE plots of two selected donors (LAU5089 and LAU5096).

3.2.2.3 Discussion

Thanks to our study, we substantiate the early appearance of SCM CD8 T cells. YFV-specific CD8 T memory cells including CM and SCM subsets are activated and expand along with the other effector subsets at the peak of the response. Our results preclude that memory subsets appear only after the acute peak. It suggests that memory cells establish early after priming. Our data indicate that memory arises very early without transition through an effector stage. Within a continuum of differentiation phenotypes, long-term memory cells persist by preserving highest “naïveness”.

Our results support models where memory CD8 T cells originate from activated CD8 T cells in parallel to the wave of effectors [258] [259]. The ontogeny of memory cells is a subject of intense debate, with recent studies supporting contrasting models. This is further discussed in Appendix 3.

3.2.2.4 Contributions

Dr. Silvia Fuertes-Marraco and I performed and analyzed the flow cytometry data, combining specimens from the YF1 and YF2 cohorts. Dr. Silvia Fuertes synthesized the data for the manuscript in preparation entitled “Human stem cell-like memory CD8 T cells establish early in the acute response to Yellow Fever virus vaccination” (Appendix 3).

4. ONGOING WORK AND PERSPECTIVES

In humans, vaccines that are routinely administered provide an ethical way to perturb the immune system in a precise and controlled setting. The exact moment of immunization is known and it is possible to collect blood samples early and long-term in order to study both the innate and adaptive responses. The YF-17D vaccine offers a unique opportunity to study the mechanisms of a persistent and powerful immune response. Indeed, it has been administered to over 600 million people worldwide with rare cases of severe adverse events. Individuals in non-endemic countries have not been exposed to Yellow fever, therefore it allows to characterize primary viral challenge. This live-attenuated vaccine results in a systemic acute viral infection within a few days. A single dose is sufficient to induce nAbs that persist for several decades and, remarkably, generates a broad and robust CD8 T cell response. The later is particularly of interest as a model to sustain the optimization of cancer immunotherapies that rely on the induction of strong cytotoxic responses.

Although the YF-17D vaccine is in use for almost 80 years, the mechanisms leading to such a successful immunogenicity remain partially unknown. This thesis provides an initial broad insight into the key immune components that are mobilized following vaccination against YFV with YF-17D in humans.

In the first part of my thesis, I characterized the genetic and structural basis of the high frequency and prevalence of the immunodominant HLA-A*02- restricted YFV-specific epitope A2/LLW, in analogy to the immunodominance of the HLA-A*02-restricted Melan-A epitope A2/ELA in melanoma. We described the TRAV12-2 bias in A2/LLW-specific CD8 T cells with functional and structural considerations of the TCR:pMHC interaction. The TCR sequences obtained during the first part of my thesis were limited to either CD8 T cell clones or T cell lines. However, the data presented in this thesis is wired within the scope of a broader characterization of the immune responses following YF-17D vaccination. The YF2 study blood specimens used in the second part of my thesis will be used further for in depth investigations thanks to recently available technologies, outlined below.

Single cell genome-wide analysis of A2/LLW-specific clonotypes during YF17D vaccination

We aim to analyze directly *ex vivo* the clonotypes before and during vaccination, including several differentiation subsets, at the single cell level. In collaboration with the group of Prof. Sarah Teichmann (Cambridge, UK), we are currently analyzing the whole transcriptome of A2/LLW-specific CD8 T cells by single-cell RNA sequencing (scRNA-seq). This group developed the TraCeR (T cell receptor sequence Reconstruction) technology, which enables the reconstruction of full-length $\alpha\beta$ paired TCR sequences and therefore to track individual clonotypes during the course of differentiation [260] [261].

In setup experiments, we first made sure that the quality of the data generated from frozen material (instead of fresh material) was suitable in order to reconstruct TCR sequences by TraCeR. Then, based on the quality of the response, the detectability of the CD8 T subsets and the availability of samples within our YF biobank, we selected four individuals from the priming group. We chose 5 out of 7 time-points (BL, D14, D28, M3, M6), without time-points D3 and D7 because our estimates on sorting yields did not calculate that sufficient events would be possibly sorted from D3 and D7. Single cells were directly sorted into plates containing lysis buffer. We isolated around 100 cells per time-point from naïve-like (CCR7+ CD45RA+), effectors (CCR7-), and CM (when possible) (CCR7+ CD45RA-). The data passed the quality check and is currently analyzed by our collaborator Dr. Santiago Carmona (Dept. of Oncology, CHUV) and our teammate Dr. Sina Nassiri (Swiss Institute of Bioinformatics & Dept. of Oncology, CHUV).

Given that the TCR sequence is a unique identity of each T cell clone, longitudinal analyses of TCR sequences may reveal the clonality of the various T cell populations in order to delineate the relationships between various differentiation subsets, with particular interest in the genealogy of SCM cells.

Some studies on YF-17D vaccination included systems biology approaches such as microarrays of PBMCs [112] [113]. However, they were limited in terms of gene expression information and protein data. Importantly, these studies were lacking the resolution of the different immune cell populations. Nowadays, technologies have improved and provide precious information on isolated leukocyte populations and also

at the single cell level. Overall, our goal is to obtain a deeper knowledge of the global and regulatory landscape of each CD8 T cell subsets. In contrast to flow cytometry, where several bias are introduced (as discussed in 3.2.1.3), the scRNASeq technique will allow having an unsupervised analysis of a myriad of parameters and potentially identifying unexpected phenomena.

Proteomic analyses of adaptive and innate populations by MS-SWATH proteomics

We collaborate with the group of Prof. Ruedi Aebersold (Zürich, Switzerland) with the aim to characterize by cutting-edge proteomics the global immune components in the blood using the technology developed in their lab called Sequential Window Acquisition of all Theoretical Mass Spectra (SWATH-MS) [262]. It is a data independent acquisition method that combines the advantages of both shotgun and Selected Reaction Monitoring methods: i) high throughput data acquisition is easy, ii) the protein and peptide detection/multiplexing is broad, iii) the reproducibility of data is high. In addition, SWATH-MS allows retrospective targeting.

We set-up the protocol to FACS-sort and analyze by MS-SWATH the proteome of total PBMC and 5 different immune populations: CD4 T cells, CD8 T cells, B cells, NK cells and monocytes. We are planning to analyze all individuals from both vaccination groups and all time-points. After optimization of the sorting protocol, reference libraries for each population have been generated based on 200'000 cells from two donors. In addition, we confirmed that 25'000 cells of each population gives enough sensitivity for further investigation by SWATH-MS.

Analysis of soluble immunomodulators by multiplex on plasma

While PBMC fractions predominate as the specimens of research in YF-17D vaccinology, a few studies also make use of plasma [263] [264]. In order to monitor parameters indicative of vaccine efficacy, we quantified neutralizing antibodies and viral titers in plasma. Alongside, we will analyze soluble immunomodulators by multiplex immunoassays on plasma samples to detect cytokines, chemokines, growth factors and soluble receptors. For this analysis, however, we have not yet decided

what particular multiplex assay or kit we will use, we hope to find an affordable and sensitive assay that includes a maximally broad panel of soluble modulators.

Broad correlation analysis across complementary datasets

Subsequently we will merge the data obtained from the aforementioned methods to seek the identification of determinants underlying the immune response elicited by YF-17D vaccination. For quantifying immunogenicity, we will establish scores that include immune events such as (i) activation of the innate arm with mechanisms dedicated to anti-viral antigen cross-presentation, (ii) titers of nAbs (B cell arm), (iii) development of plasmablasts, (iv) frequency and polyfunctionality of YFV-specific T cells, and (v) differentiation of T cells and long-lasting stem cell-like memory (SCM) T cells.

Based on the data gathered by comprehensive methods, immunogenicity scores will then be interrogated for correlation to immune determinants. Taken together, we expect to obtain high resolution of the immune response to YF-17D and better define correlates of optimal immunogenicity, and test whether these may potentially predict specific immunogenicity.

5. CONCLUDING REMARKS

Globally, my PhD thesis integrates both the analysis of specific immune interactions and multiple –omics approaches. Such high-throughput technologies generate enormous amount of data. Thus, we are facing the challenge to analyze and interpret the data. For instance, the flow cytometry data were analyzed for correlations and multiple hits were identified. However, it takes time to make “biological sense” of these individual significant correlations. Rather, we should focus on group of parameters and molecular signatures that correlate with and predict vaccine efficacy.

In conclusion, studying immune responses to YF-17D vaccination provides important insights into the determinants leading to a potent immune response. To our knowledge, the YF2 study is the first that compares in detail primary and booster vaccinations side-by-side, including the global and specific adaptive and innate parameters in parallel to nAbs and viral load. With our work, we aim to identify correlates of optimal immunogenicity, and test whether these may potentially predict specific immunogenicity. This knowledge can be further applied not only to other viral vaccines but also to cancer immunotherapies and immune-related diseases.

6. MATERIAL AND METHODS

6.1 Clinical studies: design, population and ethics statement

Peripheral blood mononuclear cells (PBMCs) were obtained in the framework of two clinical studies, approved by the Human Research Ethics Committee of the Canton de Vaud with healthy volunteers participating under written informed consent. Eligible volunteers donated blood according to the standards of the Blood Transfusion Center (Service Vaudois de Transfusion Sanguine).

The first clinical study, “YF1” (protocol 329/12), was cross-sectional and open to healthy volunteers aged 18 to 65 years having received the YF-17D vaccine (Stamaril, Sanofi Pasteur) with no limit on minimum or maximum vaccination history. The cohort consisted of 41 healthy volunteers vaccinated with YF-17D, between 3 months and 35 years ago, including four individuals having received multiple vaccines. Samples from unvaccinated blood donors were also obtained from the Blood Transfusion Center.

The second clinical study, “YF2” (protocol 324/13), was longitudinal. The study population consisted of two groups of healthy volunteers aged 18 to 65 years, who for traveling purposes were about to receive the YF-17D vaccine (Stamaril, Sanofi Pasteur). One group received the vaccine for the first time (“priming”, $n = 10$). The second group had previously received the YF-17D vaccine < 10 years ago (“boost”, $n = 6$). PBMCs, complete blood counts, and sera were obtained before vaccination at various time points following vaccination: days 3, 7, 14, 28 ± 2 days, months 3 ± 2 weeks and 6 ± 2 weeks.

6.2 Biobank: Peripheral blood collection and processing

Peripheral blood samples were collected and immediately processed for cryopreservation awaiting experimental use. PBMCs were obtained from anti-coagulated whole blood diluted 1:1 in phosphate buffered saline (PBS) and overlaid on Lymphoprep for density gradient fractionation (30 minutes at 400g without break) and were cryopreserved in complete RPMI 1640 supplemented with 40% fetal calf serum (FCS) and 10% dimethyl sulfoxide. Plasma samples were obtained from the supernatant of EDTA-coated blood tubes after centrifugation at 1'000g for 15 min at RT

followed by a second centrifugation at 8'000g for 10 minutes at 4°C, and preserved at -80°C.

6.3 Viral load quantification

Yellow Fever virus (YFV) load was quantified in plasma from EDTA-anti-coagulated blood based on a Taqman Real-time PCR assay to detect YFV genome copies as previously described, performed by our collaborator Dr. Benton Lawson in the Center For AIDS Research in Emory University (U.S.A.) [119].

6.4 Plaque reduction neutralizing test (PRNT)

Plasma samples were analyzed for YFV neutralizing antibodies by a PRNT, performed by our collaborator Dr. Rama Akondy in Emory University (U.S.A.). Briefly, plasma was heated to 56 °C for 30 minutes to inactivate complement. Various dilutions of the plasma were incubated overnight at 4 °C with 200 plaque-forming units of YFV-17D. Vero cell monolayers in drained six-well plates were incubated with this virus-plasma mixture for 1 hour at 37 °C. The wells were overlaid with a mix of agarose and 2XM199 medium and plaques counted 3–4 days later using neutral red.

6.5 Generation and maintenance of T cell clones

All A2/LLW-specific CD8⁺ T cell clones were generated in the laboratory of Prof. D. Speiser by Dr. Silvia Fuertes and Nicole Montandon, from healthy YF-17D (Stamaril, Sanofi Pasteur) vaccinees. Purified A2/LLW tetramer-positive populations were isolated by FACS as described [97] and cloned by limiting dilution in Terasaki plates, cultured in RPMI 1640 medium supplemented with 8% human serum and 150 U/ml recombinant human IL-2 (rIL-2). Thereafter, to maintain and expand T cell clones, periodic restimulation was done with 1 µg/ml PHA and 10⁶/ml irradiated allogeneic PBMC (30 Gy) as feeder cells. The MEL5 clone was generated in the laboratory of A. Sewell as previously described [135]. The clones HD421 2/5F and LAU1264 were generated in the laboratories of D. Speiser and N. Rufer as previously described [133].

6.6 Generation of T cell lines

To create T cell lines, PBMCs were cultured in priming medium (R10 with 10 mM HEPES buffer, 13 MEM nonessential amino acids, 1 mM sodium pyruvate [all from Life Technologies], and 20 IU/ml IL-2 (Proleukin; Prometheus, San Diego, CA) with 10^{-5} M LLWNGPMAV peptide and anti-human CD28 Ab (10 mg/ml) for 14 days.

6.7 TCR repertoire and clonotype analysis in A2/LLW-specific CD8⁺ T cell clones

Total RNA was isolated using the PicoPure RNA kit per manufacturer's instructions, and cDNA prepared and sequenced as previously described [129]. Briefly, for the V β repertoire, each cDNA sample was subjected to individual PCRs using a set of previously validated forward primers specific for the 22 TRBV subfamilies and one reverse primer specific for the corresponding C β gene segment. For the V α repertoire, we amplified and sequenced the TRAV12-2 segment using the TRAV12 (forward) and TRAC (reverse) primers. PCR amplicons of interest were sequenced from the reverse primer by Fasteris S.A. TRAV and TRBV segments were described according to the IMGT nomenclature [265].

6.8 TCR sequencing and analysis of the A2/LLW-specific T cell line

RNA was extracted using an RNeasy PlusMicro Kit (QIAGEN), following the manufacturer's instructions. The SMARTer RACE kit (Clontech, Paris, France) was used to generate full-length cDNA from TCR RNA, also following the manufacturer's instructions. Two sets of primers (external and internal) were designed to perform a nested PCR of the CDR3 region of the TCR alpha and beta genes. The PCR products were examined by agarose gel electrophoresis and purified by gel extraction before sample indexing. All samples were processed further to generate libraries for high-throughput Illumina sequencing. Libraries were processed with the NEBNext Ultra Library preparation kit (New England Biolabs, Cambridge, U.K.) and run on an Illumina MiSeq instrument using a MiSeq v2 reagent kit (Illumina, Cambridge, U.K.). TCR gene usage was determined using reference sequences from the ImMunoGeneTics

database (<http://www.imgt.org>), and all TCR gene segments were designated according to ImMunoGeneTics nomenclature using MiXCR software (v1.8.1).

6.9 ⁵¹Chromium release assays

The HLA-A*02⁺ human mutant cell line CEMx721.T2 (American Type Culture Collection) was used as target by labeling with ⁵¹Cr for 1 hour at 37°C, followed by extensive washing. Target cell killing was assessed by chromium release in the supernatant upon co-culture with CD8⁺ T cell clones (effector cells) at the Effector:Target ratio of 10:1 for 4 hours at 37°C in V-bottom microwells, in presence of serial dilutions of the peptide, measured using a gamma counter and calculated as:

$$\% \text{ specific lysis} = 100 \times \frac{(\text{experimental} - \text{spontaneous release})}{(\text{total} - \text{spontaneous release})}$$

6.10 Flow cytometry

- For the analysis of antigen-specific populations, CD8⁺ T cells were first enriched from cryopreserved samples using the human CD8⁺ T cell enrichment kit from StemCell Technologies (negative selection, per manufacturer's instructions). All Stainings were performed using phosphate-buffered saline with 5mM EDTA, 0.2% bovine serum albumin, and 0.02% sodium azide [fluorescence-activated cell sorting (FACS) buffer]. Tetramer stainings were performed for 40 minutes at 4°C. All tetramers were purchased from TCmetrix Sàrl. Surface antibody staining was then performed, followed by staining with LIVE/DEAD-Fixable-Aqua (Invitrogen), each step at 4°C for 30 minutes. Cells were fixed overnight in 0.36% formaldehyde (supplemented with 2% glucose and 5mM sodium azide). Samples were acquired using either a Gallios flow cytometer (Beckman Coulter, three-laser configuration) or LSRII-SORP (Beckton Dickinson). The data were processed with FlowJo (Tree Star Inc., v9.5.2). Samples with antigen-specific populations below 0.001% tetramer-positive cells in total CD8⁺ T cells were considered negative and populations consisting of less than 20 events were not considered eligible for further analysis.

- For the YF2 longitudinal study flow cytometry panels, cells were additionally fixed overnight in 1X Fix/Perm solution from the Foxp3 staining kit (eBioscience). Cells were washed and stained intranuclearly in 1X Perm solution from the Foxp3 staining kit (eBioscience). Samples were acquired using an LSRII-SORP flow cytometer (BD Bioscience). The data were processed with FlowJo (Tree Star Inc., v9.5.2). For the B cell, monocyte, dendritic cell, ILC and NK cell stainings, cells were pre-incubated with FcR blocking reagent (Miltenyi Biotec).
- For the antigen-specific staining protocol performed in Cardiff, Dextramer-PE (Immudex, Copenhagen, Denmark) and premium-grade streptavidin-PE (Life Technologies) were used with monomeric pMHC. The same batches of streptavidin-PE and each individual pMHC were used throughout this study to avoid any possibility of batch-to-batch variation. Protease inhibitors (Merck, London, U.K.) and PBS (tetramers) or dextramer buffer were added to give a final pMHC multimer concentration of 0.1 mg/ml, were stored in the dark at 4°C, and were used within 3 d of assembly. Generally, 0.4 mg of tetramer or dextramer was used per stain. Typically, 2–3 10^6 cells of a T cell line or PBMCs were stained per tube with dextramer or tetramer first on ice for 30 min. Cells were washed with PBS and then stained with LIVE/DEAD Fixable Violet Dead Cell Stain, ViViD (Life Technologies) for 5 minutes at room temperature, and then a mixture of Abs for 20 minutes on ice: anti-CD8–allophycocyanin (clone BW135/80; Miltenyi Biotec); anti-CD3–PerCP (clone BW264/56; Miltenyi Biotec); anti-CD19–Pacific Blue (clone HIB19; BioLegend), and anti-CD14–Pacific Blue (clone M5E2; BioLegend). FACS Aria (Central Biotechnology Service, Cardiff University) was used for cell sorting, with desired cells directed into RNA extraction buffer (RNeasy Plus Micro Kit; QIAGEN, Heidelberg, Germany). Data were analyzed using FlowJo software (Tree Star Inc., v9.5.2). The optimized protocol featuring two additional steps: cells were treated with 50 nM dasatinib (PKI) at 37°C for 30 minutes and were not washed prior to staining with tetramer or dextramer, and post–pHLA staining and washing, 0.5 mg (10 mg/ml) of a mouse anti-PE primary unconjugated mAb (clone PE001; BioLegend) was used.
- For t-distributed Stochastic Neighbor Embedding (t-SNE) analyses, the tSNE plugin in FlowJo 10.4.2 was used. Single live CD8 T cells from each donor were downsampled to 5'000 events and the sum of N=13 donors were concatenated into a

single file (70'000 events). This file was then gated and color-coded for the differentiation subsets. The N=13 concatenate was analysed by tSNE using the plugin from FlowJo v10, reducing nine parameters (CCR7, CD45RA, CD95, TCF1, IL7Ra, PD1, CD69, HLA-DR, CD38) to two dimensions (tSNE x- and y- axes). For the longitudinal tSNE analyses of A2/LLW-specific CD8 T cells, all single live A2/LLW-specific CD8 T cell events of the longitudinal series were concatenated and thus are represented in proportions corresponding to the original numbers of PBMC thawed, which are equal across time-points (corresponding to 10e7 PBMC thawed) except for the baseline which is 1.5-fold larger (1.5 x 10e7 PBMC thawed). The detection threshold for multimer positive populations was 0.01% of total CD8 T cells and at least 10 events. The positivity threshold for each marker was set according to distinct negative and positive populations in bulk CD8 T cells in resting and/or activated samples; for the indirect TCF1 staining, the negative signal was further validated with secondary antibody-only controls.

6.10.1 Flow cytometry: list of reagents

Target	Fluorochrome	Company	Clone	Cat no
CD58	FITC	BD	1C3	555920
HLA-DR	FITC	Biolegend	L243	307604
CD14	FITC	BC		B36297
CD15	FITC	BC		B36298
CD33	FITC	Biolegend	HIM3-4	303304
CD34	FITC	Biolegend	561	343604
CD203c	FITC	Biolegend	NP4D6	324614
CD3	FITC	BC		A07746
CD19	FITC	BC		A07768
CD20	FITC	Biolegend	2H7	302304
FcER1	FITC	Biolegend	AER-37	334608
CD138	FITC	Biolegend	1D4	344404
CD56	FITC	Biolegend	HCD56	318304
PD1 (CD279)	PerCP-eF710	eBioscience	eBioJ05	46-2799-42
CD123	PerCP-Cy5.5	eBioscience	6H6	45-1239-42
HLA-DR	PerCP-Cy5.5	Biolegend		307630
CD38	PerCP-Cy5.5	Biolegend	HIT2	303522
CD58	PE	BD		555921
IgD	PE	BD	IA6-2	555779
c-kit(CD117)	PE	Biolegend		313204
Ki-67	PE	Biolegend	Ki67	350504

secondary	PE	eBioscience		12-4739-81
CD45RA	ECD	BC		B49193
HLA-DR	ECD	BC		IM3636
CD16	ECD	BC		A33098
CD15S	PE-CF594	BD	CSLEX1	563527
CD95	PE-Cy7	Biolegend	DX2	305622
BCMA	PE-Cy7	Biolegend	19F2	357508
HLA-DR	PE-Cy7	BD		PN A40579
CD56	PE-Cy7	Biolegend	HCD56	318318
CCR10	APC	Biolegend		341506
CD83	APC	BD		551073
Nkp44 (CD336)	APC	Biolegend		325110
Foxp3	APC	eBioscience	236A/E7	17-4777-42
CD58	APC	eBioscience	TS2/9	17-0578-42
Ki-67	A647	Biolegend	Ki67	350510
CD3	A700	Biolegend	HIT3a	300324
CD86	A700	BD	2331	561124
CD38	A700	eBioscience	HIT2	56-0389-42
CD137	A700	Biolegend	4B4-1	309816
CD8	APC-AF750	BC	B9.11	A94683
CD40	APC-H7	BD		561211
CD1c (BDCA-1)	APC-Cy7	Biolegend	L161	331520
CCR7	BV421	Biolegend	G043H7	353208
CRTH2 (CD294)	BV421	BD	BM16	562992
CD14	Pacific Blue	BD	M5E2	558121
CD20	Pacific Blue	Biolegend	2H7	302320
CD141	BV510	BD	1A4	563298
CD45RA	BV510	Biol		304142
CD3	Krome Orange	BC	B00068	B00068
CD16	Krome Orange	BC	3G8	P/N B00069
CXCR5	BV605	Biolegend	J252D4	356930
CD127	BV605	Biolegend		351334
CD25	BV605	BD	2A3	562660
CD27	BV605	BD	L128	562655
CD69	BV650	Biolegend	FN50	310934
CD40	BV650	Biolegend	5C3	334338
CXCR3	BV650	Biolegend	G025H7	353730
CD4	BV785	Biolegend	OK-T4	317441
CD303 (BDCA-2)	BV785	Biolegend	201A	354221
CD138	BV711	Biolegend	MI15	356522
PD1	BV711	Biolegend	EH12-2H7	329928
FVD	eF455	eBioscience		65-0868-14
pEIF2S1	-	Abcam		ab32157

6.10.2 Intracellular cytokine staining assay

A2/LLW-specific CD8⁺ T cell clones were stimulated with peptide-loaded T2 cells at the E:T cell ratio of 1:2 for 4 hours at 37°C in the presence of Brefeldin-A (Sigma-Aldrich) and anti-CD107a-FITC antibody (BD Biosciences) or anti-CD107a-PE antibody (BD Biosciences). Then, cells were stained with anti-CD8-APC-AF750 antibody (Beckman Coulter) at 4°C for 30 minutes. After washing in PBS, cells were incubated with LIVE/DEAD-Fixable-Aqua (Invitrogen) at 4°C for 30 minutes, and fixed at 4°C overnight (0.36% formaldehyde buffer). Cells were washed and stained intracellularly with anti-IFN γ -PC7, anti-TNF α -A700 and anti-IL-2-PerPCP-Cy5.5 antibodies (BD Biosciences) or anti-IL-2-FITC antibodies (BD Biosciences) in FACS buffer with 0.1% saponin for 30 minutes at 4°C. Samples were acquired and data processed as described above.

6.10.4 Data processing and statistical analysis

Flow cytometry data processed with FlowJo (Tree Star Inc., v9.5.2). Data were plotted using the GraphPad Prism software (v.6; GraphPad). Quantifications were made on the basis of the FlowJo, Microsoft Excel, GraphPad Prism, and SPICE softwares. Statistical values were obtained using the analyses and tests (including normality tests) as detailed in the figure legends; where indicated, ns = not significant; *P < 0.05; **P < 0.01; ***P < 0.001. For statistical comparison of pie charts generated using SPICE, the built-in test in SPICE software (v5.3) was used (using 10,000 permutations).

6.10.5 Bioinformatics analysis of broad datasets

In brief, data was first normalized by log- and logit-transformation of raw counts and frequency measures, respectively. Having treated measurements prior to vaccination as baseline (day 0), we next fit a linear spline model with 4 internal knots located at days 3, 7, 14, and 28. Visually, fitting a linear spline with 4 internal knots is equivalent to fitting a piecewise linear regression with 4 breakpoints and 5 segments. We chose the location of internal knots based on the observation that most features showed temporal fluctuations up to 4 weeks post vaccination, and reached a steady state from 28 days onward. Broadly speaking, the heterogeneity of individual profiles can be

explained by either variability at the baseline (random intercepts) or variability in the slopes (random slopes). Given our sample size, we could not afford the most flexible model (by incorporating both random intercepts and random slopes). Instead, we opted for a random intercept model. Intuitively, our random intercept model assumes that individual profiles exhibit a consistent temporal dynamic, and that differences among individual profiles can be explained by variability at the baseline. Once the model was fit and unknown parameters were estimated/predicted for each feature, individual profiles were extracted for visualization and downstream analyses.

6.11 NTAmer staining and dissociation kinetic measurements

Dually labeled pMHC multimers built on NTA-Ni²⁺-His-tag interactions called NTAmers (synthesized by TCMetrix Sàrl) were used for dissociation kinetic measurements [197] [198]. Stainings with dually PE- and Cy5-labeled A2/LLW-specific NTAmers and data analysis were done as previously described [43] [197]. Briefly, staining was measured at 4°C using a thermostat device on a SORP-LSR II flow cytometer (BD Biosciences). Following 30 seconds of baseline acquisition, imidazole (100mM) was added. PE and Cy5 fluorescence were measured during the following 15min. Data were processed using the kinetic module of the FlowJo software (v.9.7.6; Tree Star), and corrected mean fluorescence intensity values were plotted and analyzed using the GraphPad Prism software (v.6; GraphPad). The Cy5 decay values of the NTAmers specific for the mutant peptides were normalized to the PE decay value of the WT NTAmer.

6.12 Sizing scan

The following mixtures were used to define the MHC-peptide length preference of individual TCRs: X⁸, X⁹, X¹⁰, X¹¹, X¹², and X¹³ (where X is any of the 19 L-amino acids excluding cysteine; Pepscan Presto) [193]. The YF5048 clones was washed and rested overnight in R5 medium (RPMI 1640 supplemented with 100 units/ml penicillin, 100 µg/ml streptomycin, 2mm l-glutamine, and 5% heat-inactivated fetal calf serum (all Invitrogen)). In U-bottom 96-well plates, 6 × 10⁴ target cells were incubated with sizing scan mixtures at 1mM in duplicate for 2 hours at 37°C. After peptide pulsing, 3 × 10⁴ YF5048 clone were added and the assay was incubated overnight at 37°C.

Subsequently, the supernatant was harvested and assayed for MIP-1 β by ELISA according to the manufacturer's instructions (R&D Systems).

6.13 Combinatorial peptide library (CPL) scans

The nonamer CPL contains a total of 4.8×10^{11} ($(9+19) \times 19^8$) different nonamer peptides divided into 180 sub-libraries with each containing 19^8 different nonamer peptides in approximately equimolar concentrations (Pepscan, Lelystad, The Netherlands) [190]. Each of the 180 sub-libraries has a fixed amino acid residue but all other positions are degenerate. Cysteine was excluded from all degenerate positions to avoid oxidation, but was included at the fixed positions. Prior to the assay, CD8⁺ T cell clones were washed and rested overnight in R5 medium (RPMI 1640 supplemented with 100 units/ml penicillin, 100 μ g/ml streptomycin, 2mm l-glutamine, and 5% heat-inactivated fetal calf serum (all Invitrogen)). For CPL screening, 6×10^4 C1R A2 cells [266] were pulsed with each sub-library at 100 μ g/ml in duplicate for 2 hours at 37°C. After peptide pulsing, 3×10^4 CD8⁺ T cells were added, and the cultures were incubated overnight at 37°C. Subsequently, the supernatant was harvested and assayed for MIP-1 β by ELISA according to the manufacturer's instructions (R&D Systems).

6.14 Protein expression, refolding and purification

HLA A*0201 α -chain and β 2m were expressed separately, without post-translational modification, as insoluble inclusion bodies (IBs) in competent Rosetta (DE3) *Escherichia coli* cells, using 0.5M IPTG to induce expression as thoroughly described recently [160]. Briefly, for a 1L pMHC refold, 30mg HLA-A*0201 α -chain was mixed with 30mg β 2m and 4mg peptide at 37°C for 15 minutes with 10mM DTT. This mixture was then added to cold refold buffer (50mM Tris, pH8, 2mM EDTA, 400mM L-arginine, 6mM cysteamine hydrochloride, and 4mM cystamine). Refolds were mixed at 4°C for > 6 h. Dialysis was performed against 10mM TRIS, pH8.1, until the conductivity of the refolds was less than two millisiemens per centimeter. The refolds were then filtered and purified first by ion exchange using a Poros50HQ™ column (GE Healthcare, Buckinghamshire, U.K.) and second by gel filtration directly into crystallization buffer

(10mM Tris pH8.1 and 10mM NaCl) or PBS buffer (137mM NaCl, 3mM KCl, 8mM Na₂HPO₄, 1mM KH₂PO₄) using a Superdex200HR™ column (GE Healthcare, Buckinghamshire, U.K.). Protein quality was analyzed by Coomassie-stained SDS-PAGE, either under non-reducing or reducing conditions.

6.15 Crystallization, diffraction data collection, and model refinement

All protein crystals were grown at 18°C by vapor diffusion via the “sitting drop” technique. 200nl of each pMHC (20 mg/ml) in crystallization buffer was added to 200nl of reservoir solution. A2/LLW-WT crystals were grown in 0.1 M Hepes, pH7, 0.2M ammonium sulphate, 20%PEG 4000. 2/LLW-4A crystals were grown in 0.1 M Sodium Cacodylate pH 6.0, 0.2 M Ammonium Sulphate, 25% PEG 4000. A2/LLW-7I crystals were grown in 0.1 M Mes pH 7.0, 0.2 M Ammonium Sulphate, 25% PEG 8000. A2/LLW-8H and A2/LLW-8Q crystals were grown in 0.1 M Sodium Cacodylate pH 6.5, 0.2 M Ammonium Sulphate, 20 % PEG 4000. All crystals were soaked in 30% ethylene glycol before cryo-cooling. All crystallization screens and optimization experiments were completed using an Art-Robbins Gryphon dispensing robot (Alpha Biotech Ltd., UK). Data were collected at 100K at the Diamond Light Source (Oxfordshire, UK) as described previously [267]. All data sets were collected at a wavelength of 0.98 Å using an ADSC Q315 CCD detector. Reflection intensities were estimated with the XIA2 package, and the data were scaled, reduced, and analyzed with the SCALA and CCP4 package. Structures were solved with molecular replacement using PHASER. A solution could be obtained with a search model taken from Protein Data Bank entry 5EU5. Sequences were adjusted with COOT, and the models were refined with REFMAC5. Graphical representations were prepared with PyMOL. The reflection data and final model coordinates were deposited in the Protein Data Bank. PDB codes are the following:

A2/LLW-WT: 5N6B

Entries in preparation for: A2/LLW-4A, A2/LLW-7I, A2/LLW-8H, and A2/LLW-8Q.

6.16 Measuring the thermal stability of HLA-A*0201–peptide complexes

Thermal stability of A2/peptide complexes was assessed by CD spectroscopy monitoring the change of ellipticities Θ at 218nm where the spectra exhibit a minimum. Data were collected on an Aviv 215 spectrometer (Aviv Biomedical Inc., Lakewood, NJ) equipped with a thermostated cell holder using a 1mm quartz cell. Proteins were dissolved in PBS at $c = 3.5 \mu\text{M}$. Denaturation was monitored from 4°C up to a temperature when protein precipitation occurred using a gradient of 0.5°C/min. Melting curves were analyzed assuming a two-state native (N) to denatured (D) transition $N_3 \leftrightarrow 3D$ with the melting temperature and van't Hoff's enthalpy at the midpoint of the transition as fitting parameters [268] [269].

6.17 *In silico* TCR:pMHC analyses: Modeling the TCR:pMHC complex and Molecular Dynamics (MD) simulations

In silico analyses on TCR:pMHC were performed by our collaborator Prof. Vincent Zoete. The 3D structure of the TRAV12-2/TRBV9 TCR in complex with HLA-A2 and the LLWNGPMAV peptide was modeled from three experimental structures: 3HG1 [135] and 4QOK [270], containing a complex between the TRAV12-2/TRBC1 TCR in complex with HLA-A2 and the ELAGIGILTV or EAAGIGILTV peptides, respectively, and the experimental structure obtained in this study for the complex between HLA-A2 and the LLWNGPMAV, LLWNGPIAV, LLWNGPMQV and LLWNGPMAV peptides. The sequence alignment between TRBV9 and TRBC1 was performed using the MUSCLE program [271]. The sequence identity between TRBV9 and TRBC1 was performed using the MUSCLE program. The sequence identity between the variable part of the TRBV9 and TRBC1 beta chains is 30%. Based on this sequence alignment, the model was obtained using the Modeller program [272] [273]. 1000 models were generated by satisfaction of spatial restraints through minimization and simulated annealing, and the model with the best Modeller objective function was retained. Molecules were visualized and analyzed using UCSF Chimera [274].

The model of A2/LLW in complex with the MEL5 TCR was obtained with the Modeller program, following the method described above to obtain the structural model of

A2/LLW with the YF5048 TCR. In this case, however, we used our experimental structure of the A2/LLW as a template for the HLA/peptide domain and the experimental structure of the complex between A2/ELA and MEL5 (PDB code: 3HG1) as a template for the MEL5 TCR.

MD simulations were performed with GROMACS [275] [276] version 2018.3 in periodic boundary conditions, using the all-atom CHARMM27 force field [277] and the TIP3P water model. The number of Na⁺ and Cl⁻ ions in solution was adjusted to neutralize the system and reach the physiological concentrations of 0.154 M. Before starting the MD simulations, missing residues and loops were modelled using the Dunbrack rotamer libraries [278] and the Modeller program [279]. Titratable side chains were protonated so as to allow hydrogen bonds with neighbouring residues. Electrostatic interactions were calculated with the Ewald particle-mesh method [280] with a grid spacing of 1.2 Å. A cut-off of 12 Å was applied for the real-space Coulomb and van der Waals interactions. Bonds involving hydrogen atoms were constrained using the P-LINCS algorithm [281]. The system was coupled to a Parinello-Rahman barostat with a relaxation time of 1 ps. The solute and the solvent were separately coupled to two nose-hoover thermostats [282], each with a relaxation time of 0.2 ps. A time integration step of 2 fs was used, with a temperature of 300 K and a pressure to 1 bar during the production trajectory. Initial Cartesian coordinates were taken from the experimental X-ray structures of pMHC molecules obtained in this study. Peptide mutations, M7I, A8H and A8Q were introduced using the *swapa* command of UCSF Chimera [274] v 1.12 and the Dunbrack backbone-dependent rotamer library [278]. Initial structures were energy optimized, heated from 0 to 300 K in 0.4 ns, equilibrated for a further 1 ns restraining each solute non-hydrogen atom to its original position, and finally equilibrated for 2 ns without restraints before data collection. 3 MD simulations were carried out for the WT and mutated peptides to assess the reproducibility of the results. Each MD simulation had a production time of 140 ns, saving coordinates every 0.05 ns.

7. REFERENCES

- [1] K. Murphy, P. Travers, M. Walport, and C. Janeway, *Janeway's immunobiology*, 8th ed. New York: Garland Science.
- [2] K. S. Kobayashi and P. J. van den Elsen, "NLRC5: a key regulator of MHC class I-dependent immune responses," *Nat. Rev. Immunol.*, vol. 12, p. 813, Nov. 2012.
- [3] J. G. Crompton, M. Narayanan, S. Cuddapah, R. Roychoudhuri, Y. Ji, W. Yang, S. J. Patel, M. Sukumar, D. C. Palmer, W. Peng, E. Wang, F. M. Marincola, C. A. Klebanoff, K. Zhao, J. S. Tsang, L. Gattinoni, and N. P. Restifo, "Lineage relationship of CD8⁺ T cell subsets is revealed by progressive changes in the epigenetic landscape," *Cell Mol Immunol*, vol. 13, no. 4. Chinese Society of Immunology and The University of Science and Technology, pp. 502–513, Jul-2016.
- [4] S. M. Gray, S. M. Kaech, and M. M. Staron, "The interface between transcriptional and epigenetic control of effector and memory CD8⁺ T-cell differentiation," *Immunol. Rev.*, vol. 261, no. 1, pp. 157–168, Sep. 2014.
- [5] R. Roychoudhuri, F. Lefebvre, M. Honda, L. Pan, Y. Ji, C. A. Klebanoff, C. N. Nichols, S. Fourati, A. N. Hegazy, J.-P. Goulet, L. Gattinoni, G. J. Nabel, M. Gilliet, M. Cameron, N. P. Restifo, R. P. Sékaly, and L. Flatz, "Transcriptional profiles reveal a stepwise developmental program of memory CD8⁺ T cell differentiation," *Vaccine*, vol. 33, no. 7, pp. 914–923, 2015.
- [6] Y. Yuzefpolskiy, F. M. Baumann, V. Kalia, and S. Sarkar, "Early CD8 T-cell memory precursors and terminal effectors exhibit equipotent in vivo degranulation," *Cell. Mol. Immunol.*, vol. 12, no. 4, pp. 400–408, Jul. 2015.
- [7] F. Crauste, J. Mafille, L. Boucinha, S. Djebali, O. Gandrillon, J. Marvel, and C. Arpin, "Identification of Nascent Memory CD8 T Cells and Modeling of Their Ontogeny," *Cell Syst.*, vol. 4, no. 3, p. 306–317.e4, 2017.
- [8] M. M. Opata and R. Stephens, "Early Decision: Effector and Effector Memory T Cell Differentiation in Chronic Infection," *Curr. Immunol. Rev.*, vol. 9, no. 3, pp. 190–206, Aug. 2013.
- [9] G. Jeannet, C. Boudousquié, N. Gardiol, J. Kang, J. Huelsken, and W. Held, "Essential role of the Wnt pathway effector Tcf-1 for the establishment of functional CD8 T cell memory," *Proc. Natl. Acad. Sci. U. S. A.*, vol. 107, no. 21, pp. 9777–9782, May 2010.
- [10] X. Zhou, S. Yu, D.-M. Zhao, J. T. Harty, V. P. Badovinac, and H.-H. Xue, "Differentiation and persistence of memory CD8(+) T cells depend on T cell factor 1," *Immunity*, vol.

- 33, no. 2, pp. 229–240, Aug. 2010.
- [11] S. M. Kaech and W. Cui, “Transcriptional control of effector and memory CD8+ T cell differentiation,” *Nat. Publ. Gr.*, vol. 12, no. 11, pp. 749–761, 2012.
- [12] D. T. Utzschneider, M. Charmoy, V. Chennupati, L. Pousse, D. P. Ferreira, S. Calderon-Copete, M. Danilo, F. Alfei, M. Hofmann, D. Wieland, S. Pradervand, R. Thimme, D. Zehn, and W. Held, “T Cell Factor 1-Expressing Memory-like CD8+ T Cells Sustain the Immune Response to Chronic Viral Infections,” *Immunity*, vol. 45, no. 2, pp. 415–427, 2016.
- [13] D. Zhao, S. Yu, X. Zhou, S. Jodie, W. Held, V. P. Badovinac, and J. T. Harty, “Constitutive Activation of Wnt Signaling Favors Generation of Memory CD8 T Cells,” 2017.
- [14] V. R. Moulton and D. L. Farber, “Committed to memory: lineage choices for activated T cells,” *Trends Immunol.*, vol. 27, no. 6, pp. 261–267, 2006.
- [15] R. Ahmed, M. J. Bevan, S. L. Reiner, and D. T. Fearon, “The precursors of memory : models and controversies,” *Nat. Publ. Gr.*, vol. 9, no. 9, pp. 662–668, 2009.
- [16] J. T. Chang, E. J. Wherry, and A. W. Goldrath, “Molecular regulation of effector and memory T cell differentiation,” vol. 15, no. 12, 2014.
- [17] Y. D. Mahnke, T. M. Brodie, F. Sallusto, M. Roederer, and E. Lugli, “The who ’ s who of T-cell differentiation : Human memory T-cell subsets,” pp. 2797–2809, 2013.
- [18] F. A. Bonilla and H. C. Oettgen, “Adaptive immunity,” *J. Allergy Clin. Immunol.*, vol. 125, no. 2, Supplement 2, pp. S33–S40, 2010.
- [19] D. G. Schatz, “V(D)J recombination,” *Immunol. Rev.*, vol. 200, no. D, pp. 5–11, 2004.
- [20] T. P. Arstila, A. Casrouge, V. Baron, J. Even, J. Kanellopoulos, and P. Kourilsky, “A Direct Estimate of the Human $\alpha\beta$ T Cell Receptor Diversity,” *Science (80-.)*, vol. 286, no. 5441, pp. 958–961, 1999.
- [21] M. M. Davis and P. J. Bjorkman, “T-cell antigen receptor genes and T-cell recognition,” *Nature*, vol. 334, no. 6181, pp. 395–402, Aug. 1988.
- [22] J. Nikolich-Žugich, M. K. Slifka, and I. Messaoudi, “The many important facets of T-cell repertoire diversity,” *Nat. Rev. Immunol.*, vol. 4, no. 2, pp. 123–132, 2004.
- [23] A. K. Sewell, “Why must T cells be cross-reactive?,” *Nat. Publ. Gr.*, vol. 12, no. 9, pp. 669–677, 2012.
- [24] C. Chothia, D. R. Boswell, and A. M. Lesk, “The outline structure of the T-cell alpha beta receptor,” *EMBO J.*, vol. 7, no. 12, pp. 3745–3755, Dec. 1988.

- [25] C. Pannetier, M. Cochet, S. Darche, A. Casrouge, M. Zöllner, and P. Kourilsky, "The sizes of the CDR3 hypervariable regions of the murine T-cell receptor beta chains vary as a function of the recombined germ-line segments," *Proc. Natl. Acad. Sci. U. S. A.*, vol. 90, no. 9, pp. 4319–4323, May 1993.
- [26] J. P. Cabaniols, N. Fazilleau, A. Casrouge, P. Kourilsky, and J. M. Kanellopoulos, "Most alpha/beta T cell receptor diversity is due to terminal deoxynucleotidyl transferase," *J. Exp. Med.*, vol. 194, no. 9, pp. 1385–1390, Nov. 2001.
- [27] E. P. Rock, P. R. Sibbald, M. M. Davis, and Y. H. Chien, "CDR3 length in antigen-specific immune receptors," *J. Exp. Med.*, vol. 179, no. 1, pp. 323–328, Jan. 1994.
- [28] D. N. Garboczi, P. Ghosh, U. Utz, Q. R. Fan, W. E. Biddison, and D. C. Wiley, "Structure of the complex between human T-cell receptor, viral peptide and HLA-A2," *Nature*, vol. 384, no. 6605, pp. 134–141, Nov. 1996.
- [29] K. C. Garcia, M. Degano, R. L. Stanfield, A. Brunmark, M. R. Jackson, P. A. Peterson, L. Teyton, and I. A. Wilson, "An $\alpha\beta$ T Cell Receptor Structure at 2.5 Å and Its Orientation in the TCR-MHC Complex," *Science (80-.)*, vol. 274, no. 5285, p. 209 LP-219, Oct. 1996.
- [30] K. C. Garcia, M. Degano, L. R. Pease, M. Huang, P. A. Peterson, L. Teyton, and I. A. Wilson, "Structural Basis of Plasticity in T Cell Receptor Recognition of a Self Peptide-MHC Antigen," *Science (80-.)*, vol. 279, no. 5354, p. 1166 LP-1172, Feb. 1998.
- [31] J. S. Bridgeman, A. K. Sewell, J. J. Miles, D. A. Price, and D. K. Cole, "Structural and biophysical determinants of $\alpha\beta$ T-cell antigen recognition," *Immunology*, vol. 135, no. 1, pp. 9–18, Jan. 2012.
- [32] M. G. Rudolph, R. L. Stanfield, and I. A. Wilson, "How Tcrs Bind Mhcs, Peptides, and Coreceptors," *Annu. Rev. Immunol.*, vol. 24, no. 1, pp. 419–466, 2006.
- [33] K. C. Garcia and E. J. Adams, "How the T Cell Receptor Sees Antigen—A Structural View," *Cell*, vol. 122, no. 3, pp. 333–336, 2005.
- [34] K. W. Wucherpfennig, E. Gagnon, M. J. Call, E. S. Huseby, and M. E. Call, "Structural biology of the T-cell receptor: insights into receptor assembly, ligand recognition, and initiation of signaling," *Cold Spring Harb. Perspect. Biol.*, vol. 2, no. 4, pp. a005140–a005140, Apr. 2010.
- [35] B. Alarcon, D. Gil, P. Delgado, and W. W. A. Schamel, "Initiation of TCR signaling: regulation within CD3 dimers.," *Immunol. Rev.*, vol. 191, pp. 38–46, Feb. 2003.

- [36] M. Huse, "The T-cell-receptor signaling network," *J. Cell Sci.*, vol. 122, no. 9, p. 1269 LP-1273, May 2009.
- [37] J. Lin and A. Weiss, "T cell receptor signalling," *J. Cell Sci.*, vol. 114, no. 2, p. 243 LP-244, Jan. 2001.
- [38] M. Katan, "The control of inositol lipid hydrolysis.," *Cancer Surv.*, vol. 27, pp. 199–211, 1996.
- [39] P. D. Holler, A. R. Lim, B. K. Cho, L. A. Rund, and D. M. Kranz, "CD8(-) T cell transfectants that express a high affinity T cell receptor exhibit enhanced peptide-dependent activation," *J. Exp. Med.*, vol. 194, no. 8, pp. 1043–1052, Oct. 2001.
- [40] S. Tian, R. Maile, E. J. Collins, and J. A. Frelinger, "CD8⁺ T Cell Activation Is Governed by TCR-Peptide/MHC Affinity, Not Dissociation Rate," *J. Immunol.*, vol. 179, no. 5, p. 2952 LP-2960, Sep. 2007.
- [41] K. Matsui, J. J. Boniface, P. Steffner, P. A. Reay, and M. M. Davis, "Kinetics of T-cell receptor binding to peptide/I-Ek complexes: correlation of the dissociation rate with T-cell responsiveness," *Proc. Natl. Acad. Sci. U. S. A.*, vol. 91, no. 26, pp. 12862–12866, Dec. 1994.
- [42] N. L. La Gruta, P. C. Doherty, and S. J. Turner, "A correlation between function and selected measures of T cell avidity in influenza virus-specific CD8⁺ T cell responses," *Eur. J. Immunol.*, vol. 36, no. 11, pp. 2951–2959, Nov. 2006.
- [43] M. Hebeisen, J. Schmidt, P. Guillaume, P. Baumgaertner, D. E. Speiser, I. Luescher, and N. Rufer, "Identification of rare high-avidity, tumor-reactive CD8⁺ T Cells by Monomeric TCR-ligand off-rates measurements on living cells," *Cancer Res.*, vol. 75, no. 10, pp. 1983–1991, 2015.
- [44] P. O. Gannon, S. Wieckowski, P. Baumgaertner, M. Hebeisen, M. Allard, D. E. Speiser, and N. Rufer, "Quantitative TCR:pMHC Dissociation Rate Assessment by NTAMers Reveals Antimelanoma T Cell Repertoires Enriched for High Functional Competence," *J. Immunol.*, vol. 195, no. 1, pp. 356–66, 2015.
- [45] M. Allard, B. Couturaud, L. Carretero-Iglesia, M. N. Duong, J. Schmidt, G. C. Monnot, P. Romero, D. E. Speiser, M. Hebeisen, and N. Rufer, "TCR-ligand dissociation rate is a robust and stable biomarker of CD8⁺ T cell potency," *JCI insight*, vol. 2, no. 14, p. e92570, Jul. 2017.
- [46] M. M. Davis, J. J. Boniface, Z. Reich, D. Lyons, J. Hampl, B. Arden, and Y. Chien, "LIGAND RECOGNITION BY $\alpha\beta$ T CELL RECEPTORS," *Annu. Rev. Immunol.*, vol. 16,

- no. 1, pp. 523–544, Apr. 1998.
- [47] D. K. Cole, N. J. Pumphrey, J. M. Boulter, M. Sami, J. I. Bell, E. Gostick, D. A. Price, G. F. Gao, A. K. Sewell, and B. K. Jakobsen, “Human TCR-Binding Affinity is Governed by MHC Class Restriction,” *J. Immunol.*, vol. 178, no. 9, p. 5727 LP-5734, May 2007.
- [48] J. D. Stone and D. M. Kranz, “Role of T Cell Receptor Affinity in the Efficacy and Specificity of Adoptive T Cell Therapies,” *Front. Immunol.*, vol. 4, p. 244, Aug. 2013.
- [49] S. Viganò, D. T. Utzschneider, M. Perreau, G. Pantaleo, D. Zehn, and A. Harari, “Functional avidity: a measure to predict the efficacy of effector T cells?,” *Clin. Dev. Immunol.*, vol. 2012, p. 153863, 2012.
- [50] E. Bianconi, A. Piovesan, F. Facchin, A. Beraudi, R. Casadei, F. Frabetti, L. Vitale, M. C. Pelleri, S. Tassani, F. Piva, S. Perez-Amodio, P. Strippoli, and S. Canaider, “An estimation of the number of cells in the human body,” *Ann. Hum. Biol.*, vol. 40, no. 6, pp. 463–471, Nov. 2013.
- [51] S. J. Turner, P. C. Doherty, J. McCluskey, and J. Rossjohn, “Structural determinants of T-cell receptor bias in immunity,” *Nat. Rev. Immunol.*, vol. 6, no. 12, pp. 883–894, 2006.
- [52] L. Gattinoni, E. Lugli, Y. Ji, Z. Pos, C. M. Paulos, M. F. Quigley, J. R. Almeida, E. Gostick, Z. Yu, C. Carpenito, E. Wang, D. C. Douek, D. A. Price, C. H. June, F. M. Marincola, M. Roederer, and N. P. Restifo, “A human memory T cell subset with stem cell – like properties,” vol. 17, no. 10, 2011.
- [53] A. Culshaw, K. Ladell, S. Gras, J. E. McLaren, K. L. Miners, C. Farenc, H. van den Heuvel, E. Gostick, W. Dejnirattisai, A. Wangteeraprasert, T. Duangchinda, P. Chotiyarnwong, W. Limpitikul, S. Vasanawathana, P. Malasit, T. Dong, J. Rossjohn, J. Mongkolsapaya, D. A. Price, and G. R. Screaton, “Germline bias dictates cross-serotype reactivity in a common dengue-virus-specific CD8+ T cell response,” *Nat. Immunol.*, vol. 18, p. 1228, Sep. 2017.
- [54] C.-Y. Wang, P.-F. Yu, X.-B. He, Y.-X. Fang, W.-Y. Cheng, and Z.-Z. Jing, “alphabeta T-cell receptor bias in disease and therapy (Review).,” *Int. J. Oncol.*, vol. 48, no. 6, pp. 2247–2256, Jun. 2016.
- [55] N. Van Braeckel-Budimir, S. Gras, K. Ladell, T. M. Josephs, L. Pewe, S. L. Urban, K. L. Miners, C. Farenc, D. A. Price, J. Rossjohn, and J. T. Harty, “A T Cell Receptor Locus Harbors a Malaria-Specific Immune Response Gene,” *Immunity*, vol. 47, no. 5, p. 835–847.e4, Nov. 2017.

- [56] E. Quiros Roldan, A. Sottini, A. Bettinardi, A. Albertini, L. Imberti, and D. Primi, "Different TCRBV genes generate biased patterns of V-D-J diversity in human T cells.," *Immunogenetics*, vol. 41, no. 2–3, pp. 91–100, 1995.
- [57] R. L. Warren, J. D. Freeman, T. Zeng, G. Choe, S. Munro, R. Moore, J. R. Webb, and R. A. Holt, "Exhaustive T-cell repertoire sequencing of human peripheral blood samples reveals signatures of antigen selection and a directly measured repertoire size of at least 1 million clonotypes," *Genome Res.*, vol. 21, no. 5, pp. 790–797, May 2011.
- [58] H. Li, C. Ye, G. Ji, X. Wu, Z. Xiang, Y. Li, Y. Cao, X. Liu, D. C. Douek, D. A. Price, and J. Han, "Recombinatorial Biases and Convergent Recombination Determine Interindividual TCR β Sharing in Murine Thymocytes," *J. Immunol.*, vol. 189, no. 5, p. 2404 LP-2413, Sep. 2012.
- [59] V. Venturi, K. Kedzierska, D. A. Price, P. C. Doherty, D. C. Douek, S. J. Turner, and M. P. Davenport, "Sharing of T cell receptors in antigen-specific responses is driven by convergent recombination.," *Proc. Natl. Acad. Sci. U. S. A.*, vol. 103, no. 49, pp. 18691–6, 2006.
- [60] D. a Price, J. M. Brenchley, L. E. Ruff, M. R. Betts, B. J. Hill, M. Roederer, R. a Koup, S. a Migueles, E. Gostick, L. Wooldridge, A. K. Sewell, M. Connors, and D. C. Douek, "Avidity for antigen shapes clonal dominance in CD8+ T cell populations specific for persistent DNA viruses.," *J. Exp. Med.*, vol. 202, no. 10, pp. 1349–1361, 2005.
- [61] G. Pantaleo, H. Soudeyns, J. F. Demarest, M. Vaccarezza, C. Graziosi, S. Paolucci, M. Daucher, O. J. Cohen, F. Denis, W. E. Biddison, R. P. Sekaly, and A. S. Fauci, "Evidence for rapid disappearance of initially expanded HIV-specific CD8+ T cell clones during primary HIV infection," *Proc. Natl. Acad. Sci. U. S. A.*, vol. 94, no. 18, pp. 9848–9853, Sep. 1997.
- [62] L. Trautmann, M. Rimbert, K. Echasserieau, X. Saulquin, B. Neveu, J. Dechanet, V. Cerundolo, and M. Bonneville, "Selection of T Cell Clones Expressing High-Affinity Public TCRs within Human Cytomegalovirus-Specific CD8 T Cell Responses," *J. Immunol.*, vol. 175, no. 9, p. 6123 LP-6132, Nov. 2005.
- [63] M. Rius and F. Lyko, "Epigenetic cancer therapy: rationales, targets and drugs," *Oncogene*, vol. 31, p. 4257, Dec. 2011.
- [64] P. Sharma, S. Hu-Lieskovan, J. A. Wargo, and A. Ribas, "Primary, Adaptive, and Acquired Resistance to Cancer Immunotherapy," *Cell*, vol. 168, no. 4, pp. 707–723,

Feb. 2017.

- [65] H. Borghaei, M. R. Smith, and K. S. Campbell, "Immunotherapy of cancer," *Eur. J. Pharmacol.*, vol. 625, no. 1–3, pp. 41–54, Dec. 2009.
- [66] M. K. Barton, "Daily aspirin may reduce mortality from prostate cancer with risk of high recurrence," *CA. Cancer J. Clin.*, vol. 65, no. 2, pp. 83–84, Mar. 2015.
- [67] W. H. Fridman, F. Pagès, C. Sautès-Fridman, and J. Galon, "The immune contexture in human tumours: impact on clinical outcome," *Nat Rev Cancer*, vol. 12, no. 4, pp. 298–306, Apr. 2012.
- [68] L. Baitsch, S. A. Fuertes-Marraco, A. Legat, C. Meyer, and D. E. Speiser, "The three main stumbling blocks for anticancer T cells," *Trends Immunol.*, vol. 33, no. 7, pp. 364–372, Jul. 2012.
- [69] T. L. Whiteside, "Immune suppression in cancer: Effects on immune cells, mechanisms and future therapeutic intervention," *Semin. Cancer Biol.*, vol. 16, no. 1, pp. 3–15, 2006.
- [70] D. Gabrilovich, "Mechanisms and functional significance of tumour-induced dendritic-cell defects," *Nat. Rev. Immunol.*, vol. 4, p. 941, Dec. 2004.
- [71] P. Allavena and A. Mantovani, "Immunology in the clinic review series; focus on cancer: tumour-associated macrophages: undisputed stars of the inflammatory tumour microenvironment," *Clin. Exp. Immunol.*, vol. 167, no. 2, pp. 195–205, Feb. 2012.
- [72] S. Ostrand-Rosenberg and P. Sinha, "Myeloid-derived suppressor cells: linking inflammation and cancer," *J. Immunol.*, vol. 182, no. 8, pp. 4499–4506, Apr. 2009.
- [73] V. Bronte and P. Zanovello, "Regulation of immune responses by L-arginine metabolism," *Nat. Rev. Immunol.*, vol. 5, p. 641, Aug. 2005.
- [74] A. Östman and M. Augsten, "Cancer-associated fibroblasts and tumor growth – bystanders turning into key players," *Curr. Opin. Genet. Dev.*, vol. 19, no. 1, pp. 67–73, 2009.
- [75] N. P. Restifo, M. E. Dudley, and S. A. Rosenberg, "Adoptive immunotherapy for cancer: harnessing the T cell response," *Nat. Rev. Immunol.*, vol. 12, no. 4, pp. 269–281, Mar. 2012.
- [76] S. A. Rosenberg, "Cell transfer immunotherapy for metastatic solid cancer--what clinicians need to know," *Nat. Rev. Clin. Oncol.*, vol. 8, no. 10, pp. 577–585, Aug. 2011.

- [77] S. Gill and D. L. Porter, "CAR-modified anti-CD19 T cells for the treatment of B-cell malignancies: rules of the road," *Expert Opin. Biol. Ther.*, vol. 14, no. 1, pp. 37–49, Jan. 2014.
- [78] D. M. Pardoll, "The blockade of immune checkpoints in cancer immunotherapy," *Nat. Rev. Cancer*, vol. 12, no. 4, pp. 252–264, Mar. 2012.
- [79] F. S. Hodi, S. J. O'Day, D. F. McDermott, R. W. Weber, J. A. Sosman, J. B. Haanen, R. Gonzalez, C. Robert, D. Schadendorf, J. C. Hassel, W. Akerley, A. J. M. van den Eertwegh, J. Lutzky, P. Lorigan, J. M. Vaubel, G. P. Linette, D. Hogg, C. H. Ottensmeier, C. Lebbé, C. Peschel, I. Quirt, J. I. Clark, J. D. Wolchok, J. S. Weber, J. Tian, M. J. Yellin, G. M. Nichol, A. Hoos, and W. J. Urba, "Improved survival with ipilimumab in patients with metastatic melanoma," *N. Engl. J. Med.*, vol. 363, no. 8, pp. 711–723, Aug. 2010.
- [80] C. Robert, L. Thomas, I. Bondarenko, S. O'Day, J. Weber, C. Garbe, C. Lebbe, J.-F. Baurain, A. Testori, J.-J. Grob, N. Davidson, J. Richards, M. Maio, A. Hauschild, W. H. Miller, P. Gascon, M. Lotem, K. Harmankaya, R. Ibrahim, S. Francis, T.-T. Chen, R. Humphrey, A. Hoos, and J. D. Wolchok, "Ipilimumab plus Dacarbazine for Previously Untreated Metastatic Melanoma," *N. Engl. J. Med.*, vol. 364, no. 26, pp. 2517–2526, Jun. 2011.
- [81] J. R. Brahmer, S. S. Tykodi, L. Q. M. Chow, W.-J. Hwu, S. L. Topalian, P. Hwu, C. G. Drake, L. H. Camacho, J. Kauh, K. Odunsi, H. C. Pitot, O. Hamid, S. Bhatia, R. Martins, K. Eaton, S. Chen, T. M. Salay, S. Alaparthi, J. F. Grosso, A. J. Korman, S. M. Parker, S. Agrawal, S. M. Goldberg, D. M. Pardoll, A. Gupta, and J. M. Wigginton, "Safety and Activity of Anti-PD-L1 Antibody in Patients with Advanced Cancer," *N. Engl. J. Med.*, vol. 366, no. 26, pp. 2455–2465, Jun. 2012.
- [82] J. Larkin, V. Chiarion-Sileni, R. Gonzalez, J. J. Grob, C. L. Cowey, C. D. Lao, D. Schadendorf, R. Dummer, M. Smylie, P. Rutkowski, P. F. Ferrucci, A. Hill, J. Wagstaff, M. S. Carlino, J. B. Haanen, M. Maio, I. Marquez-Rodas, G. A. McArthur, P. A. Ascierto, G. V Long, M. K. Callahan, M. A. Postow, K. Grossmann, M. Sznol, B. Dreno, L. Bastholt, A. Yang, L. M. Rollin, C. Horak, F. S. Hodi, and J. D. Wolchok, "Combined Nivolumab and Ipilimumab or Monotherapy in Untreated Melanoma," *N. Engl. J. Med.*, vol. 373, no. 1, pp. 23–34, May 2015.
- [83] S. L. Topalian, F. S. Hodi, J. R. Brahmer, S. N. Gettinger, D. C. Smith, D. F. McDermott, J. D. Powderly, R. D. Carvajal, J. A. Sosman, M. B. Atkins, P. D. Leming, D. R. Spigel, S. J.

- Antonia, L. Horn, C. G. Drake, D. M. Pardoll, L. Chen, W. H. Sharfman, R. A. Anders, J. M. Taube, T. L. McMiller, H. Xu, A. J. Korman, M. Jure-Kunkel, S. Agrawal, D. McDonald, G. D. Kollia, A. Gupta, J. M. Wigginton, and M. Sznol, "Safety, Activity, and Immune Correlates of Anti-PD-1 Antibody in Cancer," *N. Engl. J. Med.*, vol. 366, no. 26, pp. 2443–2454, Jun. 2012.
- [84] A. Ribas and J. D. Wolchok, "Cancer immunotherapy using checkpoint blockade," *Science (80-.)*, vol. 359, no. 6382, p. 1350 LP-1355, Mar. 2018.
- [85] T. P. Monath, "Yellow fever vaccine," *Expert Rev. Vaccines*, vol. 4, no. 4, pp. 553–574, Aug. 2005.
- [86] B. Pulendran, "Learning immunology from the yellow fever vaccine: innate immunity to systems vaccinology," vol. 9, pp. 741–747, 2009.
- [87] B. Dixon, "Microbe Hunters—Then and Now," *BMJ*, vol. 313, no. 7068, p. 1340, Nov. 1996.
- [88] M. Theiler and H. H. Smith, "THE USE OF YELLOW FEVER VIRUS MODIFIED BY IN VITRO CULTIVATION FOR HUMAN IMMUNIZATION," *J. Exp. Med.*, vol. 65, no. 6, p. 787 LP-800, Jun. 1937.
- [89] K. D. Ryman, H. Xie, T. N. Ledger, G. A. Campbell, and A. D. T. Barrett, "Antigenic Variants of Yellow Fever Virus with an Altered Neurovirulence Phenotype in Mice," *Virology*, vol. 230, no. 2, pp. 376–380, 1997.
- [90] F. Guirakhoo, Z. Zhang, G. Myers, B. W. Johnson, K. Pugachev, R. Nichols, N. Brown, I. Levenbook, K. Draper, S. Cyrek, J. Lang, C. Fournier, B. Barrere, S. Delagrave, and T. P. Monath, "A single amino acid substitution in the envelope protein of chimeric yellow fever-dengue 1 vaccine virus reduces neurovirulence for suckling mice and viremia/viscerotropism for monkeys," *J. Virol.*, vol. 78, no. 18, pp. 9998–10008, Sep. 2004.
- [91] T. P. Monath, J. Arroyo, I. Levenbook, Z.-X. Zhang, J. Catalan, K. Draper, and F. Guirakhoo, "Single mutation in the flavivirus envelope protein hinge region increases neurovirulence for mice and monkeys but decreases viscerotropism for monkeys: relevance to development and safety testing of live, attenuated vaccines," *J. Virol.*, vol. 76, no. 4, pp. 1932–1943, Feb. 2002.
- [92] A. B. de Melo, M. da P. C. da Silva, M. C. F. Magalhães, L. H. V. Gonzales Gil, E. M. Freese de Carvalho, U. M. Braga-Neto, G. R. Bertani, E. T. A. Marques Jr, and M. T. Cordeiro, "Description of a prospective 17DD yellow fever vaccine cohort in Recife,

- Brazil," *Am. J. Trop. Med. Hyg.*, vol. 85, no. 4, pp. 739–747, Oct. 2011.
- [93] S. W. Group, *Background Paper on Yellow Fever Vaccine*, no. March. 2013.
- [94] J. D. Poland, C. H. Calisher, T. P. Monath, W. G. Downs, and K. Murphy, "Persistence of neutralizing antibody 30-35 years after immunization with 17D yellow fever vaccine," *Bull. World Health Organ.*, vol. 59, no. 6, pp. 895–900, 1981.
- [95] M. Niedrig, M. Lademann, P. Emmerich, and M. Lafrenz, "Assessment of IgG antibodies against yellow fever virus after vaccination with 17D by different assays: neutralization test, haemagglutination inhibition test, immunofluorescence assay and ELISA," *Trop. Med. Int. Heal.*, vol. 4, no. 12, pp. 867–871, Dec. 1999.
- [96] M. J. Hepburn, M. G. Kortepeter, P. R. Pittman, E. F. Boudreau, J. A. Mangiafico, P. A. Buck, S. L. Norris, and E. L. Anderson, "Neutralizing antibody response to booster vaccination with the 17d yellow fever vaccine," vol. 24, pp. 2843–2849, 2006.
- [97] S. A. F. Marraco, C. Soneson, L. Cagnon, P. O. Gannon, M. Allard, S. A. Maillard, N. Montandon, N. Rufer, S. Waldvogel, M. Delorenzi, and D. E. Speiser, "Long-lasting stem cell – like memory CD8 + T cells with a naïve-like profile upon yellow fever vaccination," vol. 7, no. 282, 2015.
- [98] R. W. Wieten, E. F. F. Jonker, E. M. M. van Leeuwen, E. B. M. Remmerswaal, I. J. M. Ten Berge, A. W. de Visser, P. J. J. van Genderen, A. Goorhuis, L. G. Visser, M. P. Grobusch, and G. J. de Bree, "A Single 17D Yellow Fever Vaccination Provides Lifelong Immunity; Characterization of Yellow-Fever-Specific Neutralizing Antibody and T-Cell Responses after Vaccination.," *PLoS One*, vol. 11, no. 3, p. e0149871, 2016.
- [99] M. Kongsgaard, M. R. Bassi, M. Rasmussen, K. Skjødt, S. Thybo, M. Gabriel, M. B. Hansen, J. P. Christensen, A. Randrup, S. Buus, and A. Stryhn, "Adaptive immune responses to booster vaccination against yellow fever virus are much reduced compared to those after primary vaccination," no. March, pp. 1–14, 2017.
- [100] I. Units, T. Authors, and C. C. By-nc-nd, "Duration of post-vaccination immunity against yellow fever in adults," vol. 32, pp. 4977–4984, 2014.
- [101] M. M. De Souza, L. C. Malaquias, H. R. Persi, J. M. Pereira, A. Martins, M. Dornelas-ribeiro, A. D. A. Vinhas, T. R. Alves, M. D. L. Maia, M. S. Freire, R. D. M. Martins, A. Homma, A. P. M. Romano, C. M. Domingues, P. L. Tauil, and P. F. Vasconcelos, "Booster dose after 10 years is recommended following 17DD-YF primary vaccination," no. February, pp. 491–502, 2016.

- [102] "Brazil - recommendations.pdf." .
- [103] R. Galler, K. V Pugachev, C. L. S. Santos, S. W. Ocran, A. V Jabor, S. G. Rodrigues, R. S. Marchevsky, M. S. Freire, L. F. C. Almeida, A. C. R. Cruz, A. M. Y. Yamamura, I. M. Rocco, E. S. Travassos da Rosa, L. T. M. Souza, P. F. C. Vasconcelos, F. Guirakhoo, and T. P. Monath, "Phenotypic and Molecular Analyses of Yellow Fever 17DD Vaccine Viruses Associated with Serious Adverse Events in Brazil," *Virology*, vol. 290, no. 2, pp. 309–319, 2001.
- [104] A. Y. Khromava, R. B. Eidex, L. H. Weld, K. S. Kohl, R. D. Bradshaw, R. T. Chen, and M. S. Cetron, "Yellow fever vaccine: An updated assessment of advanced age as a risk factor for serious adverse events," *Vaccine*, vol. 23, no. 25, pp. 3256–3263, 2005.
- [105] J. L. Belsher, P. Gay, M. Brinton, J. DellaValla, R. Ridenour, R. Lanciotti, A. Perelygin, S. Zaki, C. Paddock, T. Querec, T. Zhu, B. Pulendran, R. B. Eidex, and E. Hayes, "Fatal multiorgan failure due to yellow fever vaccine-associated viscerotropic disease," *Vaccine*, vol. 25, no. 50, pp. 8480–8485, 2007.
- [106] B. Pulendran, J. Miller, T. D. Querec, R. Akondy, N. Moseley, O. Laur, J. Glidewell, N. Monson, T. Zhu, H. Zhu, S. Staprans, D. Lee, M. A. Brinton, A. A. Perelygin, C. Vellozzi, P. Brachman Jr, S. Lalor, D. Teuwen, R. B. Eidex, M. Cetron, F. Priddy, C. del Rio, J. Altman, and R. Ahmed, "Case of yellow fever vaccine--associated viscerotropic disease with prolonged viremia, robust adaptive immune responses, and polymorphisms in CCR5 and RANTES genes," *J. Infect. Dis.*, vol. 198, no. 4, pp. 500–507, Aug. 2008.
- [107] H.-G. Bae, C. Domingo, A. Tenorio, F. de Ory, J. Muñoz, P. Weber, D. E. Teuwen, and M. Niedrig, "Immune Response during Adverse Events after 17D-Derived Yellow Fever Vaccination in Europe," *J. Infect. Dis.*, vol. 197, no. 11, pp. 1577–1584, Jun. 2008.
- [108] A. D. T. Barrett and D. E. Teuwen, "Yellow fever vaccine—how does it work and why do rare cases of serious adverse events take place?," *Curr. Opin. Immunol.*, vol. 21, no. 3, pp. 308–313, 2009.
- [109] P. Hanlon, L. Hanlon, V. Marsh, P. Byass, H. Sillah, R. Hayes, H. C. Whittle, and B. M. Greenwood, "SEROLOGICAL COMPARISONS OF APPROACHES TO POLIO VACCINATION IN THE GAMBIA," *Lancet*, vol. 329, no. 8536, pp. 800–801, 1987.
- [110] A. Valsamakis, P. G. Auwaerter, B. K. Rima, H. Kaneshima, and D. E. Griffin, "Altered virulence of vaccine strains of measles virus after prolonged replication in human

- tissue," *J. Virol.*, vol. 73, no. 10, pp. 8791–8797, Oct. 1999.
- [111] G. Barba-Spaeth, R. S. Longman, M. L. Albert, and C. M. Rice, "Live attenuated yellow fever 17D infects human DCs and allows for presentation of endogenous and recombinant T cell epitopes," *J. Exp. Med.*, vol. 202, no. 9, p. 1179 LP-1184, Nov. 2005.
- [112] D. Gaucher, R. Therrien, N. Kettaf, B. R. Angermann, G. Boucher, A. Filali-Mouhim, J. M. Moser, R. S. Mehta, D. R. Drake, E. Castro, R. Akondy, A. Rinfret, B. Yassine-Diab, E. A. Said, Y. Chouikh, M. J. Cameron, R. Clum, D. Kelvin, R. Somogyi, L. D. Greller, R. S. Balderas, P. Wilkinson, G. Pantaleo, J. Tartaglia, E. K. Haddad, and R.-P. Sékaly, "Yellow fever vaccine induces integrated multilineage and polyfunctional immune responses," *J. Exp. Med.*, vol. 205, no. 13, p. 3119 LP-3131, Dec. 2008.
- [113] T. D. Querec, R. S. Akondy, E. K. Lee, W. Cao, H. I. Nakaya, D. Teuwen, A. Pirani, K. Gernert, J. Deng, B. Marzolf, K. Kennedy, H. Wu, S. Bennouna, H. Oluoch, J. Miller, R. Z. Vencio, M. Mulligan, A. Aderem, R. Ahmed, and B. Pulendran, "Systems biology approach predicts immunogenicity of the yellow fever vaccine in humans.," *Nat. Immunol.*, vol. 10, no. 1, pp. 116–25, 2009.
- [114] B. Pulendran, J. Z. Oh, H. I. Nakaya, R. Ravindran, and D. A. Kazmin, "Immunity to viruses: learning from successful human vaccines," *Immunol. Rev.*, vol. 255, no. 1, pp. 243–255, Sep. 2013.
- [115] T. Querec, S. Bennouna, S. Alkan, Y. Laouar, K. Gorden, R. Flavell, S. Akira, R. Ahmed, and B. Pulendran, "Yellow fever vaccine YF-17D activates multiple dendritic cell subsets via TLR2, 7, 8, and 9 to stimulate polyvalent immunity," *J. Exp. Med.*, vol. 203, no. 2, p. 413 LP-424, Feb. 2006.
- [116] J. D. Miller, R. G. van der Most, R. S. Akondy, J. T. Glidewell, S. Albott, D. Masopust, K. Murali-Krishna, P. L. Mahar, S. Edupuganti, S. Lalor, S. Germon, C. Del Rio, M. J. Mulligan, S. I. Staprans, J. D. Altman, M. B. Feinberg, and R. Ahmed, "Human Effector and Memory CD8+ T Cell Responses to Smallpox and Yellow Fever Vaccines," *Immunity*, vol. 28, pp. 710–722, 2008.
- [117] A. B. de Melo, E. J. M. Nascimento, U. Braga-Neto, R. Dhalia, A. M. Silva, M. Oelke, J. P. Schneck, J. Sidney, A. Sette, S. M. L. Montenegro, and E. T. A. Marques, "T-Cell Memory Responses Elicited by Yellow Fever Vaccine are Targeted to Overlapping Epitopes Containing Multiple HLA-I and -II Binding Motifs," *PLoS Negl. Trop. Dis.*, vol. 7, no. 1, 2013.

- [118] R. S. Akondy, N. D. Monson, J. D. Miller, S. Edupuganti, D. Teuwen, H. Wu, F. Quyyumi, S. Garg, J. D. Altman, C. Del Rio, H. L. Keyserling, A. Ploss, C. M. Rice, W. a Orenstein, M. J. Mulligan, and R. Ahmed, "The yellow fever virus vaccine induces a broad and polyfunctional human memory CD8+ T cell response.," *J. Immunol.*, vol. 183, no. 12, pp. 7919–7930, 2009.
- [119] R. S. Akondy, P. L. F. Johnson, H. I. Nakaya, S. Edupuganti, M. J. Mulligan, B. Lawson, J. D. Miller, B. Pulendran, R. Antia, and R. Ahmed, "Initial viral load determines the magnitude of the human CD8 T cell response to yellow fever vaccination.," *Proc. Natl. Acad. Sci. U. S. A.*, vol. 112, no. 10, pp. 3050–3055, 2015.
- [120] K. Blom, M. Braun, M. a Ivarsson, V. D. Gonzalez, K. Falconer, M. Moll, H.-G. Ljunggren, J. Michaëlsson, and J. K. Sandberg, "Temporal dynamics of the primary human T cell response to yellow fever virus 17D as it matures from an effector- to a memory-type response.," *J. Immunol.*, vol. 190, no. 5, pp. 2150–8, 2013.
- [121] E. Gotuzzo, S. Yactayo, and E. Co, "Review Article : Efficacy and Duration of Immunity after Yellow Fever Vaccination : Systematic Review on the Need for a Booster Every 10 Years," vol. 89, no. 3, pp. 434–444, 2013.
- [122] S. Kohler, N. Bethke, B. Matthias, M. Frentsch, C. Romagnani, and M. Niedrig, "The early cellular signatures of protective immunity induced by live viral vaccination," pp. 2363–2373, 2012.
- [123] M. Luiza, S. M. El, L. Ribeiro, V. Peruhype-magalh, A. Paula, V. Marciano, A. Homma, E. Geessien, and O. A. Martins-filho, "Innate immunity phenotypic features point toward simultaneous raise of activation and modulation events following 17DD live attenuated yellow fever first-time vaccination ^," 2008.
- [124] N. Marquardt, M. A. Ivarsson, K. Blom, D. Gonzalez, M. Braun, K. Falconer, A. Fogdell-hahn, J. K. Sandberg, J. Michaëlsson, M. Braun, K. Falconer, R. Gustafsson, and A. Fogdell-hahn, "The Human NK Cell Response to Yellow Fever Virus 17D Is Primarily Governed by NK Cell Differentiation Independently of NK Cell Education," 2017.
- [125] M. Â. Martins, M. L. Silva, A. P. V Marciano, V. Peruhype-Magalhães, S. M. Eloi-Santos, J. G. L. Ribeiro, R. Correa-Oliveira, A. Homma, E. G. Kroon, A. Teixeira-Carvalho, and O. A. Martins-Filho, "Activation/modulation of adaptive immunity emerges simultaneously after 17DD yellow fever first-time vaccination: is this the key to prevent severe adverse reactions following immunization?," *Clin. Exp. Immunol.*, vol. 148, no. 1, pp. 90–100, Apr. 2007.

- [126] A. Bovay, A. Bovay, V. Zoete, G. Dolton, A. M. Bulek, D. K. Cole, P. J. Rizkallah, A. Fuller, K. Beck, O. Michielin, D. E. Speiser, A. K. Sewell, and S. A. F. Marraco, "T cell receptor alpha variable 12-2 bias in the immunodominant response to Yellow fever virus," pp. 1–15, 2017.
- [127] L. Derre, M. Ferber, C. Touvrey, E. Devevre, V. Zoete, A. Leimgruber, P. Romero, O. Michielin, F. Levy, and D. E. Speiser, "A Novel Population of Human Melanoma-Specific CD8 T Cells Recognizes Melan-AMART-1 Immunodominant Nonapeptide but Not the Corresponding Decapeptide," *J. Immunol.*, vol. 179, no. 11, pp. 7635–7645, 2007.
- [128] D. K. Cole, F. Yuan, P. J. Rizkallah, J. J. Miles, E. Gostick, D. A. Price, G. F. Gao, B. K. Jakobsen, and A. K. Sewell, "Germ Line-governed Recognition of a Cancer Epitope by an Immunodominant Human T-cell Receptor," *J. Biol. Chem.*, vol. 284, no. 40, pp. 27281–27289, Oct. 2009.
- [129] S. Wieckowski, P. Baumgaertner, P. Corthesy, V. Voelter, P. Romero, D. E. Speiser, and N. Rufer, "Fine structural variations of alphabetaTCRs selected by vaccination with natural versus altered self-antigen in melanoma patients.," *J. Immunol.*, vol. 183, no. 8, pp. 5397–406, 2009.
- [130] M. A. Neller, K. Ladell, J. E. McLaren, K. K. Matthews, E. Gostick, J. M. Pentier, G. Dolton, A. J. A. Schauenburg, D. Koning, A. Isabel, C. A. Fontaine, T. S. Watkins, V. Venturi, C. Smith, R. Khanna, K. Miners, M. Clement, L. Wooldridge, D. K. Cole, D. Van Baarle, A. K. Sewell, S. R. Burrows, D. A. Price, and J. J. Miles, "Naive CD8 + T-cell precursors display structured TCR repertoires and composite antigen-driven selection dynamics," *Immunol. Cell Biol.*, no. October 2014, pp. 1–9, 2015.
- [131] S. Mantovani, B. Palermo, S. Garbelli, R. Campanelli, G. Robustelli Della Cuna, R. Gennari, F. Benvenuto, E. Lantelme, and C. Giachino, "Dominant TCR-alpha requirements for a self antigen recognition in humans," *J. Immunol.*, vol. 169, no. 11, pp. 6253–60, 2002.
- [132] M. J. M. J. Pittet, A. Gati, F.-A. Le Gal, G. Bioley, P. Guillaume, M. de Smedt, J. Plum, D. E. Speiser, J.-C. Cerottini, P.-Y. Dietrich, P. Romero, and A. Zippelius, "Ex Vivo Characterization of Allo-MHC-Restricted T Cells Specific for a Single MHC-Peptide Complex," *J Immunol*, vol. 176, no. 4, pp. 2330–2336, 2006.
- [133] P.-Y. Dietrich, F.-A. Le Gal, V. Dutoit, M. J. Pittet, L. Trautman, A. Zippelius, I. Cognet, V. Widmer, P. R. Walker, O. Michielin, P. Guillaume, T. Connerotte, F. Jotereau, P. G.

- Coulie, P. Romero, J.-C. Cerottini, M. Bonneville, and D. Valmori, "Prevalent role of TCR alpha-chain in the selection of the preimmune repertoire specific for a human tumor-associated self-antigen.," *J. Immunol.*, vol. 170, no. 10, pp. 5103–9, 2003.
- [134] F. Serana, A. Sottini, L. Caimi, B. Palermo, P. G. Natali, P. Nisticò, and L. Imberti, "Identification of a public CDR3 motif and a biased utilization of T-cell receptor V beta and J beta chains in HLA-A2/Melan-A-specific T-cell clonotypes of melanoma patients," *J. Transl. Med.*, vol. 7, no. 1, p. 21, 2009.
- [135] D. K. Cole, F. Yuan, J. Pierre, J. J. Miles, E. Gostick, D. A. Price, G. F. Gao, K. Bent, A. K. Sewell, and I. H. T. Receptor, "Germ Line-governed Recognition of a Cancer Epitope by an," *J. Biol. Chem.*, 2009.
- [136] I. Elovaara, U. Utz, S. Smith, and S. Jacobson, "Limited T cell receptor usage by HTLV-I tax-specific, HLA class I restricted cytotoxic T lymphocytes from patients with HTLV-I associated neurological disease," *J. Neuroimmunol.*, vol. 63, no. 1, pp. 47–53, 1995.
- [137] I. Elovaara, S. Koenig, A. Y. Brewah, R. M. Woods, T. Lehky, and S. Jacobson, "High human T cell lymphotropic virus type 1 (HTLV-1)-specific precursor cytotoxic T lymphocyte frequencies in patients with HTLV-1-associated neurological disease.," *J. Exp. Med.*, vol. 177, no. 6, pp. 1567–1573, Jun. 1993.
- [138] H. Li, C. Ye, G. Ji, and J. Han, "Determinants of public T cell responses.," *Cell Res.*, vol. 22, no. 1, pp. 33–42, 2012.
- [139] J. Rossjohn, S. Gras, J. J. Miles, S. J. Turner, D. I. Godfrey, and J. McCluskey, "T cell antigen receptor recognition of antigen-presenting molecules.," *Annu. Rev. Immunol.*, vol. 33, pp. 169–200, 2015.
- [140] M. Browning and P. Krausa, "Genetic diversity of HLA-A2: evolutionary and functional significance," *Immunol. Today*, vol. 17, no. 4, pp. 165–170, Apr. 1996.
- [141] D. Feng, C. J. Bond, L. K. Ely, J. Maynard, and K. C. Garcia, "Structural evidence for a germline-encoded T cell receptor-major histocompatibility complex interaction 'codon,'" *Nat Immunol*, vol. 8, no. 9, pp. 975–983, Sep. 2007.
- [142] J. P. Scott-Browne, F. Crawford, M. H. Young, J. W. Kappler, P. Marrack, and L. Gapin, "Evolutionarily conserved features contribute to $\alpha\beta$ T cell receptor specificity," *Immunity*, vol. 35, no. 4, pp. 526–535, Oct. 2011.
- [143] K. H. Piepenbrink, S. J. Blevins, D. R. Scott, and B. M. Baker, "restriction in a T cell receptor interface," *Nat. Commun.*, vol. 4, pp. 1–9, 2013.

- [144] A. Zippelius, M. J. Pittet, P. Batard, N. Rufer, M. De Smedt, P. Guillaume, K. Ellefsen, D. Valmori, D. Liénard, J. Plum, H. R. Macdonald, D. E. Speiser, J. Cerottini, and P. Romero, "Thymic Selection Generates a Large T Cell Pool Recognizing a Self-Peptide in Humans," vol. 195, no. 4, 2002.
- [145] S. Pinto, D. Sommermeyer, C. Michel, S. Wilde, D. Schendel, W. Uckert, T. Blankenstein, and B. Kyewski, "Misinitiation of intrathymic MART-1 transcription and biased TCR usage explain the high frequency of MART-1-specific T cells," *Eur. J. Immunol.*, vol. 44, no. 9, pp. 2811–2821, 2014.
- [146] J. D. Altman, P. A. H. Moss, P. J. R. Goulder, D. H. Barouch, M. G. McHeyzer-Williams, J. I. Bell, A. J. McMichael, and M. M. Davis, "Phenotypic Analysis of Antigen-Specific T Lymphocytes," *Science (80-.)*, vol. 274, no. 5284, p. 94 LP-96, Oct. 1996.
- [147] P. Batard, D. A. Peterson, E. Devêvre, P. Guillaume, J.-C. Cerottini, D. Rimoldi, D. E. Speiser, L. Winther, and P. Romero, "Dextramers: New generation of fluorescent MHC class I/peptide multimers for visualization of antigen-specific CD8+ T cells," *J. Immunol. Methods*, vol. 310, no. 1, pp. 136–148, 2006.
- [148] G. Dolton, A. Lissina, A. Skowera, K. Ladell, K. Tungatt, E. Jones, D. Kronenberg-Versteeg, H. Akpovwa, J. M. Pentier, C. J. Holland, A. J. Godkin, D. K. Cole, M. A. Neller, J. J. Miles, D. A. Price, M. Peakman, and A. K. Sewell, "Comparison of peptide–major histocompatibility complex tetramers and dextramers for the identification of antigen-specific T cells," *Clin. Exp. Immunol.*, vol. 177, no. 1, pp. 47–63, Jul. 2014.
- [149] A. Lissina, K. Ladell, A. Skowera, M. Clement, E. Edwards, R. Seggewiss, H. A. van den Berg, E. Gostick, K. Gallagher, E. Jones, J. J. Melenhorst, A. J. Godkin, M. Peakman, D. A. Price, A. K. Sewell, and L. Wooldridge, "Protein kinase inhibitors substantially improve the physical detection of T-cells with peptide-MHC tetramers," *J. Immunol. Methods*, vol. 340, no. 1, pp. 11–24, Jan. 2009.
- [150] K. Tungatt, V. Bianchi, M. D. Crowther, W. E. Powell, A. J. Schauenburg, A. Trimby, M. Donia, J. J. Miles, C. J. Holland, D. K. Cole, A. J. Godkin, M. Peakman, P. T. Straten, I. M. Svane, A. K. Sewell, and G. Dolton, "Antibody Stabilization of Peptide–MHC Multimers Reveals Functional T Cells Bearing Extremely Low-Affinity TCRs," *J. Immunol. Author Choice*, vol. 194, no. 1, pp. 463–474, Jan. 2015.
- [151] L. Wooldridge, A. Lissina, D. K. Cole, H. A. van den Berg, D. A. Price, and A. K. Sewell, "Tricks with tetramers: how to get the most from multimeric peptide–MHC," *Immunology*, vol. 126, no. 2, pp. 147–164, Feb. 2009.

- [152] G. Dolton, K. Tungatt, A. Lloyd, V. Bianchi, S. M. Theaker, A. Trimby, C. J. Holland, M. Donia, A. J. Godkin, D. K. Cole, P. Thor Straten, M. Peakman, I. M. Svane, and A. K. Sewell, "More tricks with tetramers: a practical guide to staining T cells with peptide–MHC multimers," *Immunology*, vol. 146, no. 1, pp. 11–22, Sep. 2015.
- [153] C. Rius, M. Attaf, K. Tungatt, V. Bianchi, M. Legut, A. Bovay, M. Donia, P. thor Straten, M. Peakman, I. M. Svane, S. Ott, T. Connor, B. Szomolay, G. Dolton, and A. K. Sewell, "Peptide–MHC Class I Tetramers Can Fail To Detect Relevant Functional T Cell Clonotypes and Underestimate Antigen-Reactive T Cell Populations," *J. Immunol.*, Feb. 2018.
- [154] M. P. Lefranc, V. Giudicelli, C. Ginestoux, J. Jabado-Michaloud, G. Folch, F. Bellahcene, Y. Wu, E. Gemrot, X. Brochet, J. Lane, L. Regnier, F. Ehrenmann, G. Lefranc, and P. Duroux, "IMGT®, the international ImMunoGeneTics information system®," *Nucleic Acids Res.*, vol. 37, no. SUPPL. 1, pp. 1006–1012, 2009.
- [155] D. Zehn, S. Y. Lee, and M. J. Bevan, "Complete but curtailed T-cell response to very low-affinity antigen," *Nature*, vol. 458, p. 211, Jan. 2009.
- [156] R. J. Martinez and B. D. Evavold, "Lower Affinity T Cells are Critical Components and Active Participants of the Immune Response," *Front. Immunol.*, vol. 6, p. 468, Sep. 2015.
- [157] R. J. Martinez, R. Andargachew, H. A. Martinez, and B. D. Evavold, "Low-affinity CD4+ T cells are major responders in the primary immune response," *Nat. Commun.*, vol. 7, p. 13848, Dec. 2016.
- [158] D. Haney, M. F. Quigley, T. E. Asher, D. R. Ambrozak, E. Gostick, D. A. Price, D. C. Douek, and M. R. Betts, "Isolation of viable antigen-specific CD8+ T cells based on membrane-bound tumor necrosis factor (TNF)- α expression," *J. Immunol. Methods*, vol. 369, no. 1–2, pp. 33–41, Jun. 2011.
- [159] S. Misler, W. M. Gee, K. D. Gillis, D. W. Scharp, and L. C. Falke, "Metabolite-Regulated ATP-Sensitive K⁺ Channel in Human Pancreatic Islet Cells," *Diabetes*, vol. 38, no. 4, p. 422 LP-427, Apr. 1989.
- [160] B. J. MacLachlan, A. Greenshields-Watson, G. H. Mason, A. J. Schauenburg, V. Bianchi, P. J. Rizkallah, A. K. Sewell, A. Fuller, and D. K. Cole, "Using X-ray Crystallography, Biophysics, and Functional Assays to Determine the Mechanisms Governing T-cell Receptor Recognition of Cancer Antigens," *J. Vis. Exp.*, no. 120, p. 54991, Feb. 2017.
- [161] J. M. Boulter, M. Glick, P. T. Todorov, E. Baston, M. Sami, P. Rizkallah, and B. K.

- Jakobsen, "Stable, soluble T-cell receptor molecules for crystallization and therapeutics," *Protein Eng. Des. Sel.*, vol. 16, no. 9, pp. 707–711, Sep. 2003.
- [162] K. Tsumoto, R. Abe, and D. E. and T. Arakawa, "Non-Denaturing Solubilization of Inclusion Bodies," *Current Pharmaceutical Biotechnology*, vol. 11, no. 3. pp. 309–312, 2010.
- [163] B. Wu, J. F. Nemeth, D. J. Janecki, B. Jones, G. Obmolova, T. J. Malia, A. Baker, D. Bethea, M. M. Elloso, M. Naso, and S. Taudte, "Expression, refolding and purification of a human interleukin-17A variant," *Cytokine*, vol. 53, no. 1, pp. 107–114, 2011.
- [164] J. F. Kane and D. L. Hartley, "Formation of recombinant protein inclusion bodies in *Escherichia coli*," *Trends Biotechnol.*, vol. 6, no. 5, pp. 95–101, 1988.
- [165] P. J. Bjorkman, M. A. Saper, B. Samraoui, W. S. Bennett, J. L. Strominger, and D. C. Wiley, "Structure of the human class I histocompatibility antigen, HLA-A2," *Nature*, vol. 329, p. 506, Oct. 1987.
- [166] J. M. Boulter, M. Glick, P. T. Todorov, E. Baston, M. Sami, P. Rizkallah, and B. K. Jakobsen, "Stable, soluble T-cell receptor molecules for crystallization and therapeutics," *Protein Eng*, vol. 16, no. 9, pp. 707–711, 2003.
- [167] S. J. Davis, M. J. Puklavec, D. A. Ashford, K. Harlos, E. Y. Jones, D. I. Stuart, and A. F. Williams, "Expression of soluble recombinant glycoproteins with predefined glycosylation: application to the crystallization of the T-cell glycoprotein CD2," *Protein Eng. Des. Sel.*, vol. 6, no. 2, pp. 229–232, Feb. 1993.
- [168] P. de Felipe, G. A. Luke, L. E. Hughes, D. Gani, C. Halpin, and M. D. Ryan, "E unum pluribus: multiple proteins from a self-processing polyprotein," *Trends Biotechnol.*, vol. 24, no. 2, pp. 68–75, 2006.
- [169] A. L. Szymczak, C. J. Workman, Y. Wang, K. M. Vignali, S. Dilioglou, E. F. Vanin, and D. A. A. Vignali, "Correction of multi-gene deficiency in vivo using a single self-cleaving 2A peptide-based retroviral vector," *Nat. Biotechnol.*, vol. 22, p. 589, Apr. 2004.
- [170] K. C. Garcia, L. Teyton, and I. A. Wilson, "STRUCTURAL BASIS OF T CELL RECOGNITION," *Annu. Rev. Immunol.*, vol. 17, no. 1, pp. 369–397, Apr. 1999.
- [171] T. D. Butters, L. M. Sparks, K. Harlos, S. Ikemizu, D. I. Stuart, E. Y. Jones, and S. J. Davis, "Effects of N-butyldeoxynojirimycin and the Lec3.2.8.1 mutant phenotype on N-glycan processing in Chinese hamster ovary cells: application to glycoprotein crystallization," *Protein Sci.*, vol. 8, no. 8, pp. 1696–1701, Aug. 1999.

- [172] L.-P. Li, J. C. Lampert, X. Chen, C. Leitao, J. Popović, W. Müller, and T. Blankenstein, "Transgenic mice with a diverse human T cell antigen receptor repertoire.," *Nat. Med.*, vol. 16, no. 9, pp. 1029–1034, 2010.
- [173] Y. Zhang, G. Joe, E. Hexner, J. Zhu, and S. G. Emerson, "host disease," vol. 11, no. 12, pp. 1299–1305, 2005.
- [174] L. Gattinoni, X. Zhong, D. C. Palmer, Y. Ji, C. S. Hinrichs, Z. Yu, C. Wrzesinski, A. Boni, L. Cassard, L. M. Garvin, C. M. Paulos, P. Muranski, and N. P. Restifo, "Wnt signaling arrests effector T cell differentiation and generates CD8 + memory stem cells," vol. 15, no. 7, pp. 808–814, 2009.
- [175] K. Pilipow, E. Scamardella, S. Puccio, S. Gautam, F. De Paoli, E. M. Mazza, G. De Simone, S. Polletti, M. Buccilli, V. Zanon, P. Di Lucia, M. Iannacone, L. Gattinoni, and E. Lugli, "Antioxidant metabolism regulates CD8+ T memory stem cell formation and antitumor immunity," *JCI insight*, vol. 3, no. 18, p. e122299, Sep. 2018.
- [176] A. Stokes, J. H. Bauert, and N. P. Hudson, "Experimental transmission of yellow fever virus to laboratory animals," *Int. J. Infect. Dis.*, vol. 2, no. 1, pp. 54–59, 1997.
- [177] R. A. Mason, N. M. Tauraso, R. O. Spertzel, and R. K. Ginn, "Yellow Fever Vaccine: Direct Challenge of Monkeys Given Graded Doses of 17D Vaccine," *Appl. Microbiol.*, vol. 25, no. 4, pp. 539–544, Apr. 1973.
- [178] M. C. Bonaldo, M. A. Martins, R. Rudersdorf, P. A. Mudd, J. B. Sacha, S. M. Piaskowski, P. C. Costa Neves, M. G. Veloso de Santana, L. Vojnov, S. Capuano, E. G. Rakasz, N. A. Wilson, J. Fulkerson, J. C. Sadoff, D. I. Watkins, and R. Galler, "Recombinant Yellow Fever Vaccine Virus 17D Expressing Simian Immunodeficiency Virus SIVmac239 Gag Induces SIV-Specific CD8(+) T-Cell Responses in Rhesus Macaques ," *J. Virol.*, vol. 84, no. 7, pp. 3699–3706, Apr. 2010.
- [179] P. A. Mudd, S. M. Piaskowski, P. C. C. Neves, R. Rudersdorf, H. L. Kolar, C. M. Eernisse, K. L. Weisgrau, M. G. Veloso de Santana, N. A. Wilson, M. C. Bonaldo, R. Galler, E. G. Rakasz, and D. I. Watkins, "The live-attenuated yellow fever vaccine 17D induces broad and potent T cell responses against several viral proteins in Indian rhesus macaques – implications for recombinant vaccine design," *Immunogenetics*, vol. 62, no. 9, pp. 593–600, Sep. 2010.
- [180] P. C. C. Neves, R. A. Rudersdorf, R. Galler, M. C. Bonaldo, M. G. V. de Santana, P. A. Mudd, M. A. Martins, E. G. Rakasz, N. A. Wilson, and D. I. Watkins, "CD8(+) gamma-delta TCR(+) and CD4(+) T cells produce IFN- γ at 5–7 days after yellow fever

- vaccination in Indian rhesus macaques, before the induction of classical antigen-specific T cell responses," *Vaccine*, vol. 28, no. 51, pp. 8183–8188, Nov. 2010.
- [181] A. M. Watson, L. K. M. Lam, W. B. Klimstra, and K. D. Ryman, "The 17D-204 Vaccine Strain-Induced Protection against Virulent Yellow Fever Virus Is Mediated by Humoral Immunity and CD4+ but not CD8+ T Cells," *PLoS Pathog.*, vol. 12, no. 7, p. e1005786, Jul. 2016.
- [182] A. A. Perelygin, S. V. Scherbik, I. B. Zhulin, B. M. Stockman, Y. Li, and M. A. Brinton, "Positional cloning of the murine flavivirus resistance gene," *Proc. Natl. Acad. Sci. U. S. A.*, vol. 99, no. 14, pp. 9322–9327, Jul. 2002.
- [183] K. C. Meier, C. L. Gardner, M. V. Khoretonenko, W. B. Klimstra, and K. D. Ryman, "A Mouse Model for Studying Viscerotropic Disease Caused by Yellow Fever Virus Infection," *PLoS Pathog.*, vol. 5, no. 10, p. e1000614, Oct. 2009.
- [184] J. S. Haring, V. P. Badovinac, and J. T. Harty, "Inflaming the CD8+ T Cell Response," *Immunity*, vol. 25, no. 1, pp. 19–29, Jul. 2006.
- [185] L. J. Thompson, G. A. Kolumam, S. Thomas, and K. Murali-Krishna, "Innate Inflammatory Signals Induced by Various Pathogens Differentially Dictate the IFN- γ Dependence of CD8 T Cells for Clonal Expansion and Memory Formation," *J. Immunol.*, vol. 177, no. 3, p. 1746 LP-1754, Aug. 2006.
- [186] D. Bruni, M. Chazal, L. Sinigaglia, L. Chauveau, O. Schwartz, P. Desprès, and N. Jouvenet, "Viral entry route determines how human plasmacytoid dendritic cells produce type I interferons," *Sci. Signal.*, vol. 8, no. 366, p. ra25 LP-ra25, Mar. 2015.
- [187] J. N. Mandl, R. Akondy, B. Lawson, N. Kozyr, S. I. Staprans, R. Ahmed, and M. B. Feinberg, "Distinctive TLR7 Signaling, Type I IFN Production, and Attenuated Innate and Adaptive Immune Responses to Yellow Fever Virus in a Primate Reservoir Host," *J. Immunol.*, vol. 186, no. 11, p. 6406 LP-6416, Jun. 2011.
- [188] R. B. Tesh, H. Guzman, A. P. A. T. da Rosa, P. F. C. Vasconcelos, L. B. Dias, J. E. Bunnell, H. Zhang, and S.-Y. Xiao, "Experimental Yellow Fever Virus Infection in the Golden Hamster (*Mesocricetus auratus*). I. Virologic, Biochemical, and Immunologic Studies," *J. Infect. Dis.*, vol. 183, no. 10, pp. 1431–1436, May 2001.
- [189] S.-Y. Xiao, H. Zhang, H. Guzman, and R. B. Tesh, "Experimental Yellow Fever Virus Infection in the Golden Hamster (*Mesocricetus auratus*). II. Pathology," *J. Infect. Dis.*, vol. 183, no. 10, pp. 1437–1444, May 2001.
- [190] L. Wooldridge, B. Laugel, J. Ekeruche, M. Clement, H. A. van den Berg, D. A. Price, and

- A. K. Sewell, "CD8 Controls T Cell Cross-Reactivity," *J. Immunol.*, vol. 185, no. 8, pp. 4625–4632, 2010.
- [191] B. Szomolay, J. Liu, P. E. Brown, J. J. Miles, M. Clement, S. Llewellyn-Lacey, G. Dolton, J. Ekeruche-Makinde, A. Lissina, A. J. Schauenburg, A. K. Sewell, S. R. Burrows, M. Roederer, D. A. Price, L. Wooldridge, and H. A. van den Berg, "Identification of human viral protein-derived ligands recognized by individual major histocompatibility complex class I (MHC I)-restricted T-cell receptors," *Immunol. Cell Biol.*, no. February, pp. 1–10, 2016.
- [192] M. Sospedra, C. Pinilla, and R. Martin, "Use of combinatorial peptide libraries for T-cell epitope mapping," *Methods*, vol. 29, no. 3, pp. 236–247, 2003.
- [193] J. Ekeruche-Makinde, J. J. Miles, H. A. van den Berg, A. Skowera, D. K. Cole, G. Dolton, A. J. A. Schauenburg, M. P. Tan, J. M. Pentier, S. Llewellyn-Lacey, K. M. Miles, A. M. Bulek, M. Clement, T. Williams, A. Trimby, M. Bailey, P. Rizkallah, J. Rossjohn, M. Peakman, D. A. Price, S. R. Burrows, A. K. Sewell, and L. Wooldridge, "Peptide length determines the outcome of TCR/peptide-MHC I engagement," *Blood*, vol. 121, no. 7, pp. 1112–1123, Feb. 2013.
- [194] L. Wooldridge, J. Ekeruche-Makinde, H. A. Van Den Berg, A. Skowera, J. J. Miles, M. P. Tan, G. Dolton, M. Clement, S. Llewellyn-Lacey, D. A. Price, M. Peakman, and A. K. Sewell, "A single autoimmune T cell receptor recognizes more than a million different peptides," *J. Biol. Chem.*, vol. 287, no. 2, pp. 1168–1177, 2012.
- [195] D. A. Schmid, M. B. Irving, V. Posevitz, M. Hebeisen, A. Posevitz-Fejfar, J.-C. F. Sarria, R. Gomez-Eerland, M. Thome, T. N. M. Schumacher, P. Romero, D. E. Speiser, V. Zoete, O. Michielin, and N. Rufer, "Evidence for a TCR Affinity Threshold Delimiting Maximal CD8 T Cell Function," *J. Immunol.*, vol. 184, no. 9, p. 4936 LP-4946, May 2010.
- [196] M. Nauerth, B. Weißbrich, R. Knall, T. Franz, G. Dössinger, J. Bet, P. J. Paszkiewicz, L. Pfeifer, M. Bunse, W. Uckert, R. Holtappels, D. Gillert-Marien, M. Neuenhahn, A. Krackhardt, M. J. Reddehase, S. R. Riddell, and D. H. Busch, "TCR-ligand koff rate correlates with the protective capacity of antigen-specific CD8+ T cells for adoptive transfer," *Sci. Transl. Med.*, vol. 5, no. 192, p. 192ra87-192ra87, Jul. 2013.
- [197] J. Schmidt, P. Guillaume, M. Irving, P. Baumgaertner, D. Speiser, and I. F. Luescher, "Reversible major histocompatibility complex I-peptide multimers containing Ni²⁺-nitrilotriacetic acid peptides and histidine tags improve analysis and sorting of

- CD8 + T cells," *J. Biol. Chem.*, vol. 286, no. 48, pp. 41723–41735, 2011.
- [198] J. Schmidt, D. Dojcinovic, P. Guillaume, and I. Luescher, "Analysis, isolation, and activation of antigen-specific CD4+ and CD8+ T cells by soluble MHC-peptide complexes," *Front. Immunol.*, vol. 4, no. JUL, pp. 1–14, 2013.
- [199] M. Hebeisen, L. Baitsch, D. Presotto, P. Baumgaertner, P. Romero, O. Michielin, D. E. Speiser, and N. Rufer, "SHP-1 phosphatase activity counteracts increased T cell receptor affinity," *J. Clin. Invest.*, vol. 123, no. 3, pp. 1044–1056, Mar. 2013.
- [200] C. M. Ayres, S. A. Corcelli, and B. M. Baker, "Peptide and Peptide-Dependent Motions in MHC Proteins: Immunological Implications and Biophysical Underpinnings," *Front. Immunol.*, vol. 8, p. 935, Aug. 2017.
- [201] J. D. Stone, A. S. Chervin, and D. M. Kranz, "T-cell receptor binding affinities and kinetics: impact on T-cell activity and specificity," *Immunology*, vol. 126, no. 2, pp. 165–176, Feb. 2009.
- [202] J. Ekeruche-Makinde, M. Clement, D. K. Cole, E. S. J. Edwards, K. Ladell, J. J. Miles, K. K. Matthews, A. Fuller, K. A. Lloyd, F. Madura, G. M. Dolton, J. Pentier, A. Lissina, E. Gostick, T. K. Baxter, B. M. Baker, P. J. Rizkallah, D. A. Price, L. Wooldridge, and A. K. Sewell, "T-cell receptor-optimized peptide skewing of the T-cell repertoire can enhance antigen targeting," *J. Biol. Chem.*, vol. 287, no. 44, pp. 37269–37281, Oct. 2012.
- [203] D. K. Cole, A. Fuller, G. Dolton, E. Zervoudi, M. Legut, K. Miles, L. Blanchfield, F. Madura, C. J. Holland, A. M. Bulek, J. S. Bridgeman, J. J. Miles, A. J. A. Schauenburg, K. Beck, B. D. Evavold, P. J. Rizkallah, and A. K. Sewell, "Dual Molecular Mechanisms Govern Escape at Immunodominant HLA A2-Restricted HIV Epitope," *Front. Immunol.*, vol. 8, p. 1503, Nov. 2017.
- [204] S. P. Perfetto, D. Ambrozak, R. Nguyen, P. Chattopadhyay, and M. Roederer, "Quality assurance for polychromatic flow cytometry," vol. 1, no. 3, pp. 1522–1530, 2006.
- [205] S. A. Plotkina, "Vaccination against the major infectious diseases," *Comptes Rendus l'Académie des Sci. - Ser. III - Sci. la Vie*, vol. 322, no. 11, pp. 943–951, 1999.
- [206] S. A. Plotkin and S. A. Plotkin, "Correlates of Vaccine-Induced Immunity," *Clin. Infect. Dis.*, vol. 47, no. 3, pp. 401–409, Aug. 2008.
- [207] R. A. Mason, N. M. Tauraso, R. K. Ginn, T. C. O'Brien, and R. W. Trimmer, "Yellow fever vaccine. V. Antibody response in maonkeys inoculated with graded doses of the 17D vaccine.," *Appl. Microbiol.*, vol. 23, no. 5, pp. 908–913, May 1972.

- [208] E. C. ROSENZWEIG, R. W. BABIONE, and C. L. J. WISSEMAN, "Immunological studies with group B arthropod-borne viruses. IV. Persistence of yellow fever antibodies following vaccination with 17D strain yellow fever vaccine.," *Am. J. Trop. Med. Hyg.*, vol. 12, pp. 230–235, Mar. 1963.
- [209] B. Reinhardt, R. Jaspert, M. Niedrig, C. Kostner, and J. L'age-Stehr, "Development of viremia and humoral and cellular parameters of immune activation after vaccination with yellow fever virus strain 17D: a model of human flavivirus infection.," *J. Med. Virol.*, vol. 56, no. 2, pp. 159–167, Oct. 1998.
- [210] M. P. Cancro, "The BLYS/BAFF family of ligands and receptors: key targets in the therapy and understanding of autoimmunity," *Ann. Rheum. Dis.*, vol. 65 Suppl 3, no. Suppl 3, p. iii34-iii36, Nov. 2006.
- [211] R. T. Woodland, M. R. Schmidt, and C. B. Thompson, "BLYS and B cell homeostasis," *Semin. Immunol.*, vol. 18, no. 5, pp. 318–326, 2006.
- [212] K. L. Good, D. T. Avery, and S. G. Tangye, "Resting Human Memory B Cells Are Intrinsically Programmed for Enhanced Survival and Responsiveness to Diverse Stimuli Compared to Naive B Cells," *J. Immunol.*, vol. 182, no. 2, p. 890 LP-901, Jan. 2009.
- [213] B. P. O'Connor, V. S. Raman, L. D. Erickson, W. J. Cook, L. K. Weaver, C. Ahonen, L.-L. Lin, G. T. Mantchev, R. J. Bram, and R. J. Noelle, "BCMA Is Essential for the Survival of Long-lived Bone Marrow Plasma Cells," *J. Exp. Med.*, vol. 199, no. 1, p. 91 LP-98, Jan. 2004.
- [214] V. Peperzak, I. Vikström, J. Walker, S. P. Glaser, M. LePage, C. M. Coquery, L. D. Erickson, K. Fairfax, F. Mackay, A. Strasser, S. L. Nutt, and D. M. Tarlinton, "Mcl-1 is essential for the survival of plasma cells," *Nat. Immunol.*, vol. 14, no. 3, pp. 290–297, Mar. 2013.
- [215] C. M. Prazma, N. Yazawa, Y. Fujimoto, M. Fujimoto, and T. F. Tedder, "CD83 Expression Is a Sensitive Marker of Activation Required for B Cell and CD4⁺ T Cell Longevity In Vivo," *J. Immunol.*, vol. 179, no. 7, p. 4550 LP-4562, Sep. 2007.
- [216] L. Krzyzak, C. Seitz, A. Urvat, S. Hutzler, C. Ostalecki, J. Gläsner, A. Hiergeist, A. Gessner, T. H. Winkler, A. Steinkasserer, and L. Nitschke, "CD83 Modulates B Cell Activation and Germinal Center Responses," *J. Immunol.*, vol. 196, no. 9, p. 3581 LP-3594, Apr. 2016.

- [217] M. Breloer and B. Fleischer, "CD83 regulates lymphocyte maturation, activation and homeostasis," *Trends Immunol.*, vol. 29, no. 4, pp. 186–194, Aug. 2017.
- [218] F. Sallusto, D. Lenig, R. Forster, M. Lipp, and A. Lanzavecchia, "Two subsets of memory T lymphocytes with distinct homing potentials and effector functions," *Nature*, vol. 401, no. 6754, pp. 708–712, Oct. 1999.
- [219] F. Sallusto, J. Geginat, and A. Lanzavecchia, "Central Memory and Effector Memory T Cell Subsets: Function, Generation, and Maintenance," *Annu. Rev. Immunol.*, vol. 22, no. 1, pp. 745–763, Mar. 2004.
- [220] J. C. Nolz, I. O. Health, C. Biology, and O. Health, "HHS Public Access," vol. 72, no. 13, pp. 2461–2473, 2016.
- [221] T. Nakayama, D. J. Kasprowicz, M. Yamashita, L. A. Schubert, G. Gillard, M. Kimura, A. Didierlaurent, H. Koseki, and S. F. Ziegler, "The Generation of Mature, Single-Positive Thymocytes In Vivo Is Dysregulated by CD69 Blockade or Overexpression," *J. Immunol.*, vol. 168, no. 1, p. 87 LP-94, Jan. 2002.
- [222] C. Feng, K. J. Woodside, B. A. Vance, D. El-Khoury, M. Canelles, J. Lee, R. Gress, B. J. Fowlkes, E. W. Shores, and P. E. Love, "A potential role for CD69 in thymocyte emigration," *Int. Immunol.*, vol. 14, no. 6, pp. 535–544, Jun. 2002.
- [223] P. Chu, J. Pardo, H. Zhao, C. C. Li, E. Pali, M. M. Shen, K. Qu, S. X. Yu, B. C. B. Huang, P. Yu, E. S. Masuda, S. M. Molineaux, F. Kolbinger, G. Aversa, J. de Vries, D. G. Payan, and X. C. Liao, "Systematic identification of regulatory proteins critical for T-cell activation," *J. Biol.*, vol. 2, no. 3, p. 21, Sep. 2003.
- [224] M. Matloubian, C. G. Lo, G. Cinamon, M. J. Lesneski, Y. Xu, V. Brinkmann, M. L. Allende, R. L. Proia, and J. G. Cyster, "Lymphocyte egress from thymus and peripheral lymphoid organs is dependent on S1P receptor 1," *Nature*, vol. 427, no. 6972, pp. 355–360, Jan. 2004.
- [225] L. R. Shiow, D. B. Rosen, N. Brdickova, Y. Xu, J. An, L. L. Lanier, J. G. Cyster, and M. Matloubian, "CD69 acts downstream of interferon- α / β to inhibit S1P1 and lymphocyte egress from lymphoid organs," *Nature*, vol. 440, no. 7083, pp. 540–544, Mar. 2006.
- [226] A. J. Bankovich, L. R. Shiow, and J. G. Cyster, "CD69 Suppresses Sphingosine 1-Phosphate Receptor-1 (S1P 1) Function through Interaction with Membrane Helix 4 * □," vol. 285, no. 29, pp. 22328–22337, 2010.
- [227] L. K. Mackay, A. Braun, B. L. Macleod, N. Collins, C. Tebartz, S. Bedoui, R. Carbone, T.

- Gebhardt, L. K. Mackay, A. Braun, B. L. Macleod, N. Collins, C. Tebartz, S. Bedoui, F. R. Carbone, and T. Gebhardt, "Cutting Edge: CD69 Interference with Sphingosine-1-Phosphate Receptor Function Regulates Peripheral T Cell Retention," 2017.
- [228] B. Homey, W. Wang, H. Soto, M. E. Buchanan, A. Wiesenborn, D. Catron, A. Müller, T. K. McClanahan, M.-C. Dieu-Nosjean, R. Orozco, T. Ruzicka, P. Lehmann, E. Oldham, and A. Zlotnik, "Cutting Edge: The Orphan Chemokine Receptor G Protein-Coupled Receptor-2 (GPR-2, CCR10) Binds the Skin-Associated Chemokine CCL27 (CTACK/ALP/ILC)," *J. Immunol.*, vol. 164, no. 7, p. 3465 LP-3470, Apr. 2000.
- [229] B. Homey, H. Alenius, A. Muller, H. Soto, E. P. Bowman, W. Yuan, L. McEvoy, A. I. Lauerma, T. Assmann, E. Bunemann, M. Lehto, H. Wolff, D. Yen, H. Marxhausen, W. To, J. Sedgwick, T. Ruzicka, P. Lehmann, and A. Zlotnik, "CCL27-CCR10 interactions regulate T cell-mediated skin inflammation," *Nat Med*, vol. 8, no. 2, pp. 157–165, Feb. 2002.
- [230] D. Soler, T. L. Humphreys, S. M. Spinola, and J. J. Campbell, "CCR4 versus CCR10 in human cutaneous T_H lymphocyte trafficking," *Blood*, vol. 101, no. 5, p. 1677 LP-1682, Mar. 2003.
- [231] M. Tomura, K. Itoh, and O. Kanagawa, "Naive CD4⁺ T Lymphocytes Circulate through Lymphoid Organs To Interact with Endogenous Antigens and Upregulate Their Function," *J. Immunol.*, vol. 184, no. 9, p. 4646 LP-4653, May 2010.
- [232] J. C. Nolz, "Molecular mechanisms of CD8(+) T cell trafficking and localization," *Cell. Mol. Life Sci.*, vol. 72, no. 13, pp. 2461–2473, Jul. 2015.
- [233] M. D. T. Co, E. D. Kilpatrick, and A. L. Rothman, "Dynamics of the CD8 T-cell response following yellow fever virus 17D immunization," *Immunology*, vol. 128, no. 1 Suppl, pp. e718-27, 2009.
- [234] E. A. James, R. E. Lafond, T. J. Gates, T. Mai, U. Malhotra, W. W. Kwok, E. A. James, R. E. Lafond, T. J. Gates, D. T. Mai, U. Malhotra, and W. Kwok, "Yellow Fever Vaccination Elicits Broad Functional CD4 α T Cell Responses That Recognize Structural and Nonstructural Proteins," 2013.
- [235] M. Koblishke, M. S. Mackroth, J. Schwaiger, I. Fae, K. Stiasny, F. X. Heinz, and J. H. Aberle, "Protein structure shapes immunodominance in the CD4 T cell response to yellow fever vaccination," *Sci. Rep.*, no. March, pp. 1–12, 2017.
- [236] A. P. dos Santos, A. L. Bertho, D. C. Dias, J. R. Santos, and R. Marcovistz, "Lymphocyte

- subset analyses in healthy adults vaccinated with yellow fever 17DD virus.," *Mem. Inst. Oswaldo Cruz*, vol. 100, no. 3, pp. 331–337, May 2005.
- [237] R. M. Zinkernagel and H. Hengartner, "Regulation of the Immune Response by Antigen," *Science (80-.)*, vol. 293, no. 5528, p. 251 LP-253, Jul. 2001.
- [238] R. M. Zinkernagel, "On Natural and Artificial Vaccinations," *Annu. Rev. Immunol.*, vol. 21, no. 1, pp. 515–546, Apr. 2003.
- [239] WHO, "Vaccines and vaccination against yellow fever: WHO Position Paper, June 2013—Recommendations," *Vaccine*, vol. 33, no. 1, pp. 76–77, 2015.
- [240] M. R. Bassi, M. Kongsgaard, M. A. Steffensen, C. Fenger, M. Rasmussen, K. Skjødt, B. Finsen, A. Stryhn, S. Buus, J. P. Christensen, A. R. Thomsen, M. Rasmussen, K. Skjødt, B. Finsen, A. Stryhn, and S. Buus, "CD8 + T Cells Complement Antibodies in Protecting against Yellow Fever Virus," 2015.
- [241] C. L. J. WISSEMAN and B. H. SWEET, "Immunological studies with group B arthropod-borne viruses. III. Response of human subjects to revaccination with 17D strain yellow fever vaccine.," *Am. J. Trop. Med. Hyg.*, vol. 11, pp. 570–575, Jul. 1962.
- [242] B. Christenson and M. Böttiger, "Measles antibody: comparison of long-term vaccination titres, early vaccination titres and naturally acquired immunity to and booster effects on the measles virus," *Vaccine*, vol. 12, no. 2, pp. 129–133, 1994.
- [243] H. GROOT and R. B. RIBERIRO, "Neutralizing and haemagglutination-inhibiting antibodies to yellow fever 17 years after vaccination with 17D vaccine.," *Bull. World Health Organ.*, vol. 27, pp. 699–707, 1962.
- [244] S. Y. Gomez and R. E. Ocazonez, "[Yellow fever virus 17D neutralising antibodies in vaccinated Colombian people and unvaccinated ones having immunity against dengue].," *Rev. Salud Publica (Bogota)*, vol. 10, no. 5, pp. 796–807, 2008.
- [245] H. Coulange Bodilis, G. Benabdelmoumen, A. Gergely, C. Goujon, M. Pelicot, P. Poujol, and P. H. Consigny, "[Long term persistence of yellow fever neutralising antibodies in elderly persons].," *Bull. Soc. Pathol. Exot.*, vol. 104, no. 4, pp. 260–265, Oct. 2011.
- [246] A. C. Campi-Azevedo, V. Peruhype-Magalhães, C. Costa-Pereira, C. P. de Albuquerque, L. F. Muniz, T. Yokoy de Souza, A. C. V. Oliveira, O. A. Martins-Filho, and L. M. H. da Mota, "The 17D-204 and 17DD yellow fever vaccines: an overview of major similarities and subtle differences AU - Ferreira, Clarissa de Castro," *Expert Rev. Vaccines*, vol. 17, no. 1, pp. 79–90, Jan. 2018.
- [247] "Management and control of yellow fever virus: Brazilian outbreak January-April,

- 2018 AU - Callender, David Michael," *Glob. Public Health*, vol. 14, no. 3, pp. 445–455, Mar. 2019.
- [248] I. Selemene, "Epidemiological monitoring of the last outbreak of yellow fever in Brazil – An outlook from Portugal," *Travel Med. Infect. Dis.*, 2018.
- [249] E. Muyanja, A. Ssemaganda, P. Ngauv, R. Cubas, H. Perrin, D. Srinivasan, G. Canderan, B. Lawson, J. Kopycinski, A. S. Graham, D. K. Rowe, M. J. Smith, S. Isern, S. Michael, G. Silvestri, T. H. Vanderford, E. Castro, G. Pantaleo, J. Singer, J. Gillmour, N. Kiwanuka, A. Nanvubya, C. Schmidt, J. Birungi, J. Cox, E. K. Haddad, P. Kaleebu, P. Fast, R. Sekaly, and L. Trautmann, "Clinical medicine Immune activation alters cellular and humoral responses to yellow fever 17D vaccine," vol. 124, no. 7, pp. 15–18, 2014.
- [250] P. Kvistborg, C. Gouttefangeas, N. Aghaeepour, A. Cazaly, P. K. Chattopadhyay, C. Chan, J. Eckl, G. Finak, S. R. Hadrup, H. T. Maecker, D. Maurer, T. Mosmann, P. Qiu, R. H. Scheuermann, M. J. P. Welters, G. Ferrari, R. R. Brinkman, and C. M. Britten, "Thinking outside the gate: single-cell assessments in multiple dimensions," *Immunity*, vol. 42, no. 4, pp. 591–592, Apr. 2015.
- [251] E. Lugli, M. H. Dominguez, L. Gattinoni, P. K. Chattopadhyay, D. L. Bolton, K. Song, N. R. Klatt, J. M. Brenchley, M. Vaccari, E. Gostick, D. A. Price, T. A. Waldmann, N. P. Restifo, G. Franchini, and M. Roederer, "Brief report Superior T memory stem cell persistence supports long-lived T cell memory," vol. 123, no. 2, 2013.
- [252] N. Cieri, B. Camisa, F. Cocchiarella, M. Forcato, G. Oliveira, E. Provasi, A. Bondanza, C. Bordignon, J. Peccatori, F. Ciceri, M. T. Lupo-stanghellini, F. Mavilio, A. Mondino, S. Bicciato, A. Recchia, and C. Bonini, "IL-7 and IL-15 instruct the generation of human memory stem T cells from naive precursors," vol. 121, no. 4, pp. 573–585, 2016.
- [253] S. Di, B. Evelyn, and E. S. D. Goldeck, "Impact of age , sex and CMV-infection on peripheral T cell phenotypes : results from the Berlin BASE-II Study," pp. 631–643, 2015.
- [254] S. Vigano, J. Negron, Z. Ouyang, E. S. Rosenberg, B. D. Walker, M. Lichterfeld, and G. Yu, "Prolonged Antiretroviral Therapy Preserves HIV-1-Specific CD8 T Cells with Stem Cell-Like Properties," vol. 89, no. 15, pp. 7829–7840, 2015.
- [255] M. Schmuck-henneresse, R. Sharaf, K. Vogt, B. J. D. Weist, S. Landwehr-kenzel, A. Jurisch, N. Babel, and C. M. Rooney, "Peripheral Blood – Derived Virus-Specific Memory Stem T Cells Mature to Functional Effector Memory Subsets with Self-Renewal Potency," 2016.

- [256] L. Gattinoni, D. E. Speiser, M. Lichterfeld, and C. Bonini, "review T memory stem cells in health and disease," vol. 23, no. 1, 2017.
- [257] E. Lugli, L. Gattinoni, A. Roberto, D. Mavilio, D. A. Price, N. P. Restifo, and M. Roederer, "Identification, isolation and in vitro expansion of human and nonhuman primate T stem cell memory cells," *Nat. Protoc.*, vol. 8, p. 33, Dec. 2012.
- [258] R. S. Akondy, M. Fitch, S. Edupuganti, S. Yang, H. T. Kissick, K. W. Li, B. A. Youngblood, H. A. Abdelsamed, D. J. McGuire, K. W. Cohen, G. Alexe, S. Nagar, M. M. McCausland, S. Gupta, P. Tata, W. N. Haining, M. J. McElrath, D. Zhang, B. Hu, W. J. Greenleaf, J. J. Goronzy, M. J. Mulligan, M. Hellerstein, and R. Ahmed, "Origin and differentiation of human memory CD8 T cells after vaccination," *Nature*, vol. 552, p. 362, Dec. 2017.
- [259] B. Youngblood, J. S. Hale, H. T. Kissick, E. Ahn, X. Xu, A. Wieland, K. Araki, E. E. West, H. E. Ghoneim, Y. Fan, P. Dogra, C. W. Davis, B. T. Konieczny, R. Antia, X. Cheng, and R. Ahmed, "Effector CD8 T cells dedifferentiate into long-lived memory cells," *Nature*, vol. 552, p. 404, Dec. 2017.
- [260] M. J. T. Stubbington, T. Lönnberg, V. Proserpio, S. Clare, A. O. Speak, G. Dougan, and S. A. Teichmann, "T cell fate and clonality inference from single-cell transcriptomes," *Nat. Methods*, vol. 13, no. 4, pp. 329–332, Apr. 2016.
- [261] T. Lönnberg, V. Svensson, K. R. James, D. Fernandez-Ruiz, I. Sebina, R. Montandon, M. S. F. Soon, L. G. Fogg, A. S. Nair, U. Liligeto, M. J. T. Stubbington, L.-H. Ly, F. O. Bagger, M. Zwiessele, N. D. Lawrence, F. Souza-Fonseca-Guimaraes, P. T. Bunn, C. R. Engwerda, W. R. Heath, O. Billker, O. Stegle, A. Haque, and S. A. Teichmann, "Single-cell RNA-seq and computational analysis using temporal mixture modelling resolves Th1/Tfh fate bifurcation in malaria," *Sci. Immunol.*, vol. 2, no. 9, p. eaal2192, Mar. 2017.
- [262] L. C. Gillet, P. Navarro, S. Tate, H. Röst, N. Selevsek, L. Reiter, R. Bonner, and R. Aebersold, "Targeted Data Extraction of the MS/MS Spectra Generated by Data-independent Acquisition: A New Concept for Consistent and Accurate Proteome Analysis," *Mol. & Cell. Proteomics*, vol. 11, no. 6, p. O111.016717, Jun. 2012.
- [263] U. T. Hacker, S. Erhardt, K. Tschöp, T. Jelinek, and S. Endres, "Influence of the IL-1Ra gene polymorphism on in vivo synthesis of IL-1Ra and IL-1beta after live yellow fever vaccination," *Clin. Exp. Immunol.*, vol. 125, no. 3, pp. 465–469, Sep. 2001.

- [264] C. Havenar-Daughton, M. Lindqvist, A. Heit, J. E. Wu, S. M. Reiss, K. Kendric, S. Bélanger, S. P. Kasturi, E. Landais, R. S. Akondy, H. M. McGuire, M. Bothwell, P. A. Vagefi, E. Scully, I. P. C. P. Investigators, G. D. Tomaras, M. M. Davis, P. Pognard, R. Ahmed, B. D. Walker, B. Pulendran, M. J. McElrath, D. E. Kaufmann, and S. Crotty, "CXCL13 is a plasma biomarker of germinal center activity," *Proc. Natl. Acad. Sci. U. S. A.*, vol. 113, no. 10, pp. 2702–2707, Mar. 2016.
- [265] M. P. Lefranc, "Nomenclature of the human T cell receptor genes.," *Curr. Protoc. Immunol.*, vol. Appendix 1, p. Appendix 10, 2001.
- [266] M. A. Purbhoo, J. M. Boulter, D. A. Price, A. Vuidepot, C. S. Hourigan, P. R. Dunbar, K. Olson, S. J. Dawson, R. E. Phillips, B. K. Jakobsen, J. I. Bell, and A. K. Sewell, "The Human CD8 Coreceptor Effects Cytotoxic T Cell Activation and Antigen Sensitivity Primarily by Mediating Complete Phosphorylation of the T Cell Receptor ζ Chain *," vol. 276, no. 35, pp. 32786–32792, 2001.
- [267] C. Motozono, J. A. Pearson, E. De Leenheer, P. J. Rizkallah, K. Beck, A. Trimby, A. K. Sewell, F. S. Wong, and D. K. Cole, "Distortion of the Major Histocompatibility Complex Class I Binding Groove to Accommodate an Insulin-derived 10-Mer Peptide," *J. Biol. Chem.*, vol. 290, no. 31, pp. 18924–18933, Jul. 2015.
- [268] N. J. Greenfield, "Analysis of Circular Dichroism Data," in *Numerical Computer Methods, Part D*, vol. 383, Academic Press, 2004, pp. 282–317.
- [269] A. Fuller, A. Wall, M. D. Crowther, A. Lloyd, A. Zhurov, A. K. Sewell, D. K. Cole, and K. Beck, "Thermal Stability of Heterotrimeric pMHC Proteins as Determined by Circular Dichroism Spectroscopy," *Bio-protocol*, vol. 7, no. 13, p. e2366, Jul. 2017.
- [270] F. Madura, P. J. Rizkallah, C. J. Holland, A. Fuller, A. Bulek, A. J. Godkin, A. J. Schauenburg, D. K. Cole, and A. K. Sewell, "Structural basis for ineffective T-cell responses to MHC anchor residue-improved 'heteroclitic' peptides," *Eur. J. Immunol.*, vol. 45, no. 2, pp. 584–591, 2015.
- [271] R. C. Edgar, "MUSCLE: multiple sequence alignment with high accuracy and high throughput," *Nucleic Acids Res.*, vol. 32, no. 5, pp. 1792–1797, Mar. 2004.
- [272] N. Eswar, B. Webb, M. A. Marti-Renom, M. S. Madhusudhan, D. Eramian, M. Shen, U. Pieper, and A. Sali, "Comparative Protein Structure Modeling Using MODELLER," in *Current Protocols in Protein Science*, John Wiley & Sons, Inc., 2001.
- [273] A. Šali and T. L. Blundell, "Comparative Protein Modelling by Satisfaction of Spatial Restraints," *J. Mol. Biol.*, vol. 234, no. 3, pp. 779–815, 1993.

- [274] E. F. Pettersen, T. D. Goddard, C. C. Huang, G. S. Couch, D. M. Greenblatt, E. C. Meng, and T. E. Ferrin, "UCSF Chimera—A visualization system for exploratory research and analysis," *J. Comput. Chem.*, vol. 25, no. 13, pp. 1605–1612, Oct. 2004.
- [275] M. J. Abraham, T. Murtola, R. Schulz, S. Páll, J. C. Smith, B. Hess, and E. Lindahl, "GROMACS: High performance molecular simulations through multi-level parallelism from laptops to supercomputers," *SoftwareX*, vol. 1–2, pp. 19–25, 2015.
- [276] P. Bjelkmar, P. Larsson, M. A. Cuendet, B. Hess, and E. Lindahl, "Implementation of the CHARMM Force Field in GROMACS: Analysis of Protein Stability Effects from Correction Maps, Virtual Interaction Sites, and Water Models," *J. Chem. Theory Comput.*, vol. 6, no. 2, pp. 459–466, Feb. 2010.
- [277] A. D. MacKerell, D. Bashford, M. Bellott, R. L. Dunbrack, J. D. Evanseck, M. J. Field, S. Fischer, J. Gao, H. Guo, S. Ha, D. Joseph-McCarthy, L. Kuchnir, K. Kuczera, F. T. Lau, C. Mattos, S. Michnick, T. Ngo, D. T. Nguyen, B. Prodhom, W. E. Reiher, B. Roux, M. Schlenkrich, J. C. Smith, R. Stote, J. Straub, M. Watanabe, J. Wiorkiewicz-Kuczera, D. Yin, and M. Karplus, "All-atom empirical potential for molecular modeling and dynamics studies of proteins.," *J. Phys. Chem. B*, vol. 102, no. 18, pp. 3586–3616, Apr. 1998.
- [278] R. L. Dunbrack, "Rotamer Libraries in the 21st Century," *Curr. Opin. Struct. Biol.*, vol. 12, no. 4, pp. 431–440, 2002.
- [279] N. Eswar, B. Webb, M. A. Marti-Renom, M. S. Madhusudhan, D. Eramian, M.-Y. Shen, U. Pieper, and A. Sali, "Comparative protein structure modeling using Modeller," *Curr. Protoc. Bioinforma.*, vol. Chapter 5, p. Unit-5.6, Oct. 2006.
- [280] U. Essmann, L. Perera, M. L. Berkowitz, T. Darden, H. Lee, and L. G. Pedersen, "A smooth particle mesh Ewald method," *J. Chem. Phys.*, vol. 103, no. 19, pp. 8577–8593, Nov. 1995.
- [281] B. Hess, C. Kutzner, D. van der Spoel, and E. Lindahl, "GROMACS 4: Algorithms for Highly Efficient, Load-Balanced, and Scalable Molecular Simulation," *J. Chem. Theory Comput.*, vol. 4, no. 3, pp. 435–447, Mar. 2008.
- [282] G. Bussi, D. Donadio, and M. Parrinello, "Canonical sampling through velocity rescaling," *J. Chem. Phys.*, vol. 126, no. 1, p. 14101, Jan. 2007.

APPENDIX 1: European Journal of Immunology – Cover 2/18



APPENDIX 2: T cell receptor alpha variable 12-2 bias in the immunodominant response to Yellow fever virus

Eur. J. Immunol. 2017. 00: 1–15

DOI: 10.1002/eji.201747082

Amandine Bovay et al.

1


European Journal of
Immunology

Adaptive immunity

Basic

Research Article

T cell receptor alpha variable 12-2 bias in the immunodominant response to Yellow fever virus

Amandine Bovay¹, Vincent Zoete², Garry Dolton³, Anna M. Bulek³, David K. Cole³, Pierre J. Rizkallah³, Anna Fuller³, Konrad Beck⁴, Olivier Michielin², Daniel E. Speiser¹, Andrew K. Sewell³ and Silvia A. Fuertes Marraco¹ 

¹ Department of Oncology, Lausanne University Hospital (CHUV), Epalinges, Switzerland

² SIB Swiss Institute of Bioinformatics, Molecular Modeling Group, Lausanne, Switzerland

³ Division of Infection and Immunity and Systems Immunity Research Institute, Cardiff University School of Medicine, Heath Park, Cardiff, UK

⁴ Cardiff University School of Dentistry, Heath Park, Cardiff, UK

The repertoire of human $\alpha\beta$ T-cell receptors (TCRs) is generated via somatic recombination of germline gene segments. Despite this enormous variation, certain epitopes can be immunodominant, associated with high frequencies of antigen-specific T cells and/or exhibit bias toward a TCR gene segment. Here, we studied the TCR repertoire of the HLA-A*0201-restricted epitope LLWNGPMAV (hereafter, A2/LLW) from Yellow Fever virus, which generates an immunodominant CD8⁺ T cell response to the highly effective YF-17D vaccine. We discover that these A2/LLW-specific CD8⁺ T cells are highly biased for the TCR α chain TRAV12-2. This bias is already present in A2/LLW-specific naïve T cells before vaccination with YF-17D. Using CD8⁺ T cell clones, we show that TRAV12-2 does not confer a functional advantage on a per cell basis. Molecular modeling indicated that the germline-encoded complementarity determining region (CDR) 1 α loop of TRAV12-2 critically contributes to A2/LLW binding, in contrast to the conventional dominant dependence on somatically rearranged CDR3 loops. This germline component of antigen recognition may explain the unusually high precursor frequency, prevalence and immunodominance of T-cell responses specific for the A2/LLW epitope.

Keywords: Antigen recognition · Germline · T cell receptor Alpha Variable (TRAV)-12-2 · T cell receptor bias · Yellow Fever virus



Additional supporting information may be found in the online version of this article at the publisher's web-site

Introduction

Human $\alpha\beta$ TCRs are heterodimeric proteins composed of an α - and β -chain, somatically rearranged during T cell development from

a selection of 176 variables (V), diversity (D), joining (J), and constant (C) genes [1]. The specificity of peptide-MHC (pMHC) recognition is conferred by the six highly flexible complementarity-determining region (CDR) loops that make up the antigen-binding site of the TCR. The CDR1 and CDR2 sequences are entirely encoded within the Variable genes for each α - and β -chain (T cell Receptor Alpha Variable, TRAV, and T cell Receptor Beta Variable genes, TRBV, respectively). CDR1 and CDR2 are therefore entirely

Correspondence: Dr. Silvia A. Fuertes Marraco
e-mail: silvia.fuertesmarraco@unil.ch

© 2017 WILEY-VCH Verlag GmbH & Co. KGaA, Weinheim

www.eji-journal.eu

germline-encoded. In contrast, the CDR3 loops, which generally make extensive contacts with the antigenic peptide [2, 3], are encoded by the V(D)J joints and thus hypervariable. The general consensus is that the somatic hypervariability of the CDR3 loops contributes most to the broad range of TCR specificities. However, with more atomic structures of TCR-pMHC complexes, it is becoming evident that the germline CDR1 α loop can sometimes also contact peptide residues, and in some cases dominate the contact with the peptide [4–6].

Antigen-specific CD8⁺ T cells can be biased for certain TRAV or TRBV segments or feature “public TCRs” shared across the human population. In addition, TCR bias has been observed in infection, autoimmunity, and alloreactivity, with many examples reviewed by Turner et al. [7]. The reasons behind the sharing of particular TCR segments are not yet fully understood but may have critical implications for the understanding and induction of optimal, protective antigen-specific T cell responses.

Recently, we described the remarkable decade-long persistence of human stem cell-like memory (SCM) CD8⁺ T cells specific for the HLA-A*0201-restricted Yellow Fever virus (YFV) Non-Structural protein 4b^{214–222} epitope (sequence LLWNGPMAV; hereafter, A2/LLW) in the context of YF-17D vaccination [8]. Several studies have shown that this A2/LLW epitope is highly dominant and prevalent amongst YF-17D vaccinees [9–11]. At the peak of the T cell response, up to 25% of the peripheral CD8⁺ T cells can be specific for A2/LLW [9]. In our hands, A2/LLW-specific CD8⁺ T cells could be detected in 38/41 HLA-A*0201 positive individuals after vaccination with YF-17D (>90% prevalence) [8]. Interestingly, we also revealed that naïve A2/LLW-specific CD8⁺ T cells were readily detectable in 3 out of 10 unvaccinated donors [8]. The reasons behind this unusual high frequency and prevalence of A2/LLW-specific CD8⁺ T cells warranted further investigation. Here, we show that A2/LLW-specific TCRs are highly biased for the TCR α chain germline segment TRAV12-2. This finding is in common with another human specificity for which there is an extraordinarily high frequency of naïve T cells: the HLA-A*0201-restricted epitope ELAGIGILTV (heteroclitic analog to EAAGIGILTV from Melan-A, and hereafter, A2/ELA) [12, 13]. Pertinently, A2/ELA-specific CD8⁺ T cells are also known to be biased for TRAV12-2 and the germline-encoded CDR1 α loop in an A2/ELA-specific TCR featuring TRAV12-2 (MEL5 TCR) makes major contributions to antigen recognition, thereby providing a so called “innate-like” binding of the peptide [13–18]. We performed functional and structural studies to further investigate the TRAV12-2 bias in A2/LLW-specific CD8⁺ T cells.

Results

A2/LLW-specific CD8⁺ T cells are biased for the segment TRAV12-2, before and after vaccination

Initially, genome-wide analysis of A2/LLW-specific CD8⁺ SCM and various differentiation subsets in total CD8⁺ T cells [8, 19] revealed that the most prominent feature was the highly signifi-

cant enrichment of the TRAV12-2 in A2/LLW-specific CD8⁺ T cells (Fig. 1A). We next investigated this TRAV12-2 enrichment in A2/LLW-specific CD8⁺ T cells from eight YF-17D vaccinees at the protein level (Figs. 1B and E). We also compared A2/LLW-specific CD8⁺ T cells in these vaccinees to those in unvaccinated donors in order to address whether vaccination induced the observed TRAV12-2 bias (Fig. 1E). In addition, we analyzed healthy donors for other antigen specificities such as A2/ELA, which is known to be biased for TRAV12-2 [13], and other viral antigen specificities that are not known to exhibit such bias: the HLA-A*0201-restricted epitopes BMFL1 from Epstein Barr Virus (EBV) and pp65 from cytomegalovirus (CMV) as well as two other YF epitopes that were detectable in two YF-17D vaccinees (the HLA-A*0201-restricted VMLFILAGL from NS4a protein, A2/VML, and HLA-B*07-restricted RPIDDRFGL from NS5 protein, B7/RPI). In accordance with our previous study [8], we found that vaccinees had easily detectable and largely differentiated A2/LLW-specific CD8⁺ T cells (Figs. 1B to D), while unvaccinated donors showed lower but detectable frequencies of naïve A2/LLW-specific CD8⁺ T cells (i.e. above 0.001%) (Figs. 1C and D). As expected, naïve A2/ELA-specific CD8⁺ T cells were also detectable in healthy donors, while the other viral antigen specificities were variably detected amongst donors and displayed differentiated phenotypes (Figs. 1C and D). The TRAV12-2 segment was used by the majority (median 55.5%) of A2/LLW-specific CD8⁺ T cells (Fig. 1E), in contrast to total CD8⁺ T cells (median 12.5%). The TRAV12-2 bias reached a similar extent as in Melan-A-specific CD8⁺ T cells from healthy donors (median 57.7%), in contrast to the absence of bias in the other specificities (other two YF-17D epitopes and CMV- and EBV-specific epitopes) (Fig. 1E). Interestingly, we found that the TRAV12-2 bias was already evident in naïve A2/LLW-specific CD8⁺ T cells, prior to vaccination (median 69.2%).

Despite the TRAV12-2 bias, A2/LLW-specific TCRs are mostly unique and public sequences infrequent

We generated and analyzed 57 A2/LLW-specific CD8⁺ T cell clones derived from four different YF-17D vaccinees. As shown in Fig. 2A, the V α gene segments were predominated by TRAV12-2, with 45 of 57 clones positive for TRAV12-2 (78.9%). The TRAJs were relatively more diverse, using 15 of the 61 TRAJ human genes, yet consisting predominantly of the TRAJ30 (45.1%) (Fig. 2B). In contrast, the V β repertoire was highly heterogeneous, with 10 different V β segments used, although a moderate bias for some TRBV genes was noted: TRBV9 was used by 16 clones and TRBV2 used by 10 clones (Fig. 2C). There was no evident TRBJ bias (Fig. 2D). In addition, TRAV12-2 CDR3 length consisted predominantly of 8 amino acids whereas CDR3 β sequences showed a broader distribution (Fig. 2E). Most TCRs were unique clonotypes (Supporting Information Table 1), with no conserved motif in the CDR3 loop observed. We identified two public TRAV sequences: “CAVTDDKIIFG” was shared by all four donors and “CAVGDDKIIFG” by three out of four donors.

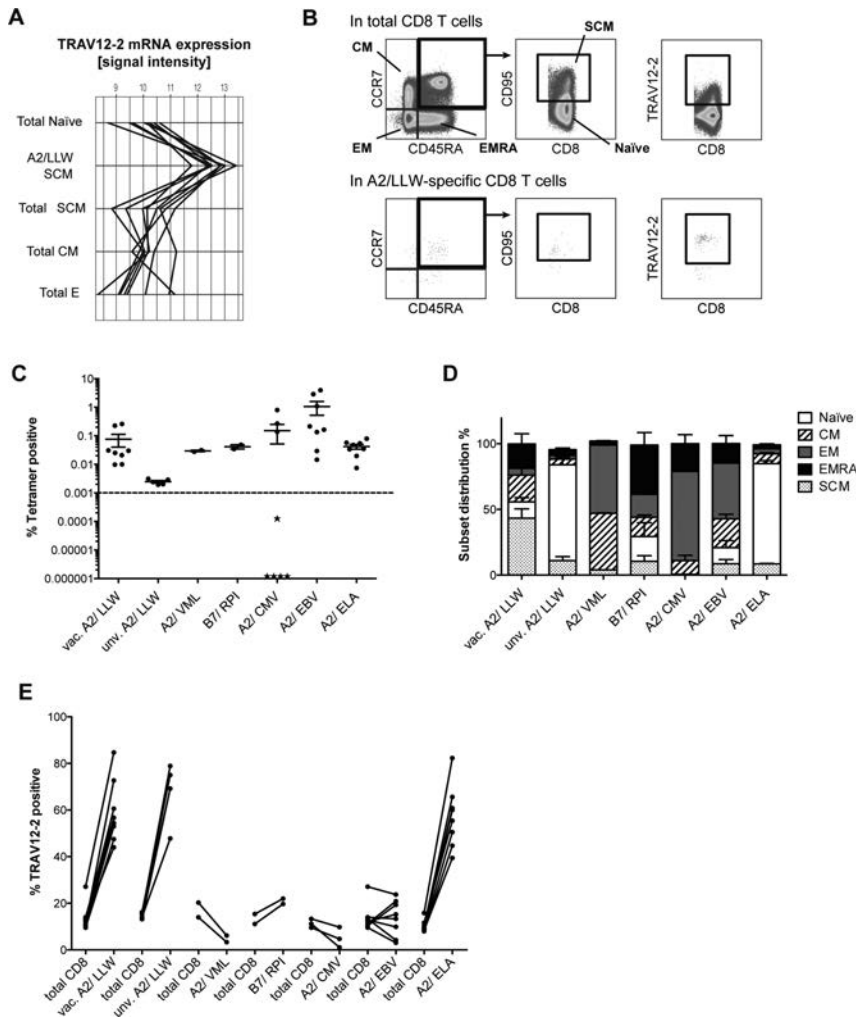


Figure 1. A2/LLW-specific CD8⁺ T cells are strongly biased for TRAV12-2 similarly to A2/ELA-specific CD8⁺ T cells. (A) TRAV12-2 mRNA expression in A2/LLW-specific stem cell-like (SCM) CD8⁺ T cells compared to reference differentiation subsets in total CD8⁺ T cells (N = 8 YF-17D vaccinees), including: Naïve, SCM, central memory (CM) and effectors (E). Samples were isolated from PBMCs by FACS and total RNA analyzed by microarray. (B) Representative gating strategy for the flow cytometry analysis of CD8⁺ T cell subsets in total or tetramer positive populations and TRAV12-2 expression therein. EM: effector memory; EMRA: effector memory CD45RA⁺. (C) Frequencies (%) of various antigen specificities amongst circulating CD8⁺ T cells (mean and SEM), including A2/LLW in YF-17D vaccinees (N = 8) and unvaccinated individuals (N = 5), A2/VML (N = 2) and B7/RPI (N = 2) in YF-17D vaccinees, as well as A2/CMV (N = 8; stars represent CMV-seronegative donors = 5/8), A2/EBV (N = 8) and A2/ELA (N = 8). Data are representative of two independent experiments. (D) Subset distribution of antigen-specific CD8⁺ T cell populations (mean and SEM). (E) Subject-paired comparison of TRAV12-2 expression between antigen-specific and total CD8⁺ T cells ("vac." = YF-17D vaccinee; "unv." = unvaccinated with YF-17D).

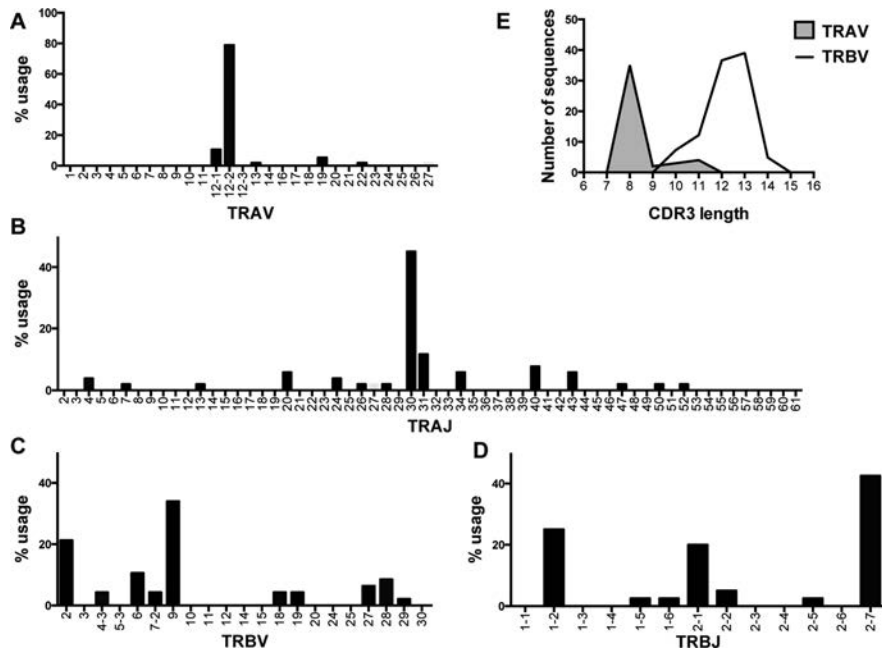


Figure 2. TCR repertoire analysis of A2/LLW-specific CD8⁺ T cell clones generated from four vaccinated donors. Total RNA was isolated from 57 A2/LLW-specific CD8⁺ T cell clones, cDNA prepared, analyzed by PCR with primers specific for each TRAV and TRBV gene segment, and sequenced. (A) TRAV gene usage. (B) TRAJ gene usage. (C) TRBV gene usage. (D) TRBJ gene usage. (E) CDR3 length distribution according to IMGT definition.

On a per cell basis, TRAV12-2 does not confer functional advantages to A2/LLW-specific CD8⁺ T cells

One hypothesis could be that TCRs with TRAV12-2 mediate increased T cell function. Analysis of various functional properties in A2/LLW-specific CD8⁺ T cell clones showed that TRAV12-2-positive clones did not differ from TRAV12-2-negative clones, whether in killing capacity (EC_{50} in Fig. 3A), TCR avidity (K_{off} in Fig. 3B) or degranulation and secretion of IFN- γ , TNF- α , and IL-2 after 4-hours peptide stimulation (Fig. 3C and D). Altogether, expression of TRAV12-2 did not confer a particular functional advantage in A2/LLW-specific CD8⁺ T cell clones.

The LLW peptide binds with high stability to HLA-A*0201

The TRAV12-2 bias in A2/LLW-specific TCRs is reminiscent of the TRAV12-2 bias observed in A2/ELA-specific CD8⁺ T cells. In the A2/ELA-specific MEL5 TCR structure, the germline-encoded

CDR1 α loop makes important interactions with the ELA peptide in complex with HLA-A*0201 providing an explanation for the preferential TRAV12-2 usage and high frequency of this specificity [5, 14–16, 20–22]. In order to determine the structural characteristics that govern the TCR recognition of the LLW peptide, we intended to solve the crystal structure of a TRAV12-2 positive TCR specific for A2/LLW in complex with its cognate pMHC (A2/LLW). Unfortunately, despite several attempts with different TCRs, we were unable to re-fold a functional A2/LLW-specific TRAV12-2 positive TCR. We were able to solve the atomic structure of the A2/LLW pMHC complex at 1.59Å resolution. Electron density around the peptide was unambiguous (Fig. 4A). The general features of the binding are similar to those observed in other peptide-HLA-A*0201 complexes: the nonamer adopts a conformation with central bulge between residues at position 4 and 6 where the side chains are protruding toward the TCR (Fig. 4B), while the peptide termini provide binding into the HLA binding pockets with many specific interactions (Figs. 4A and C).

To assay more directly the peptide binding affinity, we performed circular dichroism (CD) temperature melting experiments.

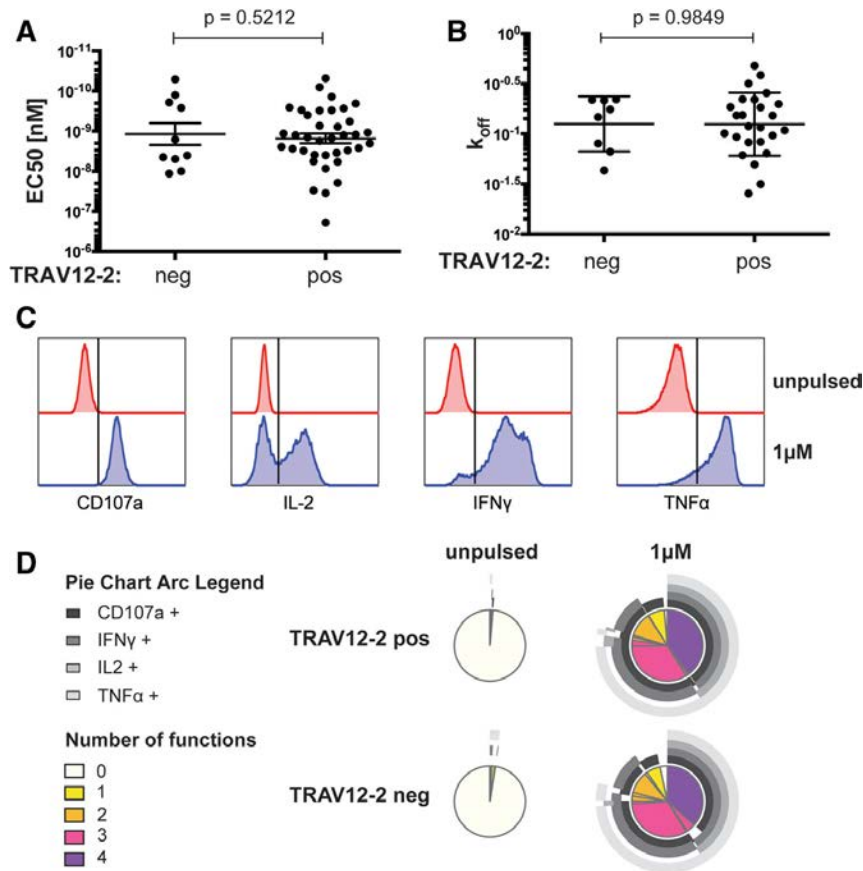


Figure 3. TRAV12-2 expression does not confer a functional advantage. Functional properties of A2/LLW-specific CD8⁺ T cell clones were assessed by various methods. (A) Killing capacity (51-chromium release assay) with LLW peptide titration in A2/LLW-specific CD8⁺ T cell clones (TRAV12-2 positive $N = 37$, TRAV12-2 negative $N = 10$). Data are representative of two independent experiments (mean and SEM; t-test p value). (B) Monomeric dissociation constant (K_{off}) rates measured in CD8⁺ T cell clones (TRAV12-2 positive $N = 25$, TRAV12 negative = 8) using NTAmers (mean and SD; t-test P value). (C and D) Intracellular cytokine staining of CD8⁺ T cell clones (TRAV12-2 positive $N = 11$, TRAV12-2 negative $N = 6$) following LLW peptide stimulation for 4 h, showing representative flow cytometry gating strategy in C. Data are representative of two independent experiments.

The A2/LLW complex showed a melting temperature T_m of 66.5°C and transition enthalpies ΔH_{vH} of ca. -500 kJ/mol (Fig. 5). Thus, the A2/LLW complex is very stable when compared to other pMHC complexes that are also recognized by TRAV12-2 positive TCRs ($T_m / \Delta H_{\text{vH}}$ 66.0°C/-610 kJ/mol and 63.0°C/-380 kJ/mol for A2/Tax from the human T-lymphotropic virus type 1 (HTLV-1) and A2/ELA, respectively).

The germline-encoded CDR1 α loop of TRAV12-2 contributes to pMHC binding

To investigate the structural determinants of a TRAV12-2 positive TCR interacting with A2/LLW, we supported our experimental A2/LLW crystal data with two complementary strategies. First, we combined our structure of the A2/LLW and the previously

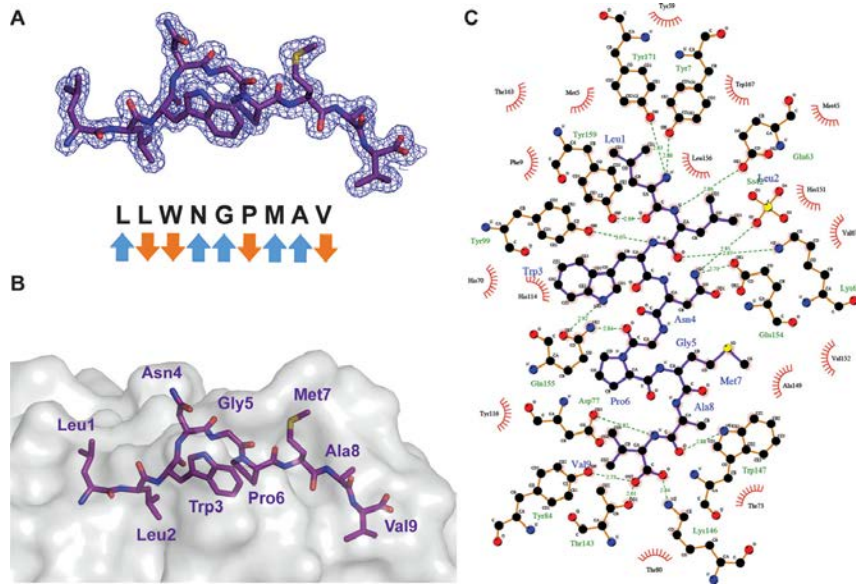


Figure 4. LLW peptide binds stably to HLA-A*0201. (A) Electron density at 1σ contour level around the peptide of the A2/LLW complex showing the overall conformation of the peptide. Blue arrows (TCR-exposed) and orange arrows (MHC-buried) indicate direction of amino acid side chains. (B) Surface and stick representation of HLA-A*0201 and peptide residues, respectively. (C) LIGPLOT schematic diagram showing the various interactions of the LLW peptide with HLA-A*0201. Purple lines are peptide covalent bonds, orange lines are HLA-A2 covalent bonds, dotted green lines are polar/H-bond contacts, and open red arcs indicate a protein atom in a non-polar contact.

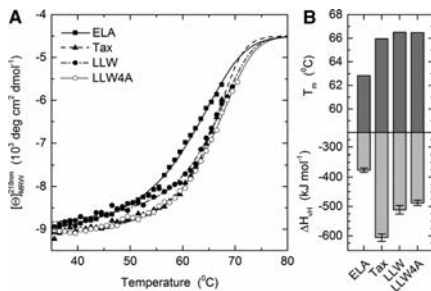


Figure 5. Thermal stability of pMHCs. (A) Temperature stability of the HLA-A2*0201 molecules with the ELA (ELAGIGILTV, square/straight line), Tax (LLFGYPVYV, triangles/dashed line), LLW (LLWNGPMAV, close circles/dash-dotted line), and LLW-4A (LLWAGPMAV, open circles/dashed line) peptides assayed by circular dichroism spectroscopy. Lines represent data fits as described in Methods. (B) Apparent melting temperature T_m and van't Hoff's enthalpy of unfolding ΔH_{vH} (mean and SD). Error bars represent S.D. resulting from the multivariable curve fitting.

solved structures of the MEL5 TCR to perform *in silico* modeling of the A2/LLW-specific YF5048 TCR (TRAV12-2/TRBV9; Fig. 6A and Supporting Information Table 2). This A2/LLW-specific TCR from clone 5048 NN4 (hereafter YF5048) was chosen out of our A2/LLW-specific clone database due to its closest similarity to the MEL5 TCR sequence for the α chain (just 3 amino acids different; Supporting Information Fig. 1A). The overall conformation of the LLW peptide binding to the MHC molecule is similar to the ELA peptide thus facilitating the modeling (Supporting Information Fig. 1B). Figure 6A and Supporting Information Table 2 show the molecular interactions taking place between the TRAV12-2 TCR and the A2/LLW complex. In this model, most of the interactions between the TCR and the peptide originate from the α chain encoded by TRAV12-2. Five peptide residues are pointing toward the TCR: Leu1, Asn4, Gly5, Met7 and Ala8; and these predominantly contact the CDR1 α loop. In particular, Asn4 extends into a polar pocket of TRAV12, where its side chain is making a network of hydrogen bonds with the side chains of CDR1 α Ser32 and CDR3 α Asp92, as well as non-polar interactions with CDR1 α Gln31. In turn, the CDR3 β loop of YF5048 expands between the Asn4 and Met7 peptide residues, and exchanges two hydrogen bonds between the backbone of Ser98 and the

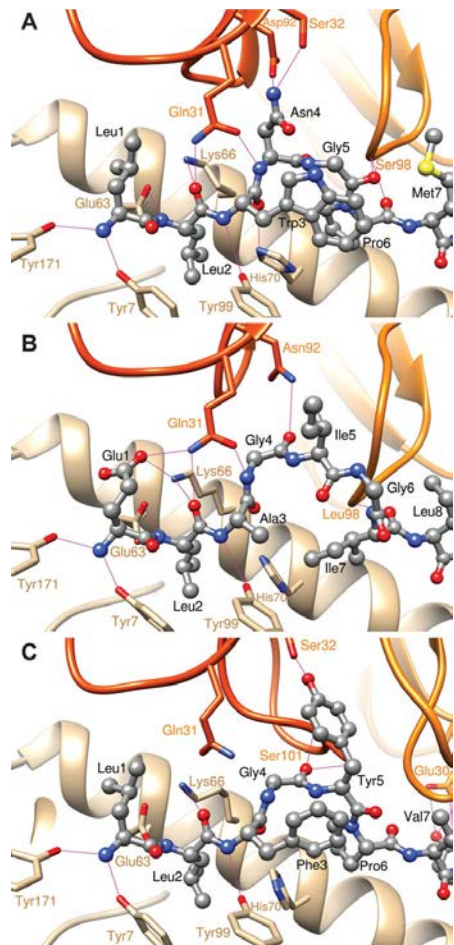


Figure 6. Molecular modeling indicates that germline-encoded CDR1 in TRAV12-2 makes major contributions to the binding with the A2/LLW complex. Calculated 3D structure of the YF5048 TRAV12/TRBV9 TCR bound to the HLA-A2/LLW peptide complex (A) and experimental structures of the MEL5 TRAV12/TRBV30 TCR bound to HLA-A2/ELA peptide complex, PDB ID 3G1 (B) or the HLA-A2/Tax peptide complex, PDB ID 4FTV (C), with ribbons representing α - and β -chains in dark and light orange, respectively; the MHC molecule in tan ribbon, and peptides in ball and stick representation. TCR and MHC side chains are shown in thick lines, with carbon atoms colored in orange and tan, respectively. Hydrogen bonds are displayed as magenta thin lines.

backbones of peptide residues Gly5 and Pro6 (Fig. 6A). This 3D model of A2/LLW/YF5048 presents important structural similarities with the experimental structures of the ELA and Tax peptides (Fig. 6). The backbone of the 3 first and last residues are nearly superimposed, and the corresponding side chains occupy the same MHC pockets: Leu2 of LLW, ELA and Tax in P2; Ala8 of LLW, Thr9 of ELA and Tyr8 of Tax in P8; Val9 of LLW and Tax, and Val10 of ELA in P9. In line with this, residues Leu1 of LLW, and Glu1 of ELA are facing the TCR α , while Met7 of LLW, Leu8 of ELA and Val7 of Tax are pointing toward the TCR β . Important structural differences arise for the central residues of the peptides. While pocket P3 of MHC is occupied by Trp3 of LLW and Phe3 of Tax, it is occupied by Gly6 and part of the Ile5 backbone of the ELA peptide, due to a large backbone rearrangement. In addition, the peptide residue pointing toward TCR α and possibly making interactions is Asn4 for LLW, Ile5 for ELA and Tyr5 for Tax.

The second strategy to investigate the structural determinants of the A2/LLW-specific TRAV12-2 was to functionally interrogate the A2/LLW-specific CD8⁺ T cell clone YF5048 using amino acid substitutions of the LLW index peptide and combinatorial peptide library (CPL) screening. Alanine substitutions at each position of the LLW peptide revealed that the central region of the peptide (positions 3–5) was key for TCR recognition as these substitutions were deleterious to recognition; in particular the Asn4→Ala4 (LLW-4A) was very informative as it completely abrogated the response of the YF5048 clone (Fig. 7A). This suggested that the TCR makes the majority of its critical contacts in the central region of the peptide, which is consistent with the conformation of the peptide accommodating into a central bulge (Figs. 4A and B). The dramatic effect of the Asn4→Ala4 mutation is in line with the critical interactions made by the TRAV12-2 CDR1 α loop of the TCR with the Asn (Fig. 6A and Supporting Information Table 2). Interestingly, both A2/LLW and the mutated A2/LLW-4A complexes were found to have the same T_m of 66.5°C, ruling out the possibility that the absence of response to the mutated peptide LLW-4A is a consequence of the instability of its complex with HLA-A*02 (Fig. 5).

To further explore the observations of the alanine scan we performed a nonamer CPL screen of the YF5048 clone, which revealed positions of the peptide where index residues gave similar (positions 1, 4 and 6) or superior (positions 2, 3, 5 and 9) activation compared to non-index amino acids (Fig. 7B). In contrast, index residues were seen minimally at positions 7 and 8, with relatively high responses seen in both cases for non-index amino acids (Fig. 7B). In concordance with the alanine scan in the LLW peptide backbone, activation toward the index residues at positions 3 (Trp) and 5 (Gly) were dominant over the other amino acid residues. Despite the dramatic loss of YF5048 activation toward the Asn4→Ala4 in the index peptide, non-index residues (namely Arg, Thr and Trp) also gave activation that was comparable or superior (Arg) to the Asn at position 4 (Fig. 7B). In light of this result, we performed an Asn4→Arg4 substitution of the index peptide, which ablated recognition of the peptide by YF5048 (Supporting Information Fig. 3A and 3B) and therefore supported the previous data that showed the importance of the Asn4 for TCR recognition. The loss

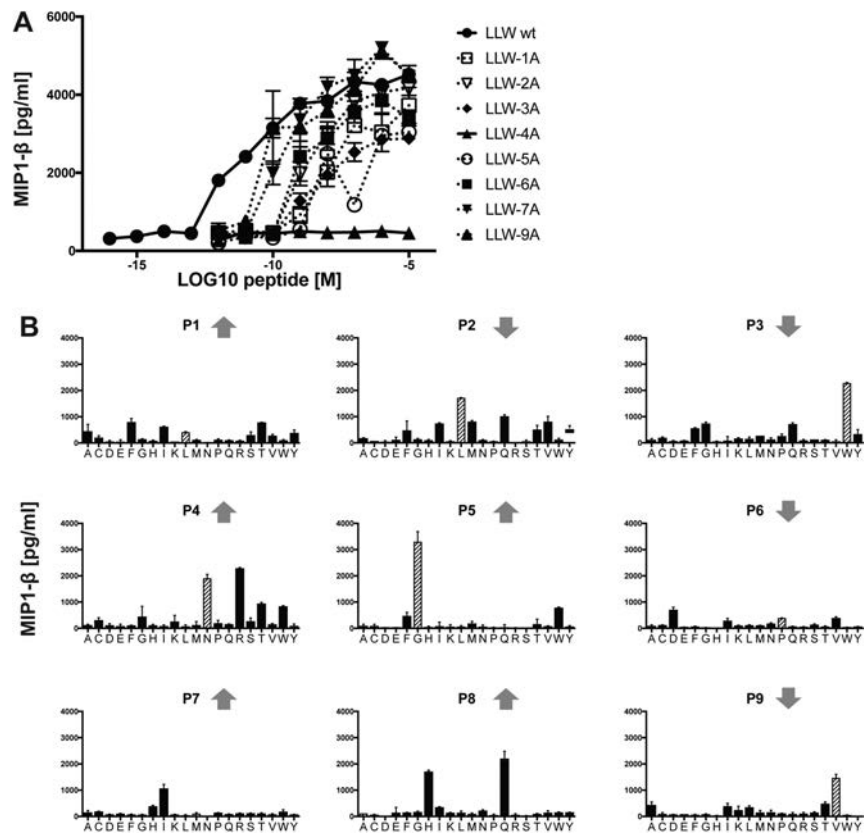


Figure 7. Peptide recognition signature of an individual TCR derived from clone YF5048. The A2/LLW-specific CD8⁺ T cell clone YF5048 was functionally interrogated using amino acid substitutions of the LLW index peptide and CPL screening (A) Alanine-scan of the LLW peptide assessed by MIP-1 β activation with graded concentrations of the peptides (mean and SEM). Data are representative of 2 independent experiments. (B) Nonamer CPL scan for clone YF5048 assayed by MIP-1 β activation (mean and SD). Index peptide residues are represented as dashed-pattern bars. Upwards arrows (TCR-exposed) and downwards arrows (MHC-buried) indicate direction of amino acid side chains. Data are representative of 3 independent experiments.

of reactivity toward the peptide LLW**R**GPMAV suggested that the Asn4→Arg4 substitution alone was not sufficient to be seen by the TCR and required further amino acid changes at other positions of the index peptide to achieve activation. The ability of a CPL to identify amino acids that can be substituted and recognized by a clone was demonstrated using second TRAV12-2 positive A2/LLW-specific clone, YF5031. CPL data for YF5031 showed that this clone preferred the index residue sub-libraries at the central positions of the peptide (Supporting Information Fig. 2A), akin to YF5048 (Fig. 7B). Maintaining this central region with substitutions at

5 other positions (**KQWNGFIPV**) substitutions in bold and underlined) gave a peptide sequence that activated YF0531 (Supporting Information Fig. 3C), thereby further highlighting the importance of the central residues for TRAV12-2 TCR recognition of the YF peptide. We also performed CPL screening of TRAV12-2 negative clones to explore their reactivity toward the central region of the peptide. Whereas the TRAV12-2 positive clones YF5048 (Fig. 7B) and YF5031 (Supporting Information Fig. 2A) were focused on index residues Trp3 and Gly5, TRAV12-2 negative clone YF5001 recognized index and multiple non-index amino acid residues at

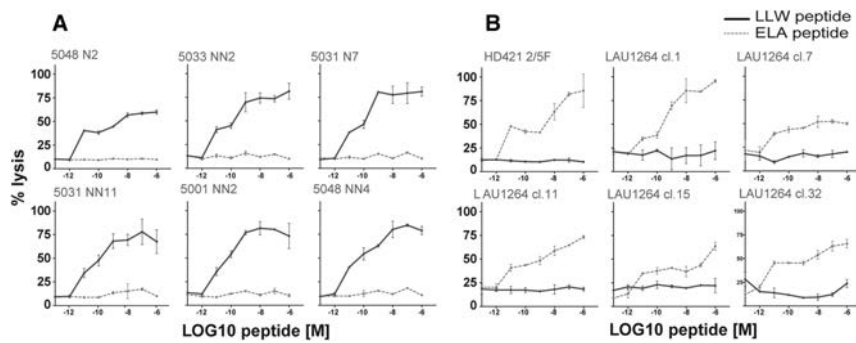


Figure 8. Absence of cross-reactivity between A2/LLW and A2/ELA epitopes. Recognition of the LLW and ELA peptides by A2/LLW-specific and A2/ELA-specific CD8⁺ T cell clones was assessed by chromium release assay. (A) Cross-reactivity analysis of TRAV12-2 positive A2/LLW-specific CD8⁺ T cell clones toward the LLWNGPMAV (LLW, solid line) and ELAGIGLTV (ELA, dashed line) (mean and SD). (B) Cross-reactivity analysis of TRAV12-2 positive A2/ELA-specific CD8⁺ T cell clones toward the LLWNGPMAV (LLW, solid line) and ELAGIGLTV (ELA, dashed line) (mean and SD).

these positions. Although YF5001 recognized the Asn4 sub-library, other amino acid sub-libraries (Ile, Arg and Try) were of comparable or greater potency (Supporting Information Fig. 2B). The second TRAV12-2 negative clone YF5048NN1, however, exhibited a focused recognition across the central region of the peptide; preferring only Trp (index) at position 3, and Gly (index) or Thr (non-index) at position 5 (Supporting Information Fig. 2C). Interestingly, any response by YF5048NN1 toward the TRAV12-2 TCR critical Asn at position 4 was unconvincing and instead dominated by activation toward the Ser-fixed sub-library (Supporting Information Fig. 2C). Taken together these data further support the importance of the central amino acid residues, especially the Asn4, of the LLW peptide in the binding of TRAV12-2 positive TCRs.

In conclusion, the complementary approaches of modeling and cell functional assays demonstrated the key elements that mediate the TRAV12-2 positive YF5048 TCR interaction with the A2/LLW complex and support that the germline-encoded CDR1 α loop of TRAV12-2 makes critical contributions to cognate peptide recognition.

A2/LLW and A2/ELA TRAV12-2 positive TCRs preserve their respective specificity

Given the germline nature of the CDR1 α loop of TRAV12-2 that is critical to peptide recognition of both A2/LLW and A2/ELA specificities, we addressed whether there was any cross-reactivity between T-cells with these TRAV12-2-dominated specificities. The TRAV12-2 positive A2/LLW-specific clones did not respond to the ELA peptide (Fig. 8A) and the TRAV12-2 positive A2/ELA-specific clones did not respond to the LLW peptide (Fig. 8B) indicating there was no common, shared TRAV12-2-mediated mode

of antigen recognition. These functional data were supported by in silico modeling of the MEL5 TCR together with the A2/LLW complex showing unfavorable interactions (Fig. 9A). In fact, the most important difference in the interaction scheme of A2/LLW with the A2/LLW-specific YF5048 TCR versus with the A2/ELA-specific MEL5 TCR involves the CDR3 β loop. In the A2/LLW/MEL5 structural model, the Asn4 residue of the LLW peptide is situated close to the Leu98 residue of the CDR3 β loop. The contact between the backbone carbonyl of Asn4 and the side chain of Leu98 prevent the former from making any hydrogen bond with its surrounding, and is unfavorable to the binding between A2/LLW and MEL5 (Fig. 9A). In contrast, in the A2/LLW/YF5048 structural model, the key residue in CDR3 β loop is Gly97, which does not sterically hinder the backbone carbonyl of the peptide Asn4 residue (Fig. 9B). In the A2/ELA/MEL5 structure, due to a different position of the peptide backbone, the Gly4 residue of ELA (corresponding to Asn4 in LLW) is situated far from Leu98 in the CDR3 β loop, and its backbone carbonyl is unhindered by this non-polar side chain (Fig. 9C). This key difference in the CDR3 β loops explains the unfavorable interaction between MEL5 and A2/LLW, compatible with the lack of cross-reactivity observed between TRAV12-2 positive TCRs toward LLW or ELA. These data highlight the importance that the CDR3 β loop plays in TCR specificity as although this loop plays a minimal role in pMHC contact it can act to interfere with engagement.

Discussion

In this study, we analyzed the TCR repertoire of CD8⁺ T cells specific for the immunodominant A2/LLW epitope in YF-17D vaccines and controls. We revealed and quantified the TRAV12-2 bias in A2/LLW-specific CD8⁺ T cells. Various functional assays

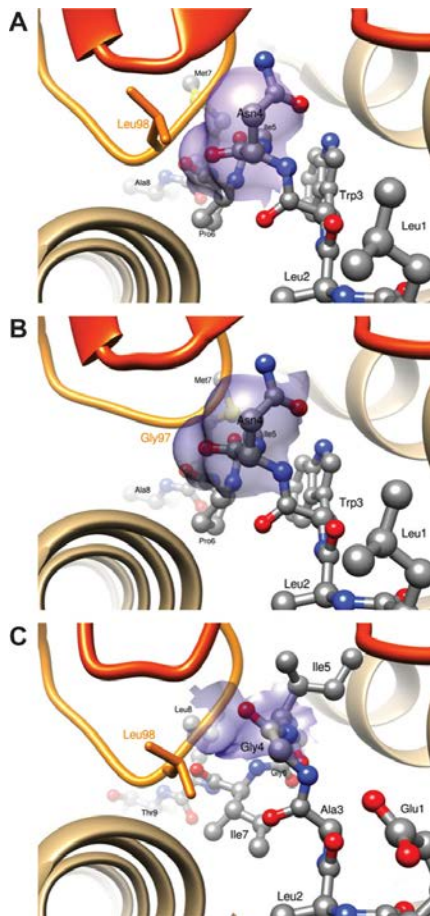


Figure 9. Calculated structures of the MEL5 and YF5048 TCRs bound to the HLA-A2/LLW peptide complex and the experimental 3D structure of the MEL5 TCR bound to the HLA-A2/ELA peptide complex. Calculated structures of the MEL5 and YF5048 TCRs bound to the HLA-A2/LLW peptide complex, (A) and (B), respectively. Experimental 3D structure of the MEL5 TCR bound to the HLA-A2/ELA peptide complex (C). Representation: α and β chains are in dark and light orange ribbons, respectively; the MHC molecule in tan ribbon; peptides in ball and stick; TCR side chains in thick lines representation, with carbon atoms colored in orange; the transparent surfaces of Asn4 (of LLW) or Gly4 (of ELA), in contact with CDR3 Leu98 (MEL5) or Gly97 (YF5048), are colored in magenta.

using T-cell clones demonstrated that TRAV12-2 does not provide a functional advantage on a per cell basis. Together with the fact that this strong TRAV12-2 bias was already present in naïve A2/LLW-specific CD8⁺ T cells before YF-17D vaccination, it rather suggests that TRAV12-2 might confer a selective advantage for high frequency and prevalence by favoring thymic output of naïve cells. We thus sought to investigate how TRAV12-2 may provide such advantage by investigating the mode of antigen binding and structural considerations of the TCR-peptide-MHC complex.

The A2/ELA epitope represents a well-known model antigen for which T cells are biased for TRAV12-2 usage [13–17]. A2/ELA-specific CD8⁺ T cells exhibit high frequency and prevalence in HLA-A*0201 healthy individuals as well as melanoma patients, showing naïve and differentiated phenotypes, respectively. Intriguingly, the binding between the MEL5 TCR expressing TRAV12-2 and the ELA peptide in complex with HLA-A*0201 occurs via dominant contacts with the CDR1 loop of TRAV12-2 [13, 18, 21, 22]. The TRAV12-2 gene is also expressed by the A6 TCR, which is specific for the A2/Tax epitope of the HTLV-1 [4]. The CDR1 α and CDR2 α loops of the A6 TCR utilize an antigen-binding mode virtually identical to that seen in the MEL5-A2/ELA complex, making contacts between the CDR1 α loop and the Tax peptide. A study in HTLV-I-Associated Myelopathy/Tropical Spastic Paraparesis (HAM/TSP) patients revealed that TRAV12-2 transcripts are predominant [23] and the frequency of naïve cells with this specificity is very high [24]. Therefore, A2/Tax-specific CD8⁺ T cells constitute another documented example of high naïve frequency associated with TRAV12-2 bias.

Unfortunately, our extensive attempts to generate a TRAV12-2 TCR A2/LLW co-crystal structure failed so we resorted to molecular modeling of this interaction taking advantage of the high sequence similarity between the A2/LLW-specific TCR YF5048 and the A2/ELA-specific TCR MEL5. Conveniently, the LLW peptide in the free A2/LLW structure we solved adopts a similar conformation to the ELA peptide in the A2/ELA/MEL5 TCR complex. Modeling showed that the YF5048 TCR α -chain positioned above the N-terminus of the peptide, making contacts predominantly with Asn4 in the middle of the peptide via the CDR1 α loop of TRAV12-2. The importance of this interaction is further supported by our results from the mutagenesis scan across the LLW peptide and CPL screen, highlighting Asn4 as a critical residue for TCR recognition by TRAV12-2 positive TCRs. Our modeling data suggests that the germline-encoded TRAV12-2 CDR1 α loop of A2/LLW-specific CD8⁺ T cells makes critical contacts with both MHC and peptide in a comparable manner to the CDR1 α loops in the MEL5 and A6 TRAV12-2 positive TCRs; the MEL5 and A6 [4, 18]. These three paralleled examples of TRAV12-2 biased responses endorse the concept that the interactions between the TCR and the antigen can rely substantially on TCR segments that already pre-exist in the germline rather than on somatic CDR3 rearrangement. However, it is important to note that this observation does not apply to all immunodominant T cell responses, as many public TCRs or immunodominant epitope-specific TCRs bind their cognate peptide predominantly via residues encoded in the CDR3 rearranged loops [6, 25].

Importantly, we showed that TCRs sharing this heritable TRAV12-2 CDR1 α component of antigen binding still preserve their respective antigen specificity. Indeed, we demonstrated that there is no cross-reactivity between the LLW and ELA specificities. Based on *in silico* modeling, the CDR3 β loop sterically hindered engagement of the non-cognate peptide. Thus, even these examples of a TRAV germline-encoded antigen binding mode are still heavily reliant on permissive sequences within the TRBV non-germline CDR3 loop.

It is intriguing that these three examples of TCRs binding their epitope with a germline component all involve the CDR1 α loop of TRAV12-2 and HLA*0201. It is conceivable that TCRs expressing the TRAV12-2 could have a selective advantage for binding to cognate antigen restricted by HLA-A*0201 or that other antigen specificities (not only restricted by HLA-A*0201) also harbor biases for certain germline-encoded TCR segments but that these have not yet been identified. The HLA-A*0201 allele and its associated antigen specificities are the most studied because HLA-A*0201 is prevalent at 30–50% in Caucasian populations and is the most prevalent HLA subtype amongst the global human population, potentially inducing a research bias [26]. Indeed, the TCR/pMHC structural database is dominated by interactions with HLA A2. More studies need to be conducted to appreciate the extent to which this phenomenon of germline-encoded TCR recognition applies to other specificities and TRAV/TRBV families.

Despite the tremendous theoretical genetic diversity of the TCR repertoire, most studies showed that the adult TCR repertoire is a consequence of a process that is far from random and TCR bias is commonly found in immune responses [27]. A specificity and/or TCR bias could reflect an evolutionary advantage during infection and other diseases. Several lines of evidence indicate that the germline-encoded TCR segments have features that promote binding to MHC molecules, suggesting co-evolution between TCR and MHC molecules [28–30]. Our data suggests that there is also co-evolution between the TCR and the cognate peptide. Indeed, we observed that TRAV12-2 TCR bias is present before YF-17D vaccination. In agreement with our functional studies on A2/LLW-specific clones, it was reported that TRAV12-2 usage in A2/ELA-specific CD8⁺ T cells was independent from functional avidity [15]. In fact, the origin of the large naïve A2/ELA-specific CD8⁺ T cell population was attributed to preferential thymic selection [31, 32]. Given that antigen recognition features a germline-encoded component, there is presumably a genetic advantage that confers higher chances for thymic output of TCR constructions involving the CDR1 α of TRAV12-2. Thus, although TRAV12-2 does not confer a functional advantage on a per cell basis, it may provide an advantage at the level of the organism by skewing the naïve CD8⁺ T cell compartment toward these specificities recognized by TRAV12-2 CDR1 α . This possibly explains the high frequency and prevalence of specificities such as A2/LLW and A2/ELA.

In summary, we discovered the TCR bias for TRAV12-2 in A2/LLW-specific CD8⁺ T cells and demonstrated that there is no functional advantage in featuring TRAV12-2 on a per cell basis. Rather, our structural modeling suggests that the germline-encoded CDR1 α loop centrally contributes to peptide binding

similar to two other TRAV12-2 positive TCR specificities. We also demonstrated that TCRs sharing this TRAV12-2 CDR1 α – mediated mode of antigen binding still preserve their own antigen specificity.

Materials and methods

Peripheral blood samples

All PBMC samples were obtained in the framework of our previously published clinical study, approved by the Human Research Ethics Committee of the Canton de Vaud (protocol 329/12) with healthy volunteers participating under written informed consent [8].

Generation of T cell clones

All A2/LLW-specific CD8⁺ T cell clones used in this study were generated in the laboratory of D. Speiser, derived from 4 healthy YF-17D (Stamaril, Sanofi Pasteur) vaccinees. Purified A2/LLW tetramer-positive populations were isolated by FACS as described [8] and cloned by limiting dilution in Terasaki plates, cultured in RPMI 1640 medium supplemented with 8% human serum and 150 U/mL recombinant human IL-2 (rIL-2). Thereafter, T cell clones were expanded by periodic restimulation with 1 μ g/mL PHA and 10⁶/mL irradiated allogeneic PBMC (30 Gy) as feeder cells. The MEL5 clone was generated in the laboratory of A. Sewell as previously described [18]. The clones HD421 2/5F and LAU1264 were generated in the laboratories of D. Speiser and N. Rufer as previously described [15].

TCR repertoire and clonotype analysis in A2/LLW-specific CD8⁺ T cell clones

Total RNA was isolated using the PicoPure RNA kit per manufacturer's instructions, and cDNA prepared and sequenced as previously described [21]. Briefly, for the V β repertoire, each cDNA sample was subjected to individual PCRs using a set of previously validated forward primers specific for the 22 TRBV subfamilies and one reverse primer specific for the corresponding C β gene segment. For the V α repertoire, we amplified and sequenced the TRAV12-2 segment using the TRAV12 (forward) and TRAC (reverse) primers. PCR amplicons of interest were sequenced from the reverse primer by FASTERIS S.A. TRAV and TRBV segments were described according to the IMGT nomenclature [33].

⁵¹Chromium release assays

The HLA-A*02⁺ human mutant cell line CEMx721.T2 (American Type Culture Collection) was used as target by labeling with

^{51}Cr for 1 h at 37°C, followed by extensive washing. Target cell killing was assessed by chromium release in the supernatant upon co-culture with CD8⁺ T cell clones (effector cells) at the Effector:Target ratio of 10:1 for 4 h at 37°C in V-bottom microwells, in presence of serial dilutions of the peptide (LLWNGPMAV or ELAGIGILTV), measured using a gamma counter and calculated as:

$$\% \text{ specific lysis} = 100 \times \frac{(\text{experimental} - \text{spontaneous release})}{(\text{total} - \text{spontaneous release})}$$

Flow cytometry

CD8⁺ T cells were first enriched from cryopreserved samples using the human CD8⁺ T cell enrichment kit from StemCell Technologies (negative selection, per manufacturer's instructions). Stainings were performed using phosphate-buffered saline with 5 mM EDTA, 0.2% bovine serum albumin, and 20 mM sodium azide [fluorescence-activated cell sorting (FACS) buffer]. Tetramer stainings were performed for 40 min at 4°C. All tetramers were purchased from TCMetrix Sàrl: HLA-A*0201/LLWNGPMAV (NS4b²¹⁴⁻²²², Yellow Fever Virus), HLA-A*0201/VMLFILAGL (NS4a⁵⁴⁻⁶², Yellow Fever Virus), HLA-B*0701/RPIDDRFGL (NS5²¹¹⁻²¹⁹, Yellow Fever Virus), HLA-A*0201/GLCTLVAML (BMFL12⁸⁰⁻²⁸⁸, Epstein Barr Virus), HLA-A*0201/NLVPMVATV (pp65⁴⁹⁵⁻⁵⁰³, Cytomegalovirus), HLA-A*0201/ELAGIGILTV (Melan-A²⁶⁻³⁵ (A27L), Melanoma). Surface antibody staining was then performed, followed by staining with LIVE/DEAD-Fixable-Aqua (Invitrogen), each step at 4°C for 30 min. Cells were fixed overnight in 0.36% formaldehyde (supplemented with 2% glucose and 5 mM sodium azide). Samples were acquired using a Gallios flow cytometer (Beckman Coulter, three-laser configuration). The data were processed with FlowJo (Tree Star Inc., v9.5.2). Samples with antigen-specific populations below 0.001% tetramer-positive cells in total CD8⁺ T cells were considered negative and populations consisting of less than 20 events were not considered eligible for further analysis.

Intracellular cytokine staining assay

A2/LLW-specific CD8⁺ T cell clones were stimulated with LLW peptide-loaded T2 cells at the E:T cell ratio of 1:2 for 4 h at 37°C in the presence of Brefeldin-A (Sigma-Aldrich) and anti-CD107a-FITC antibody (BD Biosciences). Then, cells were stained with anti-CD8-APC-AF750 antibody (Beckman Coulter) at 4°C for 30 min. After washing in PBS, cells were incubated with LIVE/DEAD-Fixable-Aqua (Invitrogen) at 4°C for 30 min, and fixed at 4°C overnight (0.36% formaldehyde buffer). Cells were washed and stained intracellularly with anti-IFN γ -PC7, anti-TNF α -A700 and anti-IL-2-PerPCP-Cy5.5 antibodies (BD Biosciences) in FACS buffer with 0.1% saponin for 30 min at 4°C. Samples were acquired and data processed as described above.

NTAmer staining and dissociation kinetic measurements

Dually labeled pMHC multimers built on NTA-Ni²⁺-His-tag interactions called NTAmers (synthesized by TCMetrix Sàrl) were used for dissociation kinetic measurements [34, 35]. Stainings with dually PE- and Cy5-labeled A2/LLW-specific NTAmers and data analysis were done as previously described [34, 36]. Briefly, staining was measured at 4°C using a thermostat device on a SORP-LSR II flow cytometer (BD Biosciences). Following 30 s of baseline acquisition, imidazole (100 mM) was added. PE and Cy5 fluorescence were measured during the following 5 min. Data were processed using the kinetic module of the FlowJo software (v.9.7.6; Tree Star), and corrected mean fluorescence intensity values were plotted and analyzed using the GraphPad Prism software (v.6; GraphPad).

Combinatorial peptide library (CPL) scans

The nonamer CPL contains a total of 4.8×10^{11} ((9+19) \times 19⁸) different nonamer peptides divided into 180 sub-libraries with each containing 19⁸ different nonamer peptides in approximately equimolar concentrations (Pepsan, Lelystad, The Netherlands) [37]. Each of the 180 sub-libraries has a fixed amino acid residue but all other positions are degenerate. Cysteine was excluded from all degenerate positions to avoid oxidation, but was included at the fixed positions. Prior to the assay, CD8⁺ T cell clones were washed and rested overnight in R5 medium (RPMI 1640 supplemented with 100 units/mL penicillin, 100 $\mu\text{g}/\text{mL}$ streptomycin, 2 mM l-glutamine, and 5% heat-inactivated fetal calf serum (all Invitrogen)). For CPL screening, 6×10^4 C1R A2 cells [38] were pulsed with each sub-library at 100 $\mu\text{g}/\text{mL}$ in duplicate for 2 h at 37°C. After peptide pulsing, 3×10^4 CD8⁺ T cells were added, and the cultures were incubated overnight at 37°C. Subsequently, the supernatant was harvested and assayed for MIP-1 β by ELISA according to the manufacturer's instructions (R&D Systems).

Protein expression, refolding, and purification

HLA A*0201 α -chain and β 2m were expressed separately, without post-translational modification, as insoluble inclusion bodies (IBs) in competent Rosetta (DE3) *Escherichia coli* cells, using 0.5 M IPTG to induce expression as thoroughly described recently [39]. Briefly, for a 1L pMHC refold, 30 mg HLA-A*0201 α -chain was mixed with 30 mg β 2 m and 4 mg peptide at 37°C for 15 min with 10 mM DTT. This mixture was then added to cold refold buffer (50 mM Tris, pH8, 2 mM EDTA, 400 mM L-arginine, 6 mM cysteamine hydrochloride, and 4 mM cystamine). Refolds were mixed at 4°C for > 6 h. Dialysis was performed against 10 mM TRIS, pH8.1, until the conductivity of the refolds was less than two millisiemens per centimeter. The refolds were then filtered and purified first by ion exchange using a Poros50HQTM column (GE Healthcare, Buckinghamshire, U.K.) and second by gel filtration directly into crystallization buffer (10 mM Tris pH8.1

and 10 mM NaCl) or PBS buffer (137 mM NaCl, 3 mM KCl, 8 mM Na_2HPO_4 , 1 mM KH_2PO_4) using a Superdex200HRM column (GE Healthcare, Buckinghamshire, U.K.). Protein quality was analyzed by Coomassie-stained SDS-PAGE, either under non-reducing or reducing conditions. HLA-A*0201 was refolded with the peptides LLWNGPMAV (A2/LLW) or LLWAGPMAV (A2/LLW-4A).

Crystallization, diffraction data collection, and model refinement

All protein crystals were grown at 18°C by vapor diffusion via the “sitting drop” technique. 200 nL of each pMHC (20 mg/mL) in crystallization buffer was added to 200 nL of reservoir solution. A2/LLW crystals were grown in 0.1 M Hepes, pH7, 0.2 M ammonium sulphate, 20%PEG 4000. All crystals were soaked in 30% ethylene glycol before cryo-cooling. All crystallization screens and optimization experiments were completed using an Art-Robbins Gryphon dispensing robot (Alpha Biotech Ltd., UK). Data were collected at 100 K at the Diamond Light Source (Oxfordshire, UK) as described previously [40]. All data sets were collected at a wavelength of 0.98 Å using an ADSC Q315 CCD detector. Reflection intensities were estimated with the XIA2 package, and the data were scaled, reduced, and analyzed with the SCALA and CCP4 package. Structures were solved with molecular replacement using PHASER. A solution could be obtained with a search model taken from Protein Data Bank entry 5EU5. Sequences were adjusted with COOT, and the models were refined with REFMAC5. Graphical representations were prepared with PyMOL. The reflection data and final model coordinates were deposited in the Protein Data Bank (PDB code: 5N6B).

Measuring the thermal stability of HLA-A*0201-peptide complexes

Thermal stability of A2/peptide complexes was assessed by CD spectroscopy monitoring the change of ellipticities Θ at 218nm where the spectra exhibit a minimum. Data were collected on an Aviv 215 spectrometer (Aviv Biomedical Inc., Lakewood, NJ) equipped with a thermostated cell holder using a 1 mm quartz cell. Proteins were dissolved in PBS at $c = 3.5 \mu\text{M}$. Denaturation was monitored from 4°C up to a temperature when protein precipitation occurred using a gradient of 0.5°C/min. Melting curves were analyzed assuming a two-state native (N) to denatured (D) transition $\text{N}_3 \leftrightarrow 3\text{D}$ with the melting temperature and van't Hoff's enthalpy at the midpoint of the transition as fitting parameters [41, 42].

Modeling the TCR-p-MHC complex

The 3D structure of the TRAV12-2/TRBV9 TCR in complex with HLA-A2 and the LLWNGPMAV peptide was modeled from three experimental structures: 3HG1 [18] and 4QOK [43], containing a complex between the TRAV12-2/TRBC1 TCR in complex with

HLA-A2 and the ELAGIGILTV or EAAGIGILTV peptides, respectively, and the experimental structure obtained in this study for the complex between HLA-A2 and the LLWNGPMAV peptide. The sequence alignment between TRBV9 and TRBC1 was performed using the MUSCLE program [44]. The sequence identity between the variable part of the TRBV9 and TRBC1 TCR beta chains is 30%. Based on this sequence alignment, the model was obtained using the Modeller program [45, 46]. 1000 models were generated by satisfaction of spatial restraints through minimization and simulated annealing, and the model with the best Modeller objective function was retained. Molecules were visualized and analyzed using UCSF Chimera [47].

The model of A2/LLW in complex with the MEL5 TCR was obtained with the Modeller program, following the method described above to obtain the structural model of A2/LLW with the YF5048 TCR. In this case, however, we used our experimental structure of the A2/LLW as a template for the HLA/peptide domain and the experimental structure of the complex between A2/ELA and MEL5 (PDB code: 3HG1) as a template for the MEL5 TCR.

Acknowledgements: We thank staff at the Flow Cytometry Facility of LICR@UNIL for providing facilities and support, Philippe Gannon for instructions to perform the TCR repertoire analyses, Charlotte Soneson for the microarray analysis of TRAV12-2, Bruce MacLachlan for data collection and processing at the Diamond Light Source, Laura Carratero Iglesias and Nathalie Rufer for the generation of the A2/ELA-specific CD8^+ T cell clones, Werner Held for discussion and support, and Nicole Montandon for technical help.

This project was supported by Ludwig Cancer Research (N.Y., U.S.A.), the Swiss National Science Foundation (320030.152856 and CRSII3.160708), SwissTransMed (KIP 18), the Swiss Cancer League (3507-08-2014) and Alfred and Annemarie von Sikk (Switzerland). A.K.S. is a Wellcome Trust Senior Investigator. The funders had no role in study design, data collection and analysis, decision to publish, or preparation of the manuscript. The authors would also like to thank Diamond Light Source for beamtime (proposals MX10462), and the staff of beamlines DLS-I03 for assistance with crystal testing and data collection.

Conflict of interest: The authors declare no commercial or financial conflict of interest.

References

- 1 Lefranc, M. P., Giudicelli, V., Ginestoux, C., Jabado-Michaloud, J., Folch, G., Bellahcene, F., IMGT[®], the international ImMunoGeneTics information system[®]. *Nucleic Acids Res.* 2009. 37(SUPPL. 1): 1006–1012.

- 2 Rudolph, M. G., Luz, J. G. and Wilson, I. A., Structural and thermodynamic correlates of T cell signaling. *Annu. Rev. Biophys. Biomol. Struct.* 2002. **31**: 121–149.
- 3 Bankovich, A. J. and Garcia, K. C., Not Just Any T Cell Receptor Will Do. *Immunity* 2003. **18**: 7–11.
- 4 Garboczi, D. N., Ghosh, P., Utz, U., Fan, Q. R., Biddison, W. E. and Wiley, D. C., Structure of the complex between human T-cell receptor, viral peptide and HLA-A2. *Nature* 1996 Nov 14. **384**: 134–141.
- 5 Cole, D. K., Yuan, F., Rizkallah, P. J., Miles, J. J., Gostick, E., Price, D. A. et al., Germ line-governed recognition of a cancer epitope by an immunodominant human T-cell receptor. *J. Biol. Chem.* 2009 Oct 2. **284**: 27281–27289.
- 6 Rossjohn, J., Gras, S., Miles, J. J., Turner, S. J., Godfrey, D. I. and McCluskey, J., T cell antigen receptor recognition of antigen-presenting molecules. *Annu. Rev. Immunol.* 2015. **33**: 169–200.
- 7 Miles, J. J., Douek, D. C. and Price D. A., Bias in the $\alpha\beta$ T-cell repertoire: implications for disease pathogenesis and vaccination. *Immunol. Cell Biol.* 2011. **89**(September 2010): 375–387.
- 8 Marraco, S. A. F., Soneson, C., Cagnon, L., Gannon, P. O., Allard, M., Maillard, S. A. et al., Long-lasting stem cell-like memory CD8+ T cells with a naïve-like profile upon yellow fever vaccination. *Sci. Transl. Med.* 2015. **7**: 282ra48.
- 9 Akondy, R. S., Monson, N. D., Miller, J. D., Edupuganti, S., Teuwen, D., Wu, H. et al., The yellow fever virus vaccine induces a broad and polyfunctional human memory CD8+ T cell response. *J. Immunol.* 2009. **183**: 7919–7930.
- 10 Blom, K., Braun, M., Ivarsson M. A., Gonzalez, V. D., Falconer, K., Moll, M. et al., Temporal dynamics of the primary human T cell response to yellow fever virus 17D as it matures from an effector- to a memory-type response. *J. Immunol.* 2013. **190**: 2150–2158.
- 11 de Melo, A. B., Nascimento, E. J. M., Braga-Neto, U., Dhalia, R., Silva, A. M., Oelke, M. et al., T-cell memory responses elicited by Yellow Fever vaccine are targeted to overlapping epitopes containing multiple HLA-I and -II binding motifs. *PLoS Negl. Trop. Dis.* 2013. **7**.
- 12 Pittet, B. M. J., Valmori, D., Dunbar, P. R., Speiser, D. E., Liénard, D., Lejeune, F. et al., T cells in a large proportion of human histocompatibility leukocyte antigen (HLA)-A2 individuals. *J. Exp. Med.* 1999. **190**: 705–715.
- 13 Neller, M. A., Ladell, K., McLaren, J. E., Matthews, K. K., Gostick, E., Pentier, J. M. et al., Naïve CD8+ T-cell precursors display structured TCR repertoires and composite antigen-driven selection dynamics. *Immunol. Cell Biol.* 2015. **93**: 625–633.
- 14 Mantovani, S., Palermo, B., Garbelli, S., Campanelli, R., Robustelli Della Cuna, G., Gennari, R. et al., Dominant TCR-alpha requirements for a self antigen recognition in humans. *J. Immunol.* 2002. **169**: 6253–6260.
- 15 Dietrich, P.-Y., Le Gal, F.-A., Dutoit, V., Pittet, M. J., Trautman, L., Zippelius, A. et al., Prevalent role of TCR alpha-chain in the selection of the preimmune repertoire specific for a human tumor-associated self-antigen. *J. Immunol.* 2003. **170**: 5103–5109.
- 16 Pittet, M. J. M. J., Gati, A., Le Gal, F.-A., Bioley, G., Guillaume, P., de Smedt, M. et al., Ex vivo characterization of allo-MHC-restricted T cells specific for a single MHC-peptide complex. *J. Immunol.* 2006. **176**: 2330–2336.
- 17 Serana, F., Sottini, A., Caimi, L., Palermo, B., Natali, P. G., Nisticò, P. et al., Identification of a public CDR3 motif and a biased utilization of T-cell receptor V beta and J beta chains in HLA-A2/Melan-A-specific T-cell clonotypes of melanoma patients. *J. Transl. Med.* 2009. **7**: 21.
- 18 Cole, D. K., Yuan, F., Pierre, J., Miles, J. J., Gostick, E., Price, D. A. et al., Germ line-governed recognition of a cancer epitope by an immunodominant human T-cell receptor. *J. Biol. Chem.* 2009. **284**: 27281–27289.
- 19 Fuertes, S. A., Soneson, C., Delorenzi, M. and Speiser, D. E., Genomics data genome-wide RNA profiling of long-lasting stem cell-like memory CD8 T cells induced by Yellow Fever vaccination in humans. *Genom. Data* 2015. **5**: 297–301.
- 20 Trautmann, L., Labarrière, N., Jotereau, F., Karanikas, V., Gervois, N., Connerotte, T. et al., Dominant TCR V α usage by virus and tumor-reactive T cells with wide affinity ranges for their specific antigens. *Eur. J. Immunol.* 2002. **32**: 3181–3190.
- 21 Wieckowski, S., Baumgaertner, P., Corthesy, P., Voelter, V., Romero, P., Speiser, D. E. et al., Fine structural variations of alphabetaTCRs selected by vaccination with natural versus altered self-antigen in melanoma patients. *J. Immunol.* 2009. **183**: 5397–5406.
- 22 Derre, L., Ferber, M., Touvre, C., Devevre, E., Zoete, V., Leimgruber, A. et al., A novel population of human melanoma-specific CD8 T cells recognizes melan-AMART-1 immunodominant nonapeptide but not the corresponding decapeptide. *J. Immunol.* 2007. **179**: 7635–7645.
- 23 Elovaara, I., Utz, U., Smith, S. and Jacobson, S., Limited T cell receptor usage by HTLV-1 tax-specific, HLA class I restricted cytotoxic T lymphocytes from patients with HTLV-1 associated neurological disease. *J. Neuroimmunol.* 1995. **63**: 47–53.
- 24 Elovaara, I., Koenig, S., Brewah, A. Y., Woods, R. M., Lehky, T. and Jacobson, S., High human T cell lymphotropic virus type 1 (HTLV-1)-specific precursor cytotoxic T lymphocyte frequencies in patients with HTLV-1-associated neurological disease. *J. Exp. Med.* 1993. **177**: 1567–1573.
- 25 Li, H., Ye, C., Ji, G. and Han, J., Determinants of public T cell responses. *Cell Res.* 2012. **22**: 33–42.
- 26 Browning, M. and Krausa, P., Genetic diversity of HLA-A2: evolutionary and functional significance. *Immunol. Today* 1996. **165**–170.
- 27 Turner, S. J., Doherty, P. C., McCluskey, J. and Rossjohn, J., Structural determinants of T-cell receptor bias in immunity. *Nat. Rev. Immunol.* 2006. **6**: 883–894.
- 28 Feng, D., Bond, C. J., Ely, L. K., Maynard, J. and Garcia, K. C., Structural evidence for a germline-encoded T cell receptor-major histocompatibility complex interaction "codon." *Nat. Immunol.* 2007. **975**–983.
- 29 Scott-Brown, J. P., Crawford, F., Young, M. H., Kappler, J. W., Marrack, P. and Gapin, L., Evolutionarily conserved features contribute to $\alpha\beta$ T cell receptor specificity. *Immunity* 2011. **35**: 526–535.
- 30 Piepenbrink, K. H., Blevins, S. J., Scott, D. R. and Baker, B. M., Restriction in a T cell receptor interface. *Nat. Commun.* 2013. **4**: 1–9.
- 31 Zippelius, A., Pittet, M. J., Batard, P., Rufer, N., De Smedt, M., Guillaume, P. et al., Thymic selection generates a large T cell pool recognizing a self-peptide in humans. *J. Exp. Med.* 2002. **195**.
- 32 Pinto, S., Sommermeyer, D., Michel, C., Wilde, S., Schendel, D., Uckert, W. et al., Misinitiation of intrathymic MART-1 transcription and biased TCR usage explain the high frequency of MART-1-specific T cells. *Eur. J. Immunol.* 2014. **44**: 2811–2821.
- 33 Lefranc, M. P., Nomenclature of the human T cell receptor genes. *Curr. Protoc. Immunol.* 2001.
- 34 Schmidt, J., Guillaume, P., Irving, M., Baumgaertner, P., Speiser, D. and Luescher, I. F., Reversible major histocompatibility complex I-peptide multimers containing Ni2+-nitrilotriacetic acid peptides and histidine tags improve analysis and sorting of CD8+ T cells. *J. Biol. Chem.* 2011. **286**: 41723–41735.
- 35 Schmidt, J., Dojcinovic, D., Guillaume, P. and Luescher, I., Analysis, isolation, and activation of antigen-specific CD4+ and CD8+ T cells by soluble MHC-peptide complexes. *Front Immunol.* 2013. **4**: 1–14.
- 36 Hebeisen, M., Schmidt, J., Guillaume, P., Baumgaertner, P., Speiser, D. E., Luescher, I. et al., Identification of rare high-avidity, tumor-reactive

- CD8⁺ T cells by monomeric TCR-ligand off-rates measurements on living cells. *Cancer Res.* 2015. 75: 1983–1991.
- 37 Wooldridge, L., Laugel, B., Ekeruche, J., Clement, M., van den Berg, H. A., Price, D. A. et al., CD8 controls T cell cross-reactivity. *J. Immunol.* 2010. 185: 4625–4632.
- 38 Purbhoo, M. A., Boulter, J. M., Price, D. A., Vuidepot, A., Hourigan, C. S., Dunbar, P. R. et al., The human CD8 coreceptor effects cytotoxic T cell activation and antigen sensitivity primarily by mediating complete phosphorylation of the T cell receptor α chain. *J. Biol. Chem.* 2001. 276: 32786–32792.
- 39 MacLachlan, B. J., Greenshields-Watson, A., Mason, G. H., Schauenburg, A. J., Bianchi, V., Rizkallah, P. J. et al., Using X-ray crystallography, biophysics, and functional assays to determine the mechanisms governing T-cell receptor recognition of cancer antigens. *J. Vis. Exp.* 2017. 54991.
- 40 Motozono, C., Pearson, J. A., De Leenheer, E., Rizkallah, P. J., Beck, K., Trimby, A. et al., Distortion of the major histocompatibility complex class I binding groove to accommodate an insulin-derived 10-mer peptide. *J. Biol. Chem.* 2015 290: 18924–18933.
- 41 Greenfield, N. J., Analysis of circular dichroism data. *Methods in Enzymology* 2004 383: 282–317.
- 42 Fuller, A., Wall, A., Crowther, M. D., Lloyd, A., Zhurov, A., Sewell, A. K. et al., Thermal stability of heterotrimeric pMHC proteins as determined by circular dichroism spectroscopy. *Bio-protocol* 2017 7: e2366.
- 43 Madura, F., Rizkallah, P. J., Holland, C. J., Fuller, A., Bulek, A., Godkin, A. J. et al., Structural basis for ineffective T-cell responses to MHC anchor residue-improved “heteroclitic” peptides. *Eur. J. Immunol.* 2015. 45: 584–591.
- 44 Edgar, R. C., MUSCLE: multiple sequence alignment with high accuracy and high throughput. *Nucleic Acids Res.* 2004 32: 1792–1797.
- 45 Eswar, N., Webb, B., Marti-Renom, M. A., Madhusudhan, M. S., Eramian, D., Shen, M. et al., Comparative protein structure modeling using MODELLER. *Current Protocols in Protein Science [Internet]*. <http://doi.org/10.1002/0471140864.ps0209s50>
- 46 Sali, A. and Blundell, T. L., Comparative protein modelling by satisfaction of spatial restraints. *J. Mol. Biol.* 1993. 234: 779–815.
- 47 Pettersen, E. F., Goddard, T. D., Huang, C. C., Couch, G. S., Greenblatt, D. M., Meng, E. C. et al., UCSF chimera—a visualization system for exploratory research and analysis. *J. Comput. Chem.* 2004 Oct 1. 25: 1605–1612.

Full correspondence: Dr. Silvia A. Fuertes Marraco, Centre Hospitalier Universitaire Vaudois & Université de Lausanne, Département d’Oncologie, Biopôle 3, Chemin des Boveresses 155, Epalinges, Vaud, Switzerland 1066
e-mail: silvia.fuertesmarraco@unil.ch

Received: 13/4/2017

Revised: 15/8/2017

Accepted: 25/9/2017

Accepted article online: 3/10/2017

APPENDIX 3: Human stem cell-like memory CD8 T cells establish early in the acute response to Yellow Fever virus vaccination

Human stem cell-like memory CD8 T cells establish early in the acute response to Yellow Fever virus vaccination

Running title : SCM CD8 T appear in the acute phase

Silvia A. Fuertes Marraco^{1*}, Amandine Bovay¹, Sina Nassiri^{1,2}, H el ene Maby-El Hajjami¹, Hajer Ouertatani-Sakouhi¹, Werner Held¹, and Daniel E. Speiser¹

1 Department of Oncology, Centre Hospitalier Universitaire Vaudois (CHUV) - University of Lausanne, Epalinges, Switzerland

2 Bioinformatics Core facility, The Swiss Institute of Bioinformatics (SIB), Lausanne, Switzerland

*** Correspondence :**

Silvia. A Fuertes Marraco
D epartement d'Oncologie CHUV-UNIL
AA-82, Biop ole 3, Centre de Laboratoires d'Epalinges
Chemin des Boveresses 155, CH-1066 Epalinges
silvia.fuertes@chuv.ch
Tel. + 41 21 692 5955

Abstract

The establishment of long-term memory is a fundamental feature of the cytotoxic CD8 T cell response. Yet when do memory cells arise, especially in humans, is poorly documented, the pathways of effector / memory cell differentiation being largely debated. Based on a cross-sectional study, we previously reported that the live-attenuated Yellow Fever virus vaccine YF-17D induces a stem cell-like memory (SCM) CD8 T cell population persisting for at least 25 years. Here we present longitudinal data revealing that CD8 T cells with an activated (I would remove “activated”) SCM T cell phenotype are distinctly detectable within two weeks following YF-17D vaccination (in the acute phase). These cells, which express the central memory transcription factor T cell factor-1 (TCF1), preferentially persist, consistent with the role of TCF1 in memory establishment. By performing t-distributed Stochastic Neighbour Embedding of flow cytometry data, we obtained a rich time-lapse representation of the dynamics of the CD8 T cell response: SCM cells appear early (2 weeks?) and remain closely related to the baseline Naïve cells (not clear what you mean, their abundance?), while effector cells burst out of baseline and gradually contract after the peak of the response. Thus we observe cells with memory phenotypes very early in the response. As opposed to models where memory cells develop from effector cells, our data support differentiation models where long-term memory cells are established by the early decision to retain proximity to the Naïve state in a memory-dedicated pool of cells.

Keywords: Stem cell-like memory, CD8 T cell, Yellow Fever virus, YF-17D vaccination, acute phase, T cell factor 1,

Introduction

The capacity to remember a pathogen and effectively protect the organism against it long-term is a fundamental property of the adaptive immune response. This is also relevant for tumour immunology since it is now well established that strong and long-lasting cytotoxic CD8 T cell responses correlate with better prognosis for cancer patients (1), and that innovative immunotherapies can defeat various types of metastatic cancers with unprecedented long-term success (2).

Once naïve T cells are primed upon antigenic encounter, the various functionalities of CD8 T cells are ensured by a heterogeneity of cells, with varying degrees of memory and effector functions. Initially classified into only two functional types (effector or memory), the heterogeneity of CD8 T cells has been more comprehensively defined over the last decade. The venue of transcriptomic and epigenetic profiling complementing functional assays has revealed a continuum of phenotypes with varying longevity, self-renewal, proliferative potential, expression of homing, costimulatory and transcription factors, and functions including cytokine secretion and cytotoxicity (3-7). Globally, effector cells display cytotoxicity and readily produce cytokines, while memory cells resemble more the naïve cells based on their high proliferative capacity and potential to generate effector progeny, together with long-term persistence and self-renewal (so called stemness) (although the latter are not features of naïve cells...). Traditionally, surface markers (including distinct homing molecules) and transcription factors have been used to define the various CD8 T cell subsets. In humans, classic subsets are primarily identified on the basis of surface C-C motif chemokine receptor 7 (CCR7) and CD45RA expression, with naïve cells being CCR7⁺ CD45RA⁺, the central memory (CM) being CCR7⁺ CD45RA⁻, and the CCR7⁻ effector memory subsets split into CD45RA⁻ effector memory (EM) and effector memory CD45RA⁺ (EMRA) cells (8). More recently, the stem cell-like memory (SCM) subset was revealed among CCR7⁺ CD45RA⁺ cells (within the classic Naïve gate) on the basis of positive expression of markers such as CD58, CXCR3, IL2Rb and the more prominently used CD95 marker (9,10).

Along with the increasingly comprehensive characterization of the heterogeneity of CD8 T cell phenotypes and functions, several models have emerged to describe the differentiation pathways of antigen-experienced CD8 T cells, starting when Naïve cells are primed, to explain the genealogy of memory and effector cells. The initially proposed model of CD8 T cell differentiation is linear: it suggests a sequential differentiation of naïve cells, first into effectors that predominate in the acute phase, followed by differentiation of a fraction of effector cells into memory cells, as the response contracts and most effector cells die out or become terminally senescent. In the mouse system, the linear model evolved to describe early effector cells (EEC) that give rise to two types of effector cells: one short-lived effector cells (SLEC) and another memory precursor effector cells (MPEC) – long-term memory predominantly originates from MPECs (11-13). Alternative models have proposed that memory cells differentiate without an obligatory acute effector stage (it is contradictory if you use effector twice). For instance, the so-called bifurcative model proposes an immediate divergence from the naïve cell: in a first asymmetric cell division, the antigen-primed naïve cell splits into distinct daughter cells, each with a distinct memory or effector fate (14,15). More recently, the proposed models integrate the large and gradual heterogeneity of memory and effector cells, based on the observed continuum of whole transcriptome and epigenetic profiles (3,16,17). These suggest that CD8 T cells may undergo progressive differentiation, from the naïve, to the SCM, CM, EM and EMRA cell stages, and all the various subsets may give rise to effector progeny or show effector function in their activated state (7,18).

To date, it is still controversial whether memory results from an early decision to diverge from effector fate or whether a fraction of effectors gives rise to memory cells. Studies in the last year continued debating whether long-lived memory cells display an epigenetic imprint that would correspond to an effector phenotype past (19,20) or whether stemness (highest memory potential) is preserved epigenetically in antigen-primed naïve cells that become memory cells and it is the silencing of memory / stemness genes that drives effector differentiation (21). One limitation is that nascent memory cells are not easily detectable or may not be distinguished from effector cells in the activated, acute phase (22). Markers such as IL7Ra have been highlighted to identify the precursors of long-lived memory cells (the MPECs in mice), distinct from the majority of activated cells that die after the acute phase (23).

One major factor that is essential to sustain central memory formation is the transcription factor T cell factor 1 (TCF1, encoded by the *TCF7* gene) (24-27). TCF1 is expressed at high levels in Naïve and memory but not in effector cells (4,28,29), and is epigenetically regulated during CD8 T cell differentiation (3,30) as one major gene involved in effector differentiation arrest and maintenance of stemness (21,31,32). Recently, we showed that inflammatory cytokines suppress TCF1 and facilitate effector differentiation (33).

•

Overall, studies on the identification of precursors and discernment of early fate decisions rely on genetic manipulation and the adoptive transfer or deletion of cells to test their progeny potential, which is limited to mouse models. Yet a major level of complexity in the study of CD8 T cell differentiation is the idiosyncrasies in mouse *versus* human systems. While fundamental phenomena may be shared, in practice, there is a basic difference in the markers used to classify CD8 T cell subsets. Therefore, and in complement to the ontological questions that can readily be addressed in the mouse experimental system, the evidence that originates from the study of human CD8 T cells is uniquely valuable. One human model that has been particularly informative to fully apprehend optimal immunogenicity in humans, including the study of CD8 T cell differentiation, is the acute response to the live-attenuated Yellow Fever virus vaccine YF-17D (34,35). We previously found that YF-17D vaccination induces a population of stem cell-like memory cells and showed that these memory cells last for decades (36,37). However, the earliest time-point after vaccination that we studied was 3.6 months, well after the acute phase that is the first 2 weeks of the response. There is currently no information on when SCM cells can be detected during an immune response in humans. Here, we aimed to study the distribution and dynamics of human CD8 T cell subsets during the first few days to months after YF-17D vaccination based on a longitudinal clinical study protocol (i.e. including the acute phase of the response), combined with analysis in the decade-long-term based on our previous cross-sectional study cohort.

Materials and Methods

Study design, population and ethics statement

Samples used in this study originated from peripheral blood of healthy volunteers aged 18 to 65 years that participated in one of two study protocols on YF-17D vaccination (Stamaril, Sanofi Pasteur). Donors from the first cohort “YF1” (study protocol 329/12) had a history of YF-17D vaccination ranging from 3.6 months to 23.74 years (cross-sectional) and donated blood in the local Blood Transfusion Center (Service régional vaudois de transfusion sanguine, 1066 Epalinges), as we described previously ((36). Donors from the second cohort “YF2” (study protocol 324/13) were in the prospect of receiving the YF-17D vaccine in view of travelling to endemic areas and participated to longitudinal sampling before and several time-points after YF-17D vaccination, in collaboration with the local vaccine center Centre de vaccination et de médecine des voyages (Policlinique Médicale Universitaire (PMU), Lausanne). The full metadata details of the two cohorts are listed in Table S1. The study protocols were approved by the Swiss Ethics Committee on research involving humans of the Canton of Vaud (CH). All participants provided written informed consent.

Peripheral blood collection and processing

Peripheral blood samples were collected and immediately processed for cryopreservation awaiting experimental use. Peripheral blood mononuclear cells (PBMC) were obtained from anti-coagulated whole blood diluted 1:1 in phosphate buffered saline (PBS) and overlaid on Lymphoprep for density gradient fractionation (30 min at 400g without break) and were cryopreserved in complete RPMI 1640 supplemented with 40% fetal calf serum (FCS) and 10% dimethyl sulfoxide. Plasma samples were obtained from the supernatant of EDTA-coated blood tubes after centrifugation at 1'000g for 15 min at RT followed by a second centrifugation at 8'000g for 10 min at 4°C.

Assay to determine copy numbers of the Yellow Fever virus YF-17D

Yellow Fever virus (YFV) load was quantified using 1ml of plasma from EDTA-anticoagulated blood based on a Taqman Real-time PCR assay to detect YFV genome copies as previously described (38).

Flow cytometry staining, acquisition and analysis

On the day of the experiment, frozen vials of PBMC were thawed in RPMI containing 10 ug / ml of DNase I (Sigma) and resuspended in fluorescence-activated cell sorting buffer (FACS buffer: PBS with 5mM EDTA, 0.2% Bovine Serum Albumin and 0.2% sodium azide). Thawed PBMC were subjected to CD8⁺ T cell selection using the negative enrichment kit from Stem Cell. CD8 T cell-enriched samples were then stained for flow cytometry according to target panels and cytometers as summarized in Table S2 and with reagents as listed in Table S3. Stainings were made in sequence depending on the target, as follows: 1) first, cells were stained with multimers for 30 min at 4°C in FACS buffer and washed in FACS buffer, 2) surface antibodies were added in FACS buffer and washed with PBS prior to 3) staining with fixable viability dye in PBS and washed with PBS, 4) cells were then fixed overnight at 4°C and washed in permeabilisation buffer before 5) intracellular staining in permeabilisation buffer at 4°C (the primary rabbit anti-TCF1 and the secondary fluorochrome-conjugated anti-rabbit IgG were stained in two subsequent steps). The fixation and permeabilisation buffers were from the Foxp3 staining kit from eBioscience. Washes were made by centrifugation at 450g for 7 min. Samples were resuspended in FACS buffer for acquisition. For samples in the YF2 study, the baseline sample vial originally contained 1.5 x 10⁷ frozen PBMC and the remainder of time-points' vials contained 10⁷ frozen PBMC – the complete volume of stained samples was finally acquired. Cytometers were the Gallios (Beckman Coulter, 3 laser, 10-color) and the LSR II Special Order Research Product (Beckton Dickinson, 5 laser including UV, 13- or 14-color). Before each acquisition, the cytometer setup and tracking (CST) was ran in order to normalize channel voltages across experiments using the same instrument configuration and experimental layout. Flow cytometry FCS data files were analyzed in FlowJo 9.7.7, except for the analyses using t-distributed Stochastic Neighbor Embedding for which the corresponding plugin in FlowJo 10.4.2 was used. Downsampling, concatenation or exports of specific populations and samples were performed as indicated in the figure legends also in FlowJo 10.4.2. For the longitudinal tSNE analyses of A2/LLW-specific CD8 T cells, all single live A2/LLW-

specific CD8 T cell events of the longitudinal series were concatenated and thus are represented in proportions corresponding to the original numbers of PBMC thawed, which are equal across time-points (corresponding to 10^7 PBMC thawed) except for the baseline which is 1.5-fold larger (1.5×10^7 PBMC thawed). The detection threshold for multimer positive populations was 0.01% of total CD8 T cells and at least 10 events (horizontal dotted line in Figure 1 C and D). The positivity threshold for each marker was set according to distinct negative and positive populations in bulk CD8 T in resting and/or activated samples; for the indirect TCF1 staining, the negative signal was further validated with secondary antibody-only controls.

Quantifications and statistical analyses

Flow cytometry data analyzed with FlowJo was quantified based on tabulated exports of the frequencies and events in the gates of interest. Calculations and data display thereafter was performed using the softwares Microsoft Excel 15.21.1, GraphPad prism 7.0c and SPICE v5.35 (for co-expression analyses). Statistical values were obtained as detailed in each figure legend (on the basis of normality tests), where trend = $p > 0.05$ and < 0.10 , * = $p < 0.05$, ** = $p < 0.01$, *** = $p < 0.001$ and ns = not significant. For the SPICE analyses, p-values originate from the built-in t-test in SPICE using 10'000 permutations. Longitudinal modeling of the flow cytometry data was achieved using linear mixed effects splines. In brief, linear splines with 3 internal knots and a random intercept was fit using the lme4 package in R (39). Pairwise comparison of fits to individual subsets was performed by fitting a null model to pooled data from the two subsets, a full model with distinct fits capturing the trends in each subset, and using the likelihood ratio test to assess the difference between these two nested models using the Chi square distribution. Resulting p-values were further adjusted for multiple comparisons using the Bonferroni method.

Results

CD8 T cells with a CCR7+ memory phenotype expand in the acute phase of YF-17D vaccination

In order to study the early dynamics of CD8 T cell differentiation, we recruited healthy volunteers that were going to receive the YF-17D vaccine in order to obtain peripheral blood samples before and at several time-points after vaccination (including early days and up to 6 months after vaccination). The study schedule and cohort are detailed in Table S1 A: “YF2 cohort”. Using peptide-MHC multimers, we detected CD8 T cells specific for the immunodominant HLA-A*02-restricted epitope of the Non-Structural 4b protein of Yellow Fever virus (the LLWNGPMAV epitope (40-42)), hereafter referred to as “A2/LLW”) in eight HLA-A*02+ vaccinees. The phenotypes of CD8 T cell differentiation were determined based on the classic markers CCR7 and CD45RA (8) as shown in Figure 1A to detect Central Memory (CM: CCR7+ CD45RA-), Effector Memory (EM: CCR7- CD45RA-) and Effector memory CD45RA+ (EMRA: CCR7- CD45RA+); within the CCR7 CD45RA double-positive gate, Naïve and stem cell-like memory (SCM) subsets were discriminated based on CD95 expression (9,10,18). Of note, the aforementioned subset nomenclature describes resting human CD8 T cells; for the purpose of longitudinal consistency we maintain this nomenclature yet highlight that acutely activated human effector cells downregulate CCR7 and phenotypically coincide with EM and EMRA (18).

We observed a massive expansion of A2/LLW-specific CD8 T cells with a peak around day 14 post-vaccination, with largely predominant CCR7- phenotypes (Figure 1B and C: “Total A2/LLW+”, “EM” and “EMRA” plots), in agreement with our prior analyses (40) (I thought this early time point has not been analyzed before?). Remarkably, detailed longitudinal quantification also showed expansion of CCR7+ memory phenotype cells: both CM and SCM cells were clearly detected and expanded by day 14 (Figure 1 C and D). After the peak at day 14, EM cells contracted, while EMRA cells continued to increase slightly until day 28. At the later time-points, especially by 6 months, it was evident that EMRA and SCM subsets

persisted, while EM and CM subsets continued to fade away. This later observation was in line with our previous report where the EMRA and SCM subsets were the two subsets predominantly detected in the long-term (range of years to decades), the SCM cells being the most stable memory cell subset described so far (36).

In addition, we determined whether CCR7⁺ memory phenotype cells detected during the early phase post-vaccination co-existed with antigen, i.e. before viral clearance. Live-attenuated vaccine virus YF-17D was detectable at days 3 and/or 7 in the plasma of five out of the eight vaccinees (Figure 1D and Figure S1). When considering samples that showed >0.01% A2/LLW⁺ CD8 T cells two donors had significant CM (in donor LAU 5088) or both CM and SCM populations (in donor LAU 5080) among A2/LLW⁺ cells at the same time-point when virus was detectable (Figure S1). These data show that cells with a memory phenotype can arise before antigen is cleared, well ahead of the contraction phase of the response.

SCM and CM phenotype cells are activated at the peak of the response

In parallel to the rise in frequencies, the acute phase of the T cell response is characterized by the expression of activation markers as previously described in total A2/LLW⁺ CD8 T cells (40,42,43). In order to address how activation compared across CD8 T cell subsets, we measured the longitudinal expression of activation markers: CD69, CD38, HLA-DR and PD1, within each subset. At the peak of the response (day 14), the analyses clearly showed that the SCM and CM subsets were extensively activated, in fact as much as the CCR7⁻ EM and EMRA subsets (Figure 2). The early activation marker CD69 was most highly expressed at days 3 and 7, while HLA-DR, CD38 and PD1 peaked at day 14 (Figure S2). Beyond day 14, CD38 clearly diminished while HLA-DR and PD1 partially persisted (Figure S2).

Of note, in the aforementioned longitudinal analyses, we observed that A2/LLW⁺ CD8 T cells were still present in the Naïve gate (as defined by CCR7⁺ CD45RA⁺ CD95⁻) after vaccination and that they remained relatively stable over time (Figure 1). Interestingly, these post-vaccination Naïve cells did show substantial activation at the

peak of the response (Figure 2 and S2). The nature of these Naïve-gated cells will be discussed. (in my mind this paragraph is a problem)

TCF1+ CD8 T cells preferentially persist for decades

Given the central function of T cell factor 1 in memory establishment (24-26,31,32), we next monitored the expression of TCF1 in the various CD8 T cell subsets following YF-17D vaccination. First, by analyzing resting total CD8 T cells in a large number of donors (N=33), we observed a wide heterogeneity in TCF1 levels in human CCR7- CD8 T cell subsets (EM and EMRA). In line with mouse and human gene expression data (3,4,28,29), we observed the hierarchical expression of TCF1: Naïve and memory subsets (including CM and SCM) expressed high levels of TCF1, while effector subsets (EM and EMRA) had low-to-negative levels of TCF1 (Figure 3). Similar to the inter-donor variability in subset distribution (Figure 3A and C), this single cell protein data in N=33 donors revealed that the fraction of TCF1+ cells was widely variable within CCR7- subsets across donors (EM and EMRA, Figure 3B and D).

We then analyzed the profiles of TCF1 in A2/LLW-specific CD8 T cells at various time-points following vaccination with YF-17D. (At 2? weeks post vaccination (? correct),

- should you not rather concentrate on Tcf1 expression by SCM and CM at the early timepoints and then describe the downregulation in effector cells
- are the late time points really of interest oin this context

the frequency of TCF1 positive cells was low among antigen-sepecific CCR7 negative subsets (EM and EMRA, Figure 4 A and B), providing evidence of TCF1 downregulation during the acute response in humans in vivo. The maximum drop in TCF1 occurred at day 28 (Figure 4 A and B), and appeared thus delayed relative to the activation peak at day 14 (Figure S2) (what do you make of this?). After day 28, the CCR7- populations (EM or EMRA) showed a gradual increase in the percentages of TCF1+ cells, particularly visible in the decade-persisting EM and EMRA cells (Figure 4B). Based on longitudinal modeling of the percentage of TCF1+ cells per

subset and the comparison of the trends across subsets, the CCR7⁻ subsets (EM and EMRA) were found to exhibit a distinct profile compared to CCR7⁺ subsets (Naïve, SCM, and CM) (Figure 4C). While CM cells showed a trend closer to the trends in Naïve and SCM, they were statistically distinct to all subsets; the trends of Naïve and SCM were not distinguishable (Figure 4C).

Within the CCR7⁻ subsets, we addressed whether the increase in the percentage of TCF1⁺ cells in the longer-term was linked to an overall or a relative increase in TCF1⁺ cells. We considered the frequencies of TCF1 positive or negative cells in each CCR7⁻ subset in relation to the total CD8 T cells and from the peak of the response (day 14), and observed that : 1) both TCF1 positive and TCF1 negative populations declined with time (Figure 4D), and 2) TCF1 positive populations declined less than TCF1 negative populations (Figure 4 D and E), in both EM and EMRA subsets. Rather than re-expression of TCF1 in CCR7⁻ cells, these relative frequencies suggest that TCF1 positive cells persist better than TCF1 negative cells in the long-term.

We further studied the expression of the Interleukin 7 Receptor alpha chain (IL7Ra) in the EMRA subset and found a pattern of IL7Ra expression globally correlating with that of TCF1 expression (Figure 5 and S5). In particular, both TCF1 and IL7Ra were enriched in EMRA cells persisting beyond six months and further co-enriched when persisting over three years. Similar trends were observed for the EM populations; however, because the EM subset in total CD8 T cells inherently features a substantial fraction of IL7Ra⁺ cells (as opposed to the scarcer fraction of IL7Ra⁺ in total EMRA), the TCF1 and IL7Ra co-enrichment was not significant; CCR7⁺ subsets express high levels of IL7Ra similar to high levels of TCF1⁺ (data not shown). This is in line with our previous analysis where A2/LLW-specific EMRA but not A2/LLW-specific EM showed significant enrichment of the IL7Ra as compared to their counterparts in total CD8 T cells (36).

SCM CD8 T cells retain proximity to the Naïve baseline (clarfy whether you mean abundance or phenotype of both), while effectors burst out of baseline and gradually contract

In order to detail the dynamics of the CD8 T cell response including multiple differentiation and activation markers, we applied multi-dimensionality reduction and unsupervised clustering to flow cytometry data using t-distributed Stochastic Neighbor Embedding (tSNE), and then further generated time-lapse representations. We applied this analysis strategy to samples from our longitudinal YF2 cohort, alone and in combination with long-term samples from the cross-sectional YF1 cohort. As detailed in the methods section, concatenated tSNE was possible for samples acquired with the same antibody panel and acquired under the same instrument configuration and normalized settings (Table S2).

First, tSNE was ran on single live total CD8 T cells from a pool of n=13 donors, analyzing nine differentiation and activation markers: CCR7, CD45RA, CD95, TCF1, IL7Ra, PD1, CD69, CD38 and HLA-DR. The differentiation subsets were then gated using the standard strategy (Figure 6A, similar to Figure 1A) in order to be located within the tSNE plots. The tSNE analysis of this n=13 donor pool of total CD8 T cells showed a distinct Naïve lobe, with SCM cells bridging this Naïve lobe into the remaining differentiation subsets which were arranged in a gradient and formed a second lobe (Figure 6 B: subset overlay, and C: individual subset populations). The localization of the subsets gated based on CCR7, CD45RA and CD95 (Figure 6 A) corresponded well with the tSNE clustering, including the expression patterns expected for the other six markers (Figure 6D) : for instance, IL7Ra and TCF1 were low while PD1 was high only in the CCR7- populations. In independent analyses, we analyzed N=16 donors, applying the 9-marker tSNE to each donor individually (Figure S6). We found that the pattern described above is reproducible across donors and tSNE runs, with donors showing variable sizes of the Naïve and differentiated lobes as expected based on the natural variability of the frequencies of CD8 T cell subsets (Figure 3). Of note, SCM were found in the bridge between lobes and also interspersed within the Naïve lobes.

We next applied this 9-marker tSNE analysis to longitudinal series of YF-17D vaccination samples, running tSNE individually on each series of 7 donors. The subset overlay tSNE plots were generated as in Figure 6, by gating subsets in each time-point of the longitudinal concatenated file (Figure S7). We then represented each

time-point and generated time-lapse animations of the data. We found a remarkable pattern of the dynamics of CD8 T cell differentiation during YF-17D vaccination across donors: SCM cells appear and remain very close to the location of baseline Naïve cells (Figure 7A; Video 1 showing N=7 subset overlays, and Video 2 showing each marker for donor LAU 5089 → *video links inserted here*). In contrast, effector CCR7- populations burst out of the baseline Naïve location, peaking their distance at days 14-28, and gradually contracting. Intriguingly, we observed a population of cells that permanently allocated to the region of the baseline cells (with a Naïve and SCM phenotype), throughout the response.

To address how do decade-persisting CD8 T cells compare to the early dynamics, in further analyses, we concatenated N=6 longitudinal series of early vaccination samples (longitudinal cohort, up to 6 months; 7 time-points per series) with N=13 samples from the long-term, cross-sectional study. We found that in both tSNE dimensions (x and y), the long-term samples also featured a population that clustered in the baseline location, in a prolongation of the cells that stay permanent in the region that Naïve cells occupy at baseline and throughout vaccination (Figure 7B).

Conclude.....

Discussion

To date, the differentiation pathways and fates of antigen-primed CD8 T cells are largely debated, a major question being whether memory cells establish from a fraction of acute effectors or from precursors that diverge from the effector fate. With respect to the existing experimental evidence, one basic question still is : how early do memory subsets appear? Specifically concerning the more recently coined SCM subset, the existing evidence is limited to one study using the macaque model of Simian Immunodeficiency Virus infection, where antigen-specific CD8 SCM cells are observed as early as day 7 of infection (supplementary data showing CM9/TL8-specific CD8 T cells in (44)). Based on our clinical studies in YF-17D vaccinees, we show first evidence in humans, in vivo, that antigen-specific CD8 T memory cells including CM and SCM subsets are activated and expand during the acute phase of the response. The analysis of samples before day 14 was challenging due to the low frequencies of antigen-specific cells and due to the medical restrictions for blood withdrawals that precluded closer intervals in our study. Nevertheless, two donors showed rising memory cells as early as day 3 and 7, while virus was still detectable (day 3). Our data clearly exclude that memory subsets appear only once the antigen is cleared or after the acute peak, and provide evidence that cells with a memory phenotype establish early after priming, within the acute phase.

The particular value of this human experimental evidence is highlighted by the challenge in studying memory development based on phenotypic markers, and the fact that these markers globally vary between mouse and human systems. In the mouse, the major differentiation markers used are CD44 (for antigen-experienced) and CD62L (for Naïve and memory), as well as IL7Ra (naïve and memory including MPECs) and KLRG1 (terminally differentiated effectors and SLECs). Human CD8 T cell subsets are classically defined on the basis of CCR7 and CD45RA (as detailed in the introduction). The SCM subset was first identified in the mouse as cells within the classic naïve-like gate that distinctly express IL2Rb, Bcl-2, CXCR3, and SCA-1 (32). Human SCM are distinguished from Naïve by the positive expression of CD95 and CD58, but these two markers are not used in mice. Conversely, the mouse SCA-1 has no human ortholog. The markers CXCR3, IL2Rb and Bcl-2 used in mice are also

considered positive in human SCM (9,10,36,44). However, these three later markers are poorly discriminative to distinguish SCM from Naïve cells: i) Bcl-2 is highly expressed in both Naïve and SCM(9) (in contrast to downregulation in cycling effectors cells(34)), ii) IL2Rb is higher in SCM but requires visualization with a second marker for Naïve/SCM discrimination, in contrast to the distinct CD95+ staining of SCM cells versus CD95- signal in naïve cells (9), and ii) CXCR3 shows high inter-donor variability and substantial positive signal even in cells that are CD58 and CD95 negative such as Melan-A-specific CD8 T cells in healthy donors, which are presumably naïve (36). A major challenge is thus the availability and choice of markers to distinctly define and visualize memory subsets. Ontogeny questions that require adoptive transfer and tracing is extremely limited in humans (only studies in the context of bone marrow transplants have successfully traced SCM generation from transferred T cells(45)) and mouse models are largely used to study CD8 T cell differentiation. Notwithstanding, the discrepancy of differentiation markers used in different model systems makes human data uniquely informative, as observations are complementary but not fully transferrable across systems such as mouse and human.

Historically, it has been particularly challenging to distinguish SCM from Naïve cells: SCM cells represent the most recent memory subset to be identified, hidden within the classic Naïve (“naïve-like”) gates. Interestingly, in our experiments, we found that there was a relatively constant level of antigen-specific CD8 T cells that fell in the naïve gate (CCR7- CD45RA- CD95-) even following priming. A hypothesis could be that these post-vaccination Naïve-gated cells have not actually been primed – this would require a compensatory replenishment of naïve cells with this antigen specificity, sufficiently rapid to immediately replenish the cells that have been primed and therefore depleted from the naïve pool. Murray et al calculated that after age 20, the naïve pool is maintained by homeostatic proliferation rather than thymic output (46) – all our donors were aged over 20, and it would be undistinguishable to know whether the naïve-gated cells proliferate due to homeostasis or due to priming. To our knowledge, in fact, there is to date no marker that can definitely prove that a given CD8 T cell has been primed. In the mouse, CD44 is often used as a marker to distinguish differentiated cells, yet there is no proof that CD44 expression is truly correlative of antigen priming experience; there is neither no such equivalent marker conventionally used in human experiments. In previous studies including ours, there

is evidence mainly substantiated from whole transcriptomic profiles, epigenetic imprints and functional assays, that subsets are arranged in a gradient, ordered from Naïve to SCM, CM, EM and EMRA (3,9,18,36). Intriguingly, we did observe that a substantial portion of cells in the naïve gate were undergoing activation, clearly visible at the peak of the response. In line with the argument that SCM amongst antigen-experienced cells preserve highest “naïveness”, we hypothesize that the cells that remain in the naïve gate after priming may have been effectively primed but are memory cells that preserve a phenotype that is very close to the naïve, even closer than SCM. Recently, Costa del Amo et al. found subpopulations of SCM cells with distinct turn-over rates in vivo (47), which highlights further potential heterogeneity within subset gates, and in support of the differentiation continuum from naïve to memory to effector.

In our animated longitudinal tSNE analyses on nine different activation and differentiation markers, it was particularly visible that a fraction of cells stayed permanently allocated in the region where cells (Naïve) located at baseline. This permanence region was observed in samples across the longitudinal series including the acute phase and prolonged in samples in the range of years-to-decades after vaccination. We observed cells with phenotypes of naïve, memory (CM and SCM, CCR7+) or effector / effector memory (EM or EMRA, CCR7+), and each of these showed activation at the peak of the response and downregulated activation markers at later time-points - this observation highlights the importance of distinguishing between displaying a memory or effector phenotype and being in an activated or resting state. The progressive differentiation model does account for activated / effector phenotypes that may rise from each of the subsets (18). To-date, methodologies used in the study of CD8 T cell differentiation include the definition of memory cells solely on the basis of the time of sampling (meaning that all cells that are detected after the acute phase are memory cells), including studies in humans vaccinated with YF-17D (20). In fact, our analyses show that there is wide heterogeneity in differentiation phenotypes very early on, within the acute phase; and particularly also in the very long-term, evidenced by the fact that EMRA cells are detectable decades after vaccination as a fraction of cells separate from SCM cells (Figure 1, Figure S3) (36). Even though they are phenotypically quite distinct (SCM vs EMRA), stem cell features such as long-term persistence and self-renewal are

likely shared in these long-term populations, at least in a fraction of them. Interestingly, we found that it is the cells that express TCF1 that preferentially persisted in the range of years-to-decades. This was pertinent not only for the SCM subset (TCF1 high from baseline and permanently thereafter) but also particularly visible in the fraction of TCF1+ cells within the EMRA subset that preferentially persisted long-term over TCF1- EMRA. The latter suggests that TCF1 may generally support cellular persistence and thus also the maintenance of long-term effector cells that are readily available in the event of reinfection.

Another historical challenge is that the classic differentiation subset nomenclature based on CCR7 and CD45RA was defined for resting human T cells, and all non-naïve subsets are termed “memory”. As a consequence, this marker-nomenclature criterium does not phenotypically distinguish acutely activated effectors (CCR7-) from the “memory”-termed effector subsets EM (CCR7- CD45RA-) and EMRA (CCR7- CD45RA+) (18). Activation and cycling markers may distinguish acute phase effectors versus resting / long-term EM and EMRA: activated CCR7- cells (HLA-DR+ CD38+) would be effectors, and CCR7- cells that are HLA-DR- and CD38- would be EM/EMRA. However, how do we define the cells that show a combined memory (CCR7+) and activated phenotype, such as the SCM and CM subsets that we detected in the acute phase being as activated as effector CCR7- subsets? The longitudinal phenotyping we hereby present clearly warrants the need for a revision of the nomenclature and marker definition of human CD8 T cell subsets with considerations of activated (acute phase) versus resting states in complement with memory and/or effector markers.

Altogether, based on clinical studies on YF-17D vaccination, we provide first evidence in humans, *in vivo*, on the early appearance of SCM CD8 T cells. The SCM phenotype that predominantly and stably persists in the decade long-term is detectable within the first week, and shows activation and expansion during the early acute phase. The results support differentiation models where memory cells arise very early without an obligatory transition through a full effector phenotype stage, yet showing an activated state on top of a memory phenotype. This would be in line with the existence of a continuum of differentiation phenotypes, where long-term memory

cells diverge from the full-blown effector burst and persist by preserving highest “naïveness” (proximity to the Naïve).

Acknowledgements

We thank Benton Lawson and the Centre for AIDS Research of Emory University (US) for the quantification of YFV load in plasma samples and the Flow Cytometry Facility of the University of Lausanne (CH) for cytometer instrument configuration and maintenance. We thank Nicole Montandon for technical assistant in processing blood specimens, and Paula Marcos Mondéjar for participating in the longitudinal study coordination. We thank Blaise Genton, Francine Widmer, Pierrette Meige and the personnel of the ‘Centre de vaccination et médecine des voyages’ at the PMU. for the coordinated efforts and collaboration with us to receive the donors and withdraw blood specimens for the longitudinal study. Finally, we warmly thank all donors that volunteered and thus preciously contributed to our findings. This study was funded by Ludwig Cancer Research and the Cancer Research Institute (both N.Y., U.S.A), the Swiss National Science Foundation (grants: 320030_152856 to DES, 310030-179459 to DES, 310030B_179570/B to WH).

Author Contributions Statement

SAFM, AB, WH and DES conceived and designed experiments, SAFM, HMEH, HOS, and DES elaborated the clinical study protocols, SAFM and AB performed experiments, SAFM, AB and SN analyzed data. All authors revised and approved the final version of the manuscript.

Conflict of Interest Statement

The authors declare that they have no conflicts of interest related to the publication of this manuscript.

References

1. Fridman WH, Pagès F, Sautès-Fridman C, Galon J. The immune contexture in human tumours: impact on clinical outcome. *Nature Publishing Group* (2012) **12**:298–306. doi:10.1038/nrc3245
2. Ribas A, Wolchok JD. Cancer immunotherapy using checkpoint blockade. *Science* (2018) **359**:1350–1355. doi:10.1126/science.aar4060
3. Crompton JG, Narayanan M, Cuddapah S, Roychoudhuri R, Ji Y, Yang W, Patel SJ, Sukumar M, Palmer DC, Peng W, et al. Lineage relationship of CD8(+) T cell subsets is revealed by progressive changes in the epigenetic landscape. *Cell Mol Immunol* (2015) doi:10.1038/cmi.2015.032
4. Roychoudhuri R, Lefebvre F, Honda M, Pan L, Ji Y, Klebanoff CA, Nichols CN, Fourati S, Hegazy AN, Goulet J-P, et al. Transcriptional profiles reveal a stepwise developmental program of memory CD8+ T cell differentiation. *Vaccine* (2015) **33**:914–923. doi:10.1016/j.vaccine.2014.10.007
5. Gray SM, Kaech SM, Staron MM. The interface between transcriptional and epigenetic control of effector and memory CD8(+) T-cell differentiation. *Immunological Reviews* (2014) **261**:157–168. doi:10.1111/imr.12205
6. Gattinoni L, Klebanoff CA, Restifo NP. Paths to stemness: building the ultimate antitumour T cell. *Nat Rev Cancer* (2012) **12**:671–684. doi:10.1038/nrc3322
7. Farber DL, Yudanin NA, Restifo NP. Human memory T cells: generation, compartmentalization and homeostasis. *Nat Rev Immunol* (2013) **14**:24–35. doi:10.1038/nri3567
8. Sallusto F, Geginat J, Lanzavecchia A. Central memory and effector memory T cell subsets: function, generation, and maintenance. *Annu Rev Immunol* (2004) **22**:745–763. doi:10.1146/annurev.immunol.22.012703.104702
9. Gattinoni L, Lugli E, Ji Y, Pos Z, Paulos CM, Quigley MF, Almeida JR, Gostick E, Yu Z, Carpenito C, et al. A human memory T cell subset with stem cell-like properties. *Nature Medicine* (2011) **17**:1290–1297. doi:10.1038/nm.2446

10. Lugli E, Gattinoni L, Roberto A, Mavilio D, Price DA, Restifo NP, Roederer M. Identification, isolation and in vitro expansion of human and nonhuman primate T stem cell memory cells. *Nat Protoc* (2012) **8**:33–42. doi:10.1038/nprot.2012.143
11. Crauste F, Mafille J, Boucinha L, Djebali S, Gandrillon O, Marvel J, Arpin C. Identification of Nascent Memory CD8 T Cells and Modeling of Their Ontogeny. *Cell Systems* (2017) **4**:306–317.e4. doi:10.1016/j.cels.2017.01.014
12. Lefrançois L, Obar JJ. Once a killer, always a killer: from cytotoxic T cell to memory cell. *Immunological Reviews* (2010) **235**:206–218. doi:10.1111/j.0105-2896.2010.00895.x
13. Yuzefpolskiy Y, Baumann FM, Kalia V, Sarkar S. Early CD8 T-cell memory precursors and terminal effectors exhibit equipotent in vivo degranulation. *Cell Mol Immunol* (2014) **12**:400–408. doi:10.4049/jimmunol.174.9.5341
14. Moulton VR, Farber DL. Committed to memory: lineage choices for activated T cells. *Trends in Immunology* (2006) **27**:261–267. doi:10.1016/j.it.2006.04.006
15. Ahmed R, Bevan MJ, Reiner SL, Fearon DT. The precursors of memory: models and controversies. *Nat Rev Immunol* (2009) **9**:662–668. doi:10.1038/nri2619
16. Restifo NP, Gattinoni L. Lineage relationship of effector and memory T cells. *Current Opinion in Immunology* (2013) **25**:556–563. doi:10.1016/j.coi.2013.09.003
17. Henning AN, Roychoudhuri R, Restifo NP. Epigenetic control of CD8. *Nat Rev Immunol* (2018) **18**:340–356. doi:10.1038/nri.2017.146
18. Mahnke YD, Brodie TM, Sallusto F, Roederer M, Lugli E. The who's who of T-cell differentiation: human memory T-cell subsets. *Eur J Immunol* (2013) **43**:2797–2809. doi:10.1002/eji.201343751
19. Ben Youngblood, Hale JS, Kissick HT, Ahn E, Xu X, Wieland A, Araki K, West EE, Ghoneim HE, Fan Y, et al. Effector CD8 T cells dedifferentiate into long-lived memory cells. *Nature* (2017)1–20. doi:10.1038/nature25144
20. Akondy RS, Fitch M, Edupuganti S, Yang S, Kissick HT, Li KW, Ben A Youngblood, Abdelsamed HA, McGuire DJ, Cohen KW, et al. Origin and

differentiation of human memory CD8 T cells after vaccination. *Nature* (2017)1–18.
doi:10.1038/nature24633

21. Pace L, Goudot C, Zueva E, Gueguen P, Burgdorf N, Waterfall JJ, Quivy J-P, Almouzni G, Amigorena S. The epigenetic control of stemness in CD8+T cell fate commitment. *Science* (2018) **359**:177–186. doi:10.1126/science.aah6499
22. Opata MM, Stephens R. Early Decision: Effector and Effector Memory T Cell Differentiation in Chronic Infection. *Curr Immunol Rev* (2013) **9**:190–206.
doi:10.2174/1573395509666131126231209
23. Kaech SM, Cui W. Transcriptional control of effector and memory CD8+ T cell differentiation. *Nat Rev Immunol* (2012) **12**:749–761. doi:10.1038/nri3307
24. Jeannot G, Boudousquié C, Gardiol N, Kang J, Huelsken J, Held W. Essential role of the Wnt pathway effector Tcf-1 for the establishment of functional CD8 T cell memory. *Proceedings of the National Academy of Sciences* (2010) **107**:9777–9782.
doi:10.1073/pnas.0914127107
25. Zhao D-M, Yu S, Zhou X, Haring JS, Held W, Badovinac VP, Harty JT, Xue H-H. Constitutive activation of Wnt signaling favors generation of memory CD8 T cells. *The Journal of Immunology* (2010) **184**:1191–1199.
doi:10.4049/jimmunol.0901199
26. Zhou X, Yu S, Zhao D-M, Harty JT, Badovinac VP, Xue H-H. Differentiation and persistence of memory CD8(+) T cells depend on T cell factor 1. *Immunity* (2010) **33**:229–240. doi:10.1016/j.immuni.2010.08.002
27. Utzschneider DT, Charmoy M, Chennupati V, Pousse L, Ferreira DP, Calderon-Copete S, Danilo M, Alfei F, Hofmann M, Wieland D, et al. T Cell Factor 1-Expressing Memory-like CD8. *Immunity* (2016) **45**:415–427.
doi:10.1016/j.immuni.2016.07.021
28. Willinger T, Freeman T, Herbert M, Hasegawa H, McMichael AJ, Callan MFC. Human naive CD8 T cells down-regulate expression of the WNT pathway transcription factors lymphoid enhancer binding factor 1 and transcription factor 7 (T cell factor-1) following antigen encounter in vitro and in vivo. *J Immunol* (2006)

176:1439–1446.

29. Kratchmarov R, Magun AM, Reiner SL. TCF1 expression marks self-renewing human CD8⁺ T cells. *Blood Adv* (2018) **2**:1685–1690. doi:10.1182/bloodadvances.2018016279
30. Abdelsamed HA, Moustaki A, Fan Y, Dogra P, Ghoneim HE, Zebley CC, Triplett BM, Sékaly R-P, Youngblood B. Human memory CD8 T cell effector potential is epigenetically preserved during in vivo homeostasis. *Journal of Experimental Medicine* (2017) **214**:1593–1606. doi:10.1002/(SICI)1521-4141(199901)29:01<284::AID-IMMU284>3.0.CO;2-C
31. Wu T, Ji Y, Moseman EA, Xu HC, Manglani M, Kirby M, Anderson SM, Handon R, Kenyon E, Elkahloun A, et al. The TCF1-Bcl6 axis counteracts type I interferon to repress exhaustion and maintain T cell stemness. *Sci Immunol* (2016) **1**: doi:10.1126/sciimmunol.aai8593
32. Gattinoni L, Zhong X-S, Palmer DC, Ji Y, Hinrichs CS, Yu Z, Wrzesinski C, Boni A, Cassard L, Garvin LM, et al. Wnt signaling arrests effector T cell differentiation and generates CD8⁺ memory stem cells. *Nature Publishing Group* (2009) **15**:808–813. doi:10.1038/nm.1982
33. Danilo M, Chennupati V, Silva JG, Siegert S, Held W. Suppression of Tcf1 by Inflammatory Cytokines Facilitates Effector CD8 T Cell Differentiation. *Cell Rep* (2018) **22**:2107–2117. doi:10.1016/j.celrep.2018.01.072
34. Miller JD, van der Most RG, Akondy RS, Glidewell JT, Albott S, Masopust D, Murali-Krishna K, Mahar PL, Edupuganti S, Lalor S, et al. Human effector and memory CD8⁺ T cell responses to smallpox and yellow fever vaccines. *Immunity* (2008) **28**:710–722. doi:10.1016/j.immuni.2008.02.020
35. Pulendran B, Oh JZ, Nakaya HI, Ravindran R, Kazmin DA. Immunity to viruses: learning from successful human vaccines. *Immunological Reviews* (2013) **255**:243–255. doi:10.1111/imr.12099
36. Fuertes Marraco SA, Soneson C, Cagnon L, Gannon PO, Allard M, Maillard SA, Montandon N, Rufer N, Waldvogel S, Delorenzi M, et al. Long-lasting stem cell-

- like memory CD8+ T cells with a naïve-like profile upon yellow fever vaccination. *Science Translational Medicine* (2015) **7**:282ra48. doi:10.1126/scitranslmed.aaa3700
37. Marraco SAF, Soneson C, Delorenzi M, Speiser DE. Genomics Data. *GDATA* (2015) **5**:297–301. doi:10.1016/j.gdata.2015.06.024
38. Akondy RS, Johnson PLF, Nakaya HI, Edupuganti S, Mulligan MJ, Lawson B, Miller JD, Pulendran B, Antia R, Ahmed R. Initial viral load determines the magnitude of the human CD8 T cell response to yellow fever vaccination. *Proceedings of the National Academy of Sciences* (2015) **112**:3050–3055. doi:10.1073/pnas.1500475112
39. Bates D, Mächler M, Bolker B, Walker S. Fitting Linear Mixed-Effects Models Using lme4. *J Stat Soft* (2015) **67**: doi:10.18637/jss.v067.i01
40. Akondy RS, Monson ND, Miller JD, Edupuganti S, Teuwen D, Wu H, Quyyumi F, Garg S, Altman JD, Del Rio C, et al. The Yellow Fever Virus Vaccine Induces a Broad and Polyfunctional Human Memory CD8+ T Cell Response. *The Journal of Immunology* (2009) **183**:7919–7930. doi:10.4049/jimmunol.0803903
41. de Melo AB, Nascimento EJM, Braga-Neto U, Dhalia R, Silva AM, Oelke M, Schneck JP, Sidney J, Sette A, Montenegro SML, et al. T-cell memory responses elicited by yellow fever vaccine are targeted to overlapping epitopes containing multiple HLA-I and -II binding motifs. *PLoS Negl Trop Dis* (2013) **7**:e1938. doi:10.1371/journal.pntd.0001938
42. Blom K, Braun M, Ivarsson MA, Gonzalez VD, Falconer K, Moll M, Ljunggren HG, Michaelsson J, Sandberg JK. Temporal Dynamics of the Primary Human T Cell Response to Yellow Fever Virus 17D As It Matures from an Effector- to a Memory-Type Response. *The Journal of Immunology* (2013) **190**:2150–2158. doi:10.4049/jimmunol.1202234
43. Querec TD, Akondy RS, Lee EK, Cao W, Nakaya HI, Teuwen D, Pirani A, Gernert K, Deng J, Marzolf B, et al. Systems biology approach predicts immunogenicity of the yellow fever vaccine in humans. *Nature Publishing Group* (2009) **10**:116–125. doi:10.1038/ni.1688

44. Lugli E, Dominguez MH, Gattinoni L, Chattopadhyay PK, Bolton DL, Song K, Klatt NR, Brenchley JM, Vaccari M, Gostick E, et al. Superior T memory stem cell persistence supports long-lived T cell memory. *J Clin Invest* (2013)
doi:10.1172/JCI66327DS1
45. Cieri N, Oliveira G, Greco R, Forcato M, Taccioli C, Cianciotti B, Valtolina V, Noviello M, Vago L, Bondanza A, et al. Generation of human memory stem T cells upon haploidentical T-replete hematopoietic stem cell transplantation. *Blood* (2015)
doi:10.1182/blood-2014-11-608539
46. Murray JM, Kaufmann GR, Hodgkin PD, Lewin SR, Kelleher AD, Davenport MP, Zaunders JJ. Naive T cells are maintained by thymic output in early ages but by proliferation without phenotypic change after age twenty. *Immunology and Cell Biology* (2003) **81**:487–495. doi:10.1046/j.1440-1711.2003.01191.x
47. Costa del Amo P, Lahoz-Beneytez J, Boelen L, Ahmed R, Miners KL, Zhang Y, Roger L, Jones RE, Marraco SAF, Speiser DE, et al. Human TSCM cell dynamics in vivo are compatible with long-lived immunological memory and stemness. *Plos Biol* (2018) **16**:e2005523. doi:10.1371/journal.pbio.2005523.s010

Figure legends

Figure 1. Quantification of A2/LLW-specific CD8 T cell subsets during the first six months after YF-17D vaccination. (A) Flow cytometry gating strategy to define CD8 T cell subsets : Central memory (CM : CCR7+ CD45RA-), Effector memory (EM : CCR7- CD45RA-) and Effector memory CD45RA+ (EMRA : CCR7- CD45RA+) cells; CCR7 and CD45RA double positive (DP) cells are further subdivided into Naïve (CD95-) and stem cell-like (SCM, CD95+) subsets. (B) Flow cytometry analysis of A2/LLW tetramer+ CD8 T cells, showing the 7 longitudinal time-points of the representative donor (LAU 5089) : CD8+ A2/LLW tetramer+ cells were analysed for subset distribution as in A. (C) and (D) Quantification of the frequency of A2/LLW tetramer+ within total peripheral CD8 T cells, in N=8 donors with 7 longitudinal time-points. In C, frequencies are shown for total A2/LLW+ or per A2/LLW+ subset, and each donor is line-connected across its dotted time-points. In D, the data is pooled showing average and standard error of the mean (N=8) per population as indicated (left y-axis) ; viral load data is complemented (right y-axis). The dotted line in C and D indicates the multimer detection threshold of 0.01% of total CD8 T cells. Time-points are BL : baseline, D3 : Day 3, D7 : Day 7, D14 : Day 14, D28 : Day 28, M3 : circa 3 months, M6 : circa 6 months (Table S1 shows full details of the cohort).

Figure 2. Activation of A2/LLW-specific CD8 T cell subsets at the peak of the response. (A) Flow cytometry profiles at day 14 showing each activation marker and subset, as indicated ; total CD8 T cells are shown as a reference. The data are from donor LAU 5089.

(B) Pie charts showing frequencies of the combinatorial expression of the four indicated activation markers, per subset : each arc designates one marker, each slice a number of markers co-expressed (representation based on SPICE software). N=7 donors were analysed at day 14 post-vaccination and only detectable populations were quantified : in Naïve (n=4/7), SCM (n=7/7), CM (n=7/7), EM (n=7/7), EMRA (n=7/7). P-values (built-in t-test in SPICE) : ns = not significant, * < 0.05, ** < 0.01, *** < 0.001.

Figure 3. Patterns of subset distribution and TCF1 expression in human CD8 T cells across donors. (A) and (B) Flow cytometry analyses of CD8 T cells for subset composition (in A) and offset overlay histograms for TCF1 expression amongst subsets (in B), showing n=3 examples. (C) Frequencies for subset composition and TCF1 expression in peripheral total CD8 T cells from N=33 donors; these correspond to non-activated cells (unvaccinated or over 6 months after vaccination). Comparative p-values are shown in matrix format below each x-axis label, based on a Friedman test (non-parametric, paired) : ns = not significant, trend = 0.05 to <0.10, * < 0.05, ** < 0.01, *** < 0.001.

Figure 4. Dynamics of TCF1 expression in A2/LLW-specific CD8 T cell subsets in the early and late phases after YF-17D vaccination. (A) Flow cytometry profiles of TCF1 expression, longitudinally in the first 6 months after vaccination, in each subset. Overlay histograms show the A2/LLW multimer+ CD8 T cells in open line (colored per subset; absence denotes a non-detectable population) and the total CD8 T cell reference in grey fill below. Donor LAU 5081 is shown. (B) Frequencies of TCF1 expression in the various A2/LLW-specific CD8 T cell subsets, longitudinally in N=8 vaccinees in the early phase (first six months, line-connected dots per donor) and N=26 vaccinees for the late phase (cross-sectional cohort: from 4 months to 23.7 years); total N=82 samples. P-values are based on Kruskal-Wallis (unpaired, non-parametric) for multiple comparisons amongst time-line groups, distributed as shown in Figure S4. (C) Statistical comparison of the % of TCF1+ cells per subset based on longitudinal modeling of the data (same dataset as in panel B) and Bonferroni adjustment of the pairwise p-values. (D) and (E) Frequencies of TCF1+ and TCF1- populations of A2/LLW-specific EM or EMRA subsets amongst total peripheral CD8 T cells. Corresponding linear regressions with least squares fit are shown for data from the peak of the response (at day 14). In D, the best-fit and standard error of the slopes from TCF1+ or TCF1- are compared, within each effector subset, with t-test p-values indicated. ns = not significant, trend = 0.05 to <0.10, * < 0.05, ** < 0.01, *** < 0.001.

Figure 5. IL7Ra co-enriches with TCF1 in the long-term in A2/LLW-specific EMRA cells. Pie charts showing frequencies of the combinatorial expression of IL7Ra and TCF1 in the EMRA subset. Baseline EMRA correspond to EMRA from

total CD8 T cells. Thereafter, post-vaccination EMRA populations that are A2/LLW-specific are shown (these are non- or insufficiently detectable for analysis before day 14). P-values (built-in t-test in SPICE, comparing to baseline) : ns = not significant, * < 0.05, ** < 0.01, *** < 0.001.

Figure 6. Gradient of differentiation in total CD8 T cells validated by t-Stochastic Neighbor Embedding (tSNE) of flow cytometry data. Total CD8 T cells from N=13 donors (ranging from 8.5 months to 23.7 years after vaccination, i.e. no acute phase samples) were analysed with the tSNE plugin from FlowJo **(A)** Analysis strategy : single live CD8 T cells from each donor were downsampled to 5'000 events and the sum of N=13 donors were concatenated into a single file (70'000 events). This file was then gated and color-coded for the differentiation subsets as previously described (Figure 1A). **(B) and (C)** The N=13 concatenate was analysed by tSNE using the plugin from FlowJo v10, reducing nine parameters (CCR7, CD45RA, CD95, TCF1, IL7Ra, PD1, CD69, HLA-DR, CD38) to two dimensions (tSNE x- and y- axes). Shown is the resulting unsupervised clustering tSNE plot, with the overlay (in B) or individual plots (in C) of the differentiation subsets gated as in panel A. **(D)** The tSNE plots showing the heatmap (based on median) of each marker, as indicated.

Figure 7. Time-lapse dynamics of CD8 T cell differentiation showing effector cell burst and permanent memory cell establishment during YF-17D vaccination. **(A)** N=7 donors were individually analysed, performing tSNE analyses on the longitudinal data series : for each donor dataset, all the single live A2/LLW-specific CD8 T cell flow cytometry events acquired were concatenated and individually ran for tSNE. The resulting tSNE plots are shown for each time-point (gated based on sample ID). Samples from donor LAU 5096 were stained with a different antibody panel (« panel D ») compared to all other donors (stained with « panel C »), as detailed in Table S2. **(B)** Single live A2/LLW-specific CD8 T cells from a pool of N=55 samples acquired with the same flow cytometry panel and instrument configuration were concatenated and ran for tSNE. These included: N=6 donors (D1 to D6) with longitudinal data (7 time-points: BL, D3, D7, D14, D28, M3 and M6 in each sequence) together with N=13 donors from the cross-sectional cohort (grouped according to years since vaccination), as indicated. Shown are the plots of the

calculated tSNE (either x- or y- dimension) versus sample ID. The black-bordered rectangle indicates the areas of permanency throughout vaccination.

Video 1. “N=7 subsets”: Dynamics of the differentiation of A2/LLW-specific CD8 T cells during YF-17D vaccination, showing subset composition for N=7 donors. Time-lapse animation of the longitudinal tSNE analysis with subset overlays in N=7 donors, as indicated. Each donor sequence is spaced by 1 second, showing subset composition, and starting from Baseline, then Day 3, Day 7, Day 14, Day 28, circa 3 Months and circa 6 Months after YF-17D vaccination. For each donor, all the single live A2/LLW-specific CD8 T cell events acquired were concatenated and ran for the 9-marker tSNE.

Video 2. “LAU 5089 markers”: Dynamics of the differentiation of A2/LLW-specific CD8 T cells during YF-17D vaccination, showing each of the 9 markers for vaccinee LAU 5089. Time-lapse animation of the longitudinal tSNE analysis of donor LAU5089, showing sequences starting from Baseline, then Day 3, Day 7, Day 14, Day 28, Day 84 (ca. 3 months) and Day 185 (ca. 6 months) after YF-17D vaccination. Each sequence is spaced by 1 second, and shows subset overlay or the indicated heatmapped marker. All the single live A2/LLW-specific CD8 T cell events acquired were concatenated and ran for the 9-marker tSNE.

Figure S1. Longitudinal differentiation of A2/LLW-specific CD8 T cells in donors with detectable Yellow Fever viral load. Data are quantified as in Figure 1D, showed for each individual donor that showed positive Yellow Fever viral load (N=5 out of 8 donors).

Figure S2. Longitudinal analysis of activation markers in A2/LLW-specific CD8 T cell subsets. The analysis is performed as in Figure 2, showing all time-points. The pie charts are translucent for the time-points and subsets with less than 3 donors with interpretable data. N values are indicated below each pie chart. P-values (built-in t-test in SPICE, comparing subsets within each time-point) : ns = not significant, * < 0.05, ** < 0.01, *** < 0.001.

Figure S3. Frequencies of A2/LLW-specific CD8 T cell subsets in subjects of the cross-sectional cohort. The frequency of A2/LLW-specific CD8 T cells within each subset is shown for the cross-sectional donors (analyzed in Figures 3 to 7 in combination with donors of the longitudinal cohort).

Figure S4: Expression of TCF1 in A2/LLW-specific CD8 T cells of donors from the longitudinal and cross-sectional cohorts. Donors were grouped according to various time intervals since vaccination, each dot representing one donor. P-values: ns = not significant, trend = 0.05 to <0.10, * < 0.05, ** < 0.01, *** < 0.001, after Kruskal-Wallis multiple comparisons (unpaired, non-parametric).

Figure S5. TCF1 and IL7Ra co-expression in total and A2/LLW-specific EMRA cells early and long-term after YF-17D vaccination. Data are analyzed as in Figure 5, showing the data corresponding to either total or A2/LLW-specific EMRA cells, in the various time-point groups. P-values (built-in t-test in SPICE, comparing total versus A2/LLW-specific within each time-point group) : ns = not significant, trend = 0.05 to <0.10, * < 0.05, ** < 0.01, *** < 0.001.

Figure S6. Individual yet conserved tSNE pattern of differentiation subsets in total CD8 T cells. A downsample of 75'000 single live total CD8 T cells was exported for each of the N=16 donors, individually running tSNE and analyzing each donor (gated and represented as in Figure 6B). The first N=13 donors correspond to the group analyzed in Figure 6 (ranging from 8.5 months to 23.7 years after vaccination, i.e. no acute phase samples); data of N=3 additional donors (ranging from 10.5 to 13.8 years after vaccination) originate from a different antibody panel configuration ("panel D", see Table S2).

Figure S7. Longitudinal dynamics of subset composition and marker expression from the tSNE analysis of donor LAU 5089. (A) For each donor dataset, all the single live A2/LLW-specific CD8 T cell flow cytometry events were concatenated and individually ran for tSNE : this generates a tSNE plot of all events. Each time-point is then gated based on sample ID, and subsets further gated and color-coded as detailed in Figure 6A. (B) Longitudinal tSNE plots showing the heatmap (based on median) of each marker, as indicated.

Figure 1

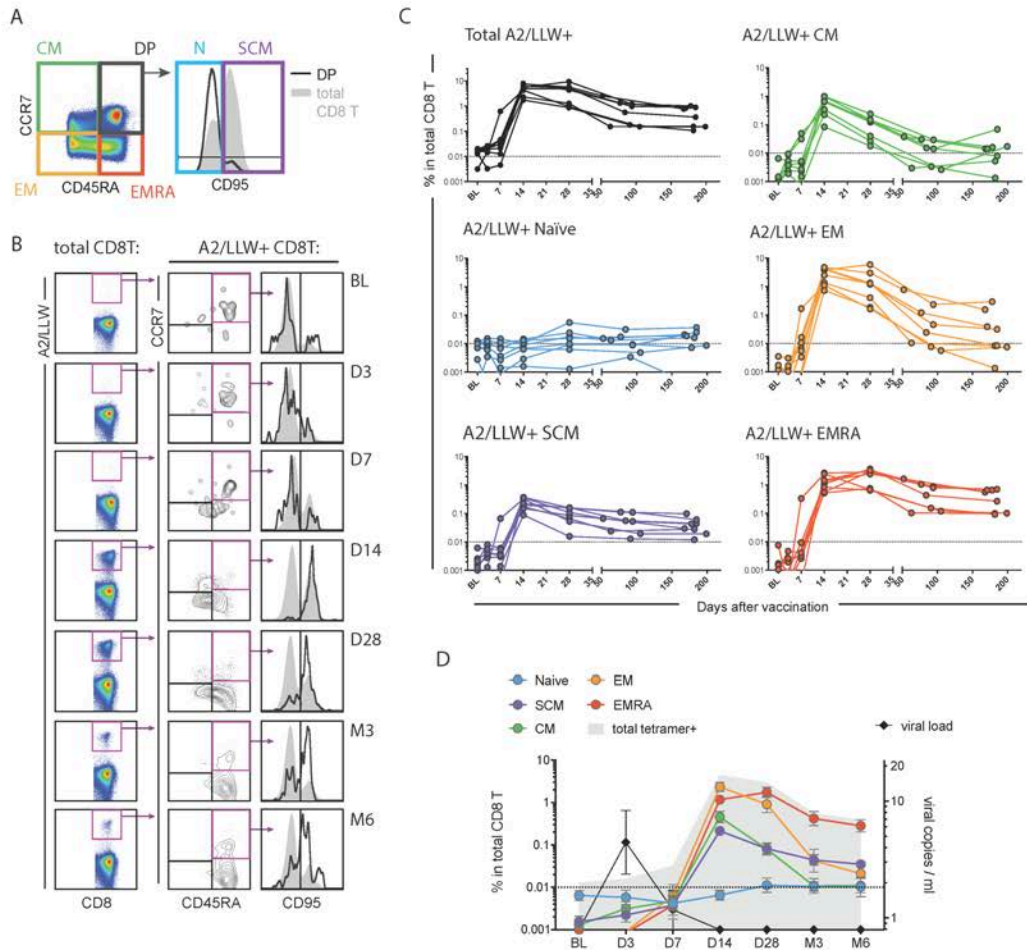


Figure 2

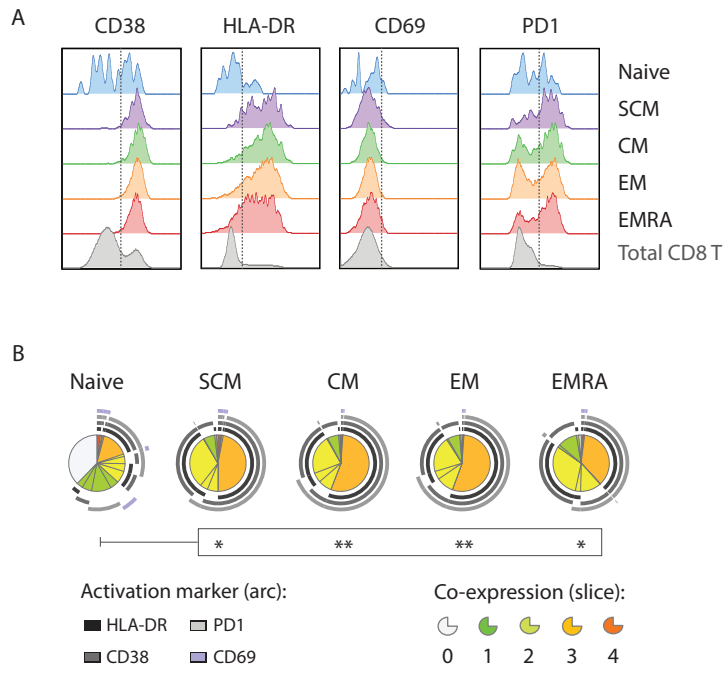


Figure 3

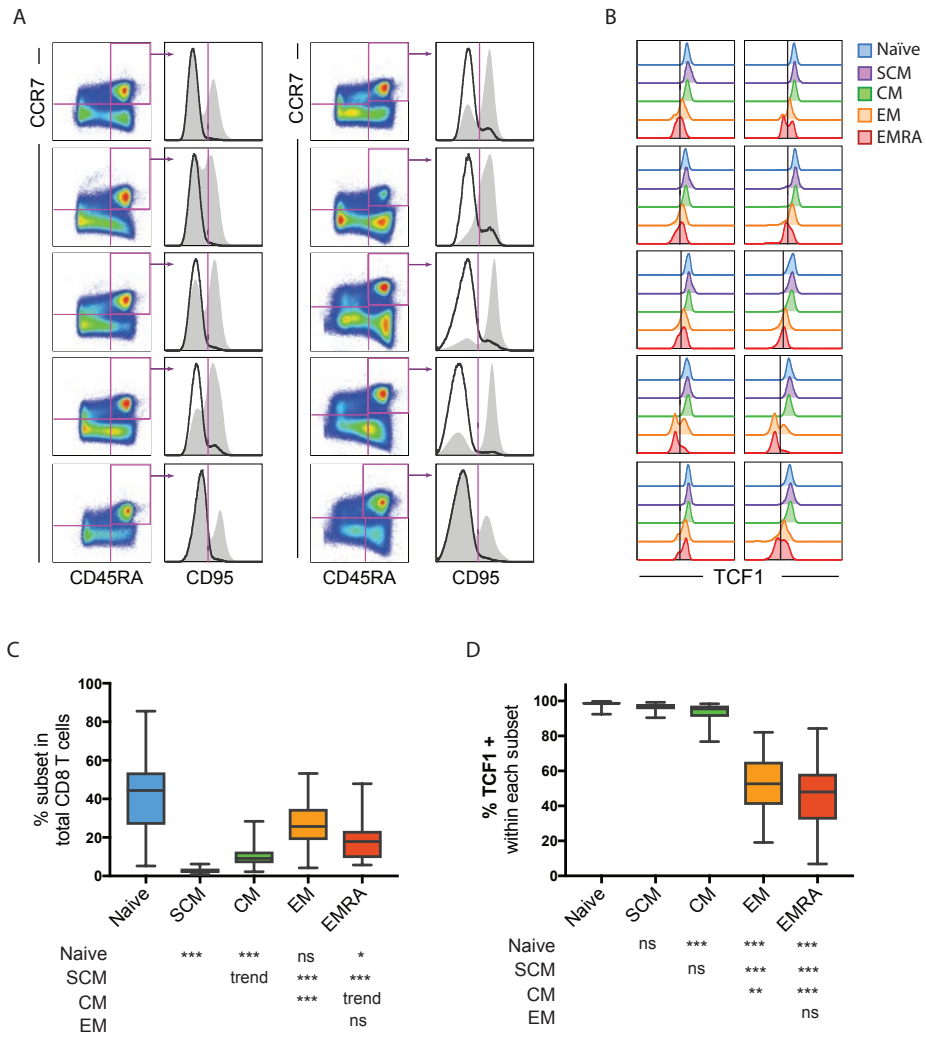


Figure 4

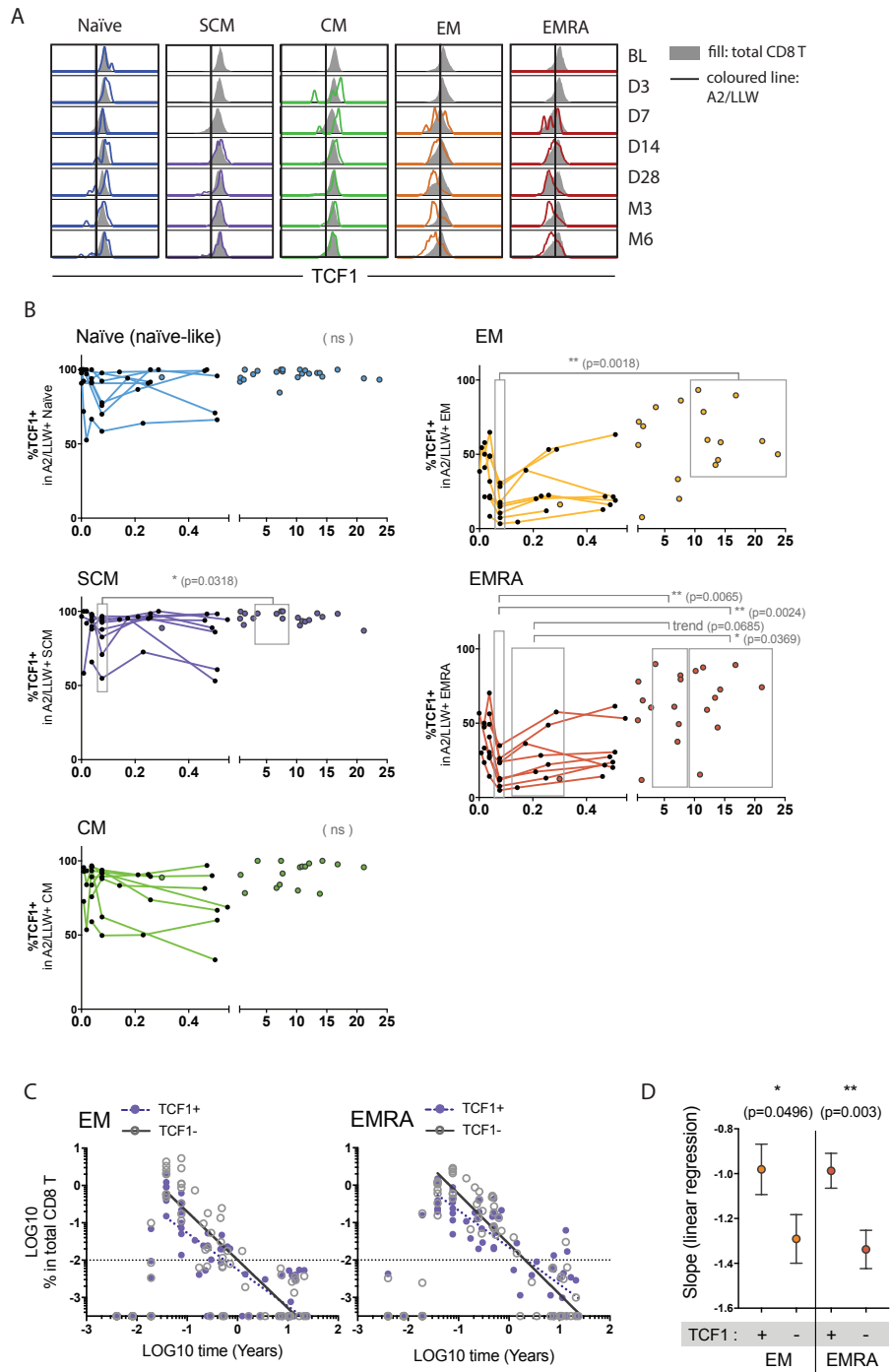


Figure 5

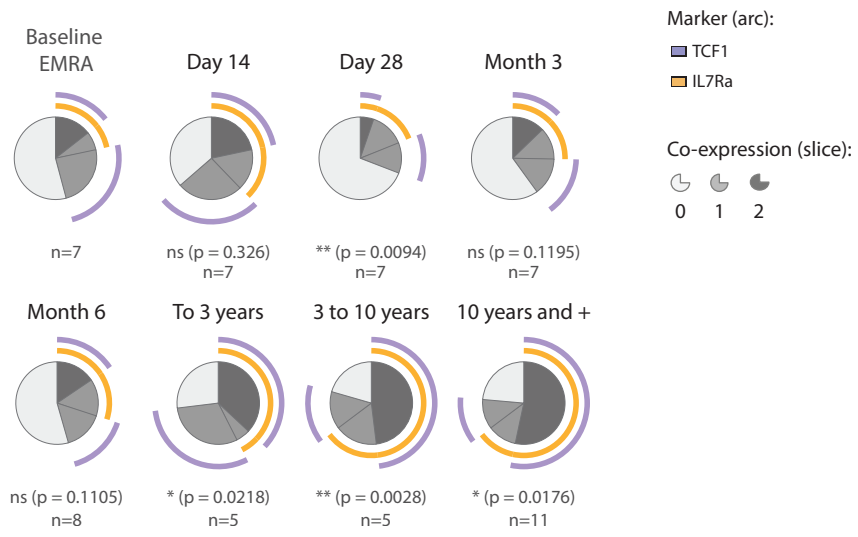


Figure 6

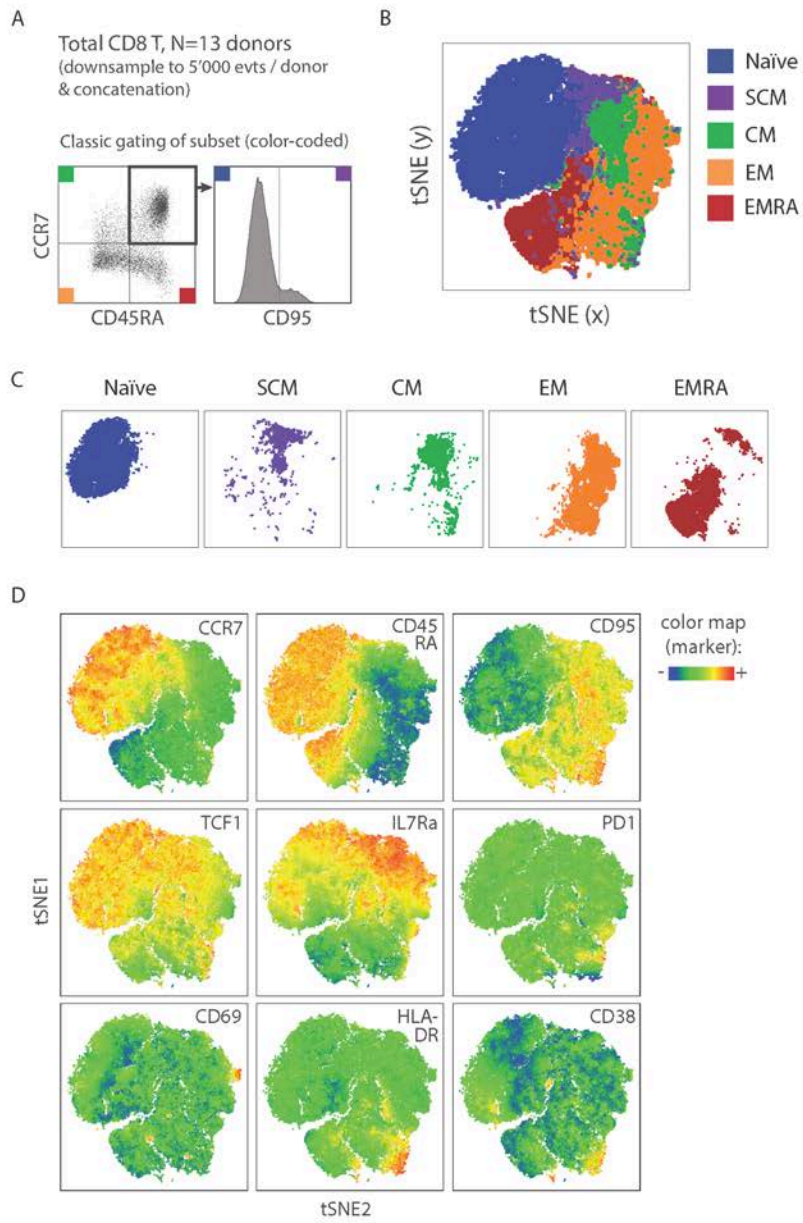
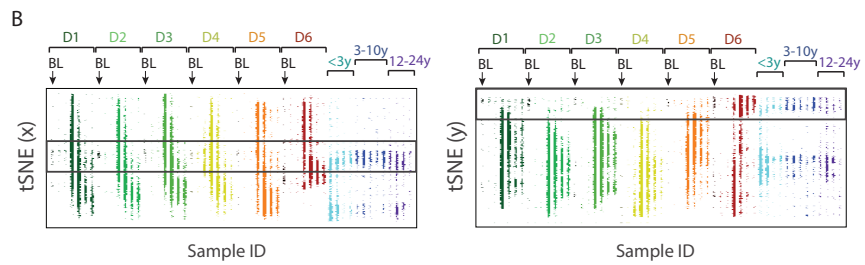
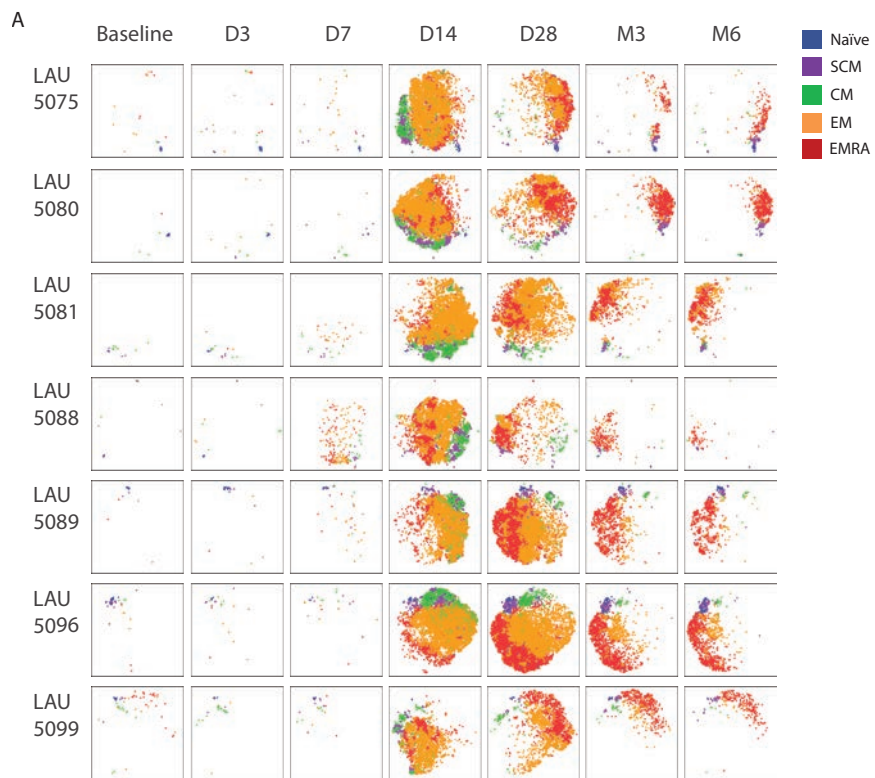


Figure 7 + animation links



CURRICULUM VITAE

Amandine Xuân Kim Bovay

Personal information

Date of birth: 08.02.1989

Citizenship: Swiss

Address: Ch. Des Roches 30, 1066 Epalinges, SWITZERLAND

Phone number: +41 79 564 33 24

E-mail: amandine.bovay@unil.ch

Education

November 2014 - present

PhD student

Prof. Dr. Daniel Speiser

Ludwig Institute of Cancer Research

University of Lausanne

PhD Thesis: "Molecular and functional characterisation of the immune responses upon Yellow Fever vaccination"

Technical skills: TCR clonotyping, ELISA, FACS, Chromium killing assay, Combinatorial peptide library, Protein expression, X-ray crystallography

June 2013

Introductory Course in Laboratory Animal Science

LTK Module 1

40 hours of training on Mice/Rats

February 2012 - March 2013

ETHZ Master program in Biochemistry

Prof. Dr. Matthias Peter

Swiss Federal Institute of Technology in Zurich (ETHZ)

Master Thesis: "The role of a Cullin 4 complex in the DNA damage response and DNA replication"

Technical skills: Western blot, siRNA transfection, Co-immunoprecipitation, Immunofluorescence, Antibody production, BrdU incorporation, Stable cell line generation

September -December 2011

ETHZ Master program in Biochemistry

Prof. Dr. Claus Azzalin

Swiss Federal Institute of Technology in Zurich (ETHZ)

Pre-master project: "Effects of telomere transcription on telomere replication"

Technical skills: Mammalian cell culture, FISH, qRT-PCR, Cell cycle analysis

2008 - 2011

Bachelor of Science in Biology

University of Lausanne

Biology and Medicine Faculty

Professional Experience

February - October 2014

Research associate

Prof. Dr. Alessandro Sartori

University of Zurich

Institute of Molecular Cancer Research
"Molecular and cellular aspects of CtIP
function in DNA Double-Strand Break
processing"

Duties: Work on research projects in progress
and contribute to the design of new ones,
Write grant applications, Operate and
maintain laboratory equipment, Purchase
laboratory consumables for the Institute,
Assist with budgetary responsibilities.

June 2013 - November 2013

Scientific collaborator

Prof. Dr. Beat Schäfer

Children's Hospital of Zurich

Experimental Infectious Diseases and
Cancer Research

"Hedgehog signaling modulation of selfrenewing
cellular compartments in eRMS"

Duties: Assist academic staff, Collect and
analyse data, Implement immunofluorescence
protocol.

July - August 2011

Intern

PD Dr. Blaise Corthésy

Lausanne University Hospital Center

Division of Immunology and Allergy
"Vaccine development"

Duties: Optimisation of protocols.

August - September 2010

Intern

Prof. Dr. Margot Thome-Miazza

University of Lausanne

Department of Biochemistry
"Analysis of the role of the protease
MALT1 in lymphocyte activation and
proliferation (SNF funding)"

Duties: Assist academic staff, Collect and
analyse data.

Award

SNF mobility grant (October 2015- September 2016):

Visiting student in the group of **Prof. Dr. Andrew Sewell, Cardiff University (UK)**.
Project: "Structural analysis of a TCR recognising the yellow fever virus epitope
NS4b₂₁₄₋₂₂₂ presented by HLA-A*0201"

Publications

- Satheesha S, Manzella G, **Bovay A**, Casanova EA, Bode PK, Belle R, Feuchtgruber S, Jaaks P, Dogan N, Koscielniak E and Schäfer BW. Targeting hedgehog signaling reduces selfrenewal in embryonal rhabdomyosarcoma. *Oncogene*. 2016 Apr 21;35(16):2020-30. doi: 10.1038/onc.2015.267.
- **Bovay A**, Zoete V, Dolton G, Bulek Am, Cole DK, Rizkallah PJ, Fuller A, Beck K, Michielin O, Speiser DE, Sewell AK, Fuertes Marraco S. T cell Receptor Alpha Variable 12-2 bias in the immunodominant response to Yellow fever virus. *Eur J Immunol*. 2018 Feb; 48(2):258-272. doi: 10.1002/eji.201747082. This article was selected for the journal front cover.
- Rius C*, Attaf M*, Tungatt K, Bianchi V, Legut M, **Bovay A**, Donia M, Straten PT, Peakman M, Svane IM, Ott A, Connor T, Szomolay B, Dolton G, Sewell AK. Peptide-MHC class I multimer staining can fail to detect relevant functional T-cell clonotypes and underestimate antigen-specific T cell populations. *J Immunol*. 2018 Feb 26;. doi: 10.4049/jimmunol.1700242.
- Fuertes Marraco SA, **Bovay A**, Nassiri S, Maby-El Hajjami H, Ouertatani-Sakouhi H, Held W, Speiser DE. Human stem cell-like memory CD8 T cells establish early in the acute response to Yellow Fever virus. *In preparation*.
- **Bovay A**, Zoete V, Rizkallah PJ, Beck K, Delbreil P, Speiser DE, Cole DK, Fuertes Marraco SA. Functionally optimized peptide rigidity in a novel superagonist mutant of the immunodominant Yellow Fever Virus epitope NS4b₂₁₄₋₂₂₂. *In preparation*.
- **Bovay A**, Nassiri S, Maby-El HAjjami H, Marcos Mondéjar P, Akondy AS, Ahmed R, Lawson B, Speiser DE, Fuertes Marraco SA. Restricted adaptive and innate immune responses to Yellow Fever virus YF-17D vaccination in individuals with pre-existing neutralizing antibodies. *In preparation*.

Conferences

Poster presentations:

- Wolfsberg meeting of Swiss PhD students in Immunology, 2015
- International Congress of Immunology, Melbourne, Australia, 2016
- EACR-AACR-SIC Special Conference, Florence, Italy, 2017

Presentations:

- Wolfsberg meeting of Swiss PhD students in Immunology, 2016
- Faculty and Staff Retreat of the Swiss Cancer Center Lausanne, Lausanne, Switzerland, 2017

Public engagement:

- Science in Health: Live!, Cardiff University, 2016

Languages

French	Mother language
English	Certificate of Advanced English, grade B
German	Basic verbal and written skills

Miscellaneous

Running
Horse riding (show jumping AVSH Merit Award 2011)
Acrylic painting